RHEOLOGICAL AND MECHANICAL PROPERTIES OF RECYCLED PAINTED AUTOMOTIVE BUMPER MATERIALS

A Thesis Submitted for the Degree of

Doctor of Philosophy

By

Rauha Tazeen Quazi

B. Sc. Eng. (Chem. Eng.)

Department of Chemical and Metallurgical Engineering

Royal Melbourne Institute of Technology

Melbourne, Australia

February, 1998.

DECLARATION

The candidate hereby declares that all the material and information reported here are original, except where due acknowledgment has been made.

The work has not been submitted previously, in whole or in part, to qualify for any other academic award.

The content of the thesis is the result of work which has been carried out since the official commencement date of the approved research program.

Rauha Tazeen Quazi

Rauha Tazeen Quazi

17/2/98

ACKNOWLEDGEMENTS

I wish to acknowledge my special gratitude to my supervisors, Prof. S. N. Bhattacharya and E. Kosior for their invaluable advice and ongoing guidance and support throughout the course of this project.

Acknowledgments are also due to CRC for Polymers for supporting the project.

I would also like to thank Prof. R. A. Shanks for his consultancy, specially regarding the use of the image analysis software.

All the technical staff at Polymer Technology Centre, Rheology and Materials Processing Centre and Chemical and Metallurgical Engineering Department were most helpful and I would like to thank them for their assistance in the use of the necessary equipment.

Thanks to my fellow post graduates for their friendship, encouragement and support during my study period at RMIT.

My special gratitude to my family, specially to my parents, who have given me constant encouragement during this period. Finally, sincere thanks are due to my husband, Nurul, for his support and patience throughout the duration of this project. Thanks to my son, Ariq, for giving me the pleasure of enjoying the motherhood beside my student life.

NOMENCLATURES

A	ligament area
a	notch depth (mm)
a_α	area of each particle
A'	constant (Pigott and Leinder equation)
A''	constant depending on suspension
A_1	cross sectional area of barrel (cm^2)
A_A	area fraction
a_T	area of a slice
B	specimen thickness (mm)
B'	constant (Pigott and Leinder equation)
C	compliance
D	specimen width (mm)
d	volume mean diameter of particles (μm)
d_1	width of a strip
d_p	particle diameter (mm)
D_S	interparticle distance (mm)
dy	thickness of a slice
$\overline{E}$	average scale reading
e	coefficient of restitution
E'	activation energy (kJ/mol)
E_C	composite modulus (MPa)
E_m	matrix modulus (MPa)
E_p	modulus of particulate phase (MPa)
g	gravitational constant (CGS units)
G'	storage modulus (Pa)
G''	loss modulus (Pa)
G^*	complex modulus (Pa)
G_C	fracture energy or critical strain energy release rate (kJ/m^2)

G_d	apparent surface energy (kJ/m^2)
H	gap between plates (mm)
k	constant
K	stress intensity factor (MN/m$^{3/2}$)
K'	constant
K_1	polymer filler interaction parameter
K_2	weightage factor
K_C	critical stress intensity factor or fracture toughness (MN/m$^{3/2}$)
L_F	final length of tensile specimen (mm)
L'	flag length (cm)
L	span of specimen (mm)
L_L	linear fraction
L_O	initial length of tensile specimen (mm)
l_T	length of a strip
m_S	mass of specimen (kg)
M	mass of striker (kg)
m	modular ratio
M'	torque (g.cm)
m'	slope of the initial straight line portion of load deflection curve (N/mm)
MFI	melt flow index
m_p	plastic constraint factor
n	Power law index
P	load (N)
P'	yield point (N)
P_C	load at fracture (N)
P_P	point fraction
r,θ	polar co-ordinates
R	gas constant (kJ/mol.K)
R'	radius of plate (mm)
r_p	radius of plastic zone (mm)
S	constant

S_1 area

T' cut off time (sec)

T temperature (K)

t travel time of flag through the photo cell (sec)

T_L line energy (J)

U elastic energy (J)

U_C energy absorbed at fracture (J)

U_{PE} potential energy (J)

U_T kinetic energy (J)

V initial velocity of striker (m/sec)

v_α volume of a slice

V_1 final velocity of striker (m/sec)

V_2 final velocity of specimen (m/sec)

VFI volume flow index

V_O initial velocity of specimen (m/sec)

v_T volume of a cube

V_V volume fraction

w average weight of extrudate (gm)

W work done (J)

W_i weight fraction of component i

w_p energy per unit volume

Y geometric factor

Y' pendulum energy (J)

Symbols

σ applied stress (Pa)

ϕ compliance calibration function

φ volume fraction of filler

Δ deflection

ρ density at room temperature (g/cm^3)

ε elongation (mm)

ν	Poisson's ratio
$\dot{\gamma}$	shear rate (sec^{-1})
τ	shear stress (Pa)
η	shear viscosity (Pa.sec)
γ	strain
θ'	shearing angle of stress head
γ'	surface energy per unit area
δA	increase in surface area
ε_C	composite elongation (mm)
γ_C	critical strain
σ_C	tensile strength of composite (MPa)
ρ_i	density of component *i* (g/cm^3)
φ_i	volume fraction of component *i*
σ_{ij}	components of the stress tensor
ε_m	matrix elongation (mm)
φ_m	maximum packing fraction
ρ_m	melt density (g/cm^3)
σ_m	tensile strength of matrix (Pa)
η_r	relative viscosity (Pa.sec)
δ_t	crack tip opening displacement
φ_v	void fraction
σ_y	uniaxial tensile stress (Pa)

TABLE OF CONTENTS

TABLE OF TABLES

TABLE OF FIGURES

SUMMARY

The use of plastics in the automotive industries has increased significantly in the past few years. Concerns for the environment and the management of waste is encouraging the recycling and proper use of scrap material. Among others, polypropylene (PP) based bumpers are targeted for recycling because of their large volume and relatively simple material composition. Most of these bumpers are coated with polyurethane based paint which becomes dispersed into the matrix during reprocessing influencing the material properties. This seemed to be an important issue to investigate as it was shown by some other workers that the lowering of properties by the presence of paint particles was more significant than the material deterioration itself. So, with the complete recycling process, it is important to understand how the dispersed phase influences the processing and later the behaviour of the matrix so that in future investigations this knowledge can be utilised in further development of the recycled material. This has been the main theme of the project with the following major objectives: (i) to remove paint particles from the painted PP bumpers by melt filtration technique (ii) to determine the rheological and mechanical properties of the rubber toughened PP based composites dispersed with paint particles and glass microspheres and (iii) to understand the effect of dispersed phase on these properties by studying the morphology of the composites.

Both commercially recycled material and real system blends prepared in the laboratory were studied to observe the effect of dispersed paint on the polymer matrix. Firstly the following materials were characterised using tensile, impact and rheological tests: virgin bumper bar grade material (PP/EPDM/talc) ; two batches of material injection moulded from the virgin grade and painted with different levels of paint layers as found on car bumpers (unfiltered and

melt filtered) and recycled painted bumpers (unfiltered and melt filtered). Extrusion melt filtration was chosen to remove the paint particles from the PP phase and the quantitative measurement of the dispersed phase was done by digital image analysis. Result of this analysis showed that only about 50% paint was removed following filtration. Little variation was observed in viscosity values for all the samples with unfiltered batches showing slightly higher and filtered samples showing slightly lower viscosity compared to the virgin material. The increased value for the first case was attributed for the paint particles acting as the particulate phase in the matrix. On the other hand, lower viscosity was caused by deterioration of material with chain scission of PP.

The elongation and impact strength of the paint dispersed batches decreased drastically compared to the virgin material as the paint particles acted as crack initiators and propagators.

For the blends prepared, well characterised paint particles were dispersed into the PP/rubber/talc and PP/rubber matrix to be used as the "real" system. Talc itself is used as a filler in the commercial grades to impart greater stiffness, so composites without talc were worth examining to compare the effect of paint over talc. Also "model" filled systems with glass microspheres were studied to observe the relative importance of particle shape and filler concentration. The choice to use glass as a model filler was primarily based on its spherical shape, non-deformable nature and relatively small surface area. The glass filled systems served as a comparison and helped in the interpretation of the rheological and mechanical properties of the paint dispersed in the rubber toughened talc filled and unfilled PP.

The rheological study over the processing temperature range showed that the presence of small fraction of the dispersed phase (upto 1.9 vol% for glass beads and 2.7 vol% for paint particles) had insignificant effect on viscosity and at these levels the effect of particle size,

particle size distribution and particle shape can be neglected. Only with increased filler fraction (5 vol%) a trend in increased viscosity was observed.

From mechanical testing it was observed that the retention of tensile yield strength was nearly 100% but elongation at break dropped significantly compared to the base matrices. This reduction was explained by poor interphase between filler and matrix. The modulus values for glass bead filled PP/rubber matrix showed an increasing tendency for high rigidity of the filler itself whereas for paint filled matrix it dropped below the base matrix value. For PP/rubber/talc matrix the scenario was different where a decrease in modulus was observed for all the composites. This was explained by the much high rigidity of talc particles over glass beads and paint particles. Though small sized talc particles acted as reinforcing fillers when added to PP/rubber system, the inclusion of second dispersed phase could not overshadow its effect on matrix thus failing as a weak structure. The drop in modulus for paint dispersed matrices was more significant indicating that irregular shaped paint particles had a smaller degree of interaction with the base matrix compared to spherical glass particles.

A sharp decrease in impact strength observed for all the composites again explained the poor adhesion between matrix and dispersed phase which was also attributed from the photomicrographs of the fractured specimens. A separated microstructure was revealed for the composites which emphasised the explanation that the inclusions reduced the ability of the elastomer phase to absorb applied energy by reducing the distance between particles. A decrease in fracture energy and toughness for all the composites was also explained by the same.

Models were proposed to predict crack propagation through glass bead and paint particle dispersed in the PP/rubber/talc matrices. For glass beads, crack propagation through the

composite was attracted to the equator of particles so fractured surfaces showed clear hemispherical holes and top surfaces of debonded particles. For irregular paint dispersed composites, crack propagated through the interphase of filler and matrix thus debonding the paint particles.

The composites under study were also related in terms of their rheology, morphology and mechanical properties. A separated microstructure of the composites as observed from the micrographs leads to the explanation of the slight increase in viscosity of filled composites over unfilled ones. Also poor interphase between filler and matrix leads to decreased property values in mechanical tests compared to base matrices.

CHAPTER ONE

INTRODUCTION

The introduction gives an overview of the use of polypropylene in automotive industries. Waste recovery of plastics by recycling technique is highlighted with attention focusing on automotive bumpers. The importance of characterisation of composite materials by rheological and mechanical property studies are stated together with the objectives of the project. The structure of the thesis is given in the last section.

1.1 Use of Polypropylene in Automotive Industries

Plastic materials are increasingly being used today in diverse fields in wide applications owing to their versatility and advantages such as corrosion resistance, light weight, energy efficiency and design flexibility over metals. The average proportion of plastic materials used in automobiles has increased substantially in the last decade and is currently of the order of 13%. The growth rate of plastics in automotive engineering over a period of thirty years is evident from figure 1.1.1 (Weber, 1991). Both thermosets and thermoplastics are used for the purpose but the manufacturers are giving priority to switch to types of plastics that are easier to recycle and more compatible with the environment. Figure 1.1.2 is a breakdown of the various types of plastics used in automobiles manufactured at Nissan Motor Company Ltd., Japan (Asakawa, 1992). The figures indicate that polypropylene (PP) has established an unassailable position as a key automobile material covering about half of the total plastics consumption with its use increasing from 34% in 1988 to 49% in 1990. European automobiles use somewhat less PP but still cover about one third of the total usage. It is estimated that more polyolefins would be used in the future and cars built in the year 2000 could contain about

70% of the total plastic used in automotive applications (Weber, 1991). A sensible balance between performance and cost and ease of recyclability has made PP a favourable material over the last decade.

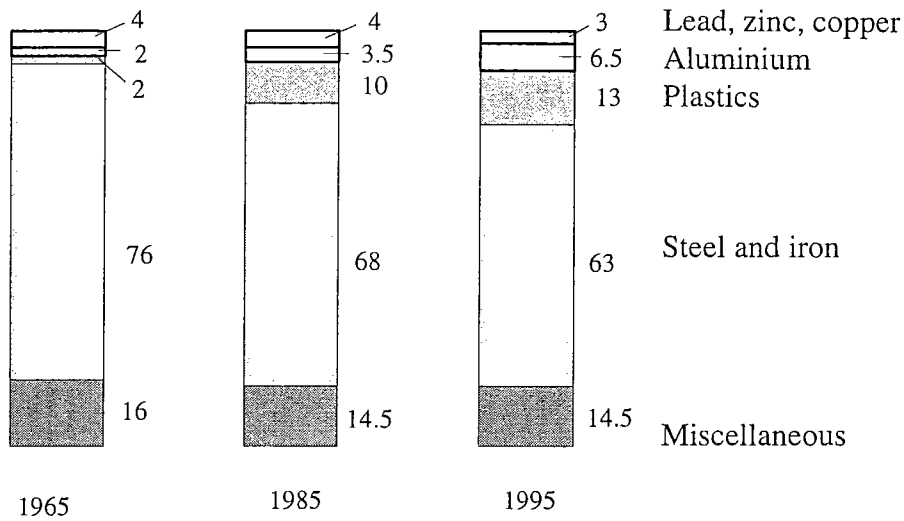

Figure 1.1.1 : Growth rate for main materials used in automobiles during the period from 1965 to 1995 (Weber, 1991).

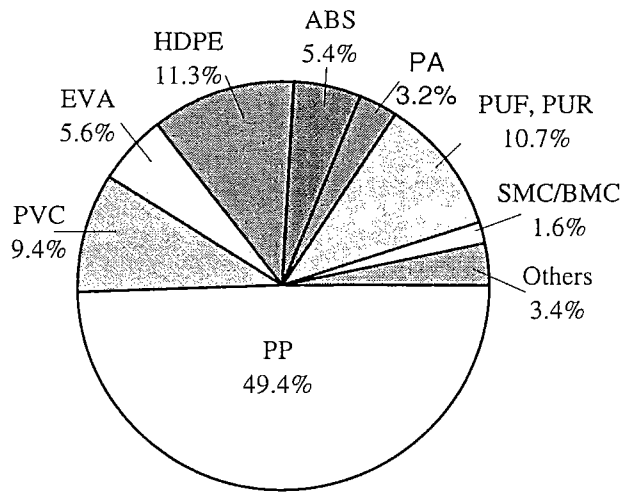

Figure 1.1.2 : Proportions of different plastics used in automobiles at Nissan Motor Company Ltd. (Asakawa, 1992).

1.2 Recycling of Plastic Waste in Automotive Industries

The increasing production and usage of plastic materials are generating more plastic waste thus creating environmental problems. This has led to serious concern about the future use of the post consumer and industrial waste. Some possible ways of disposal of materials are: landfills, steam generation, incineration, pyrolysis, hydrolysis and high temperature gasification. However, recycling of plastic waste will help reduce disposal problems as well as produce a cost reduction of raw material. Together with other industries, automobiles are producing huge amount of plastic scrap and it is estimated that three million tons of plastics waste would be generated per year from vehicles by the year 2000 (Miranda *et al.*, 1994). The Governments of Japan and Germany already require that 20% of automobiles weight be recycled and indications are there that other countries will follow too.

Automotive industries and polymer suppliers are accelerating their plastic recycling efforts following successful demonstration projects with various automotive components. Some of the vehicle parts that are being recycled are washer tank, wiper parts, heater case, cooler case, blower case, bumpers, reserve tank and dashboard. These comprise of materials such as PP, polyoxymethylene (POM), polymethyl methacrylate (PMMA), acrylonitrile butadiene styrene (ABS), polyurethane (PUR) etc. The recycled materials are reused in different parts of new cars such as floor insulator, fusible insulator, cushion pad, floor mat, door trim base, engine under cover (Asakawa, 1992) as well as in other commodities. Recycled PP has been used to make new bumpers where good retention of quality and function has been achieved. Volkswagon is the first car manufacturer to make bumpers from modified PP that contains 20% recycled resin (Hassell, 1991).

Among other plastics, attention has been focused on recycling parts made from PP as they comprise of 9 to 10% of total vehicle weight. Bumpers made from rubber toughened

polypropylene have a relatively simple material composition, and because of their large size, have become an attractive component for recycling. About a thousand ton of bumpers goes to scrap in Australia each month. The major problem with reuse of these bumpers is the polyurethane based paint coatings on them which lower the mechanical properties and qualities of recycled PP than by material deterioration or any other reasons. For example, experimental observation showed that under a tensile test, recycled PP with paint had about 50% less elongation compared to the one recycled without any paint or the virgin polymer itself (Asakawa, 1992). Similar detrimental effect was observed for impact properties as well. Presence of paint decreased impact strength of recycled material by about 25% compared to the unpainted material (Long *et al.*, 1995). Whereas, the impact strength of the unpainted material was decreased only by about 15% when recycled for a few times. The cause of reduction in this case was explained due to crosslinking of ethylene in rubber which reduced its efficiency as a toughening agent in PP. For other cases it was obvious that the dispersed paint fragments acted as stress concentrators and crack initiators thus decreasing the mechanical properties.

So attempts are being made to remove the paint from bumpers, fully or partially, before reprocessing. Numerous methods are available for paint removal but not all of them are suitable for removing paint from plastic parts. For instance, sand blasting and sanding are too expensive whereas chemical strippers create secondary pollution in the environment. So researchers are focusing on other cost effective mechanical means for paint removal. In some methods the bumpers are first shredded down to small pieces followed by passing through a pin mill (Moore, 1993) or wind mill (McCartney, 1991) to separate paint from recycled resin, the final step being melt filtration giving high grade material with low level of contamination. Some chemical solutions were also proved to be effective with low toxicity level (Studt, 1993). In all the methods filtration step is involved as it is a cheap and effective way to

remove contaminants. For the same reason this method of paint removal from bumper material was chosen in this project.

1.3 Rheological and Mechanical Properties of Polymer Composites

The demand for new materials has led to today's drive for more and better polymer composites. Polymer composites are regarded as multiphase materials of two or more components in which the polymer forms the continuous phase with fillers or reinforcing agents as the dispersed phase. Characterisation of these materials by rheological and mechanical property studies reveal information needed by diverse industries in addition to the build up of knowledge in the scientific field. Presence of fillers modifies the base polymer thereby creating a material with a prescribed set of physical, mechanical and rheological properties.

In the use of polymers, it is generally the mechanical properties which are important. However, mechanical behaviour is of little importance if the product cannot be fabricated quickly and effectively. In most of the cases, flow is involved in the processing or fabrication of such material to make useful products. The viscoelastic properties of molten polymers are of importance because it is these properties that govern flow behaviour whenever plastics are processed in molten state. For example, in order to optimise the design of an extruder, the viscosity must be known as a function of temperature and shear rate. In injection moulding, the same information is necessary in order to design the mould in such a way that the melt will completely fill it in every shot. In blow moulding, the processes of parison sag and swell are governed entirely by the rheological properties of the melt.

For filled polymers, in addition to these processes, there is an earlier stage of compounding i.e. mixing and dispersion of the filler evenly throughout the matrix polymer. By doing so, any

tendency to form a gradient in composition and properties is reduced to an acceptable level for the desired application of the composites. The most important effect of filler is on viscosity which was described above as an important design parameter for processing. The filler concentration, size, size distribution, aspect ratio, shape, fibre length for fibres, strength and interaction, related to wetting, between filler and matrix can modify the viscosity of composites. Besides, the flow behaviour is also influenced by the operating temperature of the process. It was observed that higher temperature suppresses the viscosity and the storage and loss moduli of composites (Ferry, 1980; Lepez *et al.* 1990). A vast number of studies has been performed on the rheological properties of filled polymers in molten state. Some commonly used fillers in those studies include carbon black, glass spheres, glass fibres, calcium carbonate, talc, mica, titanium dioxide, silica etc. whereas bases include polypropylene, high and low density polyethylene and a range of copolymers. Though common processes like extrusion and injection moulding are performed at higher shear rate range (> 10/s), it is important to study the low shear rate region as well, as filled composites sometimes show different behaviour specially in the lower shear rate range. This project has focused on steady shear measurements at the low shear rate region over a temperature range around the processing conditions. Also small amplitude oscillatory shear measurements were performed to investigate the structure-property relationship without destroying material structure within the same temperature window.

On the other hand, mechanical properties of polymers are probably the most important of all their properties in many ways, since whatever may be the reason for the choice of a particular composition, it must have certain characteristics of shape rigidity and strength. For polymer composites, the mechanical properties assume a dominant role as one in seeking an improvement in mechanical behaviour as a prime requirement. The filler acts through a modification of the intrinsic mechanical properties of the polymer, with such factors as

concentration, type, shape, geometrical spatial arrangement of filler within the matrix contributing to the detail of this modification.

Although it might be thought that the influence of a particulate filler on the deformability of a polymer merely distorts the molecular flow pattern in the deforming copolymer, in practice specific interactions often produce an enhanced stiffening effect (Sheldon, 1982). The micromechnical analysis of the mechanical behaviour in terms of separate contribution of the different components becomes complicated as uncertainties arise in the magnitude of interaction between filler and polymer and also from filler size distribution, agglomeration, void formation during fabrication etc. Nevertheless, theories to describe the mechanical properties of particulate filled polymers have been developed which often apply better in one situation than the other.

Published works on rheological and mechanical properties of recycled painted PP based bumper material in particular are very few in number though the ternary system of PP/rubber/talc or other similar systems have been studied by quite a few. For the study of recycled material, researchers were more interested in blends of recycled and virgin material thus evaluating their properties before end use. The presence of dispersed paint fraction resulted in poor mechanical properties although viscosity was only slightly affected (Asakawa, 1992; Long *et al.*, 1995). But none of the studies focused on determining the paint fraction in recycled material and relate that to the properties examined. This seemed to be an important issue to investigate as it was shown that the lowering of properties by the presence of paint particles was more significant than the material deterioration itself. So it is important to understand how the dispersed phase influence the processing and later the behaviour of the matrix so that in future investigations this knowledge can be utilised in further development of the recycled material. This has been the main theme of the project.

In the present work both commercially recycled and real system blends prepared in laboratory were studied to observe the effect of dispersed paint on the polymer matrix. For the "real" system, well characterised paint particles were used with the PP/rubber/talc and PP/rubber systems. Talc itself is used as a filler in the commercial grades to impart greater stiffness, so composites without talc were worth examining to compare the effect of paint over talc. Also to study the relative importance of particle size, particle size distribution, particle shape and filler concentration, "model" filled systems with glass microspheres were studied. The choice to use glass as a "model" filler was primarily based on its spherical shape, non-deformable nature and relatively small surface area. The glass filled systems served as a comparison and helped in the interpretation of the rheological and mechanical properties of the paint dispersed rubber toughened talc filled and unfilled PP.

1.4 Objectives of the Project

The project is focused on the characterisation of paint dispersed rubber toughened polypropylene by evaluating the rheological and mechanical properties. The main objectives of the project are as follows:

1. To develop a technique for analysing dispersed paint fraction in PP based polymer matrix.
2. To apply melt filtration technique for paint removal from rubber toughened PP material.
3. To produce well characterised dispersions of paint particles and glass microspheres in PP system.
4. To characterise all the above composites by evaluating their rheological behaviour at high temperatures around the processing conditions and mechanical behaviour at room temperature.

5. To develop an indepth understanding of the effect of dispersed phase on the various mechanical and rheological properties of the composites.

1.5 Structure of the Thesis

The thesis is divided into five different chapters and also includes references and appendices. The first chapter contains an introduction to the project where the consumption of PP in automotive industries, together with recycling of these materials are highlighted. The importance of material characterisation is stated followed by the objectives of the project. In the second chapter, a literature review is done on the techniques of paint removal from and recycling of polypropylene bumper materials highlighting the melt filtration method. The effect of the dispersed phase of the composite materials on the rheological and mechanical properties is discussed. Models describing mechanical properties and different toughening mechanisms of composite materials are also reviewed. Conclusions based on the literature study is made and the directions of investigations are proposed to achieve the project objectives. The third chapter elaborates the material and experimental techniques used in this work. The experimental results are analysed and discussed in chapter four. Chapter five gives the general conclusions based on the research work along with recommendations for future work. A list of symbols used in the thesis is given at the beginning although they have been defined in the text.

CHAPTER TWO

LITERATURE REVIEW

2.1 Painting of Thermoplastic Olefins

The automotive industries have seen a significant increase in the use of plastics in the past decade. Among others, thermoplastic polyolefins (TPO) comprise a major portion of the automotive plastic market as they offer many advantages over competing substrates. There is a wide selection of materials that can be used for automotive applications. Materials that compete for use with TPO are steel, thermoplastic polyurethane (TPU), actylonitrile-butadiene-styrene (ABS), polycarbonate (PC)/ polybutylene (PBT) blends and a variety of thermoplastic alloys. TPO has become the preffered plastic with major advantages as : (1) it is lighter than steel allowing better fuel economy (2) it can be recycled easily which gives it an advantage over thermosets (3) it is cost effective compared to urethane plastics and (4) it has good impact resistance and a wide range of flexural modulus thus allowing greater design flexibility (Davis and Clark, 1991).

Many applications made from TPO are also painted with various types of flexible coatings which are mainly polyurethane based, and may additionally contain melamines, acrylics, epoxies and polyesters as reactive components. All these are polar molecules having high bond energies as well as possessing reactive sites. These coatings generally cannot directly adhere to the olefinic substrate because of their low surface tension which make them hydrophobic and difficult to wet. Also their poor solubility in most organic solvents at room temperature coupled with a very crystalline surface in molded samples prevent easy diffusion of solvents across the surface creating major disadvantages for the TPO. To meet the demands

for a high quality appearance and high quality part/paint performance, plastic manufacturers, molders and paint manufacturers are working together to address this issue. Various pretreatment methods have been developed over the years to meet these demands allowing TPO to make further market share in future. The processes are discussed here briefly (Davis and Clark, 1991; Daniels, 1991; Takabori et al. , 1985; K'92 preview, 1992):

(a) Chemical oxidation :

In this process, the TPO is dipped into a strong chemical oxidising bath such as chromic/sulfuric acid bath. The disadvantage of the process is the waste disposal of chrome bath.

(b) Corona discharge:

Here high voltage electricity is released from a conductor to treat the TPO surface. This process must be done in an area free from flammable solvent vapour.

(c) Flame treatment:

In this process, open butane or propane flame is used to treat the TPO surface. This process also cannot be performed near flammable solvent vapour and it is difficult to ensure that all surfaces have been uniformly treated.

(d) Plasma treatment:

This is done in a vacuum chamber where gas is activated by an electric field. However, the difficulty and cost of running large vacuum chambers has limited the use to smaller components. Recent developments are in progress for its use with larger components.

(e) UV/ Benzophenone treatment:

This treatment is achieved by spraying the substrate with a photosensitive solution which, on exposure to high intensity ultra violet (UV) radiation, forms reactive free radicals on polymer surface. It had limited use in the last decade as TPO formulation shifted from rubber based to PP based. The current TPO used in automotive industries does not have the high level of rubber that the benzophenone oxidises to promote adhesion.

(f) Adhesion promoters:

Adhesion promoters are made from polymer such as chlorinated polyolefin. Coatings are applied to substrate using typical painting process before top coating. The promoters can be pigmented and made conductive for use in electrostatic painting. Also, they can be used wet on wet or wet on dry, with subsequent paint application. Adhesion promoters help hiding defects in moulding arising from processing.

The painting of a substrate is a multi step process comprising of :

(1) forming of substrate by injection moulding

(2) cleaning and surface preparation

(3) application of primer and /or adhesion promoter followed by

(4) application of coatings.

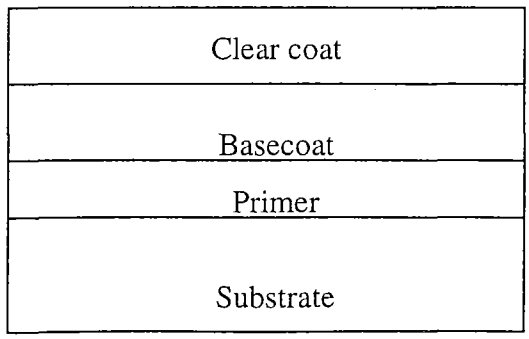

Figure 2.1.1 : Typical coated olefinic substrate.

Figure 2.1.1 shows a typical coated olefinic substrate. The primer provides a conductive surface, better gloss and increased adhesion between the coatings and substrate. The TPO substrate requires a basecoat / clearcoat technology in automotive applications to match the metal automobile body. The basecoat provides the ultimate appearance on TPO. The typical painting process of TPO bumpers followed in Ford Australia is shown in figure 2.1.2.

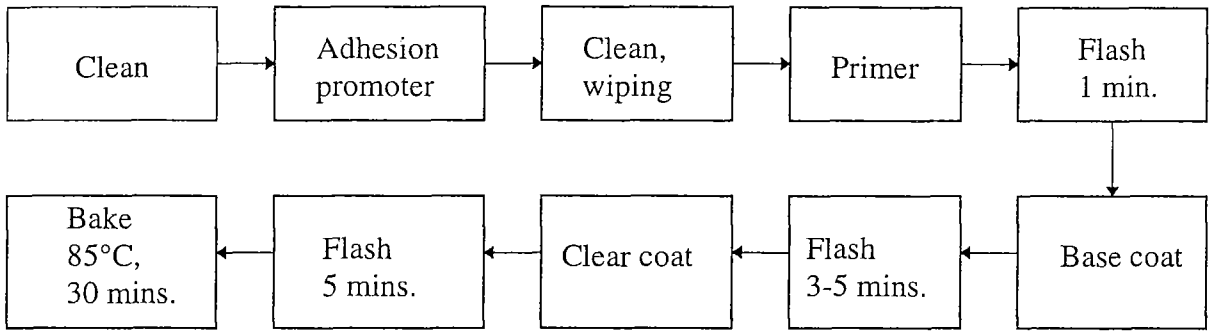

Figure 2.1.2 : Typical painting process of TPO bumpers followed in Ford, Australia.

2.2 Paint Stripping Techniques

There are numerous ways available for paint stripping from substrates but the regulations issued by the Environmental Protection Agency and Occupational Safety and Health Administration have caused industries to take a new look at these processes. Techniques such as sandblasting, abrasive particle removal and chemical stripper are now much cautiously used based on the amount of hazardous waste they generate (Alkire, 1993). Mechanical means like ultra high pressure water blasting, wheat starch blasting, crystalline ice blasting, bicarbonate blasting, plastic media blasting, CO_2 blasting and cryogenic coating removal system are used in aerospace and automotive industries to remove paint from plastic, fibre glass, graphite, aluminium, concrete and different metal substrates (Alkire, 1993; Graves, 1991; Gardner, 1985; Roberts, 1985; Abbott, 1989). In general all these methods are able to remove coatings without substrate damage and produce minimum waste.

2.2.1 Paint removal from and recycling of plastic bumpers

As bumpers account for 8-10 kg of the total automobile weight, they are targeted for many recycling efforts. But the acrylic and urethane paint coatings on their surface do not melt down with the plastic thus becoming dispersed into the matrix if not removed before or during the recycling process. As mentioned in section 2.2, there are numerous ways of paint removal but all of them are not suitable for plastic parts. For example, sandblasting and sanding are too expensive in terms of time and labour; refrigeration requires expensive equipment and chemical methods such as use of solvents lead to secondary pollution created by the chemicals itself. So attention has been focused on other mechanical means to remove the paint coating and then to recycle the plastic bumper.

Two Tokyo plastic companies claim that they have come up with an entirely mechanical means of removing majority of the coatings from painted PP parts (Moore, 1993). In the process, bumpers are firstly shredded down to small particles and then passed through a cone press. Here the particles are compressed and sheared, weakening the plastic -coating interface. Most of the coating is then removed in a pin mill the final step being extrusion through a screen exchanger and pelletising. The system removes 99.9% paint from PP.

Researchers at Nissan research Centre (NRC), Japan, have developed a recycling process that uses a water based organic salt solution to remove the paint from PP bumpers (Studt, 1993; Asakawa, 1992). The cleaned bumpers are then repelletised and remolded where the recycled PP retains more than 95% of its original physical properties. It was found that the mechanical properties of recycled PP are lowerd more by the presence of paint than by the material deterioration or any other reason. In another method, the bumpers are crushed into small pieces and then fed into a swinging crusher. Here progressively smaller plastic resin chip is produced using vibration mechanism. When the optimum size has been achieved, the resin is

fed into a wind fan which separates the paint particles from recycled resin. The material then pass through a filtering system giving high grade recycled material with extremely low level of contamination (McCartney, 1993).

Miranda *et.al.* (1994) used a continuous pressure, rotary disk filtration system for extrusion melt filtration of regrind PP bumpers contaminated with paint. A section of this rotary filter disk is always exposed to the melt channel and contaminated filter screens can be replaced on the section of the filter wheel outside of their filter blocks, which are held together under tension with pre-loaded studs. This system can be used to filter all thermoplastics to whatever degree of filtration fineness is required. The continuous exposure of the melt to a constant screen surface area assures that a consistent level of melt pressure is maintained (Brunger, 1993; Stott *et al.*, 1986). They concluded that a 100 mesh screen pack was effective in providing good surface finish and high gloss of material.

The Mitsubishi Kasei Corporation of Japan has come up with a chemical stripping technique where the thermoplastic resin (for example PP) having a thermosetting resin coating (for example polyurethane coating) is dipped into a pyrrolidone liquid and the coating film is released from the moulding. The coating film and the moulding resin are separated from each other by using the difference of specific gravity. The separated and recovered moulding is then supplied into an extruder and melt kneaded to be pelletised or moulded into a specified product. The pyrrolidone liquid is also easily recovered since the thermosetting resin may be recovered in the form of solid films. The pyrrolidone liquid has a low toxicity and no corrosive properties for metal.

None of the processes described above tried to analyse the dispersed paint fraction in the matrix which was actually causing the property deterioration. Moreover, researchers were more interested looking into blend systems made from recycled and virgin material.

2.2.1.1 Extrusion melt filtration

In all the above processes melt filtration was used at some stage of the operations to obtain better grade of recycled material. Extrusion melt filtration is a process where molten polymer is forced through a filter medium to remove foreign contaminants where the particle sizes range from about 5 μm to a few millimeters (Brokar, 1993). The basic characteristic of a filter medium is that it must be porous to the fluid phase while impervious to suspended contaminants (Stott *et al.*, 1986). In addition the filter must allow any deliberate additive particles such as anti-oxidants and ultra violet stabilisers to pass. The importance of contaminant holding capacity will depend on the quality of polymer feedstock being used. There are three important types of metallic filter medium: wire mesh, sintered powder and sintered fibre. Wire mesh comes in a square weave or a Dutch twill (woven in parallel diagonal lines). The different filter media do not perform equally with respect to their ability to hold contaminant, capture gel etc. A relative performance comparison is shown in table 2.2.1.

Table 2.2.1 : Performance comparison of different filter media.

	Wire mesh Square weave	Wire mesh Dutch twill	Sintered Powder	Metal Fibres
Gel capture	Poor	Fair	Good	Very good
Contaminant capacity	Fair	Good	Fair	Very good
Permeability	Very good	Poor	Fair	Good

Since the gaps in the woven wire are well defined in dimension, filtration can be performed with high level of confidence (Stott *et al.* 1986). As the mesh has a fair capacity to hold contaminants, its performance can be improved by combining and sintering together several layers of mesh screens. They are arranged in progressively increasing fineness, so that succeeding layers trap increasingly fine contaminate particles thus preventing early blocking of fine layer.

The screen pack is placed before the melt enters the diehead and is mechanically supported by a breaker plate. The breaker plate prevents the screens from rupturing near the holes in the breaker plate and supports the screens adequately even when the pressure increases due to the screens becoming clogged. Proper function of the breaker plate thus depends on the type of screens, flow conditions and on the actual design of the breaker plate. Correctly designed breaker plate, in conjuction with the screens, helps to acheive homogenisation of the melt. Figure 2.2.1 shows the arrangement of a screen pack and the breaker plate in an extruder.

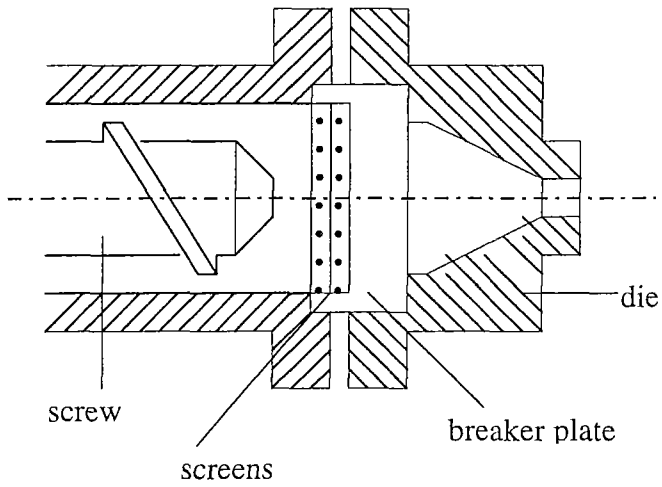

Figure 2.2.1 : Arrangement of a screen pack in an extruder.

Filtration equipment can be divided into three groups depending on different screen pack systems to be used:

(1) screen packs whose screens are changed discontinuously

(2) screen packs whose screens are changed continuously

(3) screen packs whose screens are cleaned by the melt or mechanically.

In case of discontinuous changing of screens, there is an interruption of the melt stream for varying period depending on the system which effects the performance when equipped with strip or strand granulator. It is suitable to use with low contaminated material. In the second type, screen change do not have any significant effect on melt stream with regard to throughput and viscosity (Brunger, 1993). In melt cleaned screen packs, the screens are cleaned by a backflow flushing system whereby some of the melt flow is passed in reverse direction through the dirty screen. There is also provision for mechanical cleaning.

In the present study single and combination of screen packs were used for melt filtration and no effort was made to change the screens during the whole filtration process.

2.3 Image Analysis Applied to Composite Materials

With vast development of composite materials in recent years it is important to have better understanding of their microstructure. Once the structure is established, they can be used to correlate certain physical and mechanical properties of the material. These investigations can be performed easily with automatic image analysis. This technique mainly deals with quantitative measurement and analysis of available information such as size, number, area etc. of an image. In order to perform this task it is necessary to prepare the specimen in a form suitable for this purpose. An image analysis performs in the way a human expert recognises and analyses the structure of a specimen which he examines using a microscope or

macroscope depending on the object size. A modern image analyser consists of a video processing, image processing and control processing units as shown schematically in figure 2.3.1.

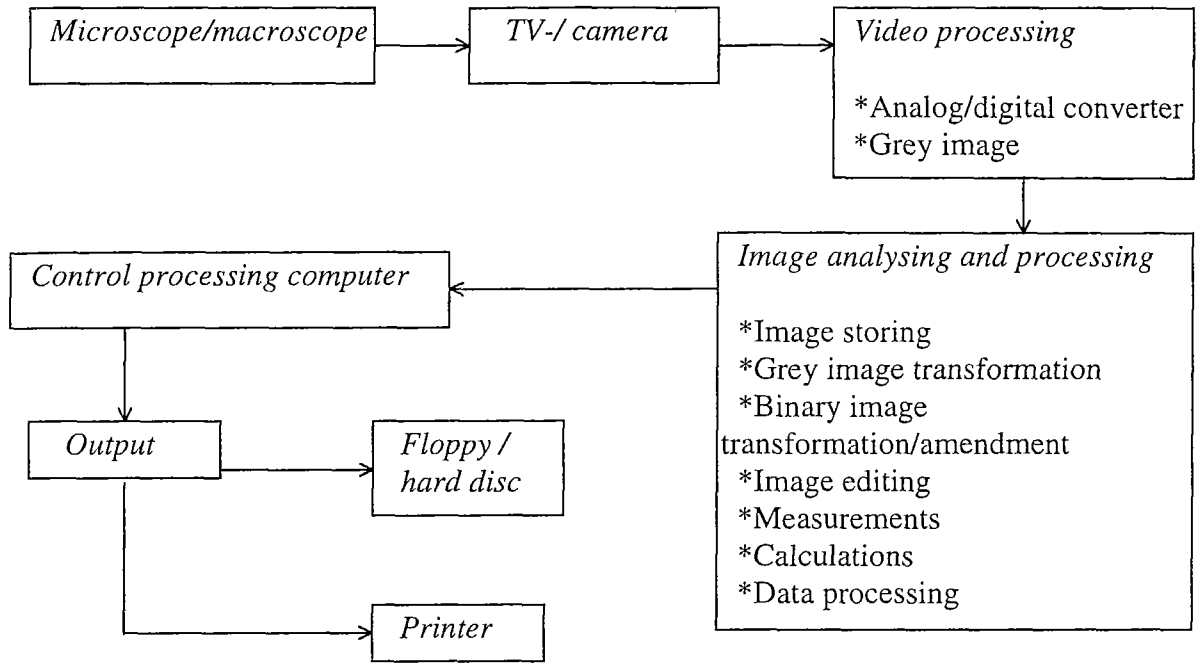

Figure 2.3.1 : Schematic diagram of the image analysing system.

2.3.1 Fundamental background to image analysis

Image analysis falls into the class of mathematical method called stereology. Stereology refers to "reconstruction of the parameters defining a material structure in space from measured values obtained on a section of the structure" (Chan, 1989). For example, volume fraction of inclusions in a material can be evaluated stereologically from the area fraction measured on a section of this material. Volume fraction is one of the most important quantities required in quantitative stereology analysis. There are three main methods available to obtain volume fraction, namely: areal analysis, linear analysis and point counting.

Areal analysis : The areal analysis is described by the principle of Delesse where the volume fraction of a second phase (α-phase) embedded in a structure can be approximated by its areal

fraction obtained in a section. To prove this concept, a cube of volume v_T containing particles of α-phase is considered (Weibel, 1979). The cube is then divided into thin parallel slices of thickness dy and area a_T as shown in figure 2.3.2.

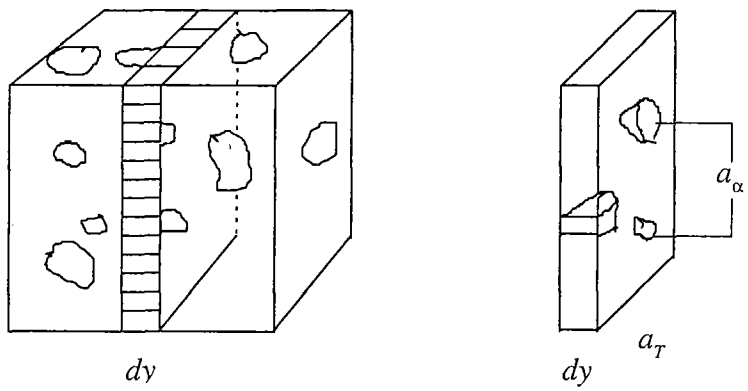

Figure 2.3.2 : Model for deriving the principle of Delesse.

Then for one slice, each volume of particles contained in that slice will be:

$$v_\alpha = a_\alpha \, dy \qquad ...(2.3.1)$$

The total volume of the slice $v_T = a_T \, dy$ ...(2.3.2)

So the volume of the α-phase contained in this cube equals :

$$\sum v_\alpha = dy \sum a_\alpha \qquad ...(2.3.3)$$

and the total volume of the cube is

$$\sum v_T = dy \sum a_T \qquad ...(2.3.4)$$

So the relationship between the volume fraction (V_v) and area fraction (A_A) becomes:

$$V_V = \sum v_\alpha / \sum v_T = dy \sum a_\alpha \, / \, dy \sum a_T = A_\alpha \, / \, A_T = A_A \qquad ...(2.3.5)$$

Linear analysis : To estimate the volume fraction of α-phase by linear analysis, Rosiwal showed that the same area section a_T can be divided into a number of strips of equal width d_1 and length l_T as shown in figure 2.3.3, so the area of this slice a_T equals $\Sigma \, l_T \, d_1$ (Chan, 1989).

Each band will cut the features of particles into numerous intercepts of lengths l_α so that:

$$a_\alpha = d\sum l_\alpha$$

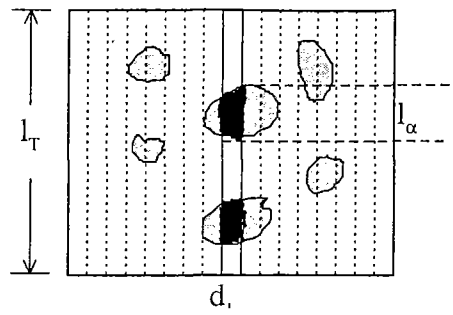

Figure 2.3.3 : Dividing the slice into thin strips.

So the relationship between the area fraction (A_A) and linear fraction (L_L) becomes:

$$A_A = a_\alpha / a_T = d\sum l_\alpha / d_1 \sum l_T = L_L = V_V \qquad ...(2.3.6)$$

Point counting : Principle of Glagolev and Thomson gives the relationship between the volume fraction and point fraction P_P. To demonstrate this a thin slice can be divided into a grid of points. The feature area can then be approximated by points falling within boundaries of the feature as shown in figure 2.3.4 (Chan, 1989). Consequently the following relationship is derived :

$$V_V = A_A = L_L = P_P \qquad ...(2.3.7)$$

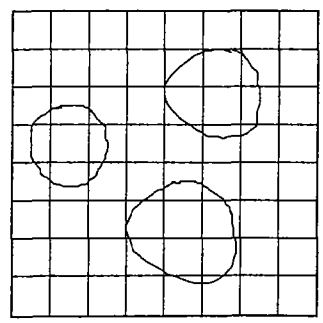

Figure 2.3.4 : Schematic derivation of the principle of Glagolev and Thomson.

Among the three, linear analysis and point counting are preferred for manual measurements, but areal analysis is generally more applicable to automatic image analysis.

2.3.2 Quantitative measurement using image analysis

Digital image analysis is widely used to study the composite materials. It is very powerful in the field of fractography in order to derive quantitative information from the fracture surface and compare this with the morphology of the bulk material in order to determine the mechanism of failure. It has been used to study the particle size and particle size distribution of different phases in polymer blends. Polymer crystallisation kinetics has been examined with it (Long *et al.* 1991, 1992). The technique was applied to determine the anisotropic particle distribution of polystyrene spheres in silicone oil under shear (Husband and Gadala-Maria, 1987). Fibre reinforced composites were also studied where spatial information on fibre distribution is gained in addition to the volume fraction data (Guild and Summerscales, 1993). Herchun and Colton (1994) studied the fibre volume fraction, fibre orientation and fibre distribution in thermoplastic composites using image analysis.

Similar concepts have been used in the present study to determine the volume fraction of the dispersed paint fraction in the rubber toughened PP as no other suitable method was available in the literature. The image acquisition and analysis techniques are described in section 3.2.1. These results can be directly compared with measurements via other methods such as gravimetric measurements.

2.4 Rubber Toughened Polymers

Plastics such as polyethylene (PE), polypropylene (PP), polystyrene (PS) and poly(vinyl chloride) (PVC) make up a large proportion of the total tonnage of polymers currently being

used mainly for consumer products. However, with increasing demand of plastics to be used in areas dominated by metals or ceramics e.g. in automobile industry, new engineering plastics, both thermoplastic and thermoset resins, have been developed providing combinations of lightness and good balance of stiffness and toughness over a wide range of temperature applications. In parallel with development of new polymers, materials are repeatedly modified and improved in the form of alloys and blends by synthesis and compounding to achieve desired properties.

Many plastics, specially glassy polymers, are susceptible to brittle fracture because energy absorbing processes in these operate only in highly localised regions around the crack tip. To increase the toughness it is therefore necessary to ensure that the volume in which the energy dissipating mechanism occurs is sufficiently large while at the same time growth and breakdown of voids and crazes are limited to prevent premature crack initiation. An approach to this is to initiate localised energy absorbing mechanism, such as crazing and shear yielding from many sites, rather than a few isolated ones, so that a much greater volume of polymer is involved. This multiple deformation mechanism has been most successfully achieved by the incorporation of a second phase of dispersed rubbery particles into the polymer matrix. The most well known example of this class of materials are high impact polystyrene (HIPS) and acrylonitrile-butadiene-styrene copolymers (ABS) which possess greatly improved toughness compared to the unmodified PS and styrene-acrylonitrile copolymer respectively. Other plastics which have been toughened using this technology include PVC, poly(methyl methacrylate) (PMMA), PP, polycarbonate (PC), poly(phenylene oxide), nylons and thermosetting resins such as epoxies, polyamide (PA) and polyesters.

The rubber phase intended for rubber toughening must be dispersed as small particles in the polymer matrix. The particle size and size distribution of the dispersed particles will depend

on the miscibility of the two phases and on the way in which they are mixed. If the miscibility is good, the particles of the rubber will be too small to promote toughening. If the two phases are immiscible, the rubber may be dispersed as macroscopic particles, too large to give toughening.

When highly dispersed, the rubbery phase can act as an effective stress concentrator and enhance both crazing and shear yielding in the matrix. A suitable processing condition constitutes one route to the desired size distribution. It has been found that rubber particle size and size distribution decreased with shear rate up to an optimum shear rate beyond which no further morphological variation is observed (Walker and Collyer, 1994). Furthermore, it has been shown that coalescence of the dispersed phase during blending can be prevented if the interfacial tension between the two phases is sufficiently low. Borggreve and Gaymans (1989) found the size distribution of ethylene-propylene-diene-monomer (EPDM) rubber in PA6 improved greatly when maleic anhydride (MA) was used as a coupling agent between the two phases.

Increasing the concentration of the rubber phase increases the impact strength up to a critical concentration level after which a marked decrease is observed. For example, a linear relationship is obtained up to 30% EPDM in PA6 but a decrease is observed in strength with higher rubber loading (Hobbs *et al.*, 1989). Increasing the concentration of the rubber phase also decreases the blend modulus and tensile strength irrespective of whether the matrix is brittle or pseudo-ductile.

The different mechanisms proposed for rubber toughening mainly rely on the dispersion of rubber particles in polymer matrix. These include energy absorption by rubber particles,

debonding at the rubber-matrix interface, matrix crazing, shear yielding and a combination of crazing and shear yielding.

The energy absorption of rubber particles in order to toughen the polymer was first proposed by Merz *et al.* (1956) where it was explained that the stress whitening accompanying elongation of HIPS was associated with the formation of microcracks inside the material. The disadvantage of the proposed theory was concerned primarily with rubber rather than the matrix. So further toughening theories concentrated on the deformation mechanism associated with the matrix, which are enhanced by the presence of rubber phase.

For matrix crazing under a tensile stress, crazes are initiated at points of maximum principal strain, typically near the equator of rubber particles and propagate outwards normal to maximum applied stress. It has been demonstrated experimentally in polymer matrices, which fail by crazing, that the optimum rubber particle size is in the range of 1-5 μm. Donald and Kramer (1982) proposed two criteria necessary for craze initiation from a rubber particle:

(1) the initial elastic stress concentration at the rubber particle must exceed the stress concentration at a static craze tip.

(2) the distance over which this critical stress acts must extend at least three fibril spacings from the particle into the glassy matrix.

The stress field around the particle is independent of particle size but the spatial extent of the stress enhancement scales with the particle diameter. The second criterion therefore explains the inability of small rubber particles to initiate crazes.

Shear yielding in matrix phase also plays a major role in rubber toughening mechanism in polymer blends. This phenomenon not only acts as an energy absorbing process but the shear

bonds also present a barrier to the propagation of crazes and crack growth, therefore delaying fracture of material. Shear yielding mechanism constitutes cavitation of rubber particles followed by extensive shear yielding throughout the matrix. Cavitation is followed by the onset of shear yielding, because on cavitation of the rubber particles the buildup of hydrostatic tension is locally relieved, lowering the yield stress. After cavitation the triaxial stresses disappear and the matrix behaves as if it were under plane stress conditions.

Shear yielding and crazing may occur simultaneously in many rubber toughened plastics. The dominant mechanism is the one by which the unmodified matrix would typically fail. However, the contribution of each mechanism to the toughening of the system depends on a number of variables such as the rubber particle size and dispersion, the concentration of the rubber particles and the rate and temperature of the test.

Though binary blends of polymer/elastomer show an improved fracture toughness and impact strength, the stiffness drops with rubber inclusions as stated before. To overcome this situation, ternary composites consisting of polymer filled with rigid inorganic particles and elastomer inclusions can be designed to obtain both stiffer and tougher composite than the neat polymer. One of the polymers that is vastly used as the basis of ternary composites is PP and the muticomponent blends made from it are widely used in automotives, home appliances, mass transportation vehicles and construction industries. Fillers used in these blends are mainly talc, calcium carbonate ($CaCO_3$) and magnesium hydroxide ($Mg(OH)_2$). Mechanical properties of these systems will depend on composition as well as on phase morphology. Phase morphology on the other hand depends on mixing conditions, rheology, surface energies of the constituents and filler geometry. Addition of coupling agent such as maleic anhydride to either PP or elastomers would give rise to different microstructure as the adhesion between filler and PP or elastomer would change. Change in morphology would

then eventually modify the properties of the system. Unlike the case of toughening binary blends, where the primary variables controlling the fracture resistance are elastomer volume fraction and the size and distribution of elastomer inclusions, the toughness of ternary blends is extremely sensitive to the relative spatial arrangement of elastomer and filler inclusions (Jancar and Dibenedetto, 1995).

In the present study, the virgin material used for bumper bar was a ternary composite with PP as the base polymer. This PP is toughened with rubber for improved impact strength specially at low temperature and filled with reinforcing talc filler for improved stiffness.

2.5 Rheology of Polymer Composites

Rheology is the science of deformation and flow of materials. There are three major objectives for rheological work of polymers (Folkes and Hope, 1993):

(a) to develop fundamental understanding of material flow behaviour in order to develop rheological equation of state

(b) to use simple investigations to find relationship with processing conditions so that processing and properties of polymer materials can be governed and predicted

(c) to study rheological properties relating polymer structure and properties in order to use these data for further characterisation such as average molecular weight, determination of branching in polymer etc.

Polymer based multiphase mixtures are categorised as alloys, blends and composites. A mixture of two or more polymers together results in polymer blends or alloys whereas polymer composites are suspension of particles of various shapes in a polymeric fluid. From detailed rheological study it is apparent that processing can provide a wide range of blend

microstructure. From the processing-structure-property correlation it is possible to overcome various processing problems in industries.

The shear viscosity of polymers can be measured under steady or oscillatory conditions. The steady shear viscosity explains the material behaviour under changing shear rate where it has passed a deformation stage. Under oscillatory shear properties the shear loss modulus measures the melt viscosity and the shear storage modulus measures the melt elasticity.

2.5.1 Steady shear viscosity

The rheological behaviour of suspensions has been a subject of research for many works and the flow behaviour has been reviewed by authors such as Han (1976), Metzner (1985), Kamal and Mutel (1985), Utracki (1988). The variables that have major influence on rheology include concentration of particles, particle size and particle size distribution, particle geometry, particle-particle and particle-fluid interaction. In general these effects can be distinguished as hydrodynamic and colloidal stability effects. Hydrodynamic effect arises from the presence and motion of particles in the flowing medium resulting in an increase in viscous energy dissipation. Colloidal stability effects are determined by the physiochemical and surface forces of colloidal origins which lead to interparticle interactions and modifications of the suspension rheology.

2.5.1.1 Effect of particle concentration

Concentration of filler is one of the most important factors controlling the melt viscosity of filled polymer composites. The usual phenomenon is the increase in viscosity with increasing filler concentration specially at lower shear rates. The flow curves tend to approach the curve of virgin polymer at high shear rates. But anomaly from this observation has been reviewed

by Fisa and Utracki (1984) where it was reported that the viscosity of silane treated mica filled PP and titanate treated calcium carbonate filled PE drops below the unfilled polymer at a shear rate greater than 1 s^{-1}. The effect was explained by improved filler dispersion, inter layer slip phenomena and shear degradation caused by the filler coupling agent. The introduction of a modifier decreases the melt viscosity of composite as formation of chemical bond between filler and polymer matrix is possible. This effect changes the hydrodynamic situation around filler particle and hence the total dissipation losses. On the other hand, Kitano *et al.* (1980) observed that for $CaCO_3$ filled LDPE and PP, the matrix does not influence the relative viscosity for untreated filler and viscosity increases with filler concentration.

A mathematical correlation was first proposed by Einstein (1911) to relate the concentration of filler with viscosity for Newtonian fluids as :

$$\eta_r = 1 + 2.5\varphi \qquad ...(2.5.1)$$

where : η_r relative viscosity (ratio of suspension viscosity to matrix viscosity)

φ concentration of filler.

This model is valid only for very low concentration of spherical fillers ($\varphi < 0.01$) where the interparticle distance is large enough to neglect particle interaction. Later Batchelor (1977) developed a model where particle-particle interaction was taken into account for dilute suspensions. His derivation was based on analysis of thermodynamic forces on particles and their effect on the bulk stress of the suspension. The numerical equation is as follows:

$$\eta_r = 1 + 2.5\varphi + 6.2\varphi^2 \qquad ...(2.5.2)$$

With increasing concentration of particles in suspensions, particle-particle interaction becomes significant and relative viscosity (ratio of viscosity of suspension to matrix) versus concentration relationship becomes non-linear which can be expressed by higher order terms

of filler concentration. Guth and Simha (1936) first proposed a relation relating particle-particle interaction as:

$$\eta_r = 1 + 2.5\varphi + 14.1\varphi^2 \qquad ...(2.5.3)$$

Kamal and Mutel (1985) reviewed correlations developed for concentrated suspensions and reported the following equation:

$$\eta_r = 1 + 2.5\varphi + 11\varphi^5 - 11.5\varphi^7 \qquad ...(2.5.4)$$

Higher order terms of φ becomes important in a situation of particle rotation and particle-particle interlocking. For dilute suspensions φ approaches zero and so equation (2.5.4) reduces to Einstein's equation (2.5.1).

Maron and Pierce (1956) developed an equation (2.5.5) which consists of theoretical and empirical components, for dilute latex particles in water. The model based on molecular parameters of the theory as a function of temperature, concentration and entropy of activation for the flow of latex particles.

$$\eta_r = \frac{1}{(1-\theta\varphi)^2} + \frac{A''\theta^2\varphi^2}{(1-\theta\varphi)^3} \qquad ...(2.5.5)$$

where θ is equal to 1.35 and A'' is a constant depending on suspension.

However, all these models disregarded parameters such as particle size, size distribution and particle shape which also affect the rheological behaviour. Therefore, to account for all these factors a parameter named maximum packing fraction (φ_m) was introduced which was defined as the maximum available volume fraction occupied by the filler. This φ_m can be calculated theoretically for different types of packing or be estimated experimentally using for example the sedimentation technique. At φ_m, there is insufficient fluid to lubricate the relative motion

of particles. Consequently, the suspension behaves as a solid substance rather than as a liquid and viscosity rises to infinity. For non-spherical particles, φ_m is less than suspensions filled with spherical particles (Kitano, 1981) and φ_m increases with increase in particle size and particle size distribution for a filled system (Baloch, 1989).

Mooney (1951) developed the semi empirical equation for viscosity of suspension where the maximum packing fraction φ_m was introduced :

$$\ln \eta_r = \frac{2.5\varphi}{1 - \frac{\varphi}{\varphi_m}} \qquad ...(2.5.6)$$

This equation was reported to be a good correlation to describe the viscosity variation of many kinds of suspensions over the entire concentration range. For example, Kataoka *et al.*(1978) reported that Mooney equation can predict relative viscosity of glass bead filled PE in the concentration range tested.

Many other mathematical models have been reported for concentrated suspensions to predict the relative viscosity as a function of concentration of particles. Most of these models are based on the assumption of uniform distribution of dispersed phase. Chong *et al.*(1971) based his prediction on many experimental results for mono and bidispersed systems and proposed a model (equation 2.5.7) with two constants which characterise particle size distribution of spherical particles in suspensions and can be determined experimentally without measuring the viscosity.

$$\eta_r = \left(1 + A\frac{\varphi / \varphi_m}{1 - (\varphi / \varphi_m)}\right)^B \qquad ...(2.5.7)$$

where, A = 0.75

B = 2

and φ_m = 0.605 for glass bead filled polyisobutylane matrix.

Quemada (1977) proposed the following model relating η_r with φ where optimisation of viscous energy dissipation principle was adopted.

$$\eta_r = \left(1 - \frac{\varphi}{\varphi_m}\right)^{-2} \qquad ...(2.5.8)$$

This model was found to be an excellent fit for Polinski *et al.*'s (1988) study on glass spheres in polybutene matrix and Van der Warff and Kruif's (1989) study on silicon particles suspended in cyclohexane.

The literature does not reveal any empirical model for concentrated suspension of irregular shaped particles excepting that proposed by Kitano *et al.*(1981) which was based on Maron-Pierce model. Many investigators found that models developed for spherical particles can effectively be applied to predict the viscosity of suspension with irregularly shaped particles provided φ_m and other shape dependent parameters are known (Ferrini *et al.*, 1979; Kitano *et al.*, 1980; Shouche *et al.*, 1994).

Increasing filler concentration also changes the rheological behaviour of composites. Non-Newtonian behaviour occurs at particle $\varphi > 0.25$ even if the particles are spherical and monodispersed. Typical behaviour includes shear thinning at intermediate concentration (φ = 0.25- 0.5) and shear thickening at high concentration ($\varphi > 0.5$). So equations which do not include shear rate factor, do not hold of suspensions showing a marked shear rate dependency on viscosity.

2.5.1.2 Effect of particle size and particle size distribution

The effect of particle size on viscosity may be difficult to determine as parameters like particle shape which characterises the system, may vary with particle size. In general, for small particles, the particle size and surface area have a direct effect on Van der Waal, electrostatic and Brownian forces in a suspension. These forces lead to an aggregation of particles which has to compete with hydrodynamic forces to break the aggregation. The effect of restoring forces is larger for small particles with high surface area. As a result, higher viscosity values were observed with aggregation of particles, when compared with larger particle filled suspensions. Tsai *et al.* (1992) studied the particle size effect on suspension viscosity of glass beads with mean diameter of 17 and 45 μm in silicon-oil-ethylene glycol and revealed no significant effect on relative viscosity of a concentrated Newtonian suspension. Bhattacharya *et al.* (1994) studied the transport properties of coarse particles of coal, ballotini and SAN in fine clay suspension and observed anomalous particle size effect in that there was increase in viscosity with increasing particle size over certain particle size range. However, variation of viscosity due to varying coarse particle size did not show any trend. They concluded that the unusual behaviour was due to the interaction between the clay flocs and coarse particles. Others explained that increased particle interaction and formation of aggregates of flocs immobilise the fluid between fillers thus increasing the effective volumetric concentration for larger particles. Pukanszky *et al.* (1985) observed that this was true for $CaCO_3$ (in the range of 78 - 0.8 μm) filled PP. Conversely talc (2-12.5 μm) filled PP showed no significant effect on viscosity. Poslinski *et al.* (1988) observed minimal effect on viscosity with variation of particle size with solid concentration less than 20% (v/v). Pukanszky *et al.* (1985) and Mayadunne (1993) suggested that at smaller shear rates decreasing particle size generally increases the composite viscosity as specific surface area of filler increases.

The particle size distribution influences the void fraction and therefore the maximum packing of the filler. In polydisperse systems closer packing of particles compared to monodisperse systems increases the φ_m and reduces the relative viscosity at a fixed volume fraction of particles. The reduction achieved depends on concentration and ratio of large particle size to small particle size. In practice bimodal mixtures produce the most significant reduction in viscosity (Chong *et al.* 1971, Poslinski *et al.*, 1988). Chong *et al.* showed a reduction of relative viscosity from 250 to 40 for 60% volume concentrated suspension. In this case the particle size ratio was 0.371 to 1. The bimodal particle size distribution effect on viscosity of colloidal dispersions was reported by Hoffman (1992). At solid concentration in between 50 and 70%, the bimodal size distribution of particles was reported to enhance the flow properties by reducing the viscosity of dispersion. The minimum viscosity was observed for the size ration of 0.14 to 1 with 80% volume of large particles in total solid volume. However, the effect of particle size distribution is only significant in more concentrated suspensions ($\varphi > 0.4$) and in systems with large variation in particle sizes (Rutgers, 1962; Eveson, 1959). A major change in φ_m is achieved by using a wide particle size distribution.

Interaction between matrix and dispersed fillers influences both properties and usefulness of composites. Utracki and Fisa (1982) proposed that particles tend to aggregate in composites as the filler-filler interactions are stronger than polymer-filler interaction. The aggregation of particles has significant effect on suspension viscosity. An aggregate can be considered as a large particle where the interior is filled with immobilised polymer liquid. Therefore the effective particle size of the suspension increases with aggregation reducing the maximum packing fraction and hence increasing suspension viscosity. The investigation of Kao *et al.* (1975) with treated and untreated glass beads in non polar polybutadiene and polar glycerol explained the interaction effect of particle and polymer on suspension flow behaviour. They showed that surface treatment produces low energy surfaces hence reducing relative viscosity

of concentrated suspensions as long as the particles are properly wet by liquid to avoid agglomeration. However, high polar liquid have higher energy surface thus influencing particles to aggregate.

2.5.1.3 Effect of particle geometry

Composite viscosity is higher for non-spherical particles compared to spherical particles at the same volume fraction. This happens as anisometric particles rotate in the shear field, producing greater perturbation and energy dissipation than those caused by spheres of same volume. Many researchers (Batchelor, 1970; Clarke, 1967; Kitano *et al.*,1981) worked on fillers with varying shapes and aspect ratios and showed that as the geometry deviates further from spherical shape, the concentration at which the viscosity starts to increase becomes markedly smaller. Maximum packing fraction was reported to be decreased with increasing aspect ratio of particles. As a result, high viscosity was observed with increasing aspect ratio even for very low concentrated suspensions.

Clarke (1967) investigated the viscosity of different shaped particles in water at different concentrations. His study showed that the suspensions of spheres and grains have much lower viscosity compared to suspensions of plates and rods. Kitano *et al.* (1981) suggested an empirical equation (equation 2.5.9) to predict relative viscosity of various organic fillers such as glass fibre, carbon fibre, talc, $CaCO_3$ and glass sphere filled polymer composites:

$$\eta_r = \left(1 - \frac{\varphi}{F}\right)^{-2} \qquad ...(2.5.9)$$

The constant F was 0.68 for glass spheres and 0.44 for $CaCO_3$ implying that glass sphere filled composites had lower viscosity. Tsai *et al.*(1992) studied the effect of irregular shaped silica sand and coal particles and spherical glass beads and polystyrene spheres on viscosity of suspensions. They found a high viscosity and small φ_m for irregular particles.

Mayadunne *et al.* (1996) investigated the dependency of rheological properties of highly concentrated polymeric composites on temperature, filler conncentration, filler size and size distribution. Their study showed that upon addition of ground rubber tyre (GRT) particles to LDPE matrix, a significant increase in viscosity was observed for the composites over the unfilled matrix but the estimated maximum packing fraction for three different sizes of GRT particles didnot show the usual trend of decreased φ_m with decreasing particle size for monodispersed systems. They concluded from the particle size analysis that the wider distribution of 45-63 μm particles was more likely a polydispersed sample than a monodispersed one. In polydispersed systems very small particles can migrate into interstices formed by large particles and reduce the void spaces. This broader distribution of particles with better packing can increase the φ_m even for irregurlarly shaped particles. This clearly indicates that size distribution plays a vital role in controlling φ_m and hence the composition viscosity.

Shapes of particles also effect the rheological behaviour through particle orientation and interaction. For example, elongated particles can form structure even in dilute solution to produce characteristics like thixotropy, shear thinning or viscoplasticity. Barne's (1989) review on shear thickening suspensions explain that more irregular particles tend to produce shear thickening more readily even at low concentration.

2.5.1.4 Effect of temperature

Effect of temperature on viscosity of suspensions has been studied by many authors. Viscosity of composites usually decreases with increasing temperature and the variation is often expressed by the Arrhenius equation over limited temperature range as :

$$\eta = A \exp(E' / RT) \qquad ...(2.5.10)$$

where A is a constant

R is gas constant (kJ/mol.K)

E' is activation energy (kJ/mol)

T is the temperature (K)

The reduction in viscosity with increase in temperature is mainly due to the rapid decrease in viscosity of the matrix phase and overall change in volume fraction of suspensions. But anomalous behaviour has been observed as well for various concentrated suspensions when increase in viscosity is observed within certain temperature regions (Le, 1991; Barro and Bhattacharya, 1980; Cohen and Richon, 1986; Lee *et al.* 1981). Viscosity of these suspensions decreased initially with increasing temperature and then suddenly increased with temperature.

In general, A and E' depend on the concentration of the dispersed phase and on molecular weight of the polymer. The variation of viscosity of polymer melts is given by the equation :

$$\frac{\Delta\eta}{\eta} = -\frac{E'}{RT^2}\Delta T \qquad ...(2.5.11)$$

Now considering $E' = 10^5$ J/mol and $T = 400$ K, we get

$(E'/RT) = 25$ and $(\Delta\eta/\eta) = 25\ (\Delta T/T)$

Therefore a 1% error in the temperature measurement could lead to a 25% error in the viscosity values.

The shape of viscosity - shear rate plots is hardly affected by temperature. The similarity accounts for the possibility of combining data, obtained at different temperatures, into a single master curve at an arbitrary reference temperature. Therefore, measuring the viscosity over 2 or 3 decades of shear rate at several temperatures and combining the results into a master curve, yields a viscosity shear rate plot which could span between say 5 and 10 decades of shear rate.

2.5.2 Oscillatory shear properties

Oscillatory shear property measurement is one of the tests carried out while performing dynamic testing. Here the sample is subjected to a sinusoidal stress or strain in wave form and effect of the wave on sample (i.e. its response) is measured. The stress signal generated can be divided into an elastic and viscous stress. The elastic stress measures the material elasticity and termed as storage modulus (G') and the viscous stress measures the viscosity and is termed as the loss modulus (G''). Complex modulus (G^*) is a measure of the materials overall resistance to deformation and can be obtained from the ratio between the storage and loss moduli.

The limit of viscoelasticity plays an important role in the oscillatory measurements as it has been found that G' and G'' are dependent on strain even at a rather small strain and are independent of strain up to a critical strain level. The physical explanation lies in the structure formed by the filler, which undergoes brittle failure at small deformation resulting in decreased linearity of composite material. So determination of the linear region is important before starting any test as it is only up to this limit the dynamic moduli and dynamic viscosity are independent of deformation.

2.5.2.1 Effect of particle concentration

As for steady shear viscosity, the oscillatory measurements are also influenced by different parameters such as filler concentration, filler size and size distribution, filler shape etc. for a dispersed system. Generally it is observed that that G' and G'' increase with increasing volume fraction as observed for glass bead and $CaCO_3$ filled LDPE (Munstedt, 1976), glass microsphere filled PS matrix (Mills, 1971), kaolin dispersed LDPE (Mills, 1971), carbon black filled PS (Lobe and White, 1979) just to name a few.

Mills (1971) observed storage and loss moduli plateau for 3 vol% kaolin (0.1-10 μm) filled LDPE at low frequency (0.05 s^{-1}) which was not evident at higher frequencies. This was explained by some filler "structure" formed at lower frequency region. The phenomena was not observed for glass bead (130 μm) filled LDPE. In contrast, for very dilute suspension (0.05 vol%) of silica (~ 4 μm) filled LDPE, both the moduli values were found to be very sensitive of frequency and increased by a factor of 2 at lower frequency. With increasing volume fraction (2 vol%), the behaviour changed and become frequency independent as frequency approached zero. Mills explained the situation by describing it as a characteristic of a very weak network in the composite containing sub-micron particles.

Bigg (1982) reported that for spheres, particle-particle interactions are not observed below concentration level of 10%. The particle geometry and degree of adhesion between filler and matrix also influenced the concentration at which interaction occur. With strong adhere between filler and polymer, force transmit from particle to particle directly through polymer molecules. With increased filler fraction, the close proximity of particles may hinder the response of neighbouring particles, thus hindering the interaction. Also for higher concentration, particles become as a "network" thus cannot move freely with respect to its neighbours.

Faulkner and Schmidt (1977) investigated the glass bead filled PP matrix and found that increasing filler fraction increased moduli values. The increase is storage modulus means that the filler allowed the polymer to store more energy elastically and increase in loss modulus means filler enables the polymer to dissipate more mechanical energy. This observation was consistent with Mills results (1971) for glass filled PS. In general, the relative storage modulus and relative loss modulus show that force required to overcome the viscous and

elastic deformation increases with the loading of filler but the viscous effect as measured by the loss modulus is greater. In other words, comparative importance of elastic force decreases with increase in filler concentration.

Composites filled with fibrous filler show an exception from this behaviour (Kitano *et al.* 1984). Kitano investigated flexible fibre and rigid fibre reinforced PE and suggested that the effect of fibre addition on storage and loss moduli was larger than observed for spherical particles. The difference was thought to be associated with a change in flow mechanism. The fibres reinforce the polymer network which stores more energy elastically and also dissipates more energy. So comparative importance of the viscous force decreases as the fibre fraction increases.

Bretas and Powell (1985) investigated the rheological properties of LDPE and PVC filled with glass beads where the filler was pretreated with silane and titanate coupling agents to observe the effect of chemical modification of filler on matrix properties. They concluded that glass beads increased the energy dissipated due to particle-particle friction or shear rate in gaps between particles. The addition of coupling agents further increased the dynamic viscosity as the entangled network was not completely disrupted for low strains used in linear viscoelastic region. It should be kept in mind that often an interfacial modification may promote opposing influence on composite properties. As for example, coupling agent added to a filled polymer may couple the filler to the polymer increasing viscous response of melt and at the same time may increase the dispersion of particles in matrix tending to reduce the viscous response.

2.5.2.2 Effect of particle size and particle size distribution

The effect of particle size on storage and loss moduli is not simple. An increase in the moduli values with decreasing particle size at a fixed volume fraction was observed for particle size

ranging from sub-micron level to around 100 mm. But anomaly in this behaviour was also observed as Li and Masuda (1990) investigated $CaCO_3$ filled PP with particle size 0-15 μm and 4 mm and observed that for low concentrations (< 20%), the loss and storage moduli were almost the same. This indicated that the effect of oscillatory behaviour on particle size is minimal for dilute suspensions. But the behaviour was different at higher concentration, which was attributed to the different dispersions of particles in each phase.

Munstedt (1976) observed increase in moduli values for $CaCO_3$ (0.15 μm) filled LDPE compared to larger sized glass beads (60 μm) filled LDPE and concluded that increasing specific surface area with smaller particle size results in an increase in moduli values. But it was not confirmed from this study that it was the particle size and not the different filler-polymer interaction influencing the result. This investigation of Gandhi and Solovey (1988) was more constructive to explain the phenomena of surface area and moduli relation. They studied the carbon black filled PS and poly(butyl methacrylate) and established that the higher surface area of the filler increases the storage and loss moduli over unfilled polymer and composites filled with lower surface area filler.

Kambe and Tanako (1963) investigated glass bead filled LDPE where the particle size ranged from 25.6 - 92.2 μm. For concentration level upto 60 vol%, the concentration dependence of storage modulus resembled that of dynamic viscosity. But for finer particles, as for $CaCO_3$ (2.9 μm) and barium sulfate (0.082 and 0.311 μm), dynamic viscosity and storage modulus increase with filler concentration with a sudden increase beyond a critical concentration level. No such critical concentration was observed in glass bead system for 0-60 vol% level which was explained as critical concentration depend on particle size and effect of filler on oscillatory shear properties.

Papadopoulos (1995) investigated glass microsphere (25.5-75.6 μm) and rubber crumb (70.4-121.9 μm) filled LDPE in the concentration range of 10-40 vol%. For increase in concentration of glass beads and increase in moduli values were reported specially at low frequency. Rubber crumb filled systems behaved quite differently compared to this. For low rubber crumb (< 20%) concentration, moduli was below the unfilled matrix value. A critical concentration level was attained at 27% where filled composites displayed equivalent moduli compared to the unfilled matrix before an increase in moduli values were obtained at higher concentration. The peculiar behaviour at lower concentration level was attributed to the slip phenomenon and presence of talc particles in the rubber crumb.

Dynamic properties are more influenced by particle size distribution than particle size of the filler. Polydispersed systems tend to reduce the viscous response of filled systems at a fixed loading level. Poslinski *et al.* (1988) worked on bimodal system of glass spheres in polybutene polymer and concluded that dynamic viscosity and storage modulus were reduced for bimodal system in comparison to the unimodal system. As in these cases the maximum packing fraction of filler increases, it is possible to achieve higher processable suspension concentration by reducing the viscosity and moduli of the suspensions at a fixed concentration.

2.5.2.3 Effect of particle geometry

Kambe and Takano (1963) reported that particle shape effects concentration dependence of oscillatory properties but did not provide any experimental data to support their conclusion. The three different fillers used in their work were approximately spherical in shape. Bigg (1982) concluded that the concentration at which particle-particle interaction becomes important is lowered as the complexity of the filler particle geometry increases. Kitano *et al.*

(1984) reported that G' and G'' increased with increasing aspect ratio for a given filler concentration.

2.5.3 Rheological properties of paint dispersed talc filled rubber toughened PP

Experimental data are available for neat PP and binary mixtures of PP/rubber blends and PP/talc composites. But as for this work commercial grade bumper material and model systems corresponding to the same were examined. Here the base polymer was PP which was toughened with rubber and had dispersed talc particles as reinforcing filler. As the main objective of the work was to evaluate the effect of dispersed paint particles in the recycled bumper material those systems were also studied. Very little work has been published on the rheological properties of paint dispersed talc filled rubber toughened PP. Miranda *et al.* (1994) investigated the effect of melt filtration on the recyclability of painted bumper material. The data generated from their tests showed that viscosity of 100% recycled material were somewhat higher at low shear rate region (10 ~ 38 s^{-1}) compared to the virgin rubber modified PP and blends of recycled and virgin material showed viscosity values in between. They claimed that the paint particles acted as fillers thus increasing the viscosity. Also as the mesh number was increased (finer mesh), the melt viscosity decreased with filtration since more paint particles were filtered effectively and particle size was lowered. But the paint fraction or the particle size and size distribution of paint particles were not measured so the above conclusions were drawn only from visual observations.

Long *et al.* (1995) worked on pure PP and three component recycled PP bumpers (PP/rubber/talc) and showed the effect of time recycled on the zero shear viscosity and molar mass distribution. They found that the zero shear viscosity decreased and molar mass

distribution increased with increasing time of recycle. These results were used later to explain the decrease in impact strength with times recycled. But again no detailed examination was carried on dispersed paint particle phase and their effect on viscosity.

2.6 Mechanical Properties of Composite Materials

Mechanical behaviour of composite materials depends not only on component properties, their miscibility and processing conditions but also on the size, shape and agglomeration of the dispersed phase and on the degree of adhesion between the filler and the matrix. The separate contributions of the different components to the overall mechanical properties sometimes complicate the analysis. The complications arise from factors such as uncertainties in filler size distribution, void formation during fabrication and imperfect adhesion between filler and matrix. Nevertheless, theories to describe the mechanical properties of particulate systems have been developed, with often one theory applying to one situation better than another. In the following sections theories for tensile properties and fracture mechanics for composite materials will be discussed together with methods of impact testing and toughening mechanism of these systems.

2.6.1 Tensile properties

2.6.1.1 Tensile strength

Theories for tensile strength of filled systems are not widely developed, however extensive work has been done by Nielsen (1966, 1967) and Leinder (Leinder and Woodhams, 1974: a,b). There are in general two main approaches in relating the strength and the filler content of the composites. Sahu and Broutman (1972) assumed that composite fails when one element is fractured as a result of stress concentration around the filler particle. It follows from this assumption that the composite strength should decrease rapidly with the first addition of filler

and then remain essentially the same with further additions of filler. They used a finite element analysis to model the composite and correlated the results with the experimental strengths of a glass sphere filled thermosetting resin. The theoretical predictions did not give good fit to the experimental results because the model neglected particle interactions. In addition the composite may not have failed as a result of the failure of the first element (Ahmed and Jones, 1990).

In the second approach it is assumed that the strength of a particulate composite is determined by the effective available area of load bearing matrix due to the presence of filler (Nielsen, 1966; Nicolais and Narkis, 1971; Nicolais and Drioli, 1973; Nicolais, 1975; Nicolais and Nicodemo, 1975). The most common expressions of composition dependence of tensile stress of two phase systems are based on the first power law (equation 2.6.1) and the two-third power law (equation 2.6.2) and expressed as :

$$\sigma_c = \sigma_m(1-\varphi) \qquad ...(2.6.1)$$

$$\sigma_c = \sigma_m(1-\varphi^{2/3}) \qquad ...(2.6.2)$$

where σ_c and σ_m are the ultimate tensile strength of the composite and the matrix and φ is the volume fraction of the filler respectively. The area fraction of the dispersed phase (inclusion or filler) depends on the volume fraction to the first power when the fracture surface can pass through the matrix for a considerable distance without intersecting a phase boundary. On the other hand, if the fracture line passes through the weak interface of the two-phase boundary, then the area fraction will depend on the volume fraction to the two-third power. These interpretations are expected to be applicable only to spherical inclusions at low concentrations (Kunori and Geil, 1980). For inclusions with different shapes and concentration levels greater than 10-20%, the anisotropy of shape and interacting stress fields need to be considered.

Nielsen (1966) proposed that for no adhesion between filler and matrix the tensile strength of the composite materials consisting of matrix with spherical inclusions can be presented as:

$$\sigma_c = \sigma_m\left(1-\varphi^{2/3}\right)S \qquad ...(2.6.3)$$

where the parameter S describes weakness in the structure created through stress concentration at the filler matrix interface. Unity in the value of S means no stress concentration effect, whereas lower the value of S greater the stress concentration effect or poorer the adhesion.

Nicolais and Narkis (1971) studied the styrene-acrylonitrile (SAN) / glass bead composites and proposed a model for no adhesion blend systems where they considered a cubic matrix with uniform dispersed spherical particles and suggested the strength equation as :

$$\sigma_c = \sigma_m\left(1-1.21\varphi^{2/3}\right) \qquad ...(2.6.4)$$

This equation can be presented in a more general form as :

$$\sigma_c = \sigma_m\left(1-K_2\varphi^{2/3}\right) \qquad ...(2.6.5)$$

where K_2 is the weightage factor describing the adhesion quality between the matrix and the inclusion and depends on the details of the model. For example, K_2 = 1.1 represents dense hexagonal packing in the plane of highest density, K_2 = 1.21 describes the case of poor adhesion with spherical inclusions for the minimum cross section between spherical beads (Nicolais and Narkis, 1971), and K_2 = 1 stands for strain consideration (Nielsen, 1966). In general lower values of K_2 below 1.21 means better adhesion (Maiti and Sharma, 1992).

Another way of representing the behaviour of poor adhesion type blend is to consider the two phase system as a matrix with pores or voids. The dispersed phase is the material filling the voids which do not play a direct role in influencing mechanical properties of the composite due to poor adhesion at the interface. This type of explanation is widely used in metallurgy to correlate the tensile strength of sintered porous metals and ceramics with their porosity

(Passmore *et al.* 1965). Nielsen (1967) and Kunori and Geil (1980) suggested the applicability of this porosity concept to polymer matrix when voids or holes are incorporated in the system and proposed the equation :

$$\sigma_c = \sigma_m \exp(-k\varphi) \qquad ...(2.6.6)$$

where the total porosity was replaced with volume fraction of dispersed phase. Here k is a constant describing stress concentration; the higher the value of k, the higher the stress concentration.

Piggott and Leidner (1974) argued that the uniform filler arrangement assumed in most models was unlikely in practice and proposed an empirical relationship :

$$\sigma_c = A'\sigma_m - B'\varphi \qquad ...(2.6.7)$$

where the parameter A' represents the weakness of the structure due to the stress concentration effect and B' is a constant dependent on matrix-filler adhesion and takes into account the volume fraction proportionality of the strength. Looking back to the previous equations, it is seen that in equation (2.6.3) the parameter S plays the role of both the parameters, A' and B', while in equation (2.6.4) the constant 1.21 is operative only on volume fraction term (Gupta and Purwar, 1984).

2.6.1.2 Elongation at break

Elongation (ε) of a specimen is defined as the change in initial (L_0) and final (L_F) length so:

$$\varepsilon = \frac{L_F - L_0}{L_F} \qquad ...(2.6.8)$$

Assuming perfect adhesion between filler and matrix, Nielsen (1966) predicted a model for the strain at break as :

$$\varepsilon_c = \varepsilon_m (1 - \varphi^{1/3}) \qquad ...(2.6.9)$$

where, ε_c and ε_m are the composite and matrix elongation respectively. It was observed that the deleterious effect of filler on elongation was relatively greater at low filler level as long as adhesion was maintained and aggregation was absent. Mitsuishi *et al.* (1985) studied the calcium carbonate filled PP system and found that the strain at break was sensitive to filler size when plotted against filler area fraction, $\varphi^{2/3}$. Smaller filler size was more sensitive to strain. They suggested a model to estimate the effect of filler polymer interaction as :

$$\varepsilon_c = \varepsilon_m (1 - K_1 \varphi^{2/3}) \qquad ...(2.6.10)$$

where, K_1 is a constant depending on the filler size and modification of filler.

2.6.1.3 Young's modulus

A polymeric matrix is strengthened or stiffened by a particulate second phase in a very complex manner. The particles appear to restrict the mobility and deformability of the matrix by introducing a mechanical restraint. The behaviour of the composite depends on the properties of both the filler and the matrix, the degree of adhesion between the filler and the matrix and also on the size, shape and state of agglomeration of the filler. The modulus of a polymer containing rigid particulate filler is generally increased, even if the filler does not interact strongly with the matrix. Lamellar or fibrous fillers raise the modulus to a greater extent than do spherical fillers.

The elastic modulus of a composite can be estimated if the elastic properties of the matrix phase, the particulate phase and the volume fraction of the particulate phase are known. In general, the particulate phase either increases or decreases the modulus of the matrix depending on whether the particulate modulus is either higher or lower than that of the matrix modulus, respectively.

As a first approach, two bounds have been predicted by Paul (1960) for the composite elastic modulus (E_c) :

upper bound $$E_c = E_p\varphi + (1-\varphi)E_m$$ (case of equal strain) (2.6.11)

and,

lower bound $$E_c = \frac{E_p E_m}{E_p(1-\varphi) + E_m\varphi}$$ (case of equal stress) (2.6.12)

where, φ is the volume fraction of the filler, E is the modulus and the subscripts m and p represents the matrix and particulate phase.

For composites having a high modular ratio ($m = E_p/E_m$), these bounding solutions are widely separated to obtain estimates of E_c and this is particularly true for m>20. A different approach is taken in this case to find the dependence of modulus on volume fraction of inclusions.

Paul (1960) proposed a two-phase model where an isolated particle was embedded in a cubic matrix and a normal uniform stress was applied at its boundary. The equation was formulated as :

$$E_c = E_m\left(\frac{1+(m-1)\varphi^{2/3}}{1+(m-1)(\varphi^{2/3}-\varphi)}\right) \quad ...(2.6.13)$$

Ishai (Ishai and Cohen, 1967) used the same model and solved it for a uniform normal displacement at the boundary with the solution as :

$$E_c = E_m\left(1+\frac{\varphi}{\frac{m}{m-1}-\varphi^{1/3}}\right) \quad ...(2.6.14)$$

Kerner (1956) proposed an equation assuming good adhesion between phases as :

$$E_c = E_m\left(\frac{(\alpha E_p-\beta)\varphi+\beta}{(\alpha E_m-\beta)\varphi+\beta}\right) \quad ...(2.6.15)$$

$$\text{where,} \quad \beta = [15(1-\nu)]^{-1}$$
$$\alpha = [(7-5\nu)E_m + (8-10\nu)E_p]^{-1}$$

where, ν is Poisson's ratio. This equation is universal in the sense that the volume fraction inclusion can vary from 0 to 100%. It was found that this equation is useful in predicting the moduli of composites of spherical fillers randomly distributed in a glassy matrix (Lewis and Nielsen, 1970).

Modification of the basic Kerner equation fits better to some experimental results and was given by Kerner and Tsai (Lewis and Nielsen, 1970) as:

$$E_c = E_m \frac{1 + A''B''\varphi}{1 - B''\varphi} \qquad ...(2.6.16)$$

$$\text{with} \quad A'' = \frac{7-5\nu}{8-10\nu}$$
$$B'' = \frac{(E_p / E_m) - 1}{(E_p / E_m) + A''}$$

This equation is a more generalised version of the equation proposed by Halpin and Tsai (Halpin and Kardos, 1976) where A'' has a value of 2 for spherical particles.

Voids and cracks

As pointed out by Ishai and Cohen (1967), incorporation of voids are unavoidable while fabricating particulate composites. This is particularly true for composites containing small particle size dispersions with φ> 0.3. Two bounds of models were predicted in this case, where the upper bound came from Paul's approximation. For a porous media m=0 and equation (2.6.13) reduces to :

$$E_c = E_m \left(\frac{1 - \varphi_v^{2/3}}{1 - \varphi_v^{2/3} + \varphi_v} \right) \qquad ...(2.6.17)$$

where, φ_v represents the void fraction. The lower bound was given by Ishai where equation (2.6.14) reduces for a porous medium to :

$$E_c = E_m(1-\varphi^{2/3}) \qquad ...(2.6.18)$$

Cracks can form either within or around the particles of the dispersed phase during fabrication due to the difference in the thermal contractions in the two phases. These cracks cannot transfer stress, similar to voids, making the material more compliable and thus reducing the modulus of the composite.

2.6.1.4 Tensile properties of recycled bumper material

The automotive bumpers made from either rubber modified PP or some other thermoplastic blends are targeted for recycling and so evaluation of their properties is vital. Miranda *et al.* (1994) examined the properties of virgin, recycled painted and blends of virgin/recycled painted material of car bumpers (rubber modified PP). Melt filtration technique was performed for paint removal where combination of 20-80 and 20-80-100-40 meshes were used. They observed that the ultimate elongation of the virgin material was about 83% higher compared to the 100% recycled material (unfiltered). However, blending recycled material with 20% or more virgin material increased the ultimate tensile elongation of recycled material to 90% of virgin material. The tensile strength at yield and modulus for 100% recycled material was higher compared to virgin material and blended material because of the presence of polyurethane paint.

Asakawa (1992) compared properties between virgin rubber modified PP, recycled rubber modified PP with primer and crushed bumper with top coat and primer and showed that the retention of properties in the third was lowest. The modulus was dropped by about 5% and the elongation decreased by about 50% of the other two. Here solvent technique was used to remove the top coat from the PP surface which gave the material recycled PP with primer.

EIN Co. Ltd. (1993) compared the properties of virgin and recycled rubber modified PP where the recycled plastic resin was processed through the EIN system to remove paint. Vibration mechanism was used to produce small resin chips which then passed through a wind fan to remove paint. Their result showed about 100% retention of tensile properties between the materials.

Long *et al.* (1995) examined the properties of recycled PP based bumpers where paint was removed by both chemical (phenol and dichloromethane) and mechanical methods. No significant difference was observed between the materials in which paint was removed by different methods.

Tao *et al.* (1993) looked at the recyclability of bumpers made from PC/PBT blend with additional rubber modifiers. The experimental result showed that the tensile and flexural strength and moduli of the recycled materials were about the same as the freshly moulded PC/PBT blends and was not affected by the inclusion of adhesives and paint. But the recycled material containing paint had a much lower elongation compared with those containing no paint.

Michael and McElhaney (1991) studied the effect of both unpainted and painted regrind on the physical properties of PUR/ABS blends used as automotive bumper material. They showed that retention of tensile strength, elongation and modulus of the 100% painted regrind was nearly 100% compared to the blends with unpainted regrind.

In all the above cases dispersed paint fragments were responsible for any deterioration of material property. However, quantitative measurement of the paint part was not performed in any cases and so the effect of paint fraction on the tensile properties was not evaluated.

2.6.2 Impact strength

2.6.2.1 Impact test methods

Impact test measures the toughness of materials. Toughness is defined as the ability of the material to absorb applied energy. In these tests, materials are subjected to high loading rates and have minimum opportunity for energy absorbing mechanisms within the material to be effective (Williams, 1988). Impact strength is one of the most widely specified mechanical properties of the polymeric materials but there are many factors affecting the impact resistance. These are the rate of loading, notch sensitivity, temperature, orientation, processing condition and types, degree of crystallinity and method of loading (Peraro, 1985). There are two aspects of 'good impact test'. Firstly it should be capable of differentiating between a wide variety of materials and secondly it should provide material ratings that correlate closely with in-service product performance.

There is a variety of impact test methods available. The specimens have been subjected to a variety of impact loads including tensile, compression, bending and torsion impacts. Impact loads have been applied using hammer, punches, pendulum, falling weight and bullets. As so many different ways have been used, it is difficult to relate the results obtained by different methods (Vincent, 1971). So it is important to examine the advantages and limitations of these methods while choosing one to provide the required comprehensive information. Some selected methods are elaborated in the following sections.

2.6.2.1.1 Pendulum impact test

This test measures the relative susceptibility of a standard test specimen to breakage by a flexural shock with a pendulum type impact load. The method assesses the total energy absorbed to break a specimen which includes not only the energy required to initiate and propagate the crack but also the kinetic energy imparted to the specimen and the energy lost through the friction and vibration of the apparatus.

There are basically two different test methods : Izod and Charpy. In Izod type, the specimen is clamped vertically at one end and struck by a swing of a pendulum released from a fixed distance from the specimen clamp. Charpy method has similar set-up except the specimen positioning. Here specimen is supported horizontally as a simple beam and fractured by a blow delivered in the middle by the pendulum. So the advantage of Charpy test over the Izod test is that as specimens are not clamped they are free from variations in clamping force. Specimens in both cases are usually notched to provide a stress concentration area.

2.6.2.1.2 Falling weight impact

In this test a free falling tup is allowed to strike a supported specimen directly and the energy is measured from the known weight and height both of which are adjustable. Advantages of this method over pendulum test is the flexibility to use specimens of different size and shape, including an actual part. It also has the ability to duplicate the multi-directional impact stresses that a part would be subjected to in actual service. However, one of the biggest disadvantages is that the test requires a large number of samples to establish an energy level to fail and thus become time consuming as well. Also it is not possible to evaluate the process of crack formation with this test method.

2.6.2.1.3 Instrumented impact test

The industrial use of instrumented impact test (IIT) method is presently an emerging technology rather than a well defined and understood one. This method relies on the application of excess energy such that specimen failure is always ensured. The data acquisition system presents the information on the impact event in the form of load-deflection signals as well as numerical results.

The descending impactor carries an outrigger with a graduated optical strip, which passes through a detector and produces pulses as the impactor moves. The data acquisition system is triggered with the first pulse from the displacement transducer and then records the output at precise intervals. The timing between the individual marks on the optical strip is also recorded and used later for velocity and position calculation. Computerised scaling routines often

assumes that the values of the first few points collected are zero and will analyse the data based on that assumption. The photodetector trigger must therefore be set to allow an adequate 'zero baseline' to be collected before the impactor strikes the specimen. Another error arises due to lack of firm and continuous contact between the specimen and the support system. Johnson *et al.* (1986) found disparities in results arose between three instrumented apparatus which differed in their facilities for signal detection and processing.

The advantages of the IIT method are that, traces obtained from tests provide information on the failure mode of the material which can be ranged from brittle to ductile, tear or punched hole. Besides, information on various other data such as impact rate, yield load, modulus, peak and failure energy can also be obtained. High speed photographic and video techniques together with this test enable the events of deformation during impact to be associated with the force-deflection curve obtained from computer. From the photographs, a mechanistic understanding of crack propagation and fracture patterns is possible.

A typical load versus displacement curve for a ductile material is shown in figure 2.6.1. The terminologies used in analysing the force versus deflection curve are as follows :

Peak force is the maximum force registered on the trace. According to Reed and Turner (1987) the peak marks the point at which the specimen lost its structural integrity rather than the material's yield point.

Energy to peak is the integrated area under the curve up to the point of peak force.

Break point is the point which registers the complete failure of the test specimen.

Total energy is the total area under the curve up to the break point.

Gradient is the slope of the initial rising part of the load trace. It is a measure of the rigidity of the material. It is defined by two points, gradient index and gradient offset. The gradient index is the upper point determining the gradient line and lies on the graph. The gradient offset is the lower point located on the baseline.

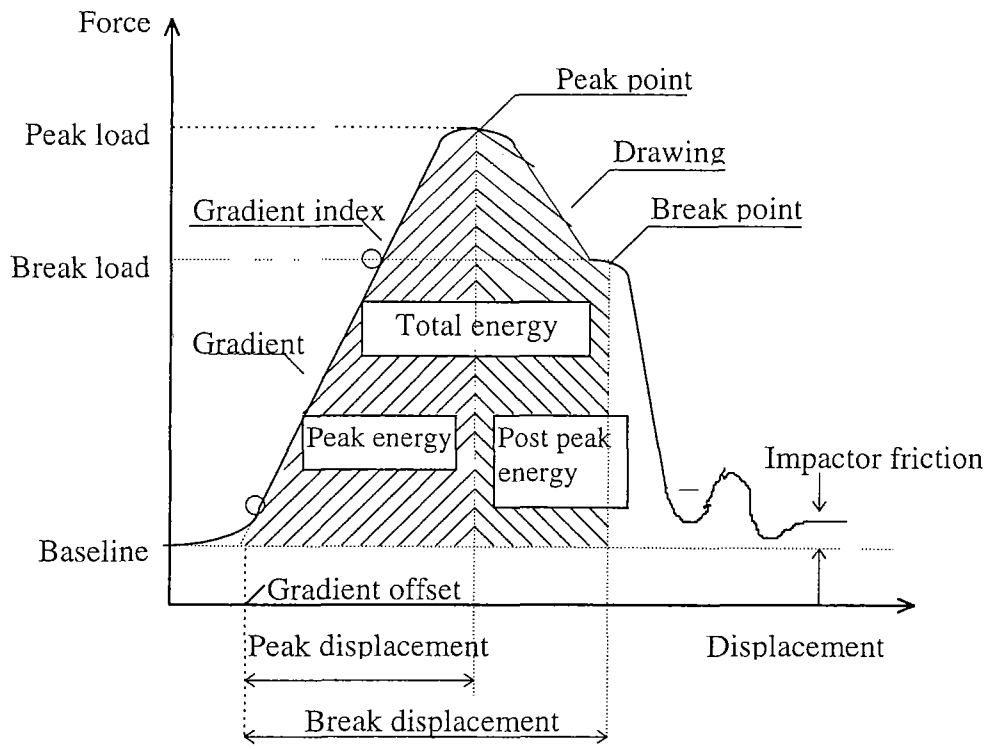

Figure 2.6.1 : Analysis of results for ductile specimen.

The limitation of the method is it requires a large number of specimens as interspecimen variability is high. Factors such as energy of impactor to penetrate the sample and energy required to toss the brittle sections of a sample contribute to the total energy failure for each specimen making it complicated to analyse.

2.6.2.2 Impact strength of recycled bumper materials

The dispersed phase of composite materials can be either rubbery or rigid and the impact strength of these materials depends on the size, shape and volume fraction of the filler phase, the adhesion between the matrix and filler and the mechanism of deformation of the matrix. Impact strength largely depends on temperature as well. At low temperature where all materials are brittle, rubbery inclusions have little effect on strength, behaving simply as rigid fillers. But the strength increases with increasing temperature and rubber content as they modify the deformation behaviour of the matrix polymer. This has led to the commercial

development of rubber toughened plastics. On the other hand, rigid particulate filled polymers usually show a decrease in strength with increasing filler fraction when the adhesion between the matrix and the filler is poor. The main reason behind it is that, the inclusions act as stress concentrators and crack initiators thus reducing the material strength. Improved adhesion between the two phases has been shown to increase the impact strength.

Different authors have examined the strength of recycled bumpers material. Miranda *et al.* (1994) performed instrumented drop impact test on recycled and blend of virgin and recycled material. Their result showed that 100% recycled material had lower impact energy and the toughness increased as the percentage of virgin material increased in the blend. Asakawa (1992) found that crushed bumper with primer and top coat had about 20% reduction in strength compared to virgin or recycled PP (paint removed by chemical means). EIN Co. Ltd. (1993) showed that removal of paint via their vibration and forced fan technique retained 100% impact strength of the recycled material compared to the virgin material. Long *et al.* (1995) observed that the presence of paint decreased the material strength by about 50% for PP based bumpers.

Tao *et al.* (1993) investigated the effect of adhesive and paint on recycled PC/PBT blends from post consumer automotive bumpers collected from various geographical locations with different conditions and exposure time. They observed that for bumpers collected from some locations (relative humidity 56% and 58%), presence of paint and adhesive did not affect the degradation of PC during processing and the impact strength of the recycled material. But for other locations (relative humidity 33% and 46%), the strength of the recycled material containing both paint and adhesive was lower than that containing paint only, indicating that the inclusion of the adhesive lowered the impact strength of the recycled material, but did not

affect the degradation of PC during processing. These findings proved that the impact strength of the bumpers decreased as exposure time, temperature and relative humidity increased.

Michael and McElhaney (1991) studied blends of TPU/ABS with both unpainted and painted regrind. They observed that notched Izod impact decreased with increasing painted regrind in the blend compared to the blends with unpainted regrind. But unlike the notched Izod impact result, the retention of impact strength based on instrumented impact was 85% or greater. Also, painted disk that was impacted with the painted surface in tension exhibited lower retention of impact strength than those impacted with the painted surface in compression.

In all the above studies though the effect of dispersed paint on the impact strength of material was studied, no attempt was made to quantify the dispersed phase and relate the volume fraction of paint to impact strength of the material.

2.6.3 Theory of fracture mechanics

Fracture mechanics is a useful technique for expressing the toughness of a plastic. In polymeric materials fracture may be brittle or ductile depending on the variables such as the processing conditions, the strain rate, the stress system, the temperature and the nature of additives. The principle external causes of fracture are : the prolonged action of a steady stress (creep or rupture), application of a stress in a very short time (impact) or the continuous application of a cyclically varying stress (fatigue) (Crawford, 1987).

The theory of fracture mechanics is based on the idea of Griffth (1920) who showed that the relatively low strength of a brittle solid can be explained by the presence of large flaws which act as stress concentrators. This hypothesis has led to the development of large body of experiments and theoretical work now termed as fracture mechanics. There are two

approaches to the fracture of the material. Firstly, the energy criterion arising from the Griffth's (1920) and later Orowan's (1948) work which supposes that fracture occurs when sufficient energy is released by growth of the crack to supply the requirements of the new fracture surfaces. The released energy comes from stored elastic or potential energy of the loading system and can be calculated for any type of test piece. Therefore it provides to measure the energy required to extend a crack over a unit area and this is termed as the fracture energy or critical strain energy release rate and is denoted by G_C. Secondly, Irwin (1964) found that the stress field around a sharp crack in a linear elastic material could be defined by a parameter named stress intensity factor, K, and stated that fracture occurs when this K value exceeds some critical value, K_C. Both G_C and K_C are material properties and independent of the geometry of the cracked body.

2.6.3.1 Linear Elastic Fracture Mechanism (LEFM)

The Linear Elastic Fracture Mechanism (LEFM) concept is essentially applied to materials obeying Hook's law. However, it may be applied to materials exhibiting inelastic deformation in the vicinity of the crack tip since the bulk body of the sample continues to exhibit linear elastic properties.

When a force is applied to a material there is work done in a sense that force moves through a distance. This work is converted to elastic energy absorbed in material and surface energy absorbed in creation of new surfaces at crack in the material. Griffth proposed that fracture would occur if the incremental change in net energy (work done, W - elastic energy, U) exceeded the energy which could be absorbed in the creation of a new surface.

Mathematically,

$$\frac{\delta}{\delta a}(W-U) \geq \gamma' \frac{\delta A}{\delta a} \qquad \text{...(2.6.19)}$$

where, γ' is surface energy per unit area and δA is the increase in surface area associated with an increment of crack growth δa.

For a crack propagation in a sheet of material of thickness B , equation (2.6.19) becomes:

$$\frac{1}{B}\frac{\delta}{\delta a}(W-U) \geq 2\gamma' \qquad \text{...(2.6.20)}$$

Where, $\delta A = 2B\delta a$

In the context of fracture mechanics the term $2\gamma'$ is replaced by G_c if it is assumed that the energy dissipation around a crack tip is independent of both the test geometry and the way forces are applied to the specimen. So fracture criterion becomes,

$$\frac{1}{B}\frac{\delta}{\delta a}(W-U) \geq G_c \qquad \text{...(2.6.21)}$$

G_c encompasses all the energy losses incurred around the crack tip. Failure occurs when the critical strain energy release rate is achieved.

Thus, considering the energy balance approach, if a cracked body of thickness B is subjected to a load P, then G_c is expressed as,

$$G_c = \frac{P_c^{\,2}}{2B}\frac{\delta C}{\delta a} \qquad \text{...(2.6.22)}$$

where P_c is the applied force at fracture and C is the compliance of the body defined as:

$$C = \Delta / P$$

Δ is the deflection of point of application of load (Kinloch and Young, 1983).

Another approach to fracture is the stress intensity approach developed by Irwin for engineering materials. This approach is concerned with the relationship between local concentration of stresses at the crack tip and applied stress. The equation proposed was:

$$\sigma_{ij} = \frac{K}{(2\pi r)^{1/2}} f_{ij}(\theta) \qquad ...(2.6.23)$$

where σ_{ij} are the components of the stress tensor at a point, r and θ are the polar coordinates of this point, taking the crack tip as the origin, and K is the stress intensity factor. This factor relates the magnitude of the stress intensity local to the crack in terms of applied loading and geometry of the structure in which the crack is located. K can be expressed in a more general way with the following equation:

$$K = Y\sigma a^{1/2} \qquad ...(2.6.24)$$

where, Y is the geometric factor, σ is the applied stress and a is the half length of a central crack and full length of an edge crack. Y may be expressed in a polynomial fashion as follows (Brown and Srawley, 1966):

$$Y = \sum_{0}^{4} A_n \left(\frac{a}{D}\right)^n \qquad ...(2.6.25)$$

where, A_n is dependent on the various specimen geometries.

A simple relationship exits between G_c and K_c in case of LEFM :

$$K_c^2 = EG_c \qquad \text{for plane stress} \qquad ...(2.6.26)$$

$$K_c^2 = \frac{E}{1-\nu^2} G_c \qquad \text{for plain strain} \qquad ...(2.6.27)$$

where, E is the Young's modulus and ν is the Poisson's ratio.

A fracture mechanics approach to impact testing was developed independently by Brown (1973) and by Marshall *et al.* (1973). It was assumed that the LEFM assumption is applicable for Izod and Charpy testing of a plastic. During these tests the energy absorbed at fracture U_c is recorded. This can be expressed in terms of applied force (P_c) and deflection (Δ) as :

$$U_c = \frac{1}{2} P_c \Delta \qquad ...(2.6.28)$$

In terms of compliance ,C, the equation becomes,

$$U_c = \frac{1}{2} P_c^2 C \qquad ...(2.6.29)$$

From equation (2.6.22) and)(2.6.29):

$$U_c = G_c B \frac{C}{\delta C / \delta A} \qquad ...(2.6.30)$$

introducing the specimen width, D, and the dimensionless geometry ϕ,

$$U_c = G_c B D \phi \qquad ...(2.6.31)$$

where, $$\phi = \frac{C}{\delta C / \delta(a / D)} \qquad ...(2.6.32)$$

If ϕ is determined as a function of *(a/D)* and the energy measured at the fracture is plotted as a function of $BD\phi$ for different specimens geometries , a straight line of slope G_c should result. Tabulated values of ϕ as a function of *(a/D)* and *(2L/D)* are given for various Charpy and Izod specimens in Plati and William's paper (1975) where L is the span of the specimen.

For high toughness material plastic yielding may occur at the crack tip region and stresses induced at the fracture tend to increase. However, if the zone is assumed to be small then it will not greatly disturb the elastic stress field and the extent of plastic zone may be defined by

the elastic stresses. Thus assumptions of LEFM can be employed and equation (2.6.31) can be used.

Irwin (1964) suggested that if a material is considered to be elastic up to the uniaxial tensile stress, σ_y, and then becomes plastic, then the extent of crack tip plasticity can be represented schematically as shown in Figure 2.6.2. Here δ_t is the crack tip opening displacement and r_p is the radius of a circular plastic zone at the tip of a 'notional' crack. The tip of this 'notional' crack is thus at the centre of the plastic zone and its length is now ($a+ r_p$). The elastic stress field ahead of this crack is regarded to be identical to the stress distribution of a real crack of length a with the extent of the plastic zone $2r_p$. The size of the plastic zone radius can be calculated as :

$$r_p = \frac{1}{2\pi}\left(\frac{K}{m_p \sigma_y}\right)^2 \qquad ...(2.6.33)$$

where, K is the fracture toughness and m_p is the plastic constraint factor which reflects the amount of constraint on the developed plastic zone created by the surrounding elastic material. This increases the stress necessary for yield to occur above that needed in uniaxial tension. In

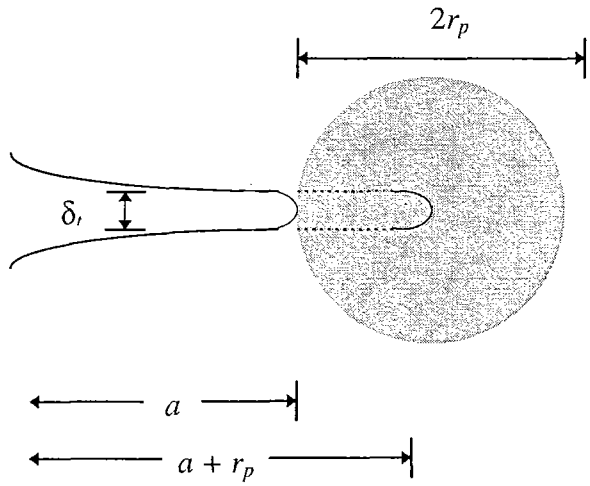

Figure 2.6.2 : Irwin's model of the plastic zone at a crack tip.

plane stress m_p has a value of unity and in plane strain it takes the value of $\sqrt{3}$ (Irwin and Paris, 1971).

In energy terms this equation becomes:

$$r_p = \frac{\pi}{16}\frac{G_c}{w_p} \qquad ...(2.6.34)$$

where w_p is the energy per unit volume. As it is difficult to calculate σ_y or w_p in impact tests, a procedure of least square fitting can be employed. In this method, small increments of r_p values are added to the original crack length a until the data for the plot of U versus. $BD\phi$ gives minimum deviation from a straight line fit calculated by least square method. This can be done numerically, and providing (r_p/D) is not too large (< 0.2), good result can be achieved. This type of failure is termed as semi-brittle failure and works well on polyethylene (PE) and polytetrafluoroethylene (PTFE) (Birch and Williams, 1977).

There is another type of impact failure for tough material termed as semi-ductile failure where a fully plastic ligament is formed upon impact followed by a subsequent unstable brittle failure. Nikpur and Williams (1978) modified equation (2.6.31) by introducing an apparent surface energy, G_d, for the plastic deformation of a ligament so that true crack propagation value, G_c can be calculated from the intercept of the equation:

$$\frac{U - U_T}{BD\phi} = G_d \frac{A}{BD\phi} + G_c \qquad ...(2.6.35)$$

where, U_T is the kinetic energy and A is the ligament area. This kind of behaviour is probably unique to rubber modified polymers, since the rubber modification results in craze initiation from the rubber particles. This is the energy absorption process which renders the system ductile but it occurs with essentially no distortion of the crack tip and consequent blunting since there is a substantial volume increase during crazing. Thus, large amounts of energy may

be absorbed in these systems without the geometry changes induced in the ductile deformation of most homogeneous materials.

2.6.3.2 Non-linear Elastic Fracture Mechanics

For materials displaying extensive crack tip plasticity, the elastic analysis is no longer valid and the concept of *J*-integral method must be invoked. Rice *et al.* (1973), found that for bulk non-linear elastic material, J is proportional to the rate of decrease of potential energy, U_{PE}, with crack length a, so that:

$$J = -\frac{1}{B}\left(\frac{\partial U_{PE}}{\partial a}\right) = cons\tan t \qquad ...(2.6.36)$$

The crack propagates when J exceeds a critical value of J_c. J_c is a material property independent of crack length and specimen geometry (Savadori *et al.*, 1984; Kinloch and Young, 1983). If full yielding is assumed in bending and this criterion is used, then J can be expressed as :

$$J = \frac{2U_{PE}}{B(D-a)} \qquad ...(2.6.37)$$

G_c and J_c measures the same property but their numerical values might be different. If the material obeys LEFM assumptions then J_c is directly equivalent to the fracture energy G_c (Plati and Williams, 1975).

2.6.3.3 Kinetic energy effects

When impact data is analysed then the measured energy contains a contribution from the kinetic energy in addition to the stored elastic energy and the graph U versus ϕ gives a positive intercept (U_T). Equation 2.6.31 then becomes:

$$U_c = U_T + G_c BD\phi \qquad ...(2.6.38)$$

This intercept may be measured separately by impacting an unsupported specimen or calculated reasonably accurately by the equation suggested by Birch and Williams (1977,1978). They considered the impact test to be modelled by a large striker of mass M impinging on a small specimen of mass m_s whose stiffness can be represented by a spring of compliance C. Considering the two bodies as rigid then from momentum :

$$MV + m_s V_0 = MV_1 + m_s V_2 \qquad ...(2.6.39)$$

where, V and V_1 are the initial and final velocities of M and V_0 and V_2 are those for m_s. If the Newtonian concept of a coefficient of restitution e is invoked, then:

$$e = \frac{V_2 - V_1}{V - V_0} \qquad ...(2.6.40)$$

If $\alpha = m_s / M$, then by combining equations (2.6.39) and (2.6.40) we have :

$$\begin{aligned} V_1 &= V\left(\frac{1-\alpha e}{1+\alpha}\right) + V_0\alpha\left(\frac{1+e}{1+\alpha}\right) \\ V_2 &= V\left(\frac{1+e}{1+\alpha}\right) - V_0\left(\frac{e-\alpha}{1+\alpha}\right) \end{aligned} \qquad ...(2.6.41)$$

For most impact tests $\alpha << 1$, and the equations become:

$$\begin{aligned} V_1 &= V \\ V_2 &= (1+e)V - eV_0 \end{aligned} \qquad ...(2.6.42)$$

The energy lost by the striker is :

$$U_T = \frac{1}{2} M\left(V^2 - V_1^2\right) = m_s V^2 (1+e)\left(1 - \frac{V_0}{V}\right) \qquad ...(2.6.43)$$

The energy of the specimen is :

$$U_2 = \frac{1}{2} m_s V_2^2 = \frac{1}{2} m_s V^2 \left(1 + e\left(1 - \frac{V_0}{V}\right)\right)^2 \qquad ...(2.6.44)$$

After impact the kinetic energy of the specimen, U_2, is converted to the strain energy in the spring. On the first impact V_0=0 and V_2 = $(1+e)V$ so that the specimen hit the striker,

compresses the spring and then as the spring recovers makes the second impact with the striker and so on.

Now for e=0, perfectly plastic impact occurs and for all V_0 values $V_2 = V$ and there is no bouncing since the specimen continues with the striker. So from equation 2.6.43 and 2.6.44 we can write:

$$U_T = m_s V^2$$
$$U_2 = \frac{1}{2} m_s V^2 \qquad \text{...(2.6.45)}$$

Here ($mV^2/2$) is lost on the first impact but $U_T = U_2 + m_s V^2/2$ thereafter.

On the other extreme case for perfectly elastic impact e=1. Here for the first impact :

$$V_2 = 2V$$
$$\frac{U_2}{U_T} = 1 \qquad \text{...(2.6.46)}$$

For subsequent impacts since V_0 is negative, there is an increase in the relative velocity at impact and more energy is impacted at each blow.

There is a critical value of $e = (\pi/2 - 1)$ which results in $V_0 = 0$ and in all cases the impacts are identical with

$$\frac{V_2}{V} = \frac{\pi}{2}$$
$$U_T = \frac{\pi}{2} m_s V^2 \qquad \text{...(2.6.47)}$$

To determine the value of e a series of tests were performed by Birch and Williams (1977) in which unrestrained specimens were knocked off the supports of a pendulum impact testing machine and the energy recorded. Four materials were tested, namely polyemthylmethacrylate (PMMA), polytetrafluoroethylene (PTFE), medium density polyethylene (MDPE) and a

thermoset resin, and the length to depth ratio of the specimens was varied between 5 and 10. The data was consistent giving an average value of e of 0.53. No trend with specimen mass or dimension was observed. Therefore for similar specimen size and shape equation (2.6.47) can be used as to calculate the kinetic energy.

2.6.4 Toughening mechanism for composite materials

Different mechanisms have been proposed to explain the improved toughness of single phase polymers by the presence of a second rubbery or rigid particulate phase and have been reviewed by Garg and Mai (1988). In short terms, the mechanisms that make G_c larger in composites are : (i) increased fracture surface area (ii) energy absorption by second phase fillers (iii) enhanced matrix plastic deformation (iv) filler matrix debonding energy and (v) interaction between crack front and dispersed fillers such as crack pinning. Some of these mechanisms which contribute to the enhanced crack resistance of multiphase polymer are discussed below.

2.6.4.1 Particle deformation

The theory of toughening mechanism in rubber modified plastics was first proposed by Merz *et al.* (1956). They observed that in high impact polystyrene (HIPS), an increase in whiteness and volume accompanied elongation of the material and concluded that multiple tiny cracks produced during the process was responsible for the phenomena. Beaumont and co-workers (1980) studied the rubber modified epoxy material and suggested that rubber particles bridge a crack as propagating through the material and dissipate the stored energy during stretching when the particles rupture thus increasing the toughness. But this mechanism failed to explain the phenomena of stress whitening and was found to be only of secondary importance in

increasing toughness. It is principally the deformation mechanism in the matrix, enhanced by the presence of the second phase, which improves the toughness.

2.6.4.2 Shear yielding

When a polymer starts to deform plastically under an applied stress it is said to have yielded. Shear deformation consists of a change of shape without significant change in volume and shear yielding of polymer is relevant to the mechanism of polymer fracture.

Though many workers have explained the shear yielding mechanism with rubbery particles, the explanation by Haaf *et al.* (1977) and Donald and Kramer (1982) have been the most convincing one. Haaf studied the mechanism in rubber modified PVC compounds and found that shear yielding deformation was accompanied by cavitation of rubber particles which explains the stress whitening. Donald and Kramer studied the deformation in thin films of two ABS polymers having different particle size distribution. They observed that shear deformation, rather than crazing promoted by rubber particle cavitation was the major toughening mechanism for the material with small rubber particles (diameter ~ 0.1 μm). On the other hand, the material with larger particles (~ 1.5 μm) initiated crazing. Kinloch and co-workers (1983) agreed with Haaf's explanation and found that cavitation was often accompanied by crack growth, specially at high temperature and was observed in hybrid particulate composites. However, they proposed that localised plastic shear yielding is the main source of energy dissipation and increased toughness. This occurred due to the interaction between the stress fields ahead of the crack and the rubber particles.

The presence of rigid particulate fillers e.g. glass beads, silica etc. may also induce shear deformation, but there are significant differences in the mechanical behaviour of these

different multiphase polymers. Rigid particles are not as effective as rubbery particles in increasing toughness which mainly arise from their post yield behaviour. The limited deformation of the former limits the energy absorbed by localised shear yield deformation and lead to crack initiation. The debonded particles cannot transmit applied loads and thus are unable to enhance yielding. On the other hand, rubbery particles either cavitate thus relieving constraints or stretch thus staying well bonded and sustain applied load.

2.6.4.3 Crack pinning

Generally it is observed that the fracture energy of a brittle material reinforced with rigid fillers is increased with filler fraction, at least for low volume fraction. Lange (1971) proposed that, a crack in a body possesses line tension and when it meets an array of impenetrable, well bonded particles it becomes pinned. In order to move past the obstacles the crack bow out between particles forming secondary cracks thus increasing fracture energy. His proposal was evident from fractographic studies which showed that as a moving crack front interacts with obstacles in the matrix, tails and steps are formed at the rear of the inclusions due to the meeting of the two arms of the crack front from different fracture planes. Lange derived an equation relating the fracture energy of composite to that of the matrix, through the line energy T_L per unit length of bowed crack front. He assumed that the crack front breaks away from the pinning position when it attains a radius of ($D_S/2$), where D_S is the interparticle distance. The equation has the following expression (Lange and Radford, 1971) :

$$G_{Ic} = G_{Ic(matrix)} + 2\frac{T_L}{D_S} \qquad ...(2.6.48)$$

where,

$$D_S = \frac{2d_p(1-\varphi)}{3\varphi}$$

d_p is the particle diameter.

However, the equation was found to be inadequate to describe the crack pinning mechanism as different initial slopes were obtained when obtained when G_{Ic} is plotted against $(1/D_S)$ for different particle sized filers in brittle polymers implying that T_L is not invariant with particle size as suggested by equation (2.6.48).

Other theoretical models have been proposed by several group of researchers to explain the phenomena of increased toughness. Evans (1972) carried out more detailed calculation of T_L and demonstrated that the line energy contribution depends upon both the particle size and shape. He suggested that when brittle particles are employed to induce crack pinning they should be impenetrable and thermal and elastic mismatch should be minimised to ensure that excessive stress concentration do not build up. Green *et al.* (1979 : a,b) explained the effect of particle shape and particle/matrix adhesion in a model system of nickel sphere filler glass matrix. They found that low adhesion of filler particle to the matrix offer little impedance to the advancing crack thus do not cause any significant change in crack shape.

At high filler fraction, tails are rarely observed due to the overlap of secondary cracks. Also, interacting stress fields lead to premature debonding of particles which then becomes ineffective pinning sites.

From these discussions some comments can be made as why brittle particles do not toughen ductile matrix. In ductile material, high stress extends well beyond crack tip and may cause debonding of particles. These debonded particles cannot act as effective sites for energy absorption via shear yielding or crazing mechanism. Moreover, when the crack front does reach the debonded particles they are unable to effectively pin crack (Owen, 1979).

2.6.4.4 Toughening mechanism of composites with elastomer inclusions and inorganic fillers

Recent development of polymeric materials concern the preparation of hybrid particulate composites obtained by incorporating both rubbery and inorganic particles in polymer matrix. By correct addition of both types of secondary phase it is possible to obtain a variety of materials with optimal performance for specific requirements. Basically, the addition of the elastomeric phase enhances the material toughness, whereas the addition of inorganic fillers increase the material stiffness.

The toughening mechanism activated by elastomer inclusion is multiple crazing and /or shear yielding, as well as rubber particle cavitation depending on the system considered (Martinatti and Ricco, 1994). On the other hand, the toughening effect of the brittle matrices with rigid particulate fillers has been mainly ascribed to crack pinning mechanism. In some hybrid particulate composites, synergism is obtained under some circumstances, where several toughening mechanisms operate simultaneously giving the composite impressive mechanical properties.

Kinloch *et al.* (1984, 1985) investigated the fracture of epoxy polymer dispersed with both rubbery and rigid glass fillers. The experimental results showed that both phases may increase toughness of epoxy polymer, but rubbery phase had a greater effect. Glass particles mainly increase the crack resistance by crack pinning mechanism whereas the rubber particles increase toughness by enhancing the extent of plastic shear deformation at the crack tip, due to interaction between the stress field ahead of the crack and the rubbery particles. The addition of glass particles to an epoxy-rubber matrix, may significantly increase the toughness of the

hybrid. At high temperature the fracture toughness value passes through a maximum at a given volume fraction of glass particles. After this debonding of glass particles decrease the toughness of the hybrid composite.

It was shown in some work (Goodier, 1933; Kinloch and Young, 1983) that for heterogeneous polymeric systems stress concentration developed around heterogeneities-filler or dispersed elastomer particles thus changing the local stress distribution in the material. Size of these heterogeneities (0.1 ~ 10 μm) often matches the notch depth (2 ~ 30 μm) creating a competition between stress concentration at heterogeneity and crack tip. Moreover, deformation mechanism changes with composition, structure, size and distribution of dispersed particles and interaction of the components, thus changing the response of the material to external load and yielding different fracture characteristics. Pukanszky *et al.* (1995) studied the fracture mechanism of PP composites filled with ethylene-propylene copolymer (EPR) elastomer and talc or $CaCO_3$ filler. They concluded that composition dependence of fracture properties are practically independent of specimen size, temperature or measurement technique.

Jancar and Dibenedetto (1995 : a,b) studied the effect of phase morphology, interfacial adhesion and filler particle shape and volume fraction on fracture toughness of PP filled with $CaCO_3$ or $Mg(OH)_2$ and EPR elastomer. They showed that presence of elastomer, as either particles dispersed uniformly in the PP matrix or as interlayer on the rigid filler surface, enhances both strain energy release rate and resistance against crack propagation. But these two morphologies differ significantly in fracture toughness under impact loading at the same material composition.

Long and Shanks (1996) studied the three component system of PP-elastomer-filler (talc and different particle sized $CaCO_3$). They proposed a model to stimulate the deformation behaviour in these systems. When elastomer and filler particles are separated in the PP matrix, the filler particles tend to produce a range of microcracks with application of an impact. Though elastomer particles can stop crack propagation, they cannot be fully effective. On the other hand, for a core-shell microstructure where the filler particles are covered by elastomer, the original microcracks initiated at the filler particles are prevented and a yielded zone around the elastomer particles are formed. In this case elastomer can be fully effective to increase the toughness of the hybrids. Similar results were obtained for both the talc and $CaCO_3$ fillers.

2.7 Structure - Property Relationship for Polymer Composites

Blends prepared under similar conditions like identical shear and thermal histories can be compared and related in terms of rheology, morphology, thermal and mechanical properties. For composites with non-deformable fillers the melt rheology depends mainly on characteristics of fillers (such as particle size, distribution, geometry etc.) and the state of dispersion and interaction between different constituents. On the other hand, the mechanical properties of multicomponent system depend on component properties, their miscibility and processing conditions of composites. The morphology of the composite arises from the blending and processing condition of the composite where the flow plays a dominant role in the structure of processed material. For the case of deformable fillers (for example polymer blends) a complete different situation exists. The morphology depends on the concentration of different components and the processing temperature. Depending upon these conditions the phases may be continuous, or one component may be dispersed in another with a third, continuous phase being itself of a different composition. Whatever the situation is, the

viscosity changes far from the initial value of the constituents. All these different structures would therefore effect the mechanical behaviour.

Kim *et al.* (1993) studied the effect of viscosity ratio on (i) the morphology of the dispersed phase and (ii) the mechanical properties of the ternary blends of PP(80)/rubber(EPM,EPDM)(10)/PE(10) and PP(80)/rubber(10)/$CaCO_3$(10) (wt%). They observed that with PE viscosity comparable to, or higher than that of rubber, the dispersed phase formed a reticulate structure. This is turn increased the hardness, modulus and elongation at break of the ternary blends. For PP/rubber/$CaCO_3$ composites, better dispersion of $CaCO_3$ in the PP matrix was obtained when the viscosity of rubber was significantly higher than that of the matrix. With better dispersion, hardness and tensile properties were improved, but the impact strength more or less decreased.

Jancar and Dibenedetto (1995) studied the ternary composite of PP with inorganic filler ($Mg(OH)_2$) and $CaCO_3$) and elastomer inclusion. They concluded that phase morphology plays a crucial role in determining the composite mechanical response. Morphology of a ternary composite PP/rubber/filler is a result of a frozen dynamic equilibrium between thermodynamic and shear forces in the melt during the mixing procedure. The thermodynamic forces are determined by the surface free energy of components and the system tends to acquire a morphology with minimum total free energy. For their systems, the free energy of the filler was greater than that of EPR which was again greater than that of PP. So the morphology possessing the lowest free energy is when filler particles are encapsulated by the elastomer layer and the core shell inclusion is embedded in PP. The shear forces on the other hand are controlled by the relative viscosities, temperature, particles size and shape and other rheological parameters (Pukanszky *et al.*, 1990) and tend to remove the elastomer from the filler surface in the course of melt mixing, leading to separate dispersion of the filler and elastomer inclusions. So they suggested that a random distribution of encapsulated, core-shell,

separated filler and elastomer inclusions in the PP matrix results from an uncontrolled mixing process. The controlled structures with complete separation or perfect encapsulation were developed from grafting of maleic anhydride (MAH) onto either PP or EPR which increased the surface free energy of the respective components. Their experimental data showed that by appropriate choice of processing conditions, filler size, shape and concentration, elastomer content and the distribution of an adhesion promoter between the phases, it is possible to tailor stiffness and strength properties over a wide range.

Long and Shanks (1996) studied the different microstructures for the ternary blend of PP/elastomer/filler (talc and $CaCO_3$) hybrid and discussed the relationship between morphologies and mechanical properties. The different microstructures were obtained by processing control and surface modification of elastomer or PP. They observed that elastic modulus increased for completely separated microstructures and impact strength increased for core-shell microstructure.

Li and Masuda (1990) showed that for PP/$CaCO_3$ composite , formation of agglomerated structure can be promoted or prevented by rheological processing. They observed that for smaller particles (0.15 μm) large surface area is available so the particles dispersed in polymer matrix agglomerate gradually with increasing time to form an agglomerated or network structure. This in turn increases the value of loss and storage moduli with lowering frequency in low frequency region. For larger particles (4 μm) better dispersion is obtained as they have small particle-particle interaction and so gradual decrease in storage and loss moduli was obtained with decrease in frequency. No mechanical testing was performed for this system.

Park and Kyn (1989) examined the rheological and mechanical properties of poly-p-phenylene terepthanide (PPTA) / nylons (nylon 6, 66, 11 and 12) molecular and particulate composites.

Different rheological behaviour of nylon 6 or 66 systems and nylon 11 or 12 systems were supposed to be caused by different phase separation behaviour of individual systems. They observed that for PPTA and nylon 6 or 66 phases separate during coagulation or melt extrusion specially at high PPTA content thus showing characteristics as of particle filled compounds. On the contrary, for PPTA and nylon 11 or 12, long PPTA fibril develops during flow thereby viscosity behaviour was similar to that of thermoplastics and thermoplastic and liquid crystalline blends. In both the cases tensile strength and elongation of the composites decreased with increased PPTA concentration.

2.8 Conclusions and Directions of Investigations

The following conclusions have been drawn as a result of analysis of literature review:

- Different techniques are available for paint removal from plastic parts but all of them are not suitable economically or environmentally. New techniques are under consideration to overcome the difficulties.

- Image analysis is now widely used to determine the volume fraction, size distribution, spatial information of different phases in polymer blends and composites. This technique is found suitable to analyse the dispersed paint fraction in PP phase.

- Rheological properties for polymer composites are influenced by filler concentration, size, geometry and interaction between filler-filler or filler-polymer interaction. In general viscosity increases with increasing filler concentration at lower shear rates. The variation due to particle size is minimum with low solid concentration (φ <20% v/v). Effect of particle size distribution is significant in more concentrated suspensions (φ > 0.4). In

practice, polydisperse systems increase the maximum allowable packing fraction, thus reducing the relative viscosity at a fixed concentration of particles. Composite viscosity also increases with increasing aspect ratio of particles.

- The mechanical properties for polymer composites are much influenced by the filler size, shape, volume fraction and adhesion between matrix and filler. Different theories have been proposed to relate these properties with volume fraction of filler.

- Very little work is published on rheological and mechanical testing of recycled PP dispersed with paint particles and attention was focused mainly on blends of recycled and virgin material. The dispersed phase particle size and particle size distribution were not considered as variables.

- Fracture mechanism of composite materials gives an insight into material behaviour under different conditions. No fracture property data was available from literature for dispersed paint in toughened polypropylene.

- Structure-property relationship for polymer composites interrelates the morphology and rheological and mechanical behaviour of the systems. Some work has been done on ternary blends of PP with elastomer inclusions and rigid fillers and described by this structure-property relationship. Generally, an increase in shear viscosity and elastic modulus was observed with decrease in extent of elongation and impact strength for completely separated microstructures compared to core-shell microstructures.

On the basis of the above conclusions the following investigations have been proposed to achieve the objectives of the project:

- Perform melt filtration for removal of paint contaminants from PP based bumper material.

- Develop a technique to analyse the dispersed paint fraction in PP matrix before and after melt filtration.

- Perform rheological and mechanical characterisation of these materials.
- Prepare real systems with controlled sized paint particles to find the effect of filler size and size distribution on properties. Also prepare model systems with glass beads to analyse the filler geometry effect on the system properties. Characterise the blends by performing rheological and mechanical tests.

- Analyse the data and fit the experimental results to different mathematical models proposed for mechanical behaviour of composites to predict the present system behaviour.

- Study the fracture mechanism of paint dispersed PP system to explain the mechanical behaviour of the composites under test conditions.

- Establish structure property relationship for the systems under study.

CHAPTER THREE

MATERIALS AND EXPERIMENTAL TECHNIQUES

3.1 Materials

The base material used for melt filtration was a thermoplastic rubber modified mineral filled polypropylene (PP), Epalex 7095, supplied as pellets by Polypacific Pty. Ltd. Australia. This high flow injection moulding grade is developed for high impact strength at sub-zero temperatures while maintaining good rigidity at high ambient temperatures. Also the lower shrinkage and high flow give good part stability at elevated temperatures used in paint ovens. The physical and mechanical properties of the material are given in Appendix A, table A.1 according to the supplier specification. Plaques (100 x 50 mm) made from the same grade was sent to Dulux, Australia to be painted in two batches. White paint system was used as found on automotive bumpers and the method described in section 2.1 was followed. Each batch had three layers of paint, namely primer, base coat and clear coat with the thicknesses shown in table 3.1.1. The average weight fraction of paint in the two batches were 2.79 and 3.92 % respectively. This was measured by direct weighing technique where the plaques were weighed before and after the paint application. The average volume fraction was then calculated from them using known density and thickness of each paint layer. The calculated values were 1.8 and 2.47% respectively.

The recycled PP based bumper bars coated with polyurethane based white paint were supplied as ground material by TP Recyclers, Australia. Only white painted bumbers were used in the experiments to keep the number of variables small. The white paint was chosen as it has the highest pigment level (Mc Elhaney and Plaver, 1991). Physical properties such as density at

room temperature, melt density and melt flow index (MFI) were measured for material charactreisation before any experimentation.

Table 3.1.1 : Thickness of paint layers.

Paint layers	Batch 1	Batch 2
Primer	3 ~ 5 μm	3 ~ 5 μm
Base coat	25 μm	40 μm
Clear coat	30 μm	40 μm

The raw materials used to prepare the "real" and "model" blends, with paint particles and glass beads as the dispersed phase, are tabulated together with their commercial names and suppliers in table 3.1.2. The base matrix for bumper grade material comprise of PP/rubber/talc with small fractions of UV stabilizer, heat stabilizers, masterbatch etc. which do not exceed more than 5% of the total formulation. In the blends prepared for the experimental investigations for this work, the main constituents were only considered and the base matrix preapred had only 70% PP, 20% rubber and 10% talc by weight. Besides, a second base matirx with 80% PP and 20% rubber (wt%) was also prepared to distinguish if talc was actullay overshadowing the effect of the second dispersed phase of paint or glass on the material behaviour. The polypropylene used was a lightly stabilized, easy flow, injection mould grade imapct copolymer (LYM 120). The rubber was a polyolefinic elastomer based modifier (VM 42E) specially designed to improve the impact strength of PP homo- or copolymer either in PP/elastomer blends or in reinforced PP or in tri-blends with high density polyethylene (HDPE). As modified with highly efficient impact strength, this grade is mainly used in injection moulding and extrusion of PP blends. The material was supplied as free flowing pellets. The talc with an average particle size of 8 μm was used as reinforcing filler for the model blends. The spherical glass beads used as the dispersed phase for the composites

were of the particle size range of 106-53 μm (average diameter 66 μm). The physical, mechanical and chemical properties of all the raw materials are given in Appendix A, tables A.2 - A.6.

Table 3.1.2 : Grades and suppliers of materials used in blends.

Materials	Grade	Supplier
PP copolymer	LYM 120	ICI Ltd., Australia
Rubber	VM 42 E	Kemcor Australia Pty.Ltd.
Talc	TALC TX	Commercial Minerals Ltd., Australia
Glass beads	AG	Potters Industries Inc., Australia

A step by step procedure was followed to obtain ground paint particles which was later used as a filler with the rubber toughened PP composites. First some polypropylene sheets were cleaned followed by application of three coats of paint namely primer, base coat and clear coat on them as found on the car bumpers. These sheets were baked in the oven at 80°C for 30 minutes for the paint to set. The paint was then scraped from the sheets manually with a scrapper as thin layers and grounded firstly with a mixer and finally with a ring grinder. The ground paint was then sieved to different sizes using BS 410 standard sieves. The portions in between sieves 150-106 and 75-53 μm were used with the blends as fillers. The average particle size determined using the Malvern Mastersizer was 135 and 63 μm respectively for the two batches. The steps are also shown as a flow diagram in Figure 3.1.1.

All blends of PP and fillers were prepared on weight fraction (W_i) basis and later converted to volume fraction (φ_i) using the formula :

$$\varphi_i = \frac{\frac{W_i}{\rho_i}}{\left(\sum_{i=1}^{n} \frac{W_i}{\rho_i}\right)} \qquad \text{...(3.1.1)}$$

where ρ_i is the density of any component *i*.

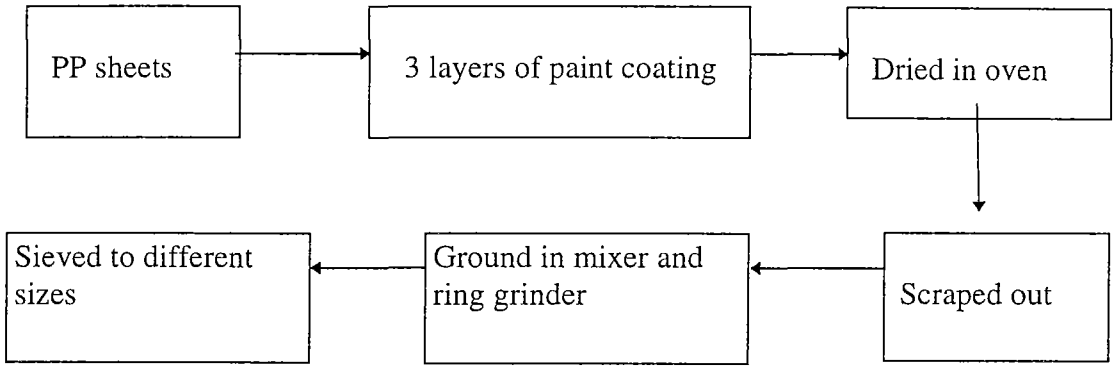

Figure 3.1.1 : Flow diagram for steps to obtain ground paint particles.

3.2 Instruments and Methods for Experimentation

3.2.1 Measurement of dispersed paint fraction

With no suitable techniques available to estimate the dispersed paint fraction in the polymer matrix, the method of image analysis was applied as a trial basis. As will be discussed in chapter four, section 4.1, the method was found to be appropriate for quantitative measurement of dispersed phase with very little percentage of error. Thus, this technique was adopted for further investigations.

3.2.1.1 Digital image analysis

The technique of digital image analysis involves image acquisition, image processing and an image analysing software. An image is divided into a grid of small square cells or pixels (picture elements). Each pixel is examined separately by the image analyser and its value at

any point is proportional to the brightness (or grey level) for the image at that point. A typical image contains 512x512 pixels with 256 grey levels if scanned in grey scale or 256 colours if scanned in colour (Gonzalez, 1992). After an image is acquired and digitised then it is available for analysis.

3.2.1.2 Software and apparatus

A wide variety of softwares (Guild and Summerscales, 1993) have been developed for image processing and analysis. In this work, the image analysis program IMAGE (1.49) was used to analyse the digital images. IMAGE (1.49) is written by W. Rasband (National Institute of Health, Research Service Branch, NIMH). IMAGE is a public domain program for the Macintosh, that can acquire, display, edit, enhance, analyse, print and animate images. It can be used to measure area, average grey value, centre and angle of orientation of a user defined regions of interest. It also incorporates a Pascal-like macro programming language that provides the ability to automate complex, and frequently repetitive, processing tasks. A Macintosh LC III computer with an Apple Color OneScanner, with a resolution of 300 dots per inch (dpi) was used to acquire and digitise images.

3.2.1.3 Image processing and analysis

Images are usually acquired by scanning of the desired object. Digitised images have to be processed in order to perform the calculations accurately. Processing includes enhancement of brightness and contrast, inverting the image, thresholding etc. Thresholding segments an image into objects of interest and background on the basis of grey scale. When threshloding is enabled, objects are displayed in black and background is white. The background pixels are ignored while the objects are measured. As the acquired images showed the paint particles as white pixels and the PP phase as the grey background, contrast enhancement and inverting the

image was necessary before thresholding was applied. The inverted images then showed the paint particles as the dark foreground and the white background was the PP phase.

To count the pixels, the image has to be in a threshlod or binary mode. The binary mode sets all the thresholded pixels to black and all the background pixels to white. Then the area fraction of each phase is directly calculated using the IMAGE program.

3.2.1.4 Application to PP/ paint system

Images were acquired directly from the specially prepared samples for the PP/ paint system. Firstly, a gram of ground material was taken and compress-moulded with a Wabash Hydraulic Press at 190°C for 5 minutes to obtain a thin sheet (0.07 ~ 0.08 mm). The sheet was then placed on the flat bed scanner and scanned. As the size of a single image for a sample was too big to handle by the program, three images were taken covering different areas for each sample and then the results were added to get the final volume fraction. The size of images used for analysis were (7x2 cm) and (10x3 cm). This was obtained by cutting three windows on a piece of paper of the above mentioned size and placed over the sample before scanning. This is schematically shown in figure 3.2.1. Figure 3.2.2 (a) shows a typical example of a digitised sample and figure 3.2.2 (b) shows the same after processing. The black area of the processed image is the paint part and the white background is the PP phase. As the shades of grey influence the result for the area fraction, so it was important to choose suitable and consistent shades of grey for a series of images. A large number of sample was made from each batch in this manner and used as specimens for image acquisition. Due to very small thickness of these sheets it has been assumed in this analysis that the area measured is directly proportional to the volume fraction of the paint. The volume fraction of paint was then quantified directly through counting the number of black pixels (paint particles) found in an image. The rest of the bachground pixels in the image belonged to the matrix phase.

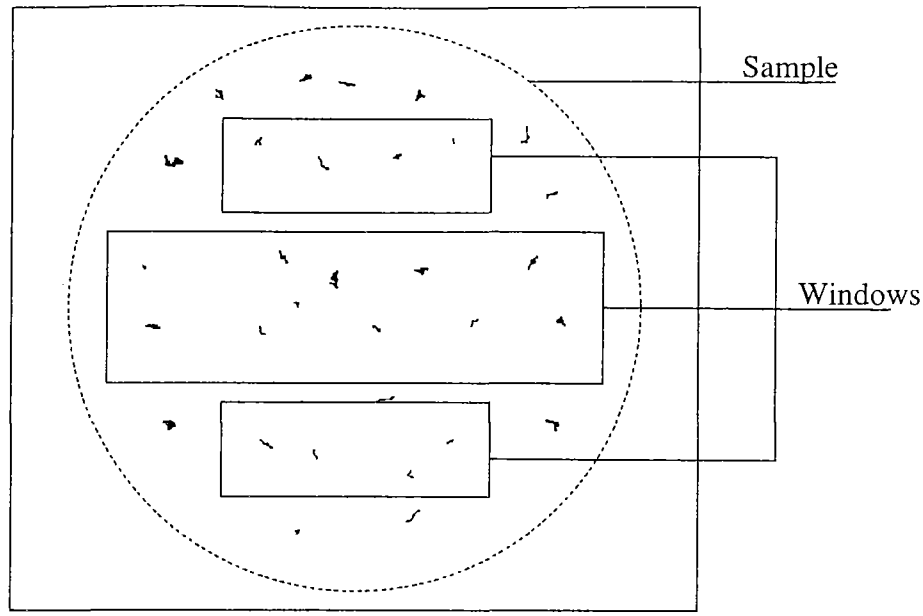

Figure 3.2.1 : Windows showing the size of images used for scanning and analysis.

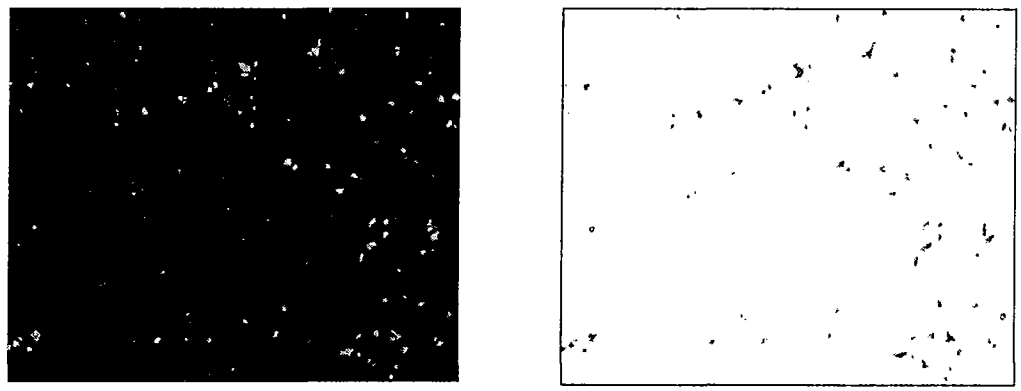

(a) (b)

Figure 3.2.2 : **(a)** Digitised and **(b)** processed image of a section of a sample.

3.2.2 Density determination

The density of the raw materials at room temperature was measured using a Beckman Air Comparison Pycnometer model 930. This instrument measures the volume of powdery, porous, granular and irregularly shaped solids within an accuracy of ±2%. The density is determined as a ratio of the mass and volume of the sample. The instrument has two chambers with pistons and a differential pressure indicator. The measurement is based on the principle

that when the pressure in both the chambers are equal then the difference between the locations of pistons is always proportional to the volume of the sample.

The density of the polymers in molten state was determined according to ASTM D1238 using a Ceast Modular Flow Indexer model 6542. The equipment consists of a vertical heated cylinder, with a die of 2.09 mm diameter, through which the polymer melt is extruded using a standard weight on the piston. The melt flow rate is obtained by measuring the mass of the length of material which has been forced out of the orifice in a certain time interval. The Melt Flow Index (MFI) is expressed as grams of material extruded per ten minutes, with temperature and load listed if other than the standard conditions. To obtain the volume flow rate, a flag of known length is attached to the piston and the time taken by the flag to pass through a photo cell timer during the extrusion is noted from the automatic timer. The Volume Flow Index (VFI) is expressed as cm^3 of material extruded per ten minutes. The melt density (ρ_m) is then calculated as a ratio of MFI and VFI :

$$\rho_m = MFI / VFI \qquad ...(3.2.1)$$

where: $MFI = 600w / T'$

and $VFI = 600A_1 L' / t$

w average weight of extrudate in grams

T' cut-off time in seconds

A_1 cross sectional area of the barrel in cm^2

L' flag length in cm

t travel time of flag through the photo cell in seconds

3.2.3 Particle size messurement using Malvern Mastersizer

The particle size measurement of talc, glass beads and ground paint particles was performed using a Malvern Mastersizer X. It is a laser scattering based instrument measuring particle size of any one material phase in another. The only requirement of the technique is that each phase must be optically distinct from the other and the medium must be transparent to the laser wavelength. The instrument allows to measure particles in the size range of 1.2-600 microns.

For glass beads the dry powder feeder MSX64 was used where the sample was dispersed in air. For talc and paint particles dispersions were made using suitable liquids. The choice of a liquid mixture in which the powder would be suspended can have a crucial effect on the accuracy of the particle size analysis result. An absolute requirement is that the particles should be insoluble in the liquid. The chart provided with the Mastersizer manual was used to select the appropriate suspending liquid, the dispersant and concentration of the liquid medium to be used for talc and paint as shown in table 3.2.1.

Table 3.2.1: Choice of liquid suspension media for particle size analysis of powders.

Material	Suspending liquid	Dispersant	Concentration
Paints(mineral)	water	Potassium citrate	0.1 mol/litre
Talc	water	Na-pyrophosphate Trisodiumphosphate	1 gm/litre

The particle size analysis results of paint particles, glass beads and talc obtained from the Malvern Mastersizer X are given in Appendix B, figures B.1-B.4. The photomicrographs of

the fillers are also given in Appendix B, figures B.5-B.8. Table 3.2.2 shows the average volume mean diameter (*d*) and the densities (ρ) of these fillers at room temperature.

TABLE 3.2.2 : Average particle size and densities of the fillers at room temperature.

	Size range (sieve analysis) (μm)	*d* (μm)	ρ (g/cm^3)
Talc		8	2.65
Paint particles	150-106	135	1.77
	75-53	63	1.77
Glass beads	106-53	66	2.50

3.2.4 Melt filtration using Haake Rheocord

Melt filtration was performed on a Haake Rheocord 90 which is equipped with a single screw extruder together with a capillary die head. The Rheocord acts as a screw speed controlling drive and the extruder provides a homogeneous melt continuously passing through the die at a sufficient pressure. A breaker plate was designed to fit the screens on it and was placed just before the die head for the filtration purpose. Meshes sized 150, 200, 250 and 350 corresponding to the aperture sizes of approximately 100, 76, 61 and 40 μm were used as combinations of screen packs. A pressure transducer was used at the end of the screw, just before the die to monitor the pressure drop across the exrtuder. The processing temperature and rotor speed were kept constant at 220°C and 60 rpm for all the experiments. Each filtration was carried out for approximately 30 minutes without changing the screen packs during the run. Figure 2.2.1 in chapter two showed the arrangement of the breaker plate and screen packs in the extruder.

3.2.5 The injection moulding equipment

A Johns injection moulding machine model 550 was used to produce specimens for mechanical testing. This machine belongs to the reciprocating screw type unit. It has a single screw with three zones namely feeding, compression and metering zone. A control console is coupled to the injection unit to set the processing conditions. The optimum processing conditions were determined by trial and error to give the best specimens. A data sheet providing the processing conditions is given in Appendix C, table C.1.

3.2.6 The counter rotating twin screw extruder

The blends of PP/rubber/filler were prepared in a Brabender counter rotating twin screw extruder model DSK 42/7. It has a capillary die head with the length and diameter of 18 and 4.9 mm respectively. The twin screw extrusion process was used to obtain a homogenised dispersion of the components throughout. A control console is coupled to the extruder for temperature and screw speed control.

For blend preparation, all the components were first preweighed and tumble mixed follwed by extrusion. The processing temperature was kept constant at 200°C along the barrel and a screw speed of 60 rpm was chosen for optimum mixing of components. The extrudate was passed over a conveyor belt provided with an air cooling system and then through a pelletiser to obtain the blended material in the final pellet form.

3.2.7 Investigation of rheological properties of polymers in molten state

The rheological behaviour of materials was examined using a Dynamic Stress Rheometer filled with a parallel plate geometry. Two models of this machine were used. RMS-605 and SR-200. The first one is a controlled strain rate rheometer whereas the later is a controlled

stress one. The melt filtered samples were examined using the RMS-605 while the PP/rubber/filler blends were examined using SR-200. Nitrogen atmosphere was used in later case to avoid degradation of PP.

Using tests supplied with the RHIOS software, either sinusoidal (dynamic) or linear (steady) stresses can be applied to the sample. Stress is applied by a stress head and a position sensor mounted on that output strain, the angular deflection of the stress head. Calculation of material properties is performed by analysis of applied stress and resulting strain. The relationship between stress (τ), strain (γ), torque (M) and shearing angle of stress head (θ') are as follows:

$$\tau\left(dyne/cm^2\right) = \left(2000g/\pi R'^3\right)M' \qquad ...(3.2.2)$$

$$\gamma = \left(R'/H\right)\theta' \qquad ...(3.2.3)$$

where M' applied torque (g.cm)

g gravitational constant (980.7, CGS unit)

R' radius of plate (mm)

H gap between plates (mm)

θ shearing angle of stress head

Samples of 25 mm diameter and 2 mm thickness were compression moulded and used with the machine for measurements.

3.2.8 Mechanical properties of polymers in solid state

Mechanical properties of materials were examined by performing tensile, flexural, impact and fracture tests at room temperature. Injection moulded samples were used for all the tests.

3.2.8.1 Tensile testing equipment

An Instron Series 4400 was used for tensile testing of the blended materials. The machine consists of two vertical crossheads. The lower crosshead is immovable and rooted to the machine base while the upper crosshead is connected to the computer system coupled to the testing machine. The control panel allows to choose the test type, perform test and produce results.

The tensile test was performed according to ASTM D638 standard and the specimens had the shape and dimension as shown in figure 3.2.3. Each specimen was clamped to the crossheads of the machine after the input of specimen dimensions and test conditions. The test was finished when the preset extension was reached or when the sample broke. The load vs. elongation curve was obtained as the experiment progressed and results were calculated from the final curve. Tensile strength at yield, elongation at break, strain at break, and youngs modulus were worked out through the installed software using the following relationships:

$$\text{Tensile strength at yield} = \frac{\text{Load at peak}}{\text{area of minimium original cross section}}$$

$$\text{Strain at break (\%)} = \frac{\text{Elongation at break} * 100}{\text{gauge length}}$$

$$\text{Youngs modulus} = \frac{(\text{Slope of the initial linear poriton of load deflection curve}) * \text{gauge length}}{\text{area of minimium original cross section}}$$

Figure 3.2.4 shows a typical load - displacement curve for the material under test. At least six specimens were examined for each batch of samples and the average of the results were taken. Statistical analysis was performed to find the standard deviation of the results.

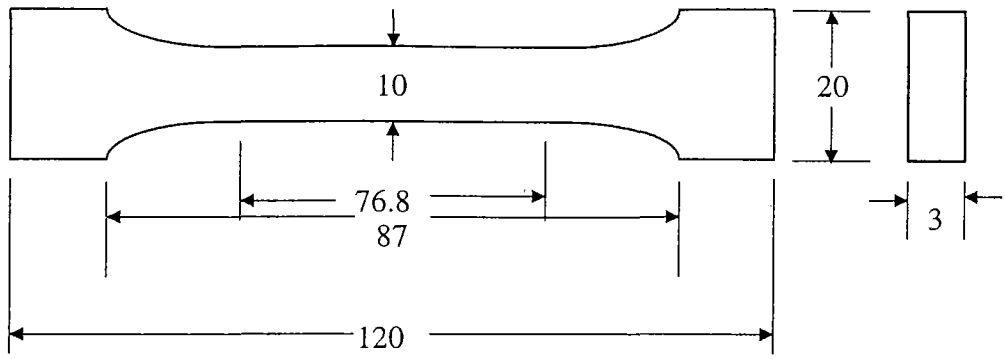

Figure 3.2.3 : Tensile test specimen (all dimensions are in mm).

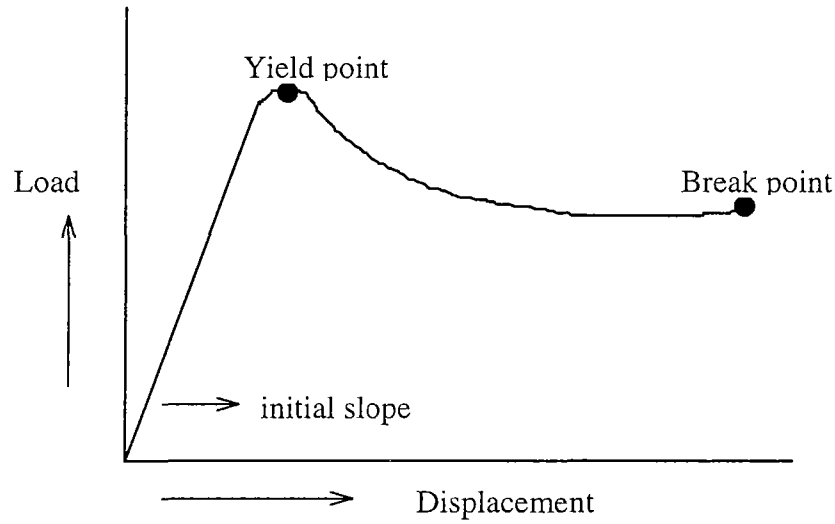

Figure 3.2.4 : Typical load displacement curve for tensile specimen.

A Lloyd machine model 2000 was also used at the beginning of the work to perform tensile test of materials before and after melt filtration. The machine had same set-up as the Instron. The test result varied by about 10% between the two machines.

3.2.8.2 Flexure testing equipment

The Instron Series 4400 was used for three point bend flexure testing as well. The set-up consists of an immovable jaw rooted to the machine base and a loading nose connected to the computer system. The test was performed according to ASTM D790 standard with specimen

dimension of 126x13x3 mm. The test bar rested on two supports of the lower jaw and was loaded by means of the loading nose midway between the suppotrs. Load was applied to the specimen at the specified crosshead rate and the test was finished when preset extension was reached. The flexural yield strength and tangent modulus was calculated according to the following equations using the provided software :

Flexural yield strength : $\frac{3P'L}{2BD^2}$

Modulus : $\frac{L^3m'}{4BD^2}$

where : P' yield point (N)

L span of specimen (mm)

B specimen thickness (mm)

D specimen width (mm)

m' slope of the initial straight line portion of load deflection curve (N/mm)

3.2.8.3 Impact testing equipment

A Davenport Izod Impact Tester was used to perform the impact test at room temperature according to ASTM D256 standard. It is a pendulum type machine where a notched specimen is broken by a blow from the pendulum of known energy. The loss of energy of pendulum equals the impact strength of the test specimen and is indicated by the movement of a pointer on a calibration scale. The calibration scale is marked from 0 - 10 where each small divison equals 0.2. The Izod imapct strength of a material is calculated using the following relationship:

Impact strength (J/m) : $\frac{\overline{E}Y'}{10D}$

where $\bar{E}$ average scale reading

Y' pendulum energy (J)

D specimen width

Depending on the toughness of the polymer being tested, the pendulum weight can be increased by attaching additional devices to the free end of the pendulum.

At least six specimens with a standard notch angle of 45° and a notch depth of 2.54 mm were tested for each batch and the average value was used to calculate the impact strength of the material. Any specimen showing much discrepancy in result was disregarded and another one was tested. The specimen dimensions are shown in figure 3.2.5.

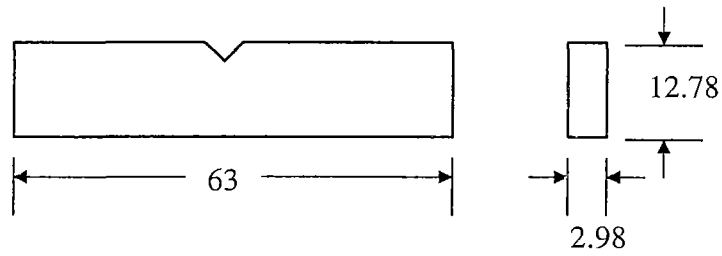

Figure 3.2.5 : Izod impact test specimen (all dimensions are in mm).

An Instrumented Impact Tester ITR-2000 equipped with the Charpy anvil was also used to perform the impact tests. This machine relies on application of excess energy such that specimen failure is always ensured and every test produces both graphical and numerical results characterising the specimen behaviour. During the test a force transducer continuously monitors the load of the impactor, while the displacement transducer monitors the distance the impactor has travelled. Subsequent analysis of the force versus displacement data carried out by the computer produces the required information on the properties of the material under test.

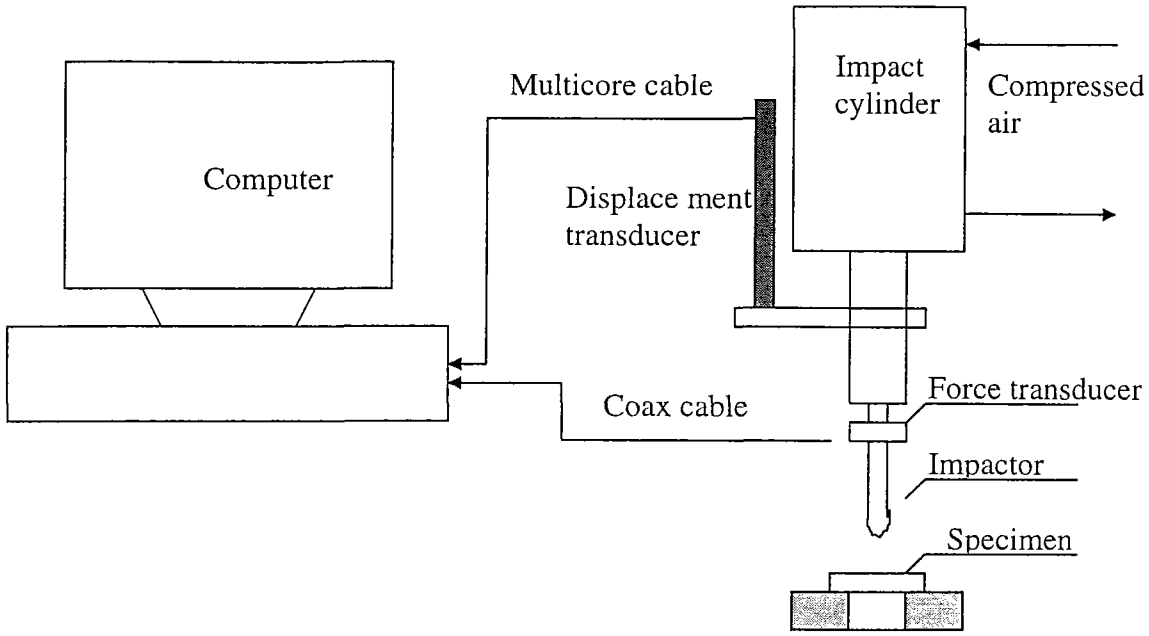

Figure 3.2.6 : General arrangement of an instrumented imapct tester (ITR 2000).

A general layout of the system is shown in figure 3.2.6. The Charpy anvil consists of two end pieces, to provide two point support for the specimen. The position of the end supports is adjustable, to allow centering of the test piece and also exact setting of the span between the anvils. A span of 51.28 mm was usd in the experimental set-up to give a span to width ratio of 4 for the specimens. A chisel shaped hardened steel impactor with a nose of 45 degrees rounded to 3.17 mm radius was used to impact the samples directly opposite to the notch. A 2kN force transducer was used for testing and the pressure regulator adjusted to keep the velocity of the impactor around 3.4 m/s.

Specimens were machine notched to six different depths (0.7 - 5.7 mm) and sharpened by pushing a razor blade slowly into them. After the test was performed the notch depth was measured using a vernier scale with a microscope mounted on it. Eight to ten specimens were tested for each notch depth. The specimen dimensions were same as the Izod impact specimens. Figure 3.2.7 shows the relation between the Charpy anvil, specimen and impactor.

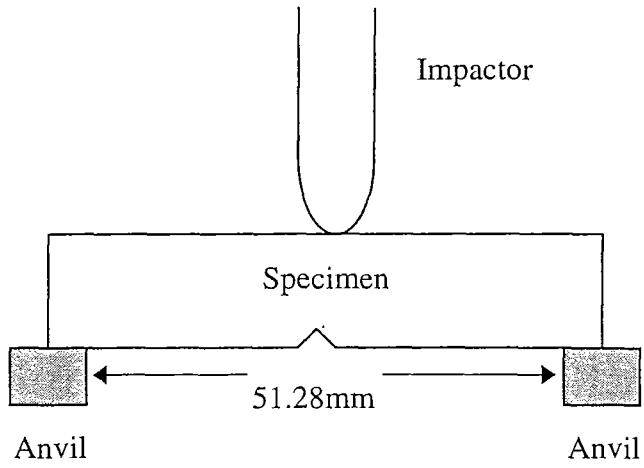

Figure 3.2.7 : Charpy anvil, specimen and impactor relation.

The terminologies used in analysing the force deflection curve has already been described in chapter two, section 2.6.2.1.3. As mentioned, the peak or total energy is the area under the curve upto the peak or break point. This was calculated with the help of the available software by integrating the area by mid point trapezoid rule.

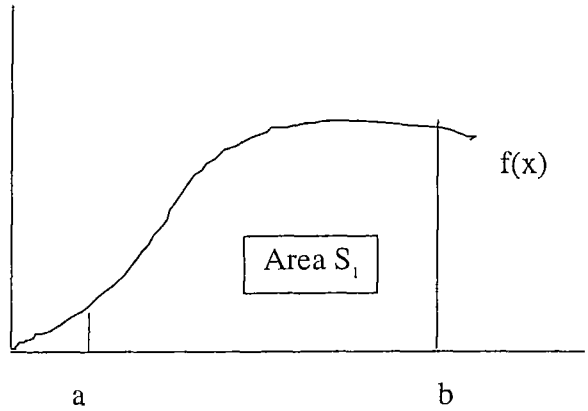

Figure 3.2.8 : Application of mid point trapezoidal rule to graph f(x).

Say the area S_1 under the graph f(x) has to be calculated between the interval $[a,b]$ (figure 3.2.8). Firstly the whole interval $[a,b]$ is divided into n parts of width h where :

$h=(b-a)/n$ and $x_0 = a,\ x_1 = a+h,$ $x_n = a+nh = b$

A midpoint between two consecutive points will be :

$$x_{j-1/2} = (x_{j-1} + x_j)/2 = a + (j-1/2)h$$

So the area under the curve f(x) from $x = a$ to b will be the sum of all the areas of these midpoint trapezoids because $f(x_{j-1/2})$ is average of bases of the jth midpoint trapezoid, h being its height :

$$S_1 = \sum_{j=1}^{n} hf(x_{j-\frac{1}{2}})$$

3.2.9 The Scanning Electron Microscope

The morphological studies were carried out on a Hitachi Scanning Electron Microscope, model S520. The machine consists of an electron-optical column and a cabinet type control console. The column has an electron gun, electromagnetic lenses and deflection coils inside and a chamber to hold the specimen at the base. The control console contains the display screens and the image recording and processing device.

Fractured samples were cut into proper size and gold coated using a Dynavac coating machine model SC100-M. Then samples were attached to a stage and placed into the column chamber for image acquisition. Once the resolution was satisfactory, photographs were taken.

3.2.10 Compression moulding

Two types of samples were produced using the compression moulding technique. Thin sheets of samples (0.07 - 0.08 mm) were compresed to be used under the scanner for the image analysis test and 2 mm thick disks, 25 mm in diameter were produced for rheology tests. A 'Wabash' 40 ton upstroking hydraulic compression press was used to serve the purpose. The

press consists of two platens the temperature of which can be adjusted by setting the controllers on the front panel. The press can be closed by depressing two close buttons simultaneously. The lower platen rises while the buttons are depressed and stops on release. The press has an automatic slow close feature which is activated by a bar depressing a switch as the platen moves up. The mould should be nearly closed when this switch is activated and once this is done the press will continue to move even when the buttons are released.

The molding pressure has to be set prior to the molding cycle. Molding requires high pressure to ensure that the plastic fills all of the cavity and has relatively uniform density throughout and to ensure better heat tranfer to the material. Proper pressure has to be applied as insufficient pressure creates molding difficulties and impair the quality of molded part.

3.3 Accuracy and Reproducability of Measurements and Error Analysis

3.3.1 Image analysis

Estimation of parameters using the image analysis software depends on the reliability of the measurements. There are some general types of errors to guard against. Inaccuracies in measurements can arise from sampling procedure, sample preparation, the quality of image and choice of threshold. To minimise error, random sampling was done and the sample preparation and image processing were kept similar for all the samples. Errors also arise from non representative samples where the prepared sample for analysis is not exactly representative of the specimen as a whole. Sufficient number of observations reduce the probability of error in sampling. Also it is expected that the reliability of the measurement would be improved if greater number of observations are performed. For this reason twenty observations were made for each batch and any one showing a big discrepancy in the pixel count was ignored while calculating the average of the others. The image quality and choice

of threshold also limit the accuracy of the measurement. These problems can be solved by editing the image before the calculation step.

3.3.2 Density determination

The density measurements of PP, rubber, talc, glass beads and paint particles were performed at room temperature using a pycnometer. The zero check was performed as per operating procedure followed by volume measurement of the samples. The density was calculated from predetermined sample weight and the volume measured. The same procedure was performed four times for all the samples and the average density was reported. The ratio of the standard deviation to mean for every sample was calculated and was reported as the percentage error in density determination as shown in table 3.3.1.

Table 3.3.1 : Percentage error in density determination at room temperature.

Sample	Average density (gm/cm^3)	% error
PP	0.906	0.62
rubber	0.906	0.12
talc	2.65	0.59
glass beads	2.51	0.94
paint particles	1.77	0.42

3.3.3 Particle size and particle size distribution

It was important to have a consistent particle size and size distribution of glass beads and paint particles for the real and model blends produced. For this random sampling was done and duplicate measurements were performed on Malvern Mastersizer X for error estimation between readings. The result analysis of the tests showed that the mode, the volume mean diameter, 10% v/v particle undersize diameter and 90% v/v particle undersize diameter were reproducible to within ±4% for both the fillers. So it was assumed that the particle size

distribution of each size range did not contribute to the error in steady viscosity and loss and storage moduli measurements.

3.3.4 Rheological measurements

3.3.4.1 Error in temperature

Temperature is an important parameter for rheological properties of polymer composites where variation of as little as 1°C can affect the obtained results. All measurements were performed within ± 0.1°C of the specified set point. Consecutive tests were resumed only when the parallel platens reached the set temperature. So error in temperature would be insignificant.

3.3.4.2 Reproducibility of steady shear measurements

The reproducibility of steady shear measurements was investigated for the 0.51% paint filled (63 μm) PP/rubber/talc composites at 190°C. Four tests were performed on separate samples over the shear rate range of 0.05 - 1/s. Statistical analysis on the test results were performed and the mean, standard deviation, standard error and other parameters were calculated for three arbitrarily chosen shear rates. The ratio of the standard deviation to mean at each shear rate, expressed as percentage, was calculated and used as an indicator of any trend in error in

Table 3.3.2 : Percentage error in shear viscosity for the 0.51% paint filled (63 μm) PP/rubber/talc composites at 190°C.

Shear rate (s^{-1})	Error in shear viscosity (%)
0.100	2.37
0.398	2.34
1.00	2.38
Average error (%)	2.36

viscosity calculation as reported in table 3.3.2. No observable trend was present in the calculated values so it can be concluded that the average error of ±2.36% is representative of the shear viscosity error over the shear rate range investigated.

3.3.4.3 Reproducibility of oscillatory shear measurements

The reproducibility of oscillatory shear measurements were investigated for the 2.7% paint filled (135 μm) PP/rubber/talc composites at 190°C. Four tests were performed on separate samples over the frequency range of 0.1 - 100 rad/s. Statistical analysis was performed for four arbitrarily chosen frequencies over the entire frequency range as in the steady shear error calculation and the average error was found to be ±0.59% and ±0.26% for the storage modulus (G') and loss modulus (G'') respectively as shown in table 3.3.3. No observable trend was noticed in the error calculation so the average was taken as the representative error over the entire range.

Table 3.3.3 : Percentage error in storage and loss moduli for the 2.7% paint filled (135 μm) PP/rubber/talc composites at 190°C.

Frequency (rad/s)	Error in storage modulus (%)	Error in loss modulus (%)
0.251	0.76	0.42
3.98	0.71	0.1
25.1	0.41	0.25
63.1	0.47	0.27
Average error (%)	0.59	0.26

3.3.5 Mechanical property testing

All the specimens moulded using an injection moulding machine were conditioned for 48 hours at 80°C and then kept at laboratory atmosphere of 23±2°C for atleast another two days

before any mechanical test was performed. The tests were then done at the same room condition with ±2°C temperature variation.

3.3.5.1 Tensile and flexural tests

At least six specimens were tested for each batch of material and the average results were reported. Statistical analysis was performed on the test results for error analysis and to check the accuracy of measurements. Table 3.3.4 gives an example of the analysis of tensile tests for 135 μm and 63 μm sized 2.7% paint dispersed PP/rubber/talc composites were the standard deviation and mean values are given along with the percentage error. All other blends tested had very similar results. Similar analysis was performed for flexural tests.

Table 3.3.4: Error analysis of tensile test for the 2.7% paint filled (135 and 63 μm) PP/rubber/talc composites at room temperature.

Sample		Tensile strength	% strain at break	Young's modulus
2.7% paint (135 μm)				
	Mean	19.0 MPa	26.7	1260 MPa
	Standard deviation	0.08	1.82	60
	% error	0.42	6.8	4.78
2.7% paint (63 μm)				
	Mean	18.6 MPa	29.5	1210 MPa
	Standard deviation	0.55	3.37	33
	% error	2.95	11.4	2.7

3.3.5.2 Impact strength

At least six individual determination of impact values were made on each sample to be tested on a pendulum impact tester with an Izod configuration. Moulded samples were all machine

notched to one particular depth with a variation of ±0.02 mm and the depth of the specimens were measured with a vernier scale. Average error of the test results were calculated from the standard deviation and the mean values and was found to be around ±5% for all the batches.

3.3.5.3 Fracture test

An instrumented impact tester (IIT) equipped with a charpy anvil was used to perform the fracture test. The samples were first machine notched to six different depths and then a natural crack was initiated by inserting a fresh razor blade. The notch depth was measured after fracture test to the nearest 0.5% accuracy using a vernier scale with a microscope mounted on it. Eight to ten specimens were tested for each notch depth. The peak load of the load-displacement curve was taken as the crack initiation point and used to calculate the fracture stress. Energy up to the peak point was used to calculate the strain energy release rate, G_c. The percentage error calculated for the peak load and the peak energy were ±10% and ±5% respectively.

CHAPTER FOUR

RESULTS AND DISCUSSIONS

In this chapter the results of the quantitative measurement of the dispersed paint fraction in polymer matrix is first discussed. The subsequent sections discuss separately the rheological and mechanical properties under investigation for the melt filtered materials and the blended systems. In all the cases, attention was focused to discuss the effect of the dispersed phase on the properties of the respective base materials. All concentration levels shown in the results are in volume fraction or volume percent unless mentioned otherwise.

4.1 Quantitative Measurement of Dispersed Paint Fraction in Polymer Matrix

As mentioned in chapter three, the technique of image analysis was applied to quantify the dispersed paint fraction in polypropylene (PP) matrix. The methods of sample preparation, image acquisition and measurement technique have already been described in section 3.2.1. Firstly it was necessary to establish the accuracy and reliability of using this method. This was done by cross checking the results obtained from here with gravimetric measurements. For this, the base polymer chosen was the commercially available bumper bar grade material (Epalex 7095). Plaques were moulded from this and then painted into two batches with different amount of paint on them. The difference was in the base coat and clear coat layers as shown in table 3.1.1. The plaques were weighed separately before and after the paint was applied and mass fraction of paint was calculated. As the densities of the constituent layers of paint were known accurately, the volume fraction of paint on the plaques was calculated. One point should be kept in mind that as the paint was applied manually, the thickness of each

layer on every plaque may not always have been exactly the same as stated in table 3.1.1. So for each batch an average of the volume fraction of paint was calculated and the values were 1.8 and 2.47% respectively. These results were then compared with those obtained from image analysis (table 4.1.1) where the average volume fraction was found to be 1.83 and 2.48% for batch 1 and 2 respectively. Though the minimum and maximum values calculated by IMAGE differed somewhat from the results obtained from direct weighing method, the average results obtained from both the techniques were very close showing only 1.67 and 0.405% error for the two batches. So it was concluded that image analysis can be used to calculate the dispersed paint fraction in the polymer matrix. This is a straightforward method and can be used for similar systems without requiring any knowledge about density values.

Table 4.1.1 : Comparison of results of volume fraction of paint obtained by two different techniques.

Volume fraction of paint							
Batch	by direct weighing	by image analysis					
	avg.	avg.	% error	min.	% error	max.	% error
1	0.018	0.0183	1.67	0.0163	9.44	0.0204	13.33
2	0.0247	0.0248	0.405	0.0238	3.64	0.0265	7.28

Inaccuracies in the measurement arise from sampling procedure, sample preparation, the quality of image and choice of threshold. To minimise error, random sampling was done and the sample preparation and image processing were kept similar for all the samples. It is also expected that greater number of observations involved in a measurement increase the accuracy of result. For this reason twenty observations were made for each batch and any one showing a big discrepancy in the pixel count was ignored while calculating the average of the others. Table 4.1.2 shows some results for volume fraction of paint of batch 1 samples.

This method was then applied to calculate the paint fraction in the polymer matrix before and after the melt filtration so that the amount of paint removed can be directly quantified. It was found that about 50% paint was removed from unfiltered samples by using melt filtration, where different combination of meshes were used. The results are tabulated in appendix E, table E.1 along with the tensile test results.

Table 4.1.2: Some results of volume fraction of paint of batch 1 samples.

Sample	Black pixels (paint particles)	White pixels (PP phase)	Total pixels	Fraction of paint
1	16544*	795064	811608	0.0204
2	13335	798273	811608	0.0164
3	13215	798393	811608	0.0163
4	16565	795043	811608	0.0204
5	14222	797386	811608	0.0175
6	16309	795299	811608	0.0201
7	13562	798046	811608	0.0167
8	13562	798046	811608	0.0167

*(Pixels count is the added result of the three images for each sample)

The same image analysis technique was also used to study the average particle size of the paint particles after the filtration process. The software was able to calculate the size and number of particles from which the average size was calculated. The mean particle size for the mesh combinations 250/250 and 150/150 were 255 and 280 μm respectively. The result indicates that, decrease in aperture opening with increasing mesh number disintegrated the paint particles to even smaller sizes thus lowering the average particle size.

4.2 Effects of Interfacial Adhesion Between Filler and Matrix on Properties of Composite Materials

The behaviour of composites depends not only on the individual properties of the components and on their relative proportions but also on the size, shape, state of agglomeration of the minor component and on the degree of adhesion between them. Particulate phases are usually called fillers, or if the interphase adhesion is high then reinforcing fillers. Fillers can be fibrous which are usually referred to as reinforcing, since the fibres themselves bear an important fraction of any load imposed on the composite.

Polymers, being organic materials, exhibit little tendency to wet and cover the surface of inorganic filler particles during compounding. Optimum properties in composites usually cannot be realised with fillers in agglomerated forms. Improving the polymer-filler compatibility through the wetting agent or coupling agent surmounts the problem. A wetting agent modifies the surface tension of the filler in such a way that the polymer will wet the filler particles, allowing them to separate and distribute in a better manner than obtained by shear mixing only. A coupling agent, on the other hand, is a bifunctional molecule having an organic end and an inorganic end. The inorganic end is designed to bond to the filler and the organic end to the polymer, resulting in a chemical bond between filler particles and polymer.

With good adhesion, the fracture strength of composites are usually the same as that of the unfilled matrices. Whereas, poor adhesion of filler to matrix reduces the composite strength with increasing volume fraction of filler (Spanoudakis and Young, 1984). Many authors concluded that increased adhesion between filler and matrix improved tensile properties (i.e. tensile yield strength, elongation and modulus) because of higher wettability of filler with the matrix. Silane based bonding agents were generally used for glass fibre and beads, mica and

calcined clays and coupling agents were used for mica, talc, $CaCO_3$ (Xavier *et al.*, 1990; Maiti and Sharma, 1992; Maiti and Mahapatro, 1991) and silver powder (Ghosh and Maiti, 1996) filled composites, which seem to plasticise/lubricate the matrix thus improving the tensile properties. Interfacial adhesion has been shown to influence flow properties as well. Kao *et al.* (1975) showed that treated glass beads in polar glycerol produce low energy surface giving reduced composite viscosity.

In the present study no effort was made to improve the interface between the matrix and the fillers (talc, glass beads and paint particles) used as the dispersed phase. Still, different composite behaviour was observed with different fillers. Addition of much larger sized glass beads (66 μm) or paint particles (63 and 135 μm) to PP/rubber system showed poor interface between matrix and inclusion which was evident from fractographs of these composites. Figure 4.2.1 is an impact fractograph of a glass filled composite where clean exposed surface of glass beads and clear hemispherical holes proves debonding of particles.

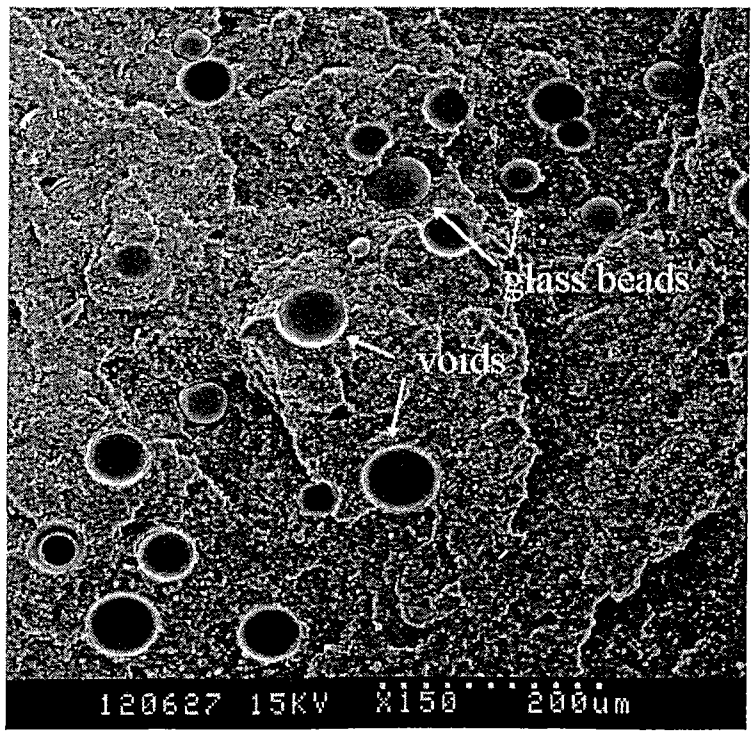

Figure 4.2.1 : SEM of an impact fractured surface of 1.9% glass bead filled PP/rubber composite.

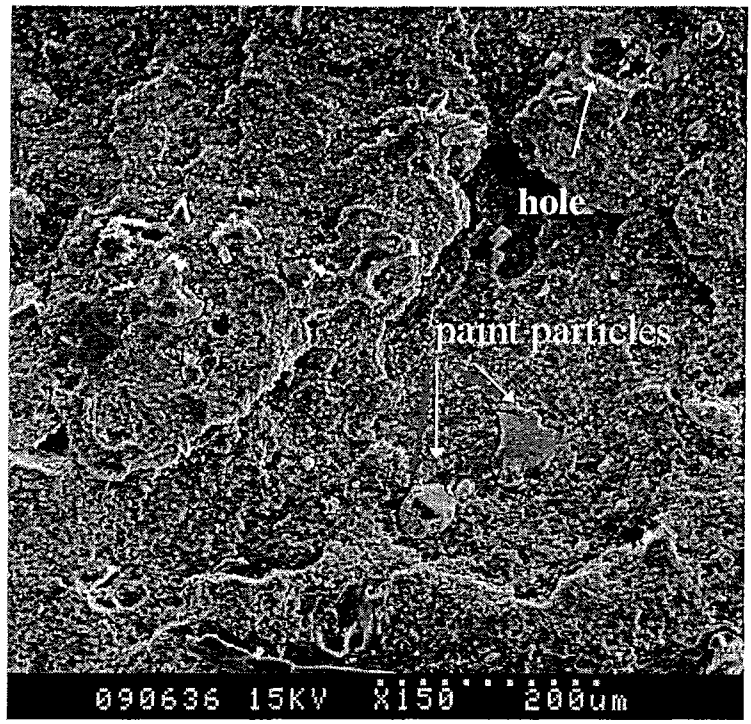

Figure 4.2.2: SEM of an impact fractured surface of 2.7% paint particle filled PP/rubber composite.

Paint filled composites showed similar structure where irregular holes were observed instead as shown in figure 4.2.2. These poor interfaces led to decreased impact strength and lower elongation at break in tensile test for the composites. But when talc was added to PP/rubber composite, increased rigidity and fracture strength was obtained over the unfilled composite. The small particle size of talc (~ 8 μm) and its ability to interact strongly in a physiochemical sense let allowed it to fit between polymer molecules making a filler-polymer network thus improving its rigidity.

Because there is adhesion between the talc and polymer, stress transfer takes place across the interface even at low strains, thus allowing the filler to share the stress. This in turn provides a reinforcing effect. Also good wetting of talc particles by matrix as shown in figure 4.2.3

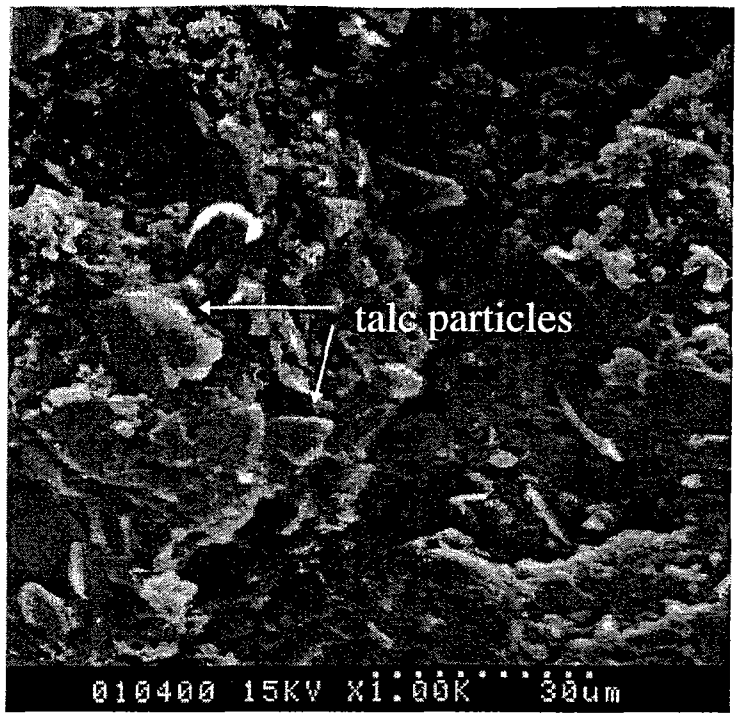

Figure 4.2.3 : SEM of an impact fractured specimen of PP/rubber/talc (3.6%) composite.

limited debonding of particles. These observations led to the conclusion that PP/rubber/talc system can be described as a continuum phase.

The dispersion of glass beads or paint particles into PP/rubber/talc composite showed a separated microstructure with poor interface between the disperse phase and the matrix. The fractrograph of the tensile specimens of glass filled PP/rubber/talc composite as in figure 4.2.4 showed relatively clean exposed surface of particles pointing to the fact that they have cleaved during the fracture process whereas the talc particles were still bonded to the matrix. Particle matrix interface decohesion also indicates the interfacial weakness over the matrix. Similar observation for paint particle dispersed composite is shown in figure 4.2.5. Poor interface was also observed in impact fractured specimens which would be presented in later sections (figure 4.4.36 and 4.4.37). So it can be concluded that large size and poor wetting of glass beads or paint particles to the matrix led to detrimental effect on tensile and impact properties for the present composites with the absence of any wetting or coupling agents.

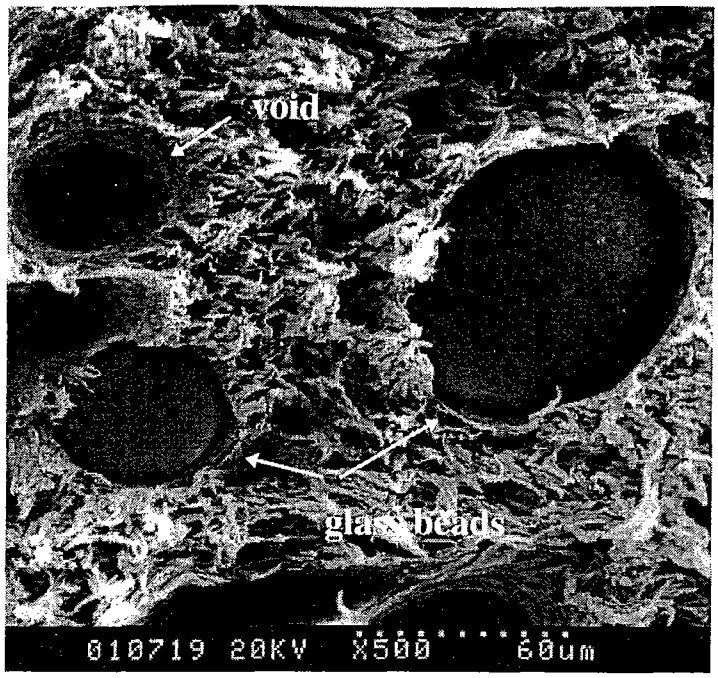

Figure 4.2.4 : SEM of a tensile fractured specimen of glass bead filled PP/rubber/talc composite.

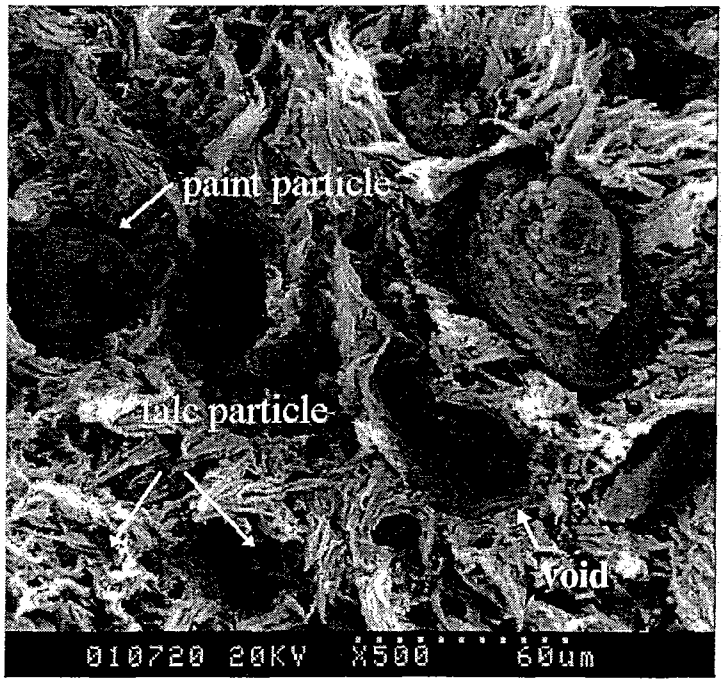

Figure 4.2.5 : SEM of a tensile fractured specimen of paint particle filled PP/rubber/talc composite.

4.3 Rheological Properties

The rheological properties of paint dispersed recycled material and blended samples of paint particle or glass bead dispersed PP/rubber and PP/rubber/talc systems were studied and are discussed in this section. As in recycled material, the paint fraction was found to be only upto 1 vol%, the maximum concentration level of paint phase added to the blends was kept to 5 vol%. The two different sized particles of paint used in the blends were smaller than the ones found in recycled material. The use of smaller size was intentional as to observe the effect of particle size on flow properties. The test temperature range chosen was around the processing conditions of these materials. The small change of filler particle concentration, size and temperature showed limited variation in rheological properties. However, the result of the steady shear and oscillatory measurements of these systems has been useful in understanding how rheology and therefore processing is likely to be affected by these variables.

4.3.1 Steady shear measurements

4.3.1.1 Base material and melt filtered material

The steady shear measurements were performed on the commercial grade bumper material, Epalex 7095 (virgin material), the two batches of painted material with dispersed paint phase (batch 1 and 2) and the recycled ground painted bumper material (batch 3) (unfiltered and melt filtered). The effect of filtration and the presence of paint phase on the polymer matrix was observed in the temperature range of 190-240°C.

Figure 4.3.1 shows a typical plot of viscosity versus shear rate curves for the virgin material and batch 1 samples (unfiltered and filtered) at 190°C. No significant Newtonian plateau was observed for these materials at low shear rate region. The viscosity of the unfiltered material

was around 20% higher compared to the virgin material for the presence of 1.83% dispersed paint fraction. Similar observation was made by Miranda *et al.* (1994) where they worked

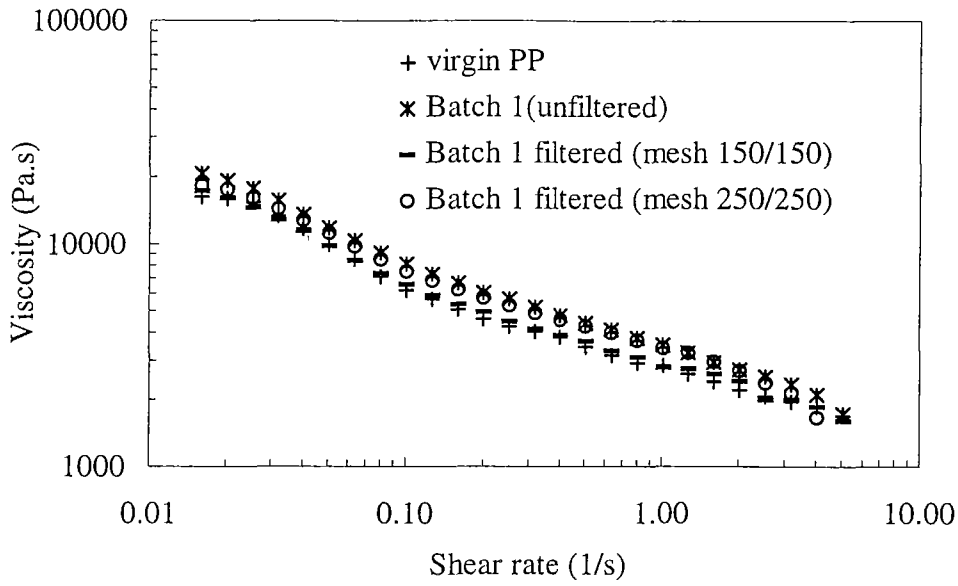

Figure 4.3.1 : Flow curves for virgin material and batch 1 samples containing 1.83% paint (unfiltered and filtered) at 190°C.

with paint dispersed recycled bumper material. With filtration process, the viscosity decreased below the unfiltered material. Also a decrease in viscosity was observed by around 5-20% for the filtered batches below the virgin material in the higher temperature range (220, 240°C) as shown in appendix D, figure D.1 and D.2. The low values for viscosity can be explained in two ways. Firstly, the filtered material had less paint content (0.92 and 0.94%) thus having lower viscosity as, generally, for composite materials increase in viscosity becomes smaller with decrease in filler concentration. Secondly, as these material went through a second heat history stage with filtration process, deterioration of material with chain scission of PP is possible thus lowering composite viscosity.

It was observed from the scanned images that the paint particles were more evenly dispersed after the filtration process. So particle aggregation was minimised to have an effect on

composite viscosity. Also, as noted from figure 4.3.1, the material passed through the mesh combination 150/150 had about 10% lower viscosity compared to those filtered through 250/250 mesh. Higher mesh number corresponds to low size of aperture opening. So a possibility for this reduced values can be that decreased aperture opening broke the paint particles to even smaller sizes so an increase in composite viscosity was observed as specific surface area of the paint particles increased in the later mesh combination (250/250) filtration process. The mean diameters of the paint particles were calculated from the scanned images after the filtration process through 150/150 and 250/250 meshes which gave values of 280 and 255 μm. As seen, smaller sized particles were attained using finer meshes as expected. Though the size variation was not dramatic, it might have some influence on lowering viscosity as stated above. Pukanszky *et al.*(1985) and Mayadunne *et al.*(1993) observed similar phenomena where they examined the effect of particle size on viscosity. Batch 2 and 3 material showed similar behaviour over the entire temperature range as shown in appendix D, figures D.3-D.6.

4.3.1.1.1 Flow behaviour model

Figure 4.3.2 shows the shear stress (τ) versus shear rate ($\dot{\gamma}$) curves for unfiltered batch 1 samples at 190, 220 and 240°C respectively. In the shear rate range of 0.05 to 1.27s^{-1} the material obeyed the power-law equation (4.3.1):

$$\tau = K'\dot{\gamma}^n \qquad ...(4.3.1)$$

where K' is a constant and n is the power law index. The effect of temperature on n values is shown in table 4.3.1 for the virgin and unfiltered samples. The low values of n (<1) indicated that the materials are pseudoplastic in nature, which decreased with increasing temperature. This increase in nonlinearity in the flow curve may be due to the occurrence of increased crosslinking in the paint with increase in temperature.

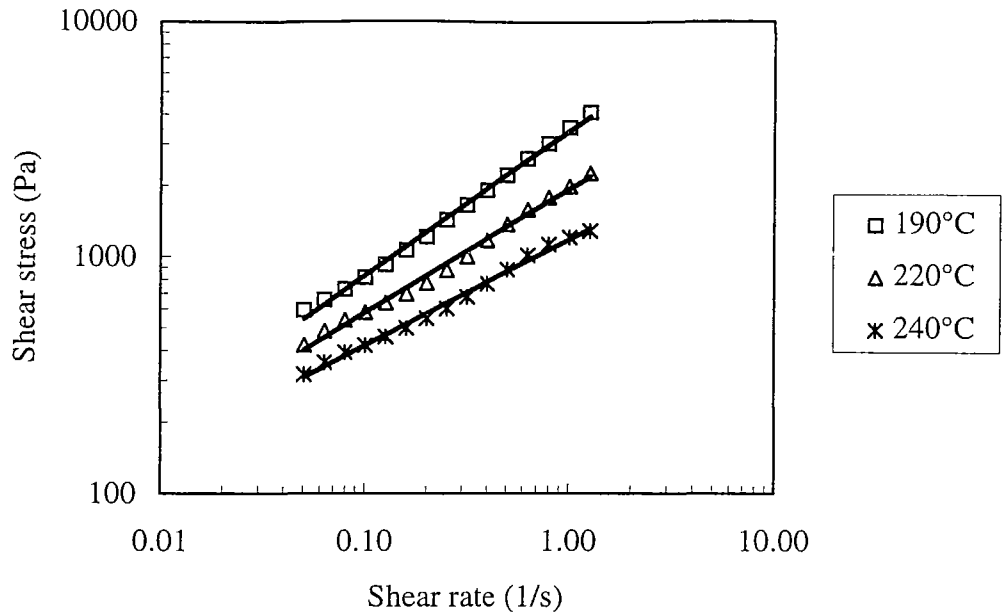

Figure 4.3.2 : Shear stress versus shear rate for unfiltered batch 1 samples at different temperatures.

Table 4.3.1 : Power-law index (n) at different temperatures for virgin and unfiltered materials.

Sample	Paint content	Temperature (°C)		
		190	220	240
Virgin material	-	0.607	0.515	0.515
Batch 1 (unfiltered)	1.83	0.612	0.524	0.448
Batch 2 (unfiltered)	2.48	0.588	0.529	0.461
Batch 3 (unfiltered)	1.00	0.590	0.507	0.431

4.3.1.1.2 Effect of temperature on shear viscosity

A typical example of the effect of temperature on shear viscosity can be seen from figure 4.3.3 for virgin and batch 1 (unfiltered and filtered) material at two different shear rates. It was observed that the viscosity values converged with increased temperature particularly for the paint dispersed samples.

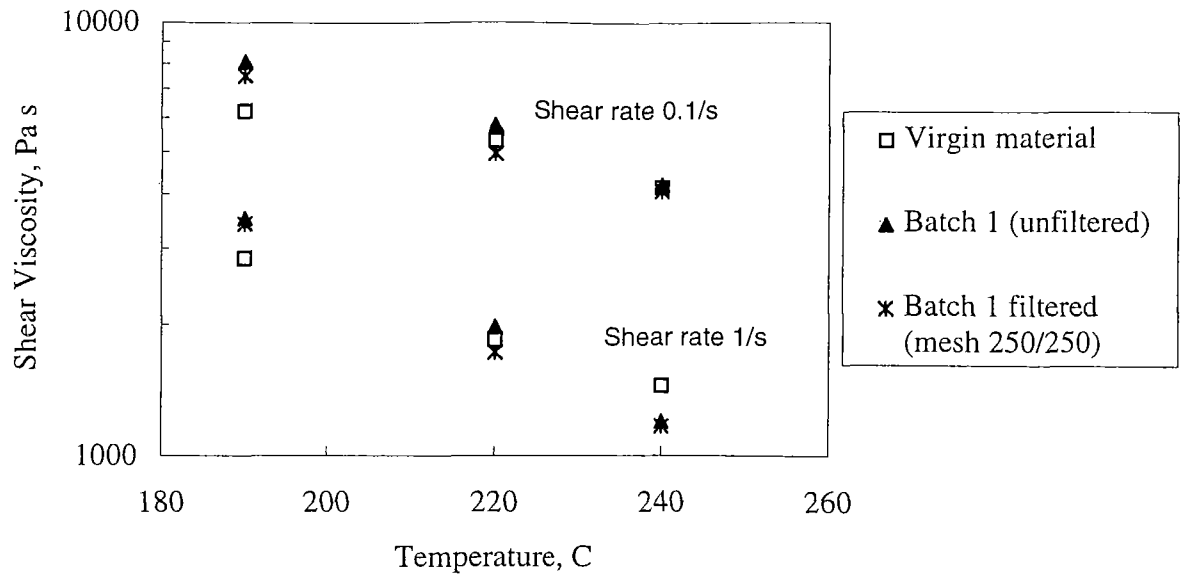

Figure 4.3.3 : Shear viscosity versus temperature at different shear rates for virgin and batch 1 sample.

The activation energy, E' (kJ/mol), for the materials were derived from the Arrhenius type relation valid for power law fluids as described in section 2.5.1.4 from the relation :

$$\eta = Ae^{E'/RT} \qquad ...(2.5.10)$$

From the gradient of the graph of logη versus ($1/T$) (K^{-1}) the activation energies of the above materials were estimated (figure 4.3.4) and are tabulated in table 4.3.2. At higher shear rates, the polymeric systems showed lower activation energies than at lower shear rates. Also the activation energies increased as the paint fraction increased in the unfiltered samples compared to the virgin material containing no paint which was more evident at lower shear rate range. The filtered samples had lower values than corresponding unfiltered samples which was again more apparent at low shear rate. No literature evidence was available for such system to explain the variation of activation energies which keeps the matter open for further investigation.

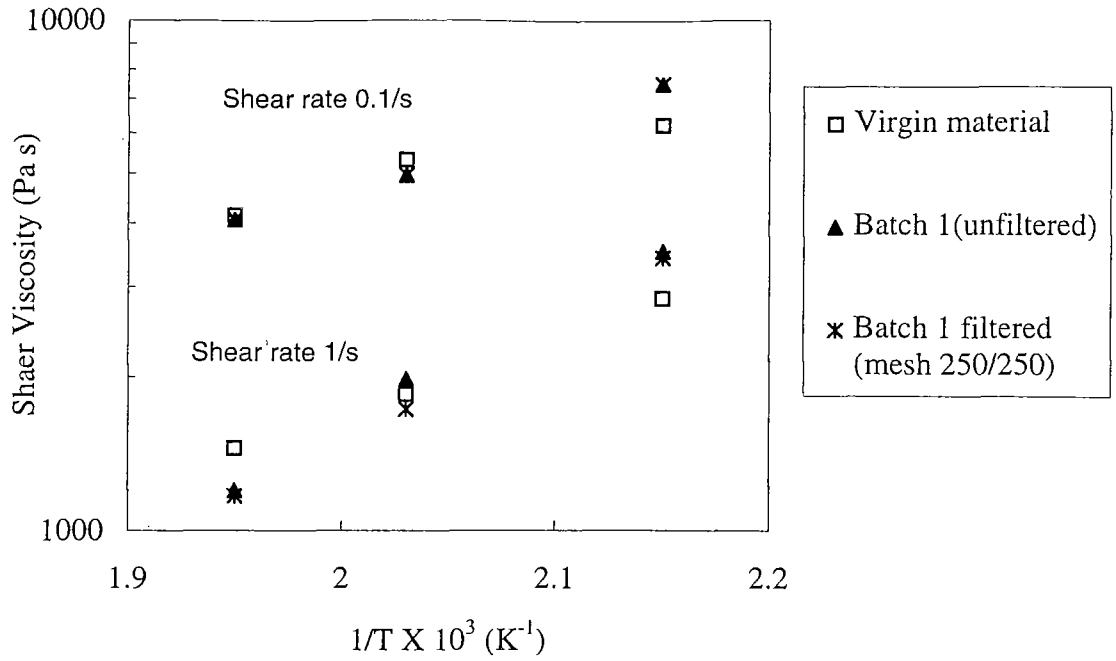

Figure 4.3.4 : Log (shear viscosity) versus reciprocal temperature at two different shear rates for virgin and batch 1 sample.

Table 4.3.2 : Activation energies (kJ/mol) for virgin, unfiltered and melt filtered samples at two different shear rates.

		Shear rate (s^{-1})	
Sample	paint content (%)	0.1	1.0
Virgin material (Epalex 7095)	-	84.12	58.63
Batch 1 (unfiltered)	1.83	162.01	96.82
Batch 1 filtered (mesh 250/250)	0.94	145.6	94.95
Batch 1 filtered (mesh 150/150)	0.92	121.5	74.55
Batch 2 (unfiltered)	2.48	181.3	93.2
Batch 2 filtered (mesh 250/250)	1.07	169.5	89.8
Batch 2 filtered (mesh 150/150)	1.4	145.3	81.4
Batch 3 (unfiltered)	1.00	99.7	70.4
Batch 3 filtered (mesh 250/250)	0.52	59.6	57.4
Batch 3 filtered (mesh 150/150)	0.49	56.9	48.2

4.3.1.2 PP/rubber based composites

The steady shear measurements of PP/rubber based composites dispersed with glass beads or paint particles were performed in the temperature range of 180-220°C. Nitrogen atmosphere was used for the tests to avoid any degradation of the material. The effect of particle concentration, particle size, particle geometry and temperature effect on viscosity was examined for the composites.

4.3.1.2.1 Effect of particle concentration

The shear viscosity of glass bead filled PP/rubber composites was slightly higher over the PP/rubber matrix values, which was more significant at lower shear rate (0.03 s^{-1}). At higher shear rate (1 s^{-1}), the flow curves of the filled composites approached the curve of base material (figure 4.3.5).

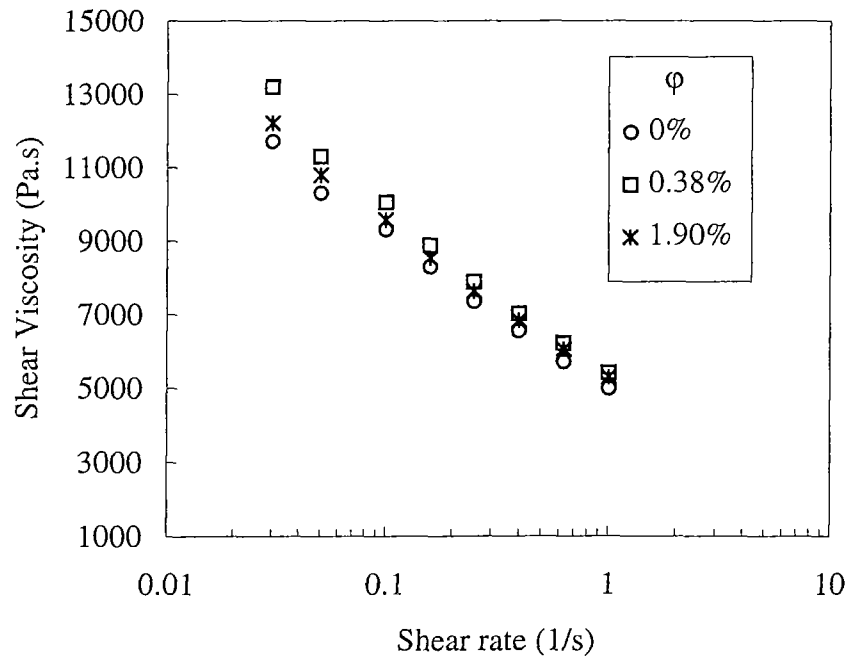

Figure 4.3.5 : Steady shear viscosity versus shear rate for glass bead filled PP/rubber composites at 180°C.

Similar behaviour was observed for paint dispersed PP/rubber composites where the variation was less significant as shown in figure 4.3.6.

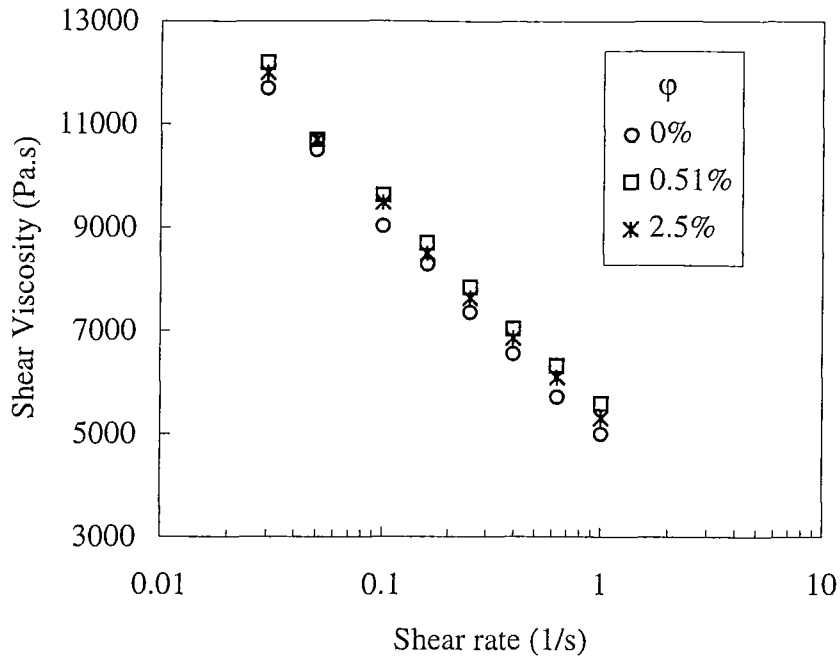

Figure 4.3.6 : Steady shear viscosity versus shear rate for paint particle (63 μm) filled PP/rubber composites at 180°C.

Increase in shear viscosity with filler was observed by many others for composite materials. Kim *et al.* (1993) showed increase in viscosity for ternary blends of PP/rubber/$CaCO_3$ over the base material when the dispersion of $CaCO_3$ in the matrix was good. It was also observed that the viscosity of lower concentrated glass bead or paint particle filled material were slightly higher (~4%) compared to the higher concentrated one but the variation was within experimental error. The small variation in viscosity with small change in concentration of dispersed phase was usual as in these cases the flow behaviour is dominated by the matrix rather than the dispersed particles. This can be explained by Einstein's equation (2.5.1) relating filler fraction and composite and matrix viscosity. As seen from the equation:

$$\eta_r = 1 + 2.5\varphi \qquad \text{...(2.5.1)}$$

with dilute suspensions $\varphi \rightarrow 0$, and composite viscosity tends to matrix viscosity which is similar to the present case. At high temperature the composites behaved in similar fashion. The flow curves for glass bead and paint particle dispersed PP/rubber composites at 190 and 220°C are given in appendix D, figures D.7-D.10.

4.3.1.2.2 Effect of particle size and particle size distribution

Two different sized paint particles were studied in the present investigation with mean particle diameters of 135 and 63 μm respectively. Figure 4.3.7 shows the change in viscosity with shear rate for the two sized paint particles dispersed in PP/rubber at 180°C at a constant volume fraction of 2.5%.

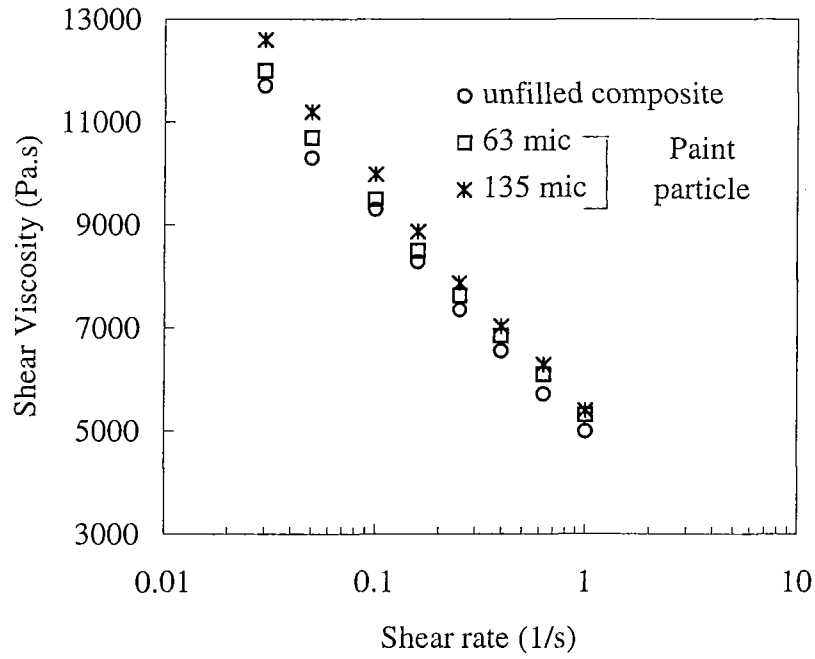

Figure 4.3.7 : Steady shear viscosity versus shear rate for 2.5 vol% paint particle filled PP/rubber composites at 180°C.

As observed from the data, the larger sized particles had about 8% higher values over the unfilled matrix but only about 5% increase in viscosity was observed from smaller to the

larger sized particle. This increased value was negligible as around 2.5% error was reported in the measurements. Poslinki *et al.*(1988) also observed insignificant effect on viscosity with variation of particle size with concentration < 20 vol%. The average size of glass spheres used in their investigation had the size of 15 and 78 μm diameter. So it can be concluded that for these dilute concentrated composites, variation of particle size has minimum effect on viscosity. Figure D.11 in appendix D shows the effect of particle size on shear viscosity at 190 and 220°C which also depict negligible variation.

4.3.1.2.3 Effect of particle geometry

As the real systems were dispersed with irregular paint particles it was worthwhile to investigate the effect of particle geometry by studying the composites dispersed with spherical glass beads.

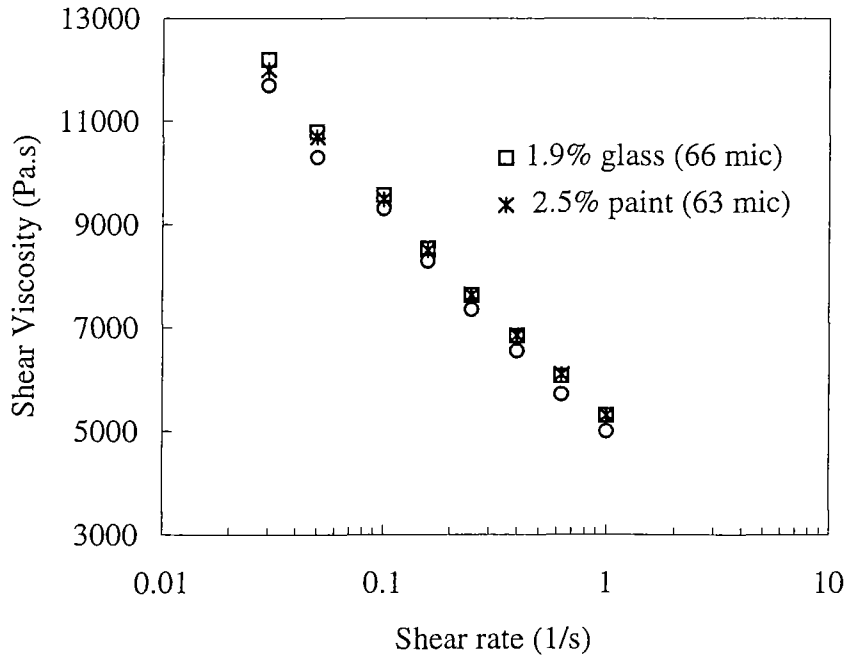

Figure 4.3.8 : Steady shear viscosity versus shear rate for glass bead and paint particle filled PP/rubber composites at 180°C.

Figure 4.3.8 shows the flow curves for 2.5 vol% paint particle (63 μm) and 1.9 vol% glass bead (66 μm) filled PP/rubber composites at 180°C which corresponds to 5 wt% for both. As observed, both the composites showed similar values for viscosity. Though non-spherical particles usually show higher viscosity compared to spherical particles, this was not the case in this situation for low concentrated composites. Figure D.12 in appendix D shows the effect of particle geometry at higher temperatures.

4.3.1.2.4 Effect of temperature

All the tests were performed in the temperature range of 180-220°C to find the temperature effect on viscosity for the composites. The influence of temperature on shear viscosity can be seen from figure 4.3.9 for paint dispersed PP/rubber composites. As observed, increasing temperature shifted the flow curves down retaining their original shape.

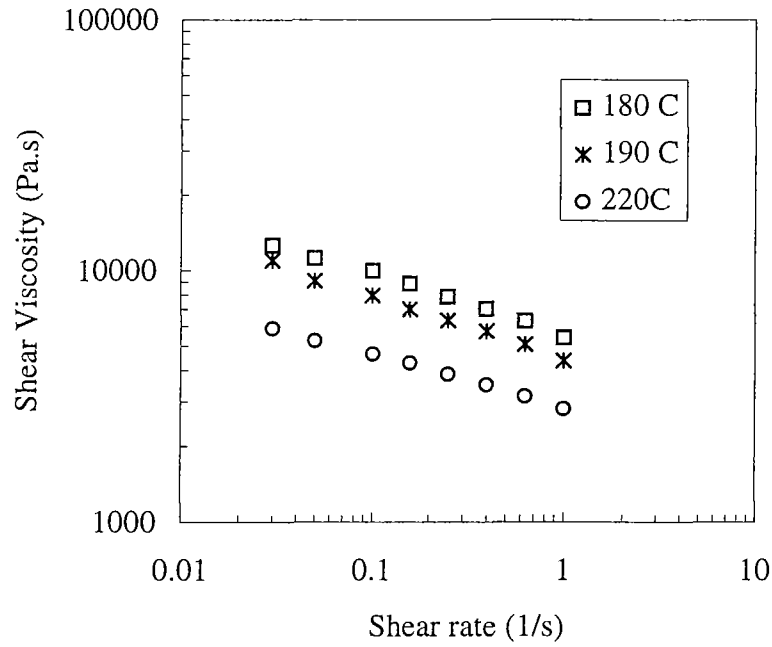

Figure 4.3.9 : Flow curves for 2.5% paint (135 μm) dispersed PP/rubber composites at different temperatures.

The activation energies for the composites were derived from the slope of the graph of logη versus ($1/T$) (K^{-1}) and are tabulated in table 4.3.3. An example of such a curve is given in figure 4.3.10 for shear rates 0.1 and 1/s.

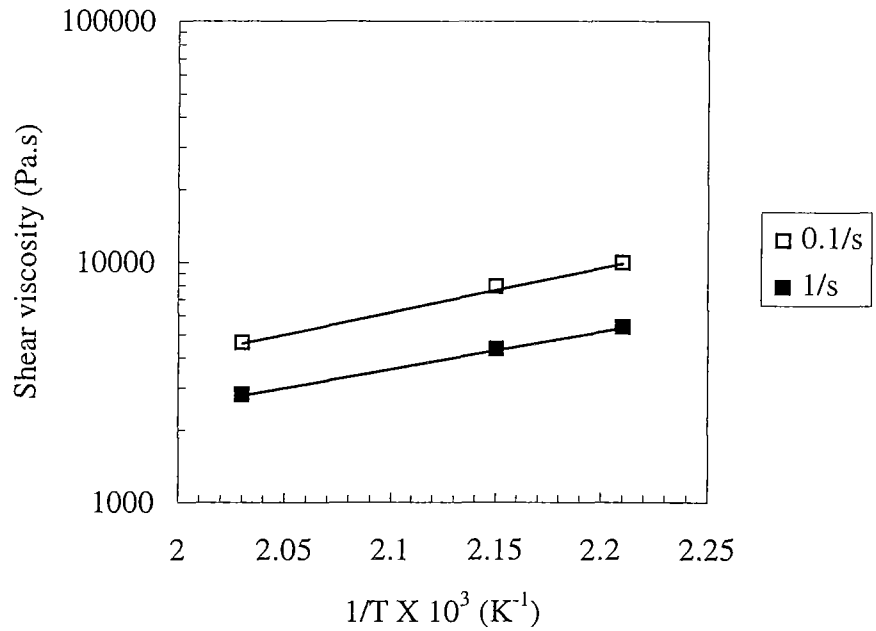

Figure 4.3.10 : Log (shear viscosity) versus reciprocal temperature at two different shear rates for 2.5% paint (135 μm) dispersed PP/rubber composites.

As seen from the table 4.3.3, the activation energy of the filled composites is higher compared to unfilled PP/rubber composite implying that addition of filler has some effect on temperature dependence of viscosity. This means that particle-particle interaction or particle-polymer interaction for the filled composites are affected by temperature. Also the activation energy values at lower concentration levels were somewhat higher compared to the higher concentration level implying that particle-polymer interaction is more predominant in the first case. This was also evident from their flow curves where lower concentrated composites showed slightly higher viscosity values over the entire temperature range. Different sized paint particles also showed variation in activation energies but no conclusions can be drawn from the available results as the data is limited showing no particular trend. Mayadunne *et*

al.(1996) reported similar decrease in activation energies with increasing filler volume fraction for smaller sized ground rubber tyre particle (90-125 μm and 45-63 μm) filled LDPE. No such variation was observed for larger sized particles (180-125 μm). But no evidence in literature was revealed to explain such variation in activation energy with change in filler concentration and particle size keeping the matter unclear and thus requiring further investigations.

Table 4.3.3 : Activation energies (kJ/mol) for glass bead and paint particle dispersed PP/rubber composites at two different shear rates.

Material	Shear rate (s^{-1})	
	0.1	1
PP/rubber	218.54	98.47
Glass composites		
66 μm, 0.38% (v/v)	238.33	114.5
66 μm, 1.9% (v/v)	224.58	106.1
Paint composites		
63 μm, 0.51% (v/v)	225.46	125.3
63 μm, 2.5% (v/v)	222.1	115.1
135 μm, 0.51% (v/v)	272.18	112.74
135 μm, 2.5% (v/v)	244.07	117.48

4.3.1.3 PP/rubber/talc based composites

A comparison between shear measurements of the PP/rubber and PP/rubber/talc base materials was performed to find the effect of talc on melt viscosity before the composites were tested with the addition of a second dispersed phase. The concentration levels of talc added to the PP/rubber composites were 0.34%, 1.7% and 3.6% (vol%) respectively. Figure 4.3.11 shows the effect of talc on viscosity at 180°C. As seen from the graph, at lower concentrations, the presence of talc had negligible effect on the melt viscosity of the PP/rubber composites. But as the concentration was increased upto 3.6% (v/v) (i.e. 10% wt/wt), an increase in viscosity was observed specially at the lower shear rate range, similar to many other filled systems. At high shear rates, all the flow curves for talc filled composites approached the curve for the unfilled PP/rubber matrix. This phenomena was explained by Ottani *et al.* (1988) where they observed the same behaviour for $CaCO_3$ filled LDPE matrix.

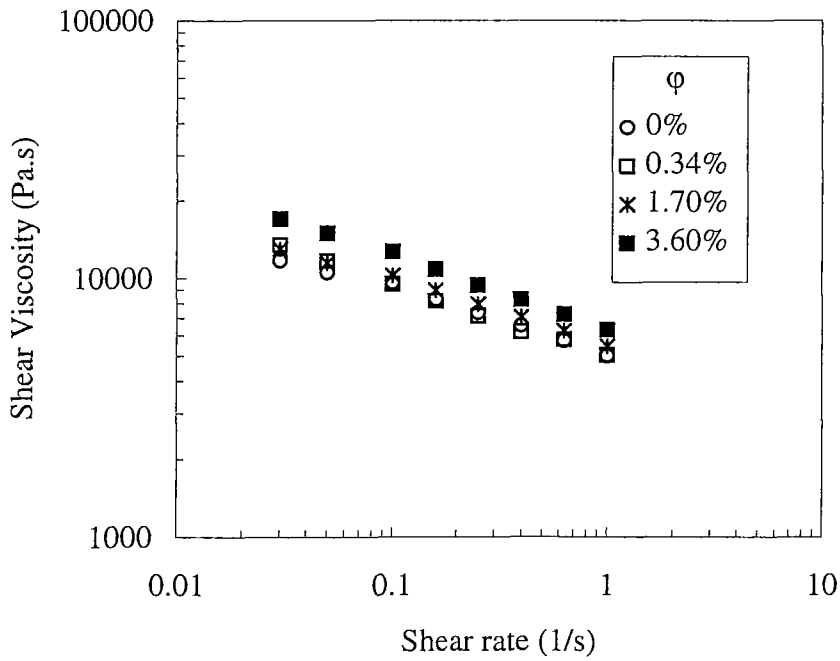

Figure 4.3.11 : Steady shear viscosity versus shear rate for PP/rubber/talc composites at 180°C.

flow exist between the filler and the macromolecules. Similar behaviour was found for the whole temperature range. As the highest concentration level of 3.6% talc was used as a standard amount for all the PP/rubber/talc composites hereafter, it is worth noting that an increased viscosity would be expected for the composites over the PP/rubber ones.

The steady shear measurements of PP/rubber/talc based composites dispersed with glass and paint particles were then performed in the temperature range of 180-220°C. Nitrogen atmosphere was used for the tests to avoid any degradation of the material. The effect of particle concentration, particle size and particle size distribution, particle geometry and temperature effect on viscosity was examined for the composites.

4.3.1.3.1 Effect of particle concentration

The flow curves of glass bead filled PP/rubber/talc composites are shown in figure 4.3.12. At lower shear rates (upto $0.05s^{-1}$), the 0.38% glass filled composite had viscosity values even lower than the unfilled base material which was apparent over the entire temperature range. With increasing shear rate, the flow curves converged. Though it was considered that the dispersed phase is only the glass beads but actually the composite would behave as a bimodal system with the presence of talc particles. It is known that the composite viscosity decreases for polydisperse systems. Also, the diameter ratio of small to large particles and the volume fraction of the smaller size particles in the total solid concentration are two important parameters characterising a bimodal system. No reduction in relative viscosity is observed when the ratio of particle size is ~ 0.1 as small particles can easily migrate through the

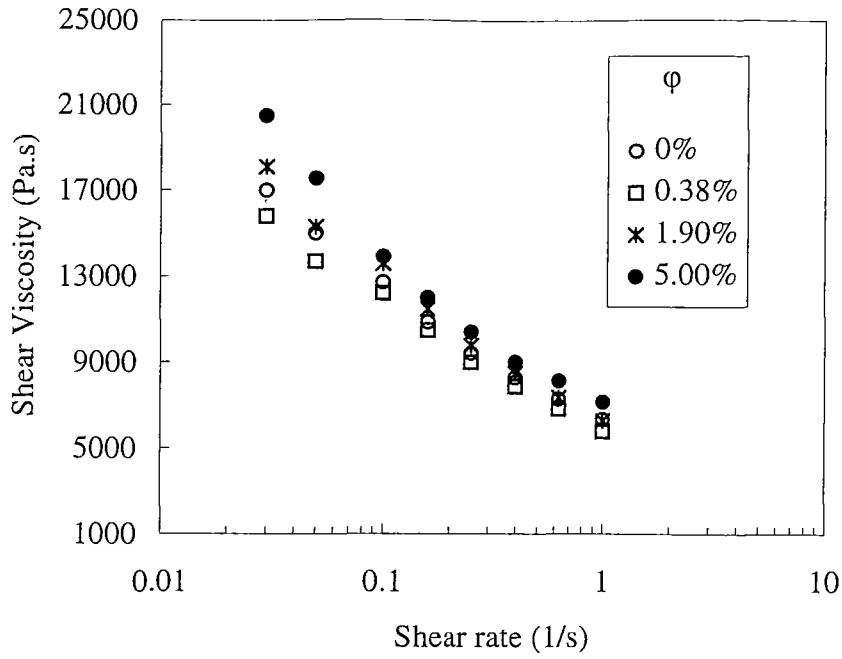

Figure 4.3.12 : Steady shear viscosity versus shear rate for glass bead filled PP/rubber/talc composites at 180°C.

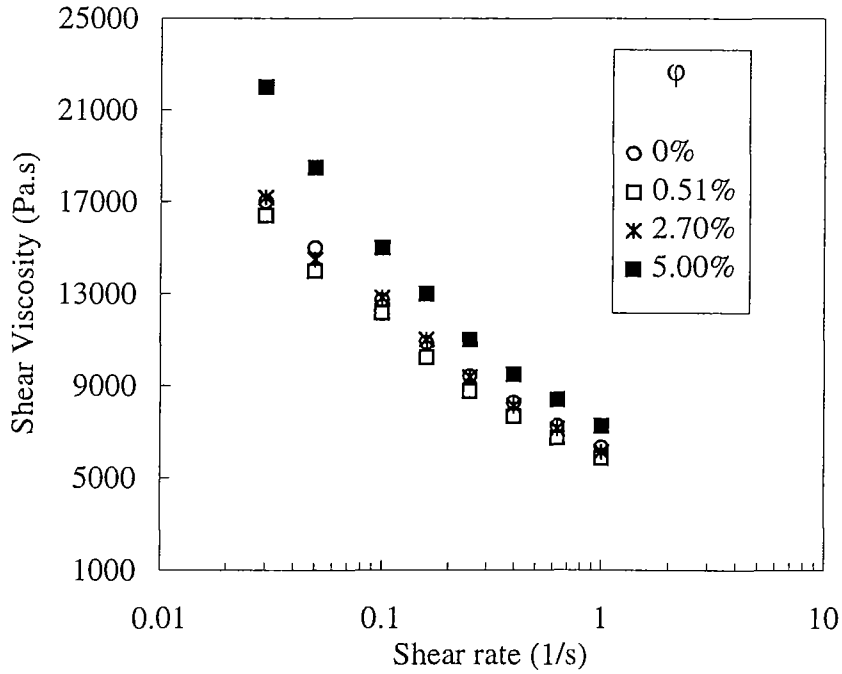

Figure 4.3.13 : Steady shear viscosity versus shear rate for paint particle (63 μm) filled PP/rubber/talc composites at 180°C.

interstices of large particles. Lastly an optimum level of smaller particles are necessary in total filler concentration to minimise the viscosity value (Polinski *et al.*, 1988). Considering all these points, lower viscosity values for 0.38% glass filled composites compared to the PP/rubber/talc composite can be justified. With increasing volume fraction of larger sized glass beads an increase in viscosity occurred specially at lower shear rate range indicating influence of talc diminishes slowly. But the overall increase in viscosity for 5% glass filled system was only about 25-15% over the unfilled system showing less effect of concentration on viscosity for dilute suspensions. Similar behaviour was observed for paint dispersed PP/rubber/talc composites as shown in figure 4.3.13. Figures D.13-D.16 in appendix D show the concentration effect of the dispersed systems at higher temperatures.

4.3.1.3.2 Effect of particle size

Figure 4.3.14 shows the effect of particle size on the shear viscosity of paint dispersed composites at 180°C at a constant volume fraction of 2.7%. As observed larger sized particles showed slightly higher viscosity values over the smaller sized and unfilled PP/rubber/talc composites at low shear rate regions. The smaller particle dispersed system had similar viscosity values as the unfilled system. The explanation already used in the earlier section can also be used to describe the behaviour here. Considering these composites as bimodal systems, it is found that the diameter ratio for the smaller sized particle (63 μm) to talc (8 μm) is 0.126. So theoretically a reduction in composite viscosity can be achieved. But for the larger sized particle (135 μm) the diameter ratio is 0.06 and reduction in composite viscosity would not be effective as a bimodal system as it is less than 0.1. Rather, it would behave as a unimodal system thus showing increased viscosity as evident from the experimental observation. Figure D.17 shows the negligible effect of size variation of viscosity at higher temperatures.

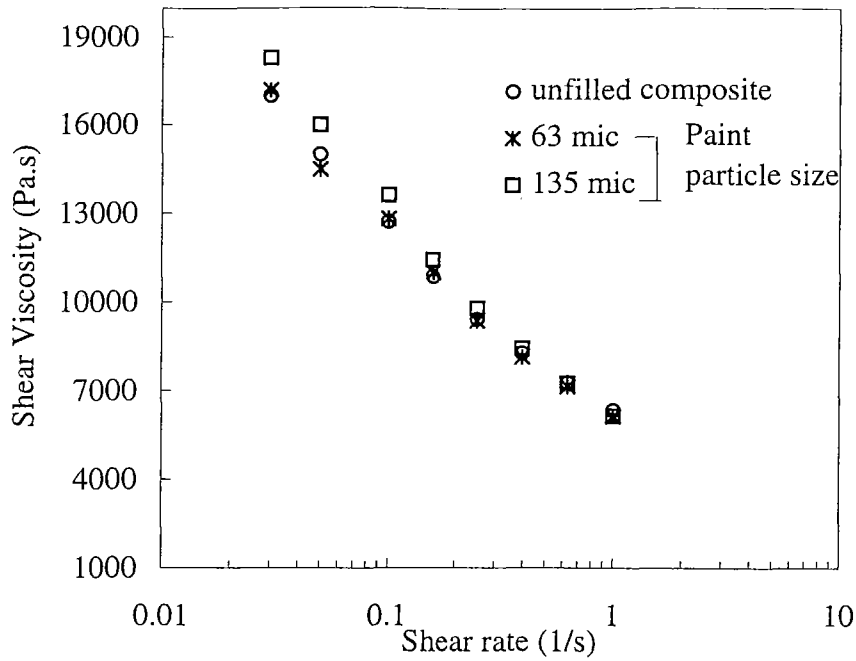

Figure 4.3.14 : Steady shear viscosity versus shear rate for different sized paint particle filled PP/rubber/talc composites at 180°C.

4.3.1.3.3 Effect of particle geometry

Figure 4.3.15 shows the flow curves for 5% paint particles (63 μm) and glass bead (66 μm) filled talc based composites at 180°C. The normal scale plots showed that the irregular sized paint particles had slightly higher viscosity values (at most 12%) compared to the spherical glass bead filled system. This was in accordance with results published in literature (Kitano *et al.*, 1981; Tsai *et al.*, 1992) where it was observed that composite viscosity increases for non-spherical particles. But this variation was only noticed when the concentration reached the 5% level. For lower concentration of fillers, the change in viscosity values for the two different shaped particles was insignificant. Figure D.18 in appendix D shows the effect of geometry on viscosity at higher temperatures.

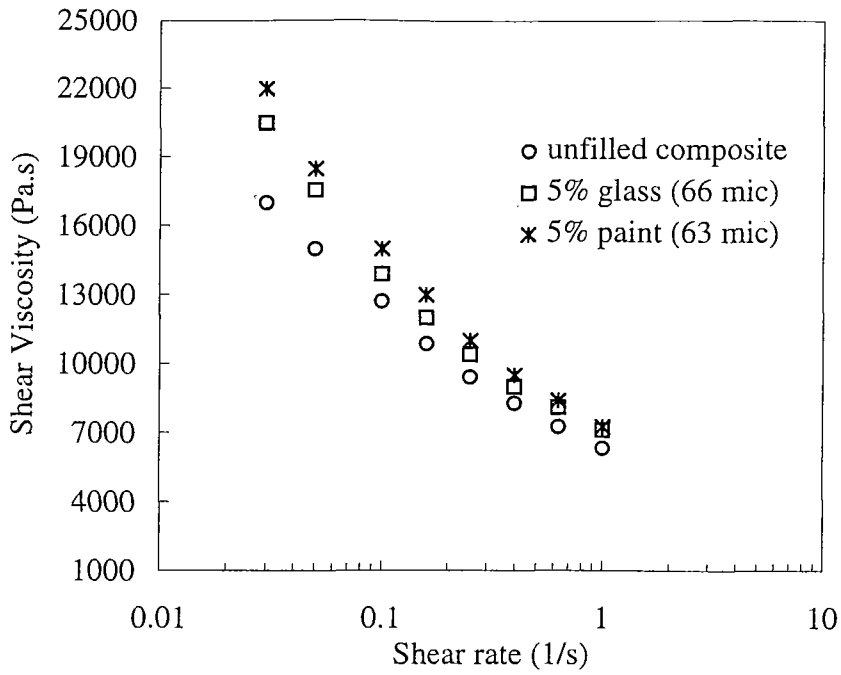

Figure 4.3.15 : Steady shear viscosity versus shear rate for glass bead and paint particle filled PP/rubber/talc composites at 180°C.

4.3.1.2.4 Effect of temperature

Figure 4.3.16 shows a typical plot of effect of temperature on viscosity with changing shear rates. The flow curves were shifted downwards with increase in temperature but retained their nature of gradual decreasing value as shear rate increased.

The activation energies for the composites were derived from the slope of the graph of logη versus ($1/T$) (K^{-1}) and are tabulated in table 4.3.4. Figure 4.3.17 is a typical example of such a curve for shear rate 0.1 and 1/s for a paint dispersed composite. The activation energy of PP/rubber/talc composite was much higher compared to the PP/rubber composite (324.6 kJ/mol and 218.54 kJ/mol respectively) implying that greater interaction was present between talc and PP/rubber system. Also, a different scenario was noticed for glass bead or paint particle dispersed composites where lower activation energy was obtained for low

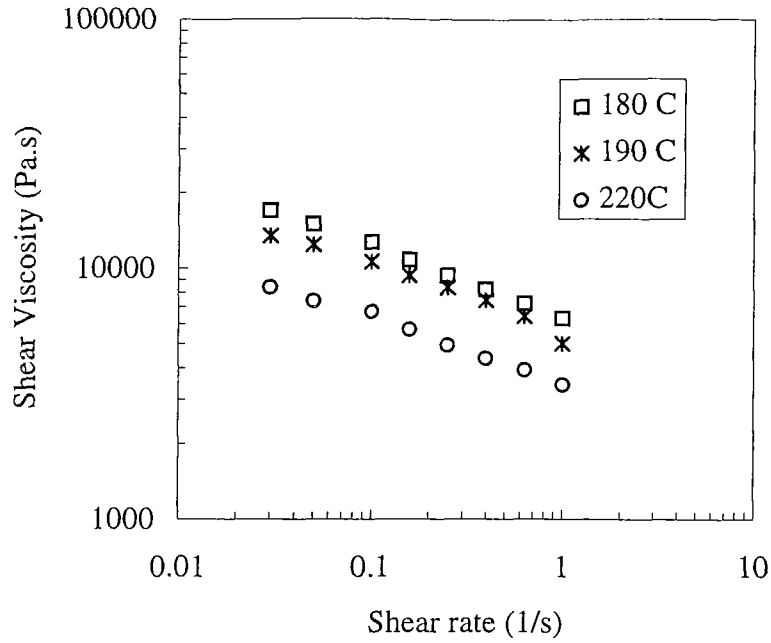

Figure 4.3.16 : Flow curves for 2.7% paint (135 μm) dispersed PP/rubber/talc composites at different temperatures.

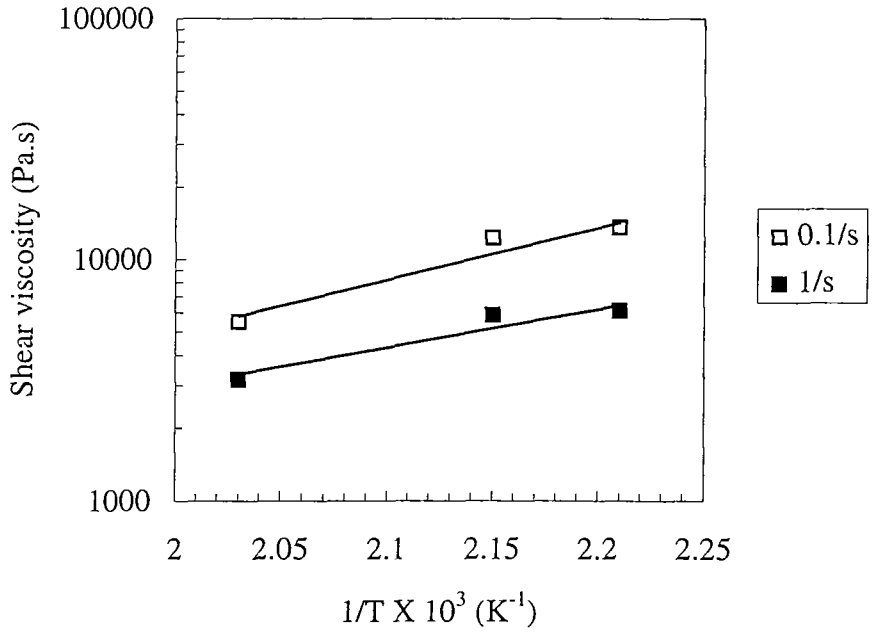

Figure 4.3.17 : Log (shear viscosity) versus reciprocal temperature at two different shear rates for 2.7% paint (135 μm) dispersed PP/rubber/talc composites.

concentrated suspensions compared to unfilled matrix and the high concentration level of dispersed phase. This might be related to the reduced viscosity of the composites for polydisperse systems at low concentration level of dispersed phase. But no explanation was found for this kind of behaviour in the literature in terms of activation energy and further study is required to understand the system properly.

Table 4.3.4 : Activation energies (kJ/mol) for glass bead and paint particle dispersed PP/rubber/talc composites at two different shear rates.

Material	Shear rate (s^{-1})	
	0.1	1
PP/rubber/talc (3.6%)	324.6	129.65
Glass composites		
0.38% (v/v)	301.88	103.42
1.9% (v/v)	360.27	131.93
Paint composites		
63 μm, 0.54% (v/v)	322.16	127.08
63 μm, 2.7% (v/v)	347.4	144.4
135 μm, 0.54% (v/v)	328.1	122.93
135 μm, 2.7% (v/v)	387.49	143.91

Looking at the results for these systems, a general conclusion can be drawn that the flow behaviour of paint dispersed systems is not greatly affected by the presence of small volume fraction of dispersed phase over the processing temperature range. Also, the effect of filler concentration on viscosity is most pronounced at low shear rates, where the flow behaviour is restricted by the presence of dispersed phase. Keeping this in mind, the present tests were performed at the lower shear rate range (upto 1/s) where no significant variation in viscosity was observed. Then tests at higher shear rate range would also show small variation in

viscosity between filled and unfilled matrices. So, it can be demonstrated that, the dispersed systems containing paint particles can easily be used in processing such as extrusion or injection moulding where the shear rate is over 10/s. Moreover, the maximum volume fraction of paint examined here was 5 vol%, although the concentration of paint in the recycled material is unlikely to exceed 1 vol%. This indicates that, the recycling operations would not pose any difficulty in the processing of these materials.

4.3.2 Oscillatory shear measurements

Oscillatory shear measurements were performed on PP/rubber and PP/rubber/talc based composites only.

4.3.2.1 Thermal stability of composites

To illustrate thermal stability of the test samples, a time sweep was performed over the entire test temperature range of 180°-220°C for selective composites. The frequency and stain were kept constant at 10 rad/s and 5% respectively and the test was carried out under nitrogen blanket for an hour. Figure 4.3.18 shows a typical plot of the most sensitive rheological function, storage modulus (G') versus time for PP/rubber/talc composite at 180° and 220°C. It was observed that G' increased by 4 and 13% respectively at the two temperatures over the entire test period. Since the frequency sweeps carried on later lasted for a time $t \leq 10$ minutes or 600 seconds , the samples were considered thermally stable within the experimental time limit. Time sweep was also carried out for composites dispersed with glass and paint particles showing thermal stability within the experimental time limit.

Similar effect was observed by Utracki *et al.* (1984) for PP/mica systems. At low filler concentration, the decrease in G' was small for time $\leq$ 40 minutes but at higher mica

concentration, a rapid decrease in G' was noted during the same period. After 40 minutes, the reduction in value was slower, occurring approximately at the same rate for all samples. They explained the phenomena for higher concentration level as an ordering of mica flakes in the sample.

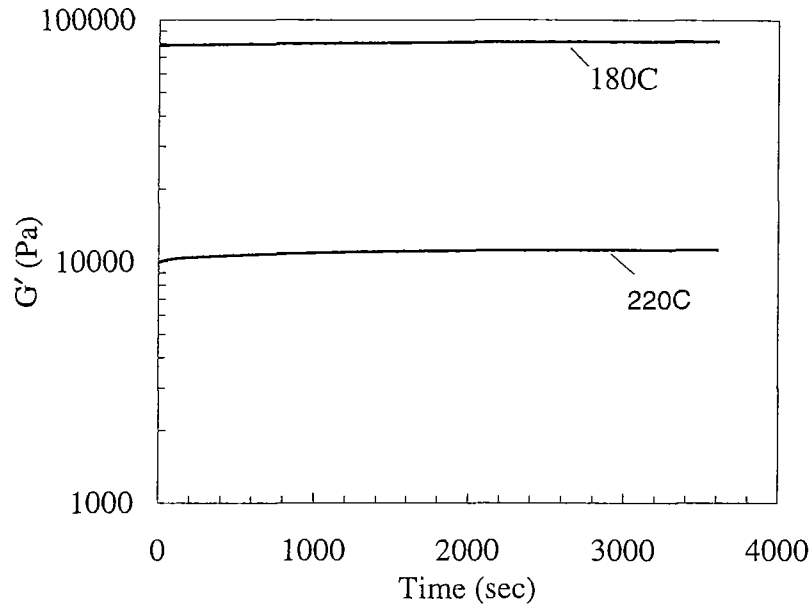

Figure 4.3.18 : Time sweep of PP/rubber/talc composite at frequency 10 rad/s and 5% strain.

4.3.2.2 Strain dependence of storage and loss moduli for PP/rubber and PP/rubber/talc composites

The most important step in oscillatory measurement is the determination of the linear viscoelastic region by performing strain sweeps. The linear region is the region in which the deformation is small enough for the dynamic moduli and dynamic viscosity to be independent of the deformation. Usually, the rheological properties of a viscoelastic material are independent of strain up to a critical strain level (γ_c), beyond which the material's behaviour is nonlinear. The effect of strain on storage modulus at 180°C for PP/rubber/talc system is shown in figure 4.3.19 over several frequencies. As frequency increased, the critical strain value decreased. So a critical strain of 4 ~ 5% was chosen for frequency sweep as at this level

the highest frequency of 100 rad/s also showed a linear region. For the temperature of 220°C, no linear region was observed for the strain over the frequency value of 60 rad/s. So the highest frequency that can be used in that temperature was 60 rad/s.

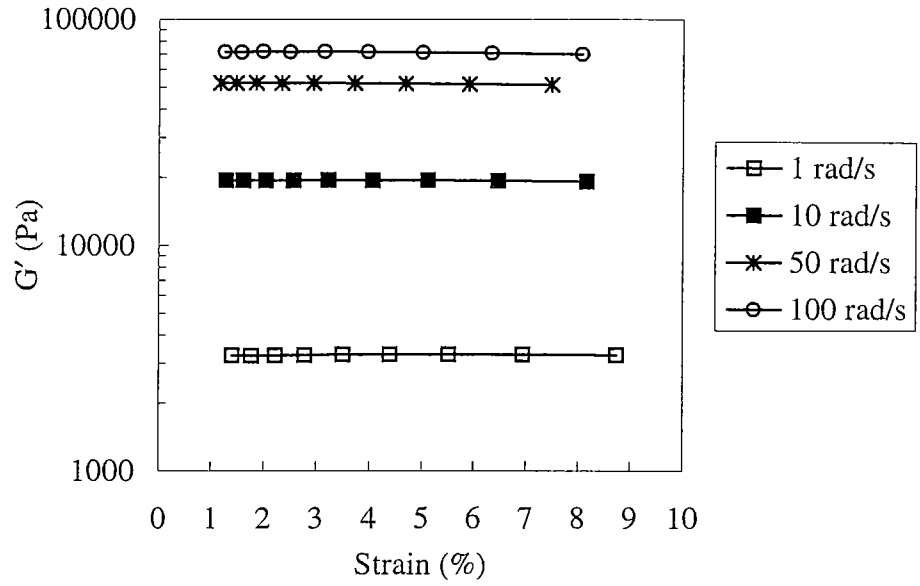

Figure 4.3.19 : Strain sweep of PP/rubber/talc composites at 180°C at different frequencies.

4.3.2.3 Effect of concentration on storage and loss moduli for PP/rubber and PP/rubber/talc composites

For the different particle sized paint dispersed PP/rubber composites, the storage and loss moduli at a lower concentration level (0.51%) were slightly lower than that for the unfilled matrix, whereas at a higher concentration level (2.7%) the loss and storage moduli were higher than those for the unfilled system (figure 4.3.20). Similar behaviour was observed for glass filled systems as well over the entire temperature range (figure D.19).

For paint dispersed PP/rubber/talc composites, the lower concentrated filled system (0.51%) showed decreased value below the unfilled system and the higher concentrated filled systems (2.7 and 5%) showed increased values. Figure 4.3.21 is a typical example of such a composite.

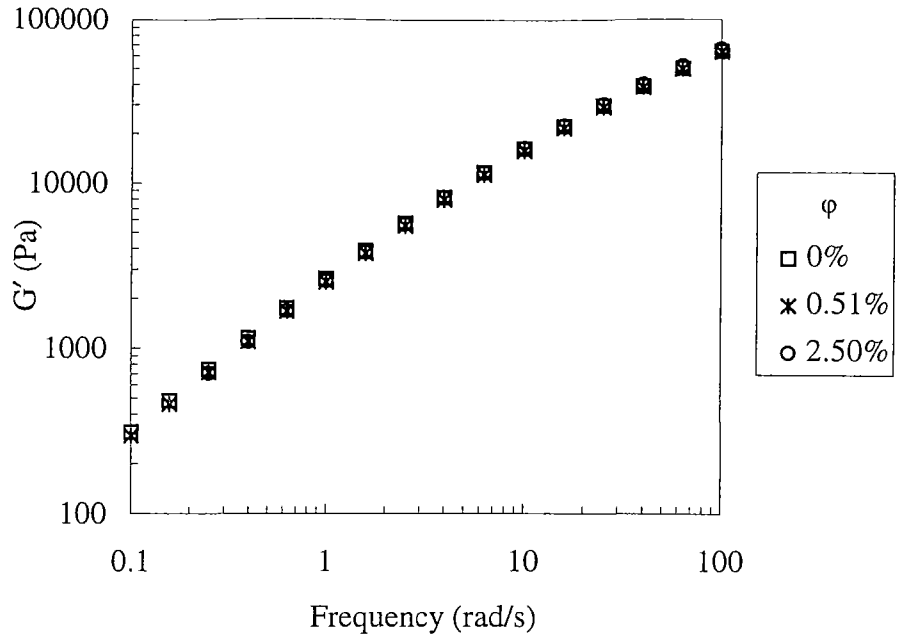

Figure 4.3.20.a : Storage modulus of paint particle (135 μm) filled PP/rubber composites at 180°C and 5% strain.

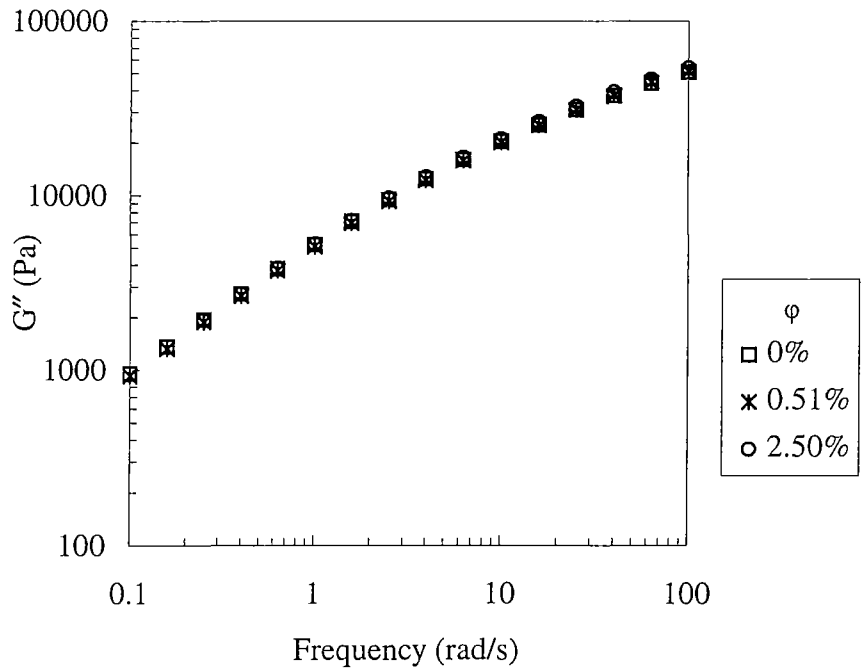

Figure 4.3.20.b : Loss modulus of paint particle (135 μm) filled PP/rubber composites at 180°C and 5% strain.

It seems from the experimental data that there is a critical concentration level of the dispersed phase at which the storage and loss moduli will become equal to that of the unfilled composite. The dispersed phase concentration below this critical concentration level is not commonly used in polymer composites. Similar behaviour was cited by Papadolopous (1995) for rubber crumb filled LDPE composites below the critical level of 24% filler. The phenomena was explained as due to improved dispersion of rubber crumb in polymer matrix for the presence of talc particles and inter layer slip phenomena caused by incompatible filler coupling agent. Utracki and Fisa (1984) also noted similar behaviour for mica/PP, $CaCO_3$/PE and $CaCO_3$/PP systems. As the present systems also had dispersed talc particles, it is reasonable to assume that the talc particles aided in improved dispersion of the second dispersed phase at the lower concentration level. The glass bead dispersed PP/rubber/talc composites showed similar nature as shown in appendix D, figure D.20.

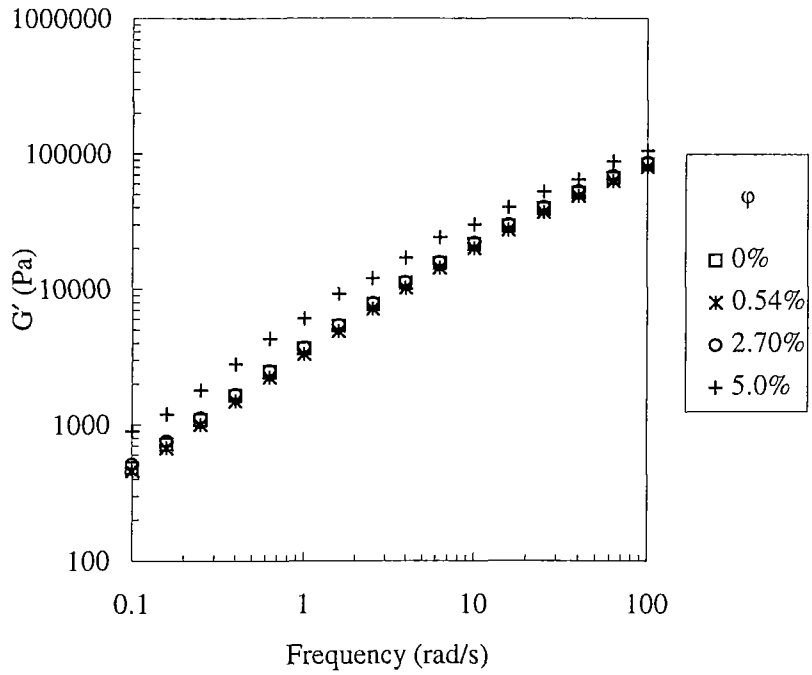

Figure 4.3.21.a : Storage modulus of paint particle (63 μm) filled PP/rubber/talc composites at 180°C and 5% strain.

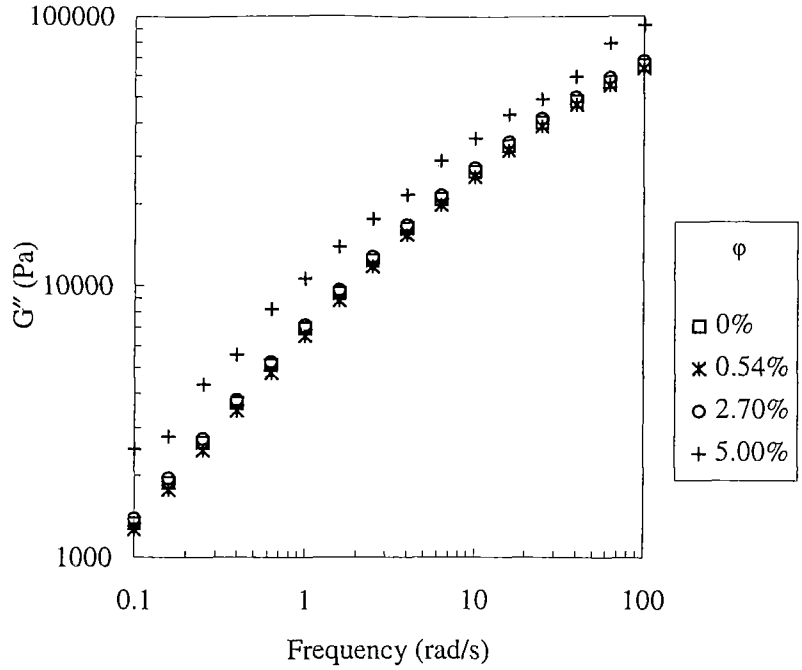

Figure 4.3.21.b : Loss modulus of paint particle (63 μm) filled PP/rubber/talc composites at 180°C and 5% strain.

4.3.2.4 Effect of particle size on storage and loss moduli for PP/rubber and PP/rubber/talc composites

The effect of particle size on storage and loss moduli for PP/rubber/talc systems at 180°C is shown in figure 4.3.22 for two different sized paint particles used in this investigation showing marginal difference in the values. Similar observation was cited by Li and Masuda (1990) where they showed that viscoelastic behaviour is determined mainly by particle content, not by particle size, when the content is low (< 20%). Also, small particles with large surface area tends to form agglomerated structure which increases the moduli values dramatically. In this case, as the mean size of the particles used was quite high (135 and 63 μm), the particles would have less tendency to form agglomerates thus influencing the moduli values. Similar behaviour was observed at higher temperature as well as for PP/rubber composites as shown in appendix D, figures D.21 and D.22.

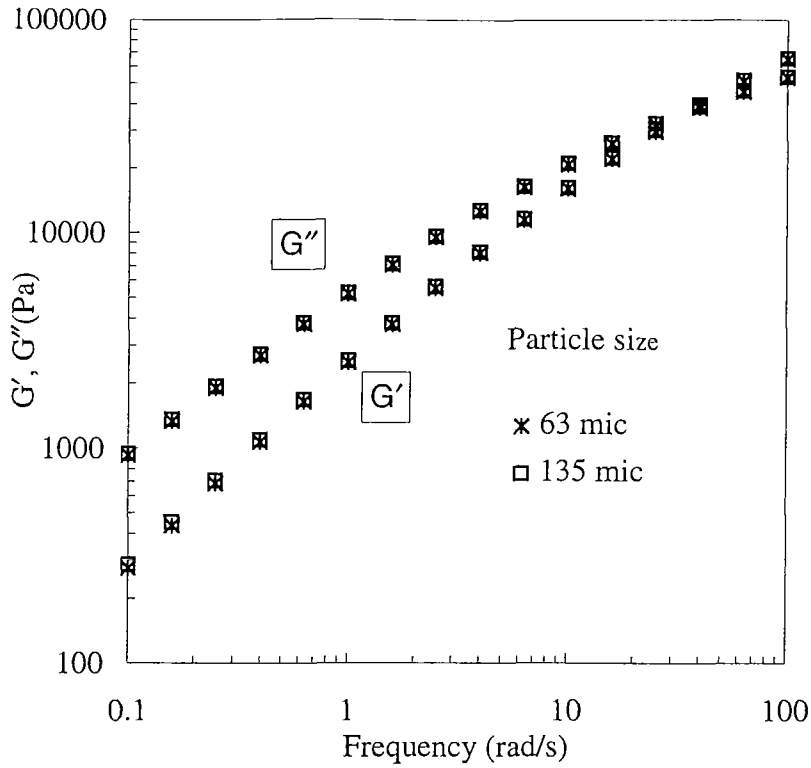

Figure 4.3.22 : Storage and loss moduli of paint particle filled PP/rubber/talc composites at 180°C and 5% strain.

4.3.2.5 Effect of particle geometry on storage and loss moduli for PP/rubber and PP/rubber/talc composites

Figure 4.3.23 shows the effect of particle geometry on the storage and loss moduli values for PP/rubber/talc system at 180°C. As observed, similar sized spherical and irregular particles showed very similar nature at the concentration level considered. Negligible effect of particle geometry was observed for PP/rubber systems as well, as shown in appendix D, figure D.23.

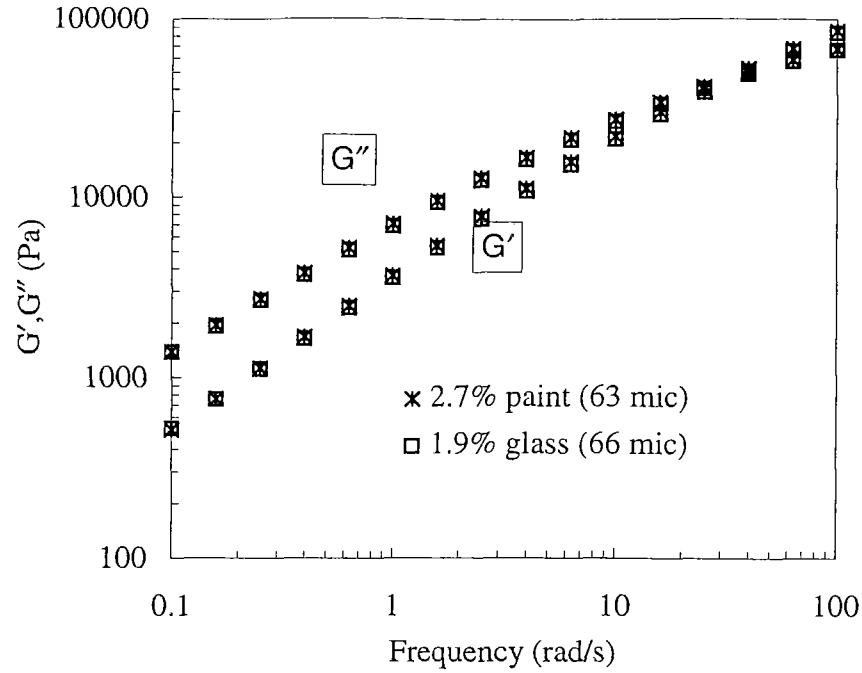

Figure 4.3.23 : Storage and loss moduli of glass bead and paint particle filled PP/rubber/talc composites at 180°C and 5% strain.

4.3.2.6 Effect of temperature on storage and loss moduli for PP/rubber and PP/rubber/talc composites

As expected, the storage and loss moduli curves for all the composites were shifted downwards with increasing temperature retaining their original shape. Examples of such curves are given in appendix D, figure D.24. Arrhenius type relationship can be applied to calculate the activation energies for the composites similar to steady shear measurements. No such calculation was performed for this investigation for oscillatory measurements.

4.4 Mechanical Properties

In many ways the mechanical properties of polymers are probably the most important of all their properties, since whatever may be the reason for the choice of a particular polymer for some application, it must still have certain characteristics of shape rigidity and strength. For composite polymers, these properties invariably assume a dominant role as one is usually seeking an improvement in mechanical behaviour as a prime requirement.

The most common way of recording deformation behaviour of polymers is to carry out a load-extension measurement, using some kind of tensile testing equipment. These measurements give the idea about the rigidity and strength of composites under a certain applied strain rate at a specific temperature. On the other hand, the fracture behaviour of polymers is usually connected with impact tests where a material is subjected to high rates of strain which results in multiaxial stressing. The fracture type might be either brittle or tough depending on the strain rate and the nature of composite. Considering these points, mechanical properties such as tensile, flexural, impact and fracture properties were studied for both commercially available composite material as well as for model systems in the present investigation. In the following sections each of them will be discussed separately relating property dependency with volume fraction of the dispersed phase.

4.4.1 Tensile properties

4.4.1.1 Base material and melt filtered material

The base material used for melt filtration studies was the rubber modified talc filled polypropylene, Epalex 7095. The two batches of material with 1.83% (batch 1) and 2.48% (batch 2) paint along with the recycled ground painted bumper material (batch 3) were

investigated before and after filtration. The results of yield strength, elongation and modulus of all the filtered and unfiltered material are tabulated in Appendix E, table E.1.

4.4.1.1.1 Effect of dispersed phase on tensile yield strength

The dispersed phase in all the materials studied here refers to the paint particles. Figure 4.4.1 shows the effect of paint concentration (%) on tensile yield strength before and after filtration of batch 1 and 2 material at two different test speeds. As observed, both the unfiltered batches had somewhat higher yield strength compared to the virgin material without any paint and all the filtered materials had slightly lower values compared to the corresponding unfiltered materials. But the average values did not vary by more than 6% with the standard deviation varying from 0.1 to 0.3 for all the samples. This leads to the conclusion that both the unfiltered and melt filtered samples retained nearly 100% of the yield strength as the virgin material. As noticed from figure 4.4.1, the test speed did not influence the material behaviour as well.

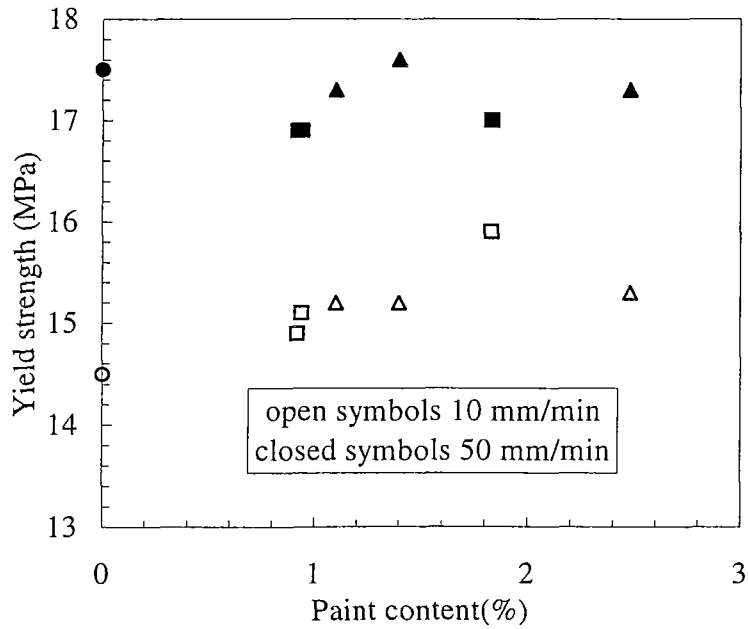

Figure 4.4.1 : Effect of paint content on tensile strength before and after melt filtration for (□) batch 1, (Δ) batch 2 and (•, o) virgin material.

The polypropylene based recycled bumper materials (batch 3) were also characterised and their yield strength is plotted against the paint content in figure 4.4.2. The filtered materials again retained strength between unpainted and painted regrind. Similar behaviour was observed by Tao *et al.* (1993) where the base material was rubber modified polycarbonate (PC)/polybutylene terepthalate (PBT) used in passenger cars. Miranda *et al.* (1994) also worked on rubber modified PP bumper material and found that the yield strength of virgin material was about 7% lower than the paint dispersed recycled material. None of the above studies quantified the paint content at any stage before and after the filtration process.

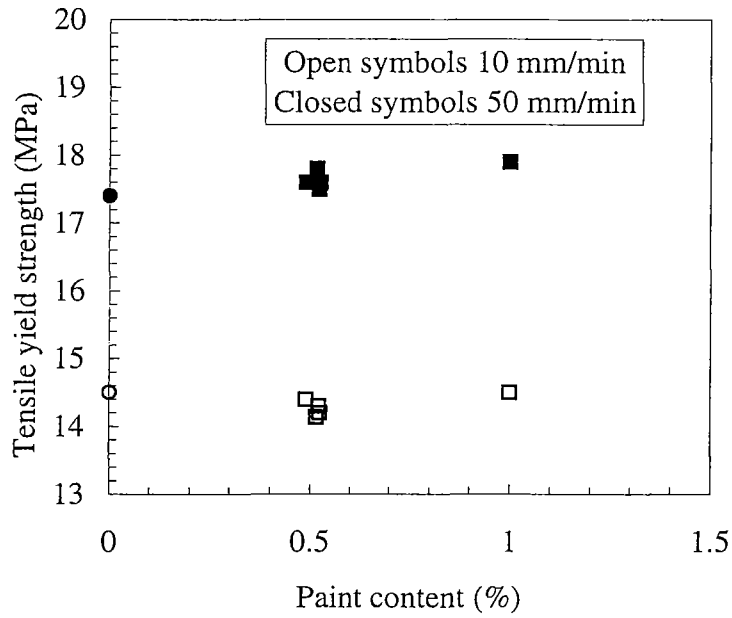

Figure 4.4.2 : Effect of paint content on tensile strength before and after melt filtration for recycled bumper material (batch 3).

4.4.1.1.2 Effect of dispersed phase on elongation at break

The elongation at break for all the paint dispersed materials (filtered and unfiltered) was much lower (around 10% of the original value) compared to the unfilled base material (figure 4.4.3). It was obvious from this result that the large paint particles acted as crack initiators thus reducing the strain at break. Similar result was reported by Miranda *et al.* (1994) where they

observed about 80% reduction in elongation at break for paint dispersed composites compared to the virgin material. Asakawa (1992) noticed about 55% retention of strain at break for recycled bumper material containing paint compared to unpainted recycled material. In all the cases the contaminants put restrain on matrix deformation. The melt filtered materials had very similar elongation compared to the unfiltered paint dispersed batches explaining that filtration did not effect much on elongation as filtered materials also contained some fraction of contaminants present. With test speed, the ultimate strain values decreased but the trend was similar for both the speeds. Tao *et al.* (1993) observed massive shear bands in the gauge section during tensile testing of paint contained PC/PBT blends and concluded that it was the flakes of paint in the material which caused these, decreasing the ultimate elongation by about 84%.

4.4.1.1.3 Effect of dispersed phase on Young's modulus

The calculated Young's modulus of most of the filtered and unfiltered batches were within experimental deviation without showing any particular trend at the test speed of 10 mm/min (appendix E, table E.1). The modulus values increased with test speed of 50 mm/min and a decreasing trend was observed with filtered samples with respect to their unfiltered batch of material (appendix E, table E.2). But the values were still within the standard deviation. So it is difficult to draw any conclusion regarding the effect of filtration process and paint content on modulus as any particular trend in result was absent. Figures 4.4.3.a and 4.4.3.b show the variation of strain at break and modulus with paint content for batch 1 material at the test speed of 10 and 50 mm/min respectively. Results for batch 2 and 3 samples were not provided in figure 4.4.3 as all the batches showed similar trend in strain at break (%) and Young's modulus.

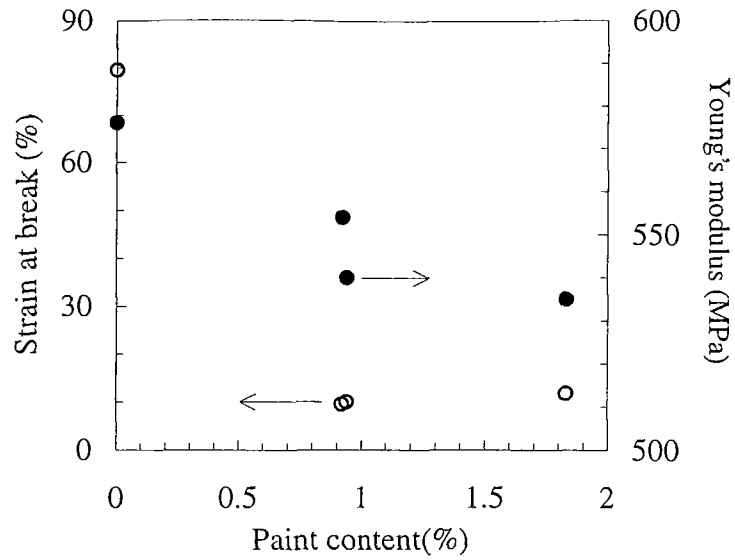

Figure 4.4.3.a : Effect of paint content on (o) strain at break (%) and (•) and Young's modulus for batch 1 sample before and after melt filtration at test speed 10 mm/min.

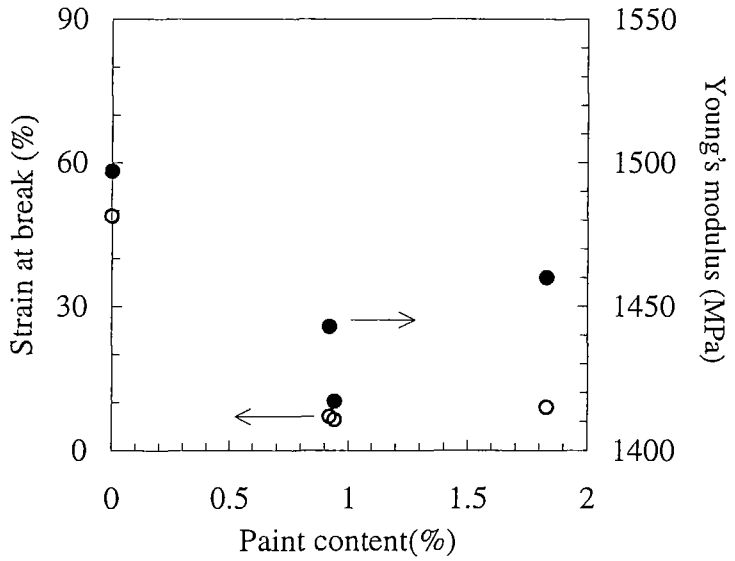

Figure 4.4.3.b : Effect of paint content on (o) strain at break (%) and (•) and Young's modulus for batch 1 sample before and after melt filtration at test speed 50 mm/min.

4.4.1.2 PP/ rubber based composites

As a starting point, it is assumed that the base matrices PP/rubber and PP/rubber/talc behave as a continuum and the added glass and paint particles are the second phase of the composite. Then, in principle, it should be possible to calculate the properties of the multiphase materials in terms of the properties of its constituents. Table E.3 in appendix E gives the tabulated values of tensile yield strength, percentage strain at break and young's modulus of all the composites at the test speed of 50 mm/min. In the following sections each of these are discussed separately focusing on the effect of dispersed phase on them.

4.4.1.2.1 Effect of dispersed phase on tensile yield strength

Figure 4.4.4 shows the tensile yield strength as a function of the dispersed phase fraction. Though the variation in strength was small, a decreasing trend was observed with increasing volume fraction of filler, the lowest strength being for a paint dispersed composite ($\varphi = 0.027$) where a 13% reduced strength was noted compared to the base matrix. The reduction in strength is common for a particulate composite particularly when there is no binding between the various phases as then the material response as if the matrix contained holes of shape identical to that of the filler (Sheldon, 1982). As no surface treatment was done to the filler particles and no coupling agent was added to the matrix polymer to enhance adhesion between phases, poor binding was expected for the composites studied, explaining a reduction in strength values. Also the decrease in strength value was small as the dispersed phase fraction was small and it can be concluded that greater reduction in strength would occur with increasing filler volume for poor binding between the matrix and filler.

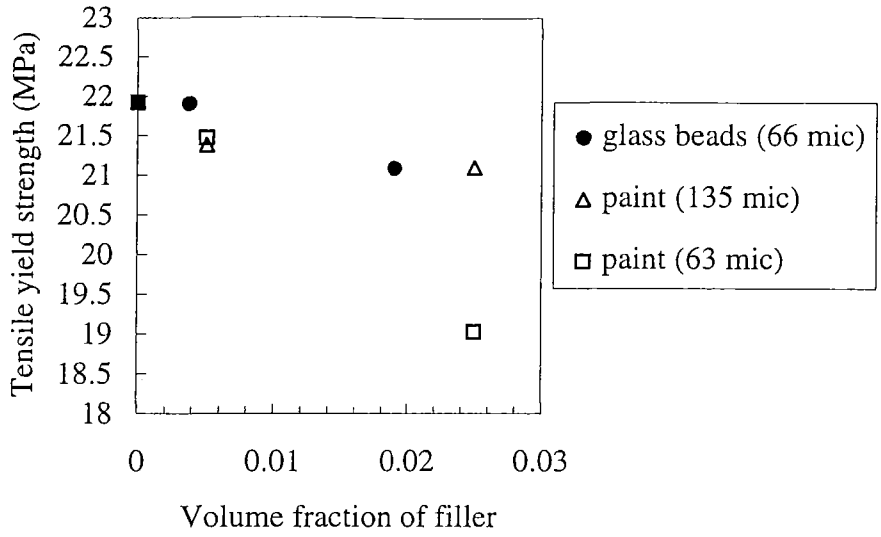

Figure 4.4.4 : Tensile yield strength versus volume fraction of filler for PP/rubber composites.

4.4.1.2.2 Effect of dispersed phase on elongation at break

The strain at break decreased significantly with the addition of small fraction of paint particles and glass beads and was gradual after the initial low value. This indicates that the poor wetting of the dispersed phase by the matrix allows filler-matrix separation causing cavitation as the composites are stretched along the direction of applied load, which is possible for even a small fraction of dispersed phase.

As displayed in figure 4.4.5, Nielsen's predictive model for perfect adhesion between filler and matrix (chapter two, section 2.6.1.2) showed higher values than the experimental points indicating poor adhesion as well.

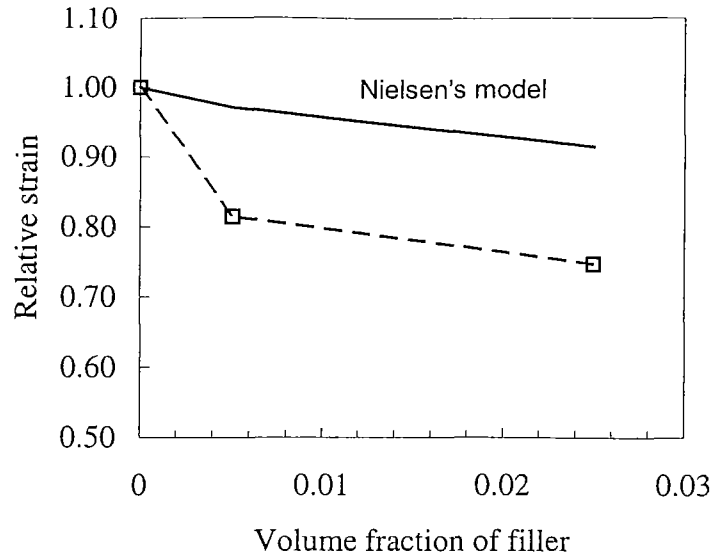

Figure 4.4.5 : Variation of relative strain ($\varepsilon_c/\varepsilon_m$) of PP/rubber composites with volume fraction of dispersed paint particles (63 μm). (Solid curve represents the predictive behaviour according to Nielsen's equation and the dashed curve represents variation of experimental data)

4.4.1.2.3 Effect of dispersed phase on Young's modulus

The Young's modulus of the filled composites behaved quite differently depending on the dispersed phase used. For the paint dispersed composites (figure 4.4.6.a), a decreasing trend was observed in modulus values with increasing volume fraction of fillers. The result was obvious as, in general, particulate phase decreases the elastic modulus of the matrix phase if the particulate modulus is lower than that of the matrix modulus. Here, the modulus of paint particle was taken as 887 MPa (Takabori *et al.*, 1985) and the modulus of PP/rubber matrix was measured as 910 MP, making the modular ratio of filler to matrix , *m*, equal to 0.97. Now using equations 2.6.13-14 to calculate the limiting bounds, no change in moduli value was observed from the matrix modulus for the volume fraction considered. But looking at the

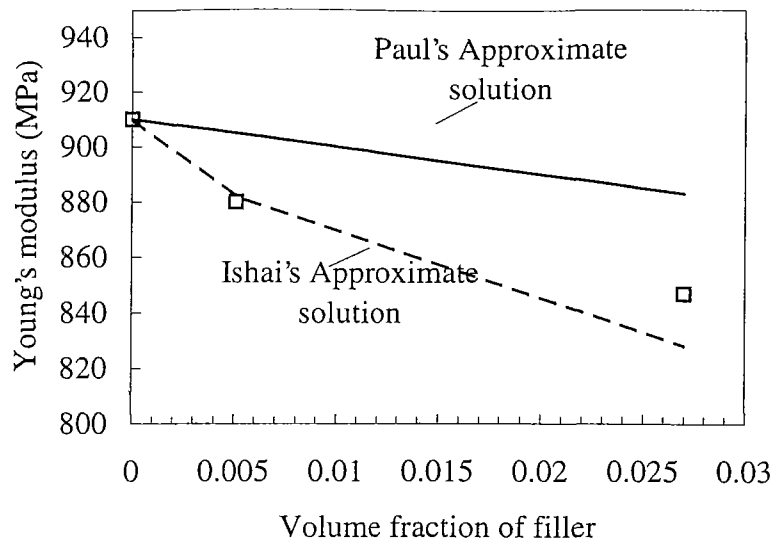

Figure 4.4.6.a : Young's modulus versus filler volume fraction for paint particle (63 μm) dispersed PP/rubber composites.

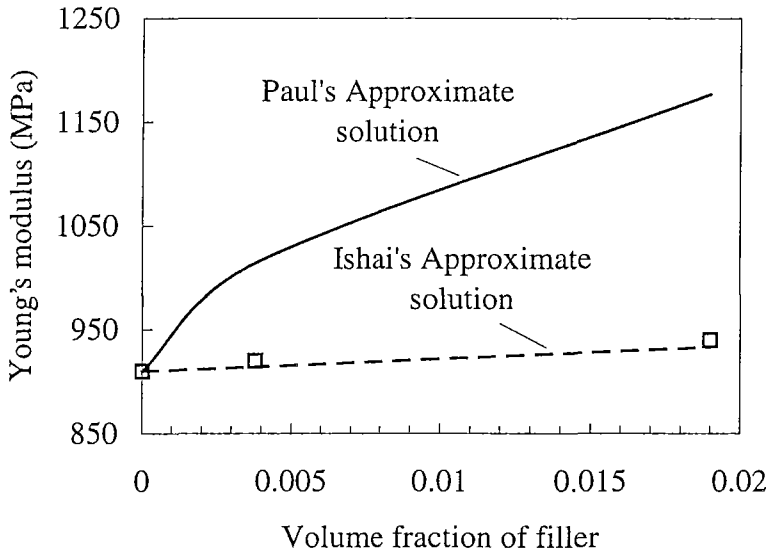

Figure 4.4.6.b : Young's modulus versus filler volume fraction for glass bead (66 μm) dispersed PP/rubber composites.

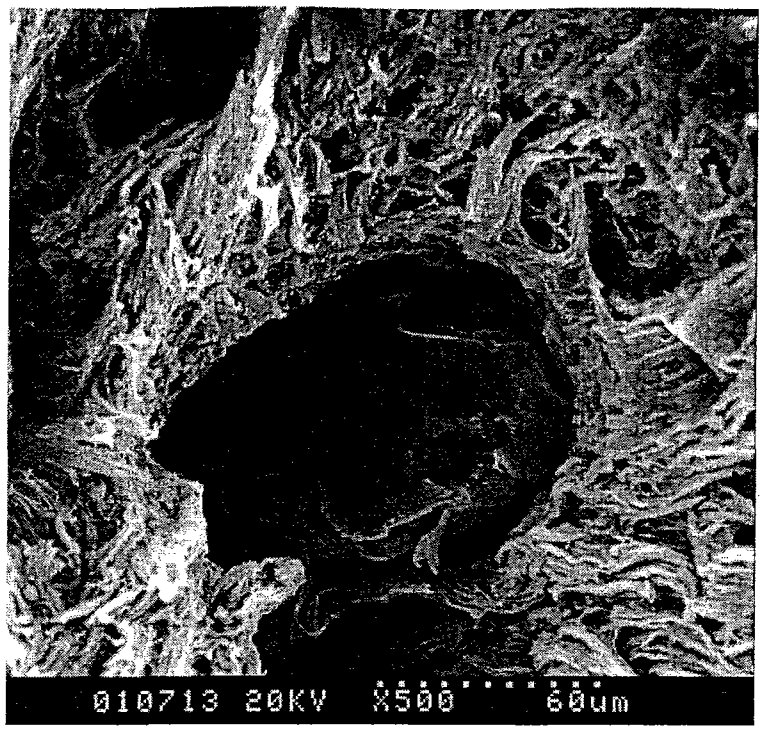

Figure 4.4.7.a : SEM of a tensile fractured specimen of paint particle filled PP/rubber composite.

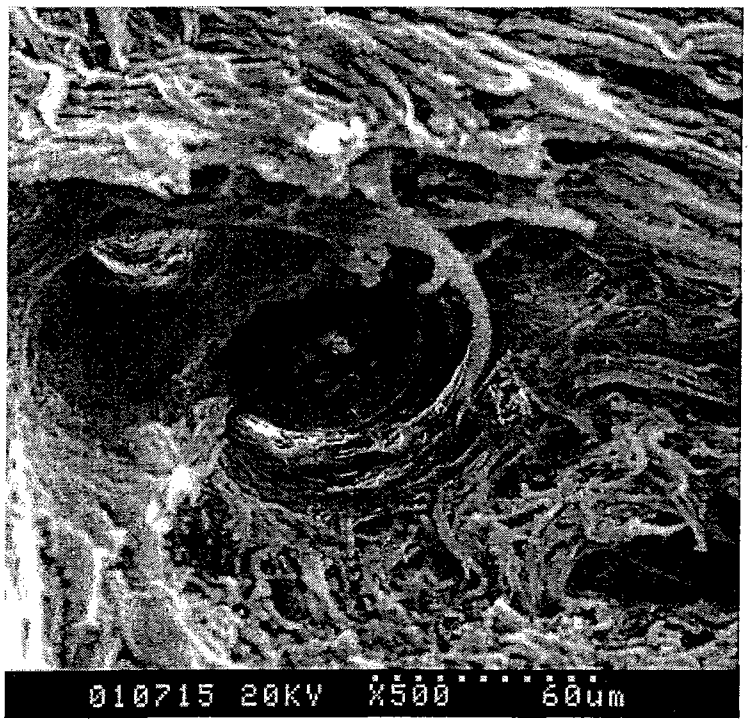

Figure 4.4.7.b : SEM of a tensile fractured specimen of glass bead filled PP/rubber composite.

tensile fractograph of such a sample (figure 4.4.7.a), a clear separation between the paint particle and matrix was observed leading to the conclusion that debonding of filler from matrix is possible which would give the matrix a porous structure. Then equations 2.6.17-18 can be used to calculate the bound moduli values which are suitable for a porous media. The curves in figure 4.4.6.a represent these upper and lower limits.

On the other hand, for the glass filled composites, the composite modulus showed a tendency to increase with increasing filler fraction (figure 4.4.6.b). This corresponds to the theory that particulate phase would increase matrix modulus if particulate modulus (here glass beads with modulus of 73 GPa (Young *et al.* 1986)) is higher than matrix modulus itself. In general, if the modulus of the filler is very high relative to that of the matrix, the polymer modulus does not have much effect on the variation of moduli values with changing filler fraction. Also it was shown by many authors that the modulus of a polymer composite containing a rigid particulate filler generally increased even if the filler does not interact strongly with the matrix. The tensile fractograph of a glass bead filled PP/rubber composite as shown in figure 4.4.7.b shows that the glass bead is only partially adhered to the matrix on the left side and is debonded from the matrix on the right giving an overall poor interaction. The bounds of modulus values were calculated using equation 2.6.13-14 and are plotted in figure 4.4.6.b along with the experimental data points. The experimental data fit quite well to the lower bound approximating Ishai's equation. Similar observation was explained by Manson and Sperling (1971) as polymers containing large particle size (low surface area) fillers tend to exhibit lower bound behaviour.

4.4.1.3 PP/ rubber/ talc based composites

4.4.1.3.1 Effect of dispersed phase on tensile yield strength

The gradual weakness in the composite structure introduced by the increased dispersed phase fraction was attempted to be estimated by comparing the tensile strength data with some theoretical predictive models as described in section 2.6.1.1. The equations were as follows:

$$\sigma_c = \sigma_m\left(1-\varphi^{2/3}\right)S \qquad \text{Nielsen model} \qquad ...(2.6.3)$$

$$\sigma_c = \sigma_m\left(1-K_2\varphi^{2/3}\right) \qquad \text{Nicolais and Narkis model} \qquad ...(2.6.5)$$

$$\sigma_c = \sigma_m \exp(-k\varphi) \qquad \text{Porosity model} \qquad ... (2.6.6)$$

Table 4.4.1 presents the values of S, K_2 and k at each individual dispersed phase concentration obtained from the experimental results together with their average values. According to Nielsen's model, the average values of S were slightly lower than unity indicating moderate stress concentration effect for both paint particles and glass spheres. The same was with Nicolais and Narkis model where the average values of K_2 were around unity. From porosity model higher values of k from unity indicated greater stress concentration.

Comparison of the data with the predictive models is also graphically represented. Figure 4.4.8.a shows the relationship between tensile yield strength against volume fraction of glass beads and the lines represent predictive behaviour according to Nielsen's model (equation 2.6.3). Some of the experimental data points lay below the theoretical curve of S=1 which represents no stress concentration effect and all the points were bounded between S=1 to 0.86. Figure 4.4.8.b shows similar representation for 63 μm paint particle dispersed composites. Here the stress concentration values lay between 1 and 0.95 with the average value being 0.97.

This indicated moderate stress concentration according to this model as lower value of S than unity indicate greater stress concentration effect or poorer adhesion.

Table 4.4.1 : Values of stress concentration parameters S, K_2 and k in PP/rubber/talc composites.

Filler	Volume fraction	S (equ. 2.6.3)	K_2 (equ. 2.6.5)	k (equ. 2.6.6)
Glass beads	0	-	-	-
(66 μm)	0.0038	1.014	0.406	2.61
	0.019	1.014	0.814	3.14
	0.027	0.936	1.64	5.90
	0.050	0.910	1.573	4.80
	0.100	0.858	1.516	3.95
	Mean	0.946	1.19	4.08
Paint particles	0.0054	1.01	0.628	3.61
(63 μm)	0.027	0.962	1.378	4.89
	0.05	0.948	1.33	3.97
	Mean	0.974	1.11	4.16
Paint particles	0.0054	1.00	0.843	4.86
(135 μm)	0.027	0.98	1.16	4.11
	Mean	0.99	1.00	4.48

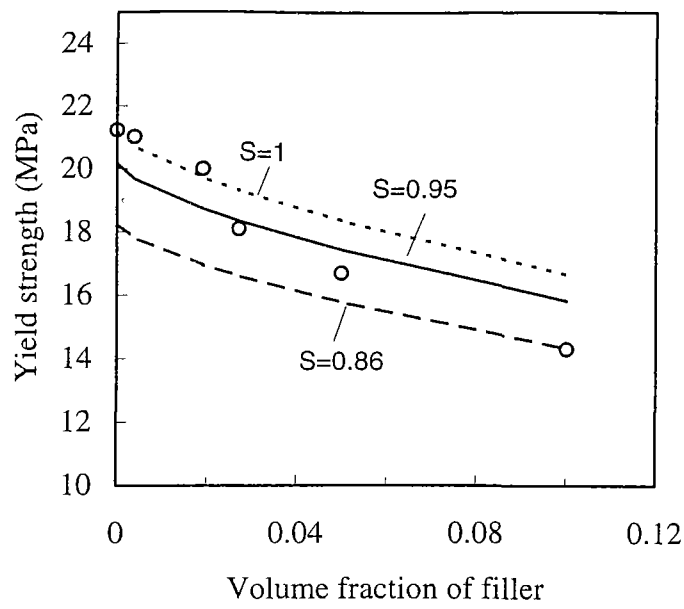

Figure 4.4.8.a : Tensile yield strength versus volume fraction of glass beads for PP/rubber/talc composites (The lines represent predicted behaviour according to equation (2.6.3) with *S* values indicated).

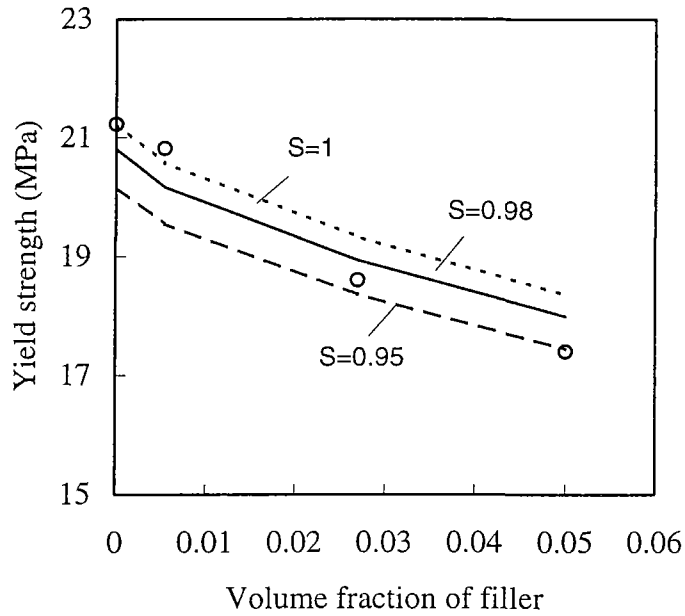

Figure 4.4.8.b : Tensile yield strength versus volume fraction of paint particles (63 μm) for PP/rubber/talc composites (The lines represent predicted behaviour according to equation (2.6.3) with *S* values indicated).

The Nicolais and Narkis model (equation 2.6.5) showed good agreement with glass filled composites as shown in figure 4.4.9 indicating poor adhesion between the matrix and dispersed phase. The parameter K_2 in the equation is the weightage factor and describes the adhesion quality between the matrix and filler and depends on the details of the model. The data lay around the curve with the adhesion parameter K_2 =1.21 which is applicable for no adhesion type composites with spherical fillers (Kunori and Geil, 1980).

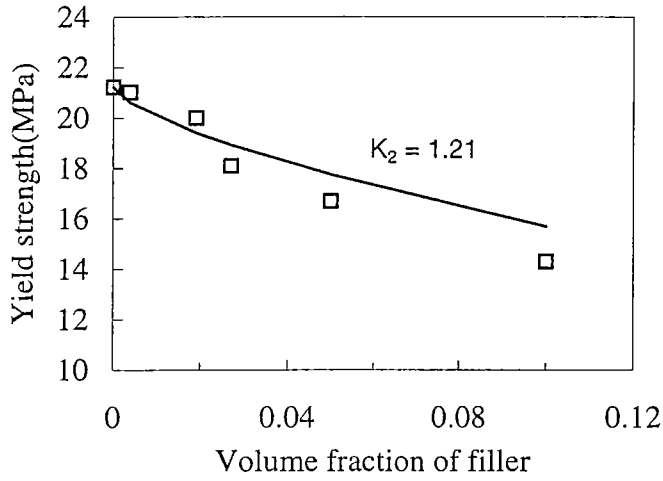

Figure 4.4.9 : Tensile yield strength versus volume fraction of glass beads for PP/rubber/talc composites (The solid line represents the predicted behaviour according to equation (2.6.5) with K_2 = 1.21).

For irregular paint particle filled systems the value of the adhesion parameter went higher than 1.21 with increasing dispersed phase fraction for 63 μm paint particle dispersions (table 4.4.1). In general lower values of K_2 below 1.21 means better adhesion (Maiti and Sharma, 1992) so higher K_2 values would indicate more stress concentration effect. For larger sized paint particles (135 μm) an increasing trend in K_2 value was also observed.

Figure 4.4.10 showed the applicability of porosity model (equation 2.6.6) to the experimental data of paint (63 μm) dispersed PP/rubber/talc matrix. As discussed in section 2.6.1.1, higher values of k corresponds to increase in stress concentration. The solid line on the plot for the average k = 4.2 for 63 μm paint particles indicated that the model fits quite well.

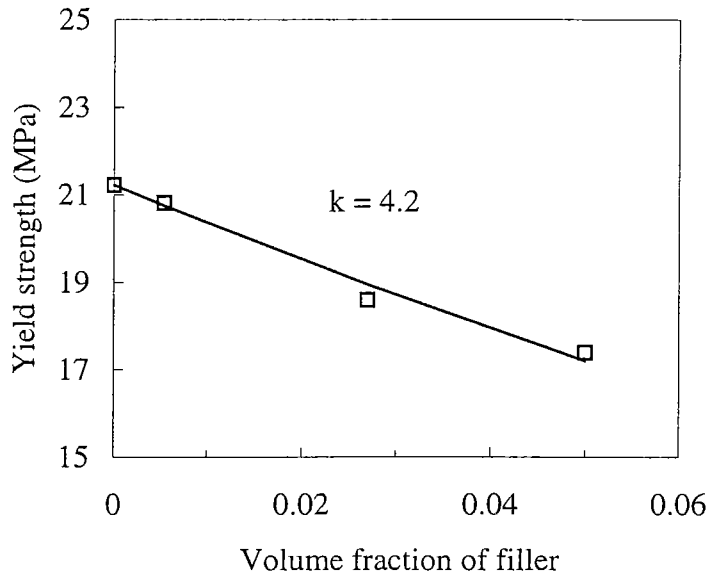

Figure 4.4.10 : Tensile yield strength versus volume fraction of paint particles (63 μm) for PP/rubber/talc composites (The solid line represent the predicted behaviour according to equation (2.6.6) with k = 4.2).

The decrease in yield strength with increasing filler volume fraction for composite materials was also predicted by Piggott and Leinder where they gave a linear relation as :

$$\sigma_f = A'\sigma_m - B'\varphi \qquad ...(2.6.7)$$

The experimental data was fitted to this model and as shown in table 4.4.2, the values of the stress concentration factor, A', and the constant B', which depend on the filler matrix adhesion, are not significantly affected by the different fillers used. Figure 4.4.11 is the graphical representation of the model fitted to the results.

Table 4.4.2 : Constant values for Piggott and Leinder equation (tensile yield strength).

Filler	A'	B'
glass (66 μm)	0.99	71.12
paint (63 μm)	0.99	78.90
paint (135 μm)	0.99	81.20

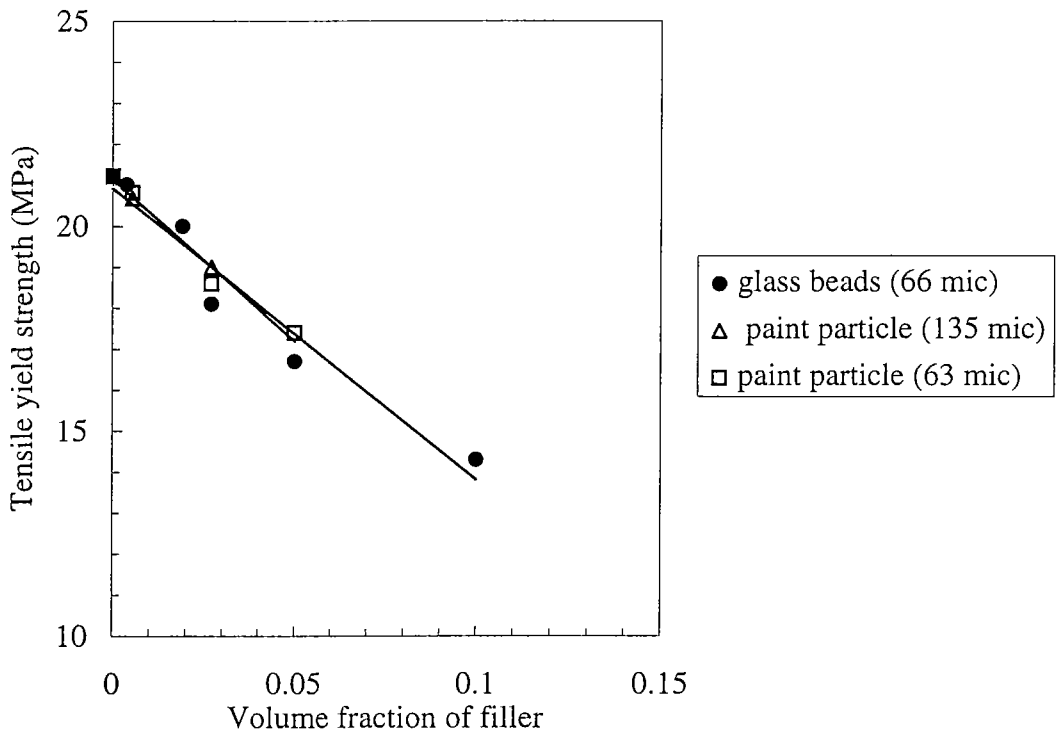

Figure 4.4.11 : Tensile yield strength versus volume fraction of dispersed phase for PP/rubber/talc composites (the solid line represent the predicted behaviour according to Piggott and Leinder equation).

4.4.1.3.2 Effect of dispersed phase on elongation at break

The relative strain at break (i.e. the ratio of the composite strain (ε_c) to the matrix strain (ε_m) showed a decrease with increase in dispersed phase fraction as shown in figure 4.4.12. Nielsen's (1966) predictive model for perfect adhesion between filler and matrix exhibited higher values than all the composites. The low values in elongation occurred from low adhesion of large sized dispersed particles which restrict the deformability of matrix. Also the filler particles that do not wet properly by the matrix and are poorly bonded caused cavitation thus reducing the matrix from providing strength between particles.

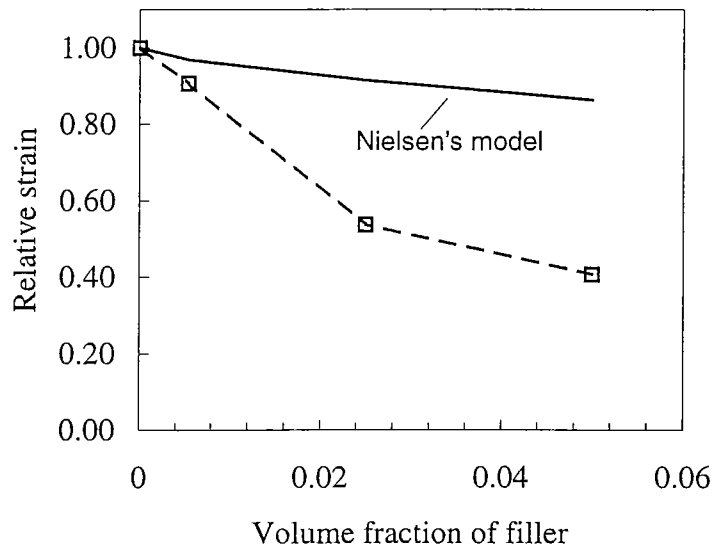

Figure 4.4.12 : Variation of relative strain ($\varepsilon_c/\varepsilon_m$) of PP/rubber/talc composites with volume fraction of dispersed paint particles (63 μm). (Solid curve represents the predictive behaviour according to Nielsen's equation and the dashed curve represents variation of experimental data)

The decrease in strain than that predicted by Neilsen model, indicates that the elongation is related to filler fraction as $\varphi^{2/3}$. Figure 4.4.13 shows a plot of relative strain versus $\varphi^{2/3}$. The plot reveals that for paint particles the elongation was quite sensitive to filler surface area upto

$\varphi^{2/3} = 0.089$ (i.e. $\varphi = 0.027$) after which the sensitivity was lowered with further increase in φ. But elongation was not that sensitive to filler surface area for glass bead fillers where the decrease in strain was rather gradual. This indicates that irregular shaped particles were more detrimental in reduction of strain with increasing volume fraction of dispersed phase compared to spherical particles.

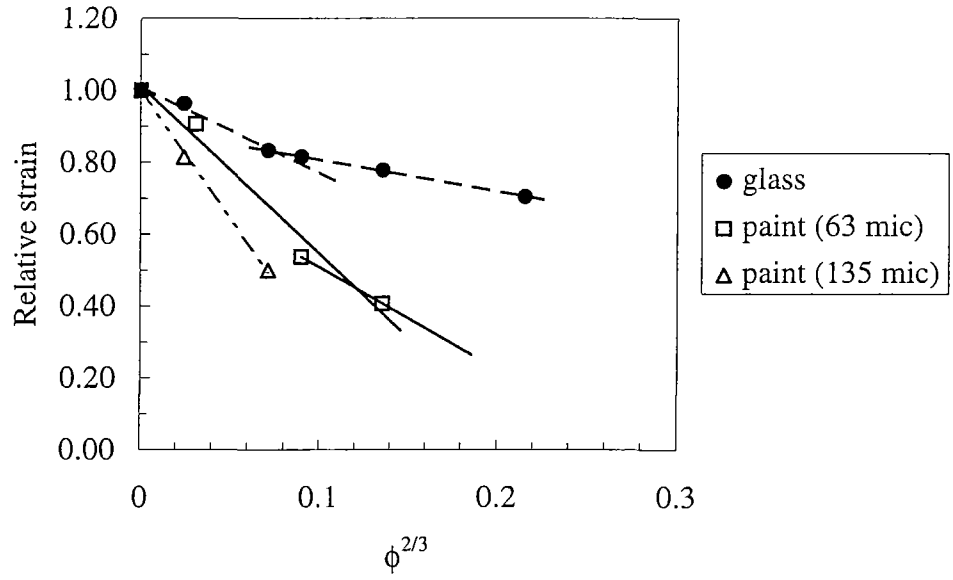

Figure 4.4.13 : Variation of relative strain at break of PP/rubber/talc composites with filler area fraction $\varphi^{2/3}$.

The experimental data were treated according to Mitsuishi's model to study the filler polymer interaction and the value of K_1 obtained from equation 2.6.10 (model presented in section 2.6.1.2) are tabulated in table 4.4.3 where higher value of K_1 indicates a smaller degree of interaction between phases:

$$\varepsilon_c = \varepsilon_m(1 - K_1\varphi^{2/3}) \qquad ...(2.6.10)$$

The mean values of K_1 determined for glass fillers were much lower compared to the paint fillers indicating better adhesion of glass to the matrix. Figure 4.4.14 is a graphical representation of the model for paint dispersed composites.

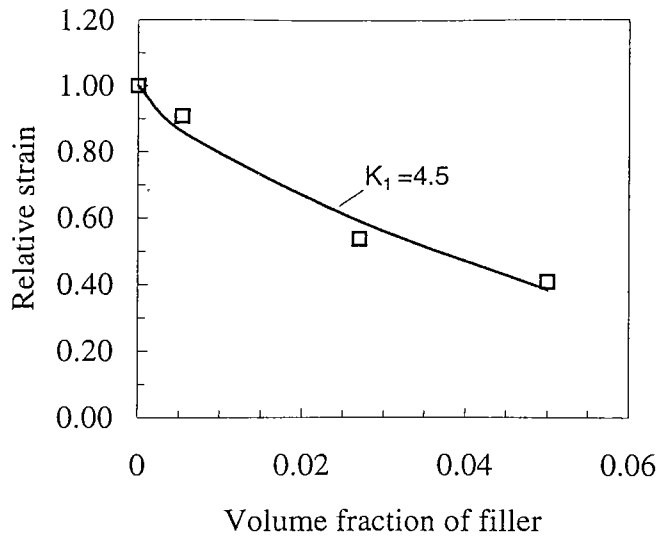

Figure 4.4.14 : Variation of relative strain at break of PP/rubber/talc composites dispersed with paint particles (63 μm) (The solid represent equation 2.6.10 with $K_1 = 4.5$).

Table 4.4.3 : Values of polymer filler interaction parameter, K_1, for PP/ rubber/ talc composites dispersed with paint particles and glass beads.

	K_1		
Volume fraction	paint (63 μm)	paint (135 μm)	glass (66 μm)
0	-	-	-
0.0038	-	-	1.52
0.0054	3.01	6.02	-
0.0190	-	-	2.35
0.0270	5.15	5.56	2.05
0.0500	4.37	-	1.64
0.1000	-	-	1.37
Mean value	4.18	5.8	1.79

Mitsuishi also showed that smaller filler size was more sensitive to strain which does not correspond to the present situation. K_1 also depends on filler surface modification and the variation was insignificant for smaller sized filler particles for PP/$CaCO_3$ composites (Mitsuishi, 1985). Maiti and Sharma (1992) and Ghosh and Maiti (1996) also concluded that

for talc filled and silver powder filled PP composites the surface treated fillers decreased the interaction parameter only marginally.

Observation of tensile fractured specimens under the SEM also revealed the interface between the matrix and filler particles. As observed in figure 4.4.16, the talc (~ 8 μm) filled rubber toughened PP composite showed fairly good dispersion and wetting of talc particles in the polymer matrix and so considering the PP/rubber/talc as a continuum phase is justified. Figure 4.2.5 showed the tensile fractograph of a paint dispersed PP/rubber/talc specimen. As observed large sized paint particles were very obvious in the matrix compared to the talc particles which were present as a part of the continuum matrix. Decohesion of the paint particles were clear by observing the clean voids. Also, no matrix layer covers or bonds with the paint part indicating poor adhesion between them. Glass bead filled systems showed similar clear voids from which they were pulled out (figure 4.2.4). Clean exposed surfaces of the filler particles indicate poor interaction with the matrix.

4.4.3.1 Effect of dispersed phase on Young's modulus

The effect of addition of talc particles into PP/rubber binary system was first examined before looking at the composites of PP/rubber/talc system. As seen in figure 4.4.16, increased talc fraction increased the modulus values of the binary composite as talc acted as a reinforcing filler. Smaller particle size actually increases the modulus of a composite in greater extent perhaps because a larger total surface interaction occurs between the filler and matrix or as the value of the maximum packing fraction increases (Sheldon, 1982). The small sized talc particles (~ 8 μm) fit between the polymer chains making a filler-polymer network and thus increasing the rigidity of the whole composite. The maximum level of talc added was 3.6 vol% (10 wt%) which was later chosen as the base matrix. As mentioned in the last section,

good dispersion and wetting of talc particles in the binary system were revealed from the tensile fractograph (figure 4.4.16) and so consideration of PP/rubber/talc as a continuum matrix was justified.

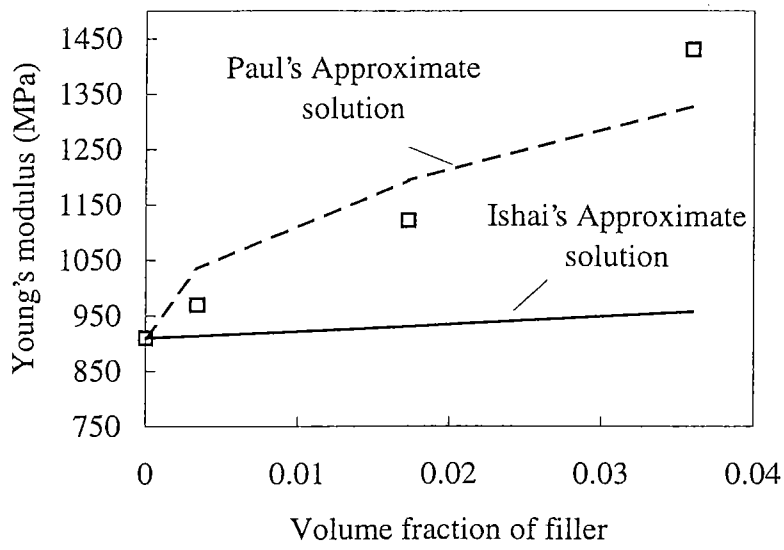

Figure 4.4.15 : Young's modulus versus filler volume fraction for talc dispersed PP/rubber composites.

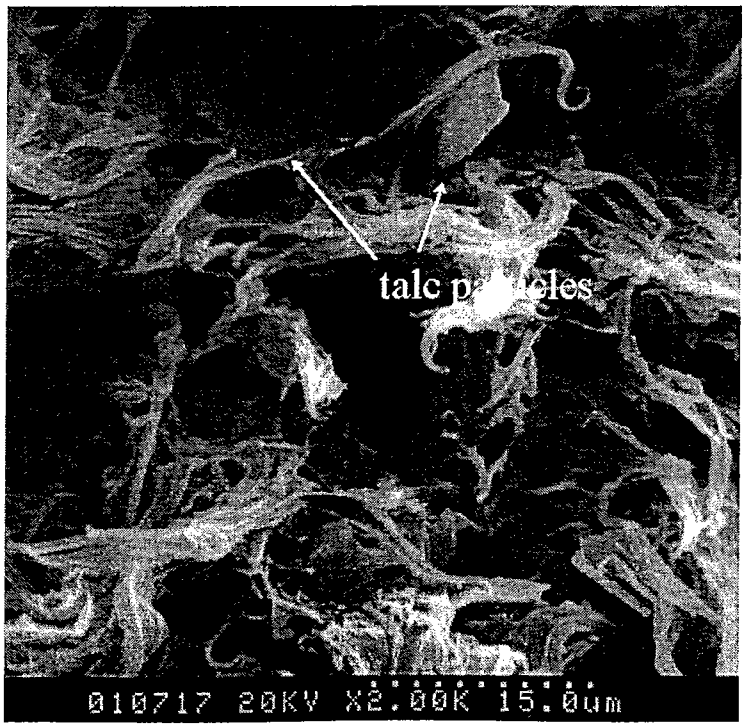

Figure 4.4.16 : SEM of a tensile fractured specimen of PP/rubber/talc (3.6%) composite.

For the addition of paint particles or glass beads as inclusions in the PP/rubber/talc matrix, the Young's modulus showed a decrease as dispersed phase fraction increased implying that the addition of inclusions into the matrix formed a weak structure. The decrease in value was significant upto $\varphi = 0.027$ beyond which it was only marginal for paint particles (figure 4.4.17.a). Also modulus decreased slightly with decreasing particle size (Appendix E, table E.4), the reason for which is unclear and needs further investigation. For glass spheres the decrease was more gradual as shown in figure 4.4.17.b implying that much small degree of interaction was present between irregular shaped paint particles compared to glass spheres.

If it is assumed that there is no interaction between the dispersed phase and the matrix then the fillers can be considered as voids or pores and the modulus can be compared with the predictive theories of Paul (1960) and Ishai (Ishai and Cohen, 1967) using the following equations:

$$E_c = E_m\left(\frac{1-\varphi^{2/3}}{1-\varphi^{2/3}+\varphi}\right) \qquad \text{upper bound} \qquad ...(2.6.17)$$

$$E_c = E_m\left(1-\varphi^{2/3}\right) \qquad \text{lower bound} \qquad ...(2.6.18)$$

Figure 4.4.17.a represents the modulus values of paint dispersed composites together with the upper and lower bound curves according to the above equations. As observed, the experimental data fell far below these limits for $\varphi > 0.0054$, implying that a much larger extent of non interaction between the matrix and the dispersed phase existed with increasing dispersed particles. Similar behaviour was observed by Ghosh and Maiti (1996) for silver (Ag) powder filled PP composites. They proposed that one possibility for lack of adhesion between Ag and PP may be that, PP always has a tendency to crystallise excluding the Ag particles as foreign matter.

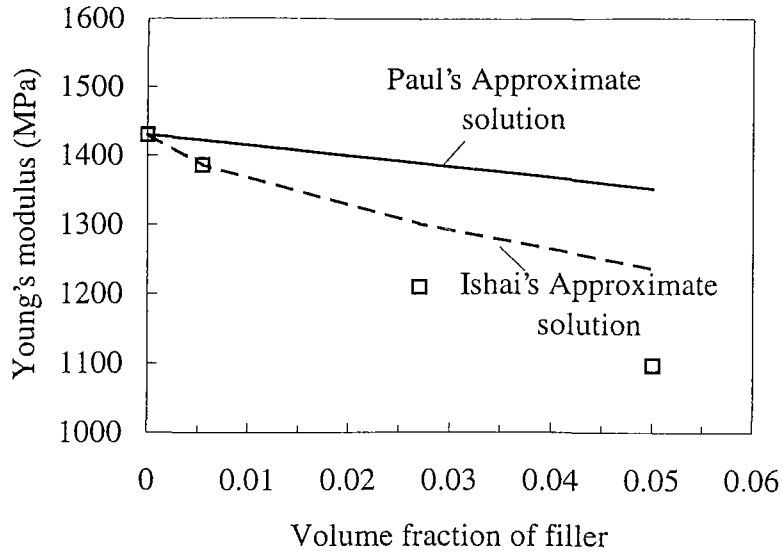

Figure 4.4.17.a : Young's modulus versus filler volume fraction for paint particle (63 μm) dispersed PP/rubber/talc composites.

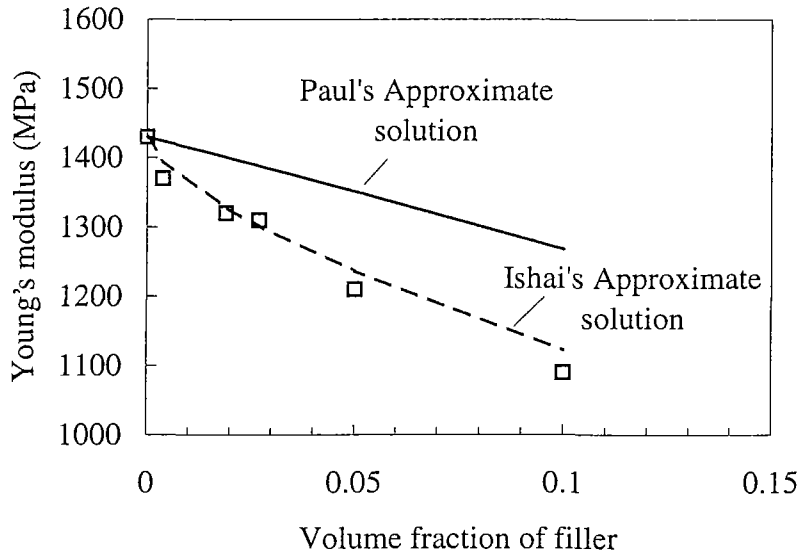

Figure 4.4.17.b : Young's modulus versus filler volume fraction for glass bead dispersed PP/rubber/talc composites.

The nature of data observed in figure 4.4.17.b for glass bead filled PP/rubber/talc composite was contrary to the glass bead dispersed PP/rubber system where a trend of increase in modulus was observed with increasing filler fraction for the later. It was explained that for

PP/rubber system, the composite modulus increased with inclusion of glass beads as the particulate modulus itself (73 GPa for glass) was much higher than of the matrix (910 MPa). In this case poor interface between matrix and filler did not influence the increase in modulus value.

On the other hand, a decrease in composite modulus was observed for glass dispersed PP/rubber/talc systems. Possibly the presence of talc in the present composite played a role in such behaviour. As seen, the addition of 3.6% talc particles (modulus 170 GPa) increased the overall modulus of the PP/rubber system from 910 to 1430 MPa which can be explained as just mentioned in the last paragraph. Now, PP/rubber/talc system was considered as a continuum phase but the composite modulus would be governed by talc particles as it has much higher rigidity than the other two components. Dispersing glass beads into this system showed detrimental effect in modulus as the independent modulus of glass was less than half of the talc. So instead of reinforcing, the composites failed as a weak structure and poor interface between glass beads and the matrix also aided the process.

4.4.2 Flexural properties

Flexural properties were investigated for the "real" and "model" blends prepared with paint particles and glass beads as the dispersed phase respectively. The tests were performed with a three point flexure configuration on an Instron machine at room temperature and at a crosshead speed of 10 mm/min. The flexural strength and the flexural modulus were calculated for each composites using the equations given in chapter three, section 3.2.8.2. It was found that all composite samples were capable of undergoing plastic deformation during testing and none of them failed completely at the specified test speed. The flexural yield strength was calculated taking the maximum load on curve as the yield point. The calculated values are tabulated in appendix E, table E.3 and E.4 along with the tensile results.

4.4.2.1 Effect of dispersed phase on flexural strength

The flexural strength versus volume fraction of dispersed phase for PP/rubber system is plotted in figure 4.4.18. The addition of low fraction of glass or paint did not effect the strength much and the values obtained were within the standard deviation of the experimental results.

For PP/rubber/talc based composites a gradual decrease was noticed with increased dispersed phase fraction (glass beads or paint particles). In three point bending, the loaded surface undergoes compression while the surfaces on the opposite sides undergoes tension (Nielsen, 1974). Also in tension any flaw or defect magnifies whereas in compression the defects become plugged. For talc based composites the talc particles stay well bonded with the matrix and shows higher rigidity (32.17 MPa for 3.6 vol% talc) in bending compared to PP/rubber binary composite (28.9 MPa). As the second dispersed phase was introduced, interfacial

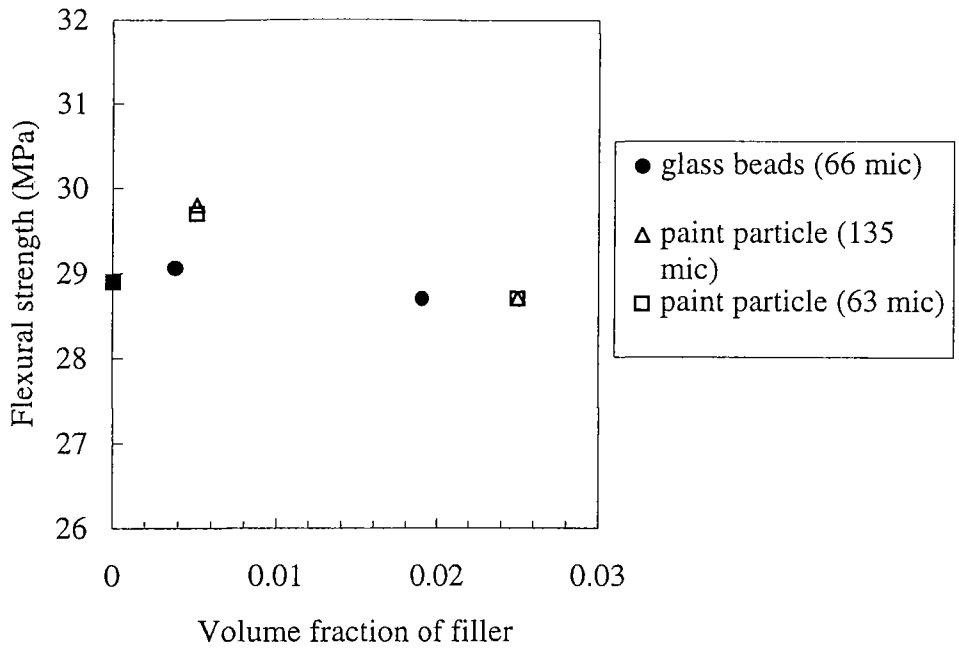

Figure 4.4.18 : Flexural strength versus volume fraction of filler for PP/rubber composites.

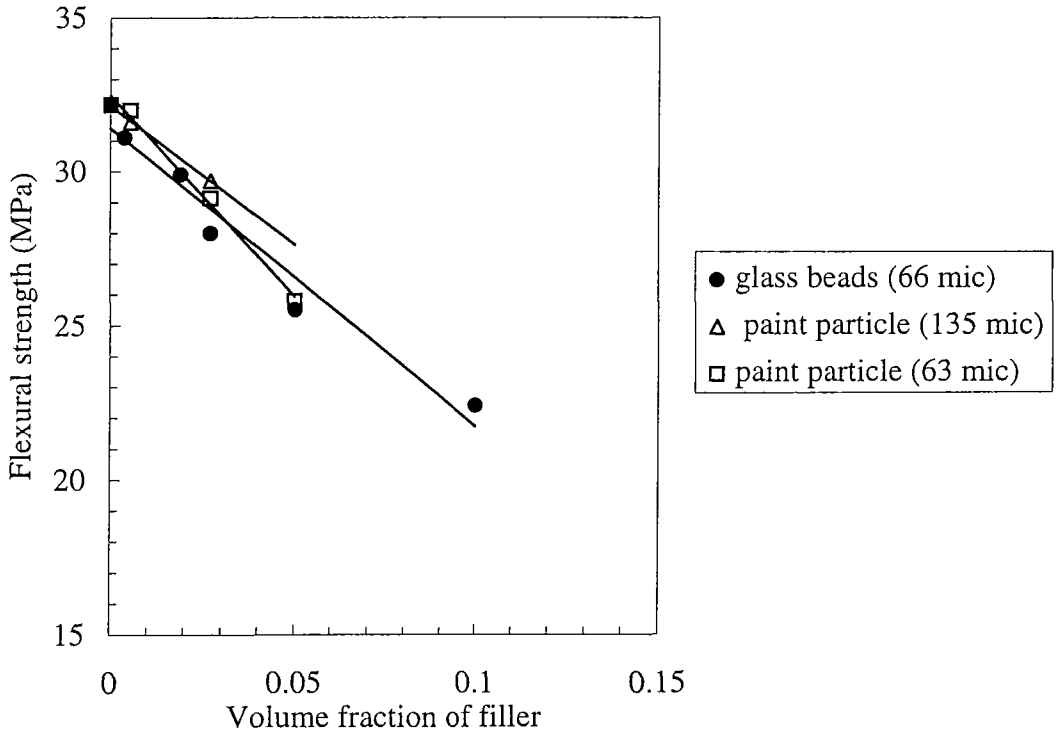

Figure 4.4.19 : Flexural strength versus volume fraction of filler for PP/rubber/talc composites (the solid lines represent the prediction according to Piggott and Leinder equation).

debonding of large particles occurred during deformation thus lowering the strength below that of the PP/rubber/talc matrix.

The decrease in strength with increasing volume fraction was predicted by Piggott and Leinder equation and shown in figure 4.4.19 for PP/rubber/talc composites. The constant values of A' and B' are tabulated in table 4.4.4 showing larger value of B' for similar sized paint particle dispersed composite compared to the glass beads. As the constant B' depends on the filler-polymer adhesion, it is apparent that irregular paint particle adhesion to the matrix is poorer. Though the larger sized paint particle dispersed composite showed much lower value for B', no conclusion should be drawn from this as the volume fraction added was only upto 0.027 which is not enough to show the trend in composite strength.

Table 4.4.4 : Constant values for Piggott and Leinder equation (flexural strength).

Filler	A'	B'
glass (66 μm)	0.98	96.78
paint (63 μm)	1.00	130.76
paint (135 μm)	0.99	90.48

Also for three point flexure test, failure takes place by a crack propagating from the tension side to the compression side of the beam. The presence of dispersed phase hinders the crack propagation which could lead to higher strengths in flexural specimens compared to tensile specimens under the same test speed. These conclusions were drawn by Nabi and Hashimi (1996) when they worked with glass filled acrylonitrile/styrene/acrylate copolymers. They observed greater difference between tensile and flexural strength with increased volume fraction of dispersed phase as crack propagation became more difficult. No such conclusion

can be drawn in the present study as tensile and flexural tests were performed at different speeds.

4.4.2.2 Effect of dispersed phase on flexural modulus

The modulus values obtained in flexure test were lower than those from tensile test. The result was obvious as the tests here were performed with a slower speed (10 mm/min) compared to the tensile tests (50 mm/min). Slow speed permits more disentanglement of molecular chains thus giving lower modulus. The binary blend of PP/rubber gave lower modulus (924 MPa) compared to the virgin PP (1244 MPa) for the inclusion of rubbery phase in the matrix. The flexural modulus values for PP/rubber composites differed with the different dispersed phases used. For glass filled composites a slight increase in modulus was noticed (figure 4.4.20.a) whereas for paint dispersed composites a decreasing trend was observed with increasing filler fraction (figure 4.4.20.b).

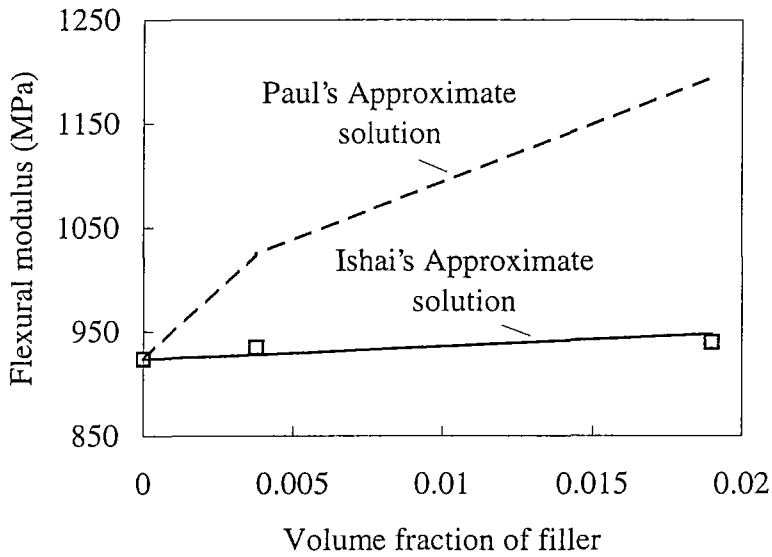

Figure 4.4.20.a : Flexural modulus versus filler volume fraction for glass bead dispersed PP/rubber composites.

The phenomena can be attributed from the differing stiffness of glass beads (~ 73 GPa) to paint particles (~ 887 MPa). In case of glass filled systems, as the modulus of the filler itself is

very high relative to that of the matrix (924 MPa), they influence the composite modulus more compared to the matrix. Also as the degree of adhesion between the filler-polymer is poor, so a dramatic increase in modulus is not seen. For the paint dispersed composites, comparable

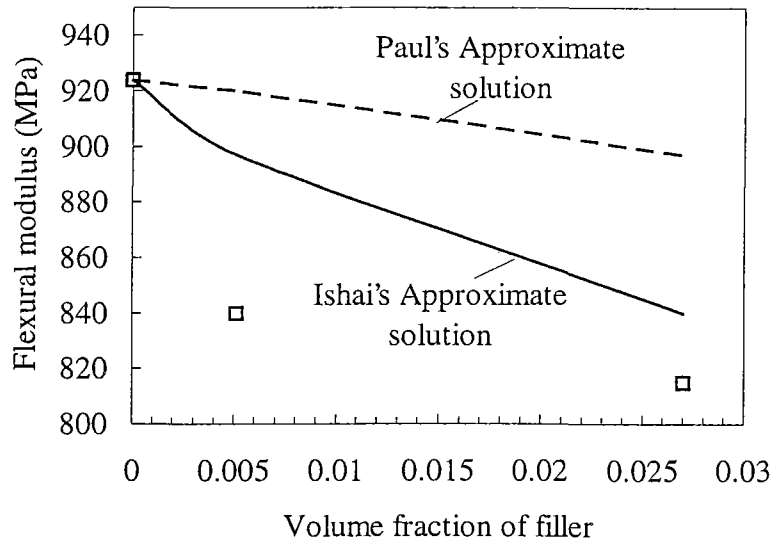

Figure 4.4.20.b : Flexural modulus versus filler volume fraction for paint particle (63 μm) dispersed PP/rubber composites.

values of filler and polymer modulus is observed and for poor interphase between them a reduction in modulus is noticed with increased filler fraction. The solid and dotted lines in the graph represent Paul and Ishai's approximate solution respectively. For glass filled composites, the experimental data points correlate quite well with the lower bound curve as seen in the Young's modulus case as well. For paint dispersed composites, the deviation of experimental points from the upper and lower bound curves imply that a large extent of non interaction exists between the polymer and the dispersed phase.

When talc was added to the PP/rubber matrix a gradual increase in modulus value was noticed as observed in figure 4.4.21. Talc acted as a reinforcing filler and left a reduced degree of

room for compressive deformation of the PP/rubber matrix. The modulus values were within the bounds approximated by Paul and Ishai.

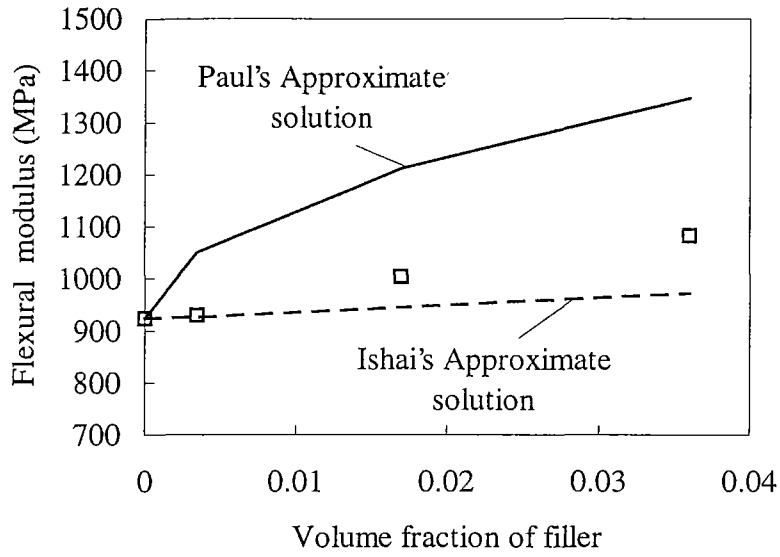

Figure 4.4.21 : Flexural modulus versus filler volume fraction for talc particle dispersed PP/rubber composites.

For both the glass bead or paint particle dispersed PP/rubber/talc composites, a gradual decrease in flexural modulus was observed. Though glass beads increased modulus of binary PP/rubber composites the same was not the case here. With the presence of much rigid talc particles (~ 170 GPa), the glass beads could not provide enough strength to the matrix and so failed as a weak structure. The same happened for paint dispersed composites which had even lower modulus value. Figure 4.4.22 shows the variation of modulus values against the filler fraction along with the upper and lower bounds according to Paul and Ishai's approximation for these composites.

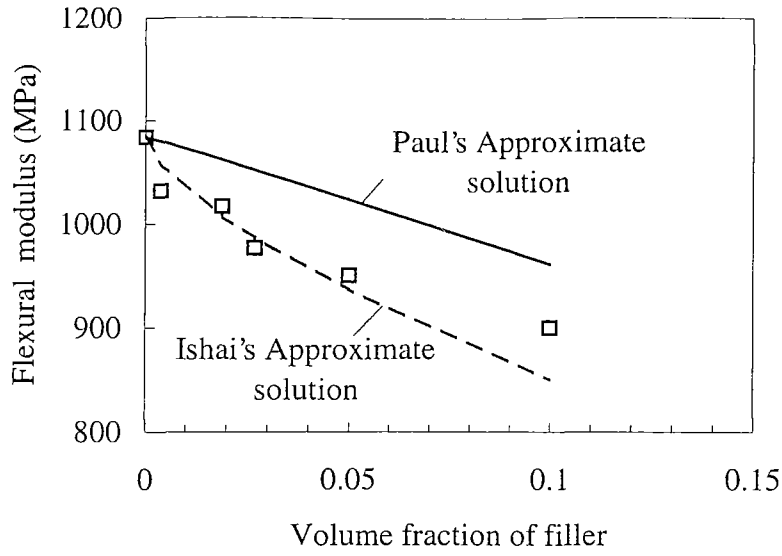

Figure 4.4.22.a : Flexural modulus versus filler volume fraction for glass bead dispersed PP/rubber/talc composites.

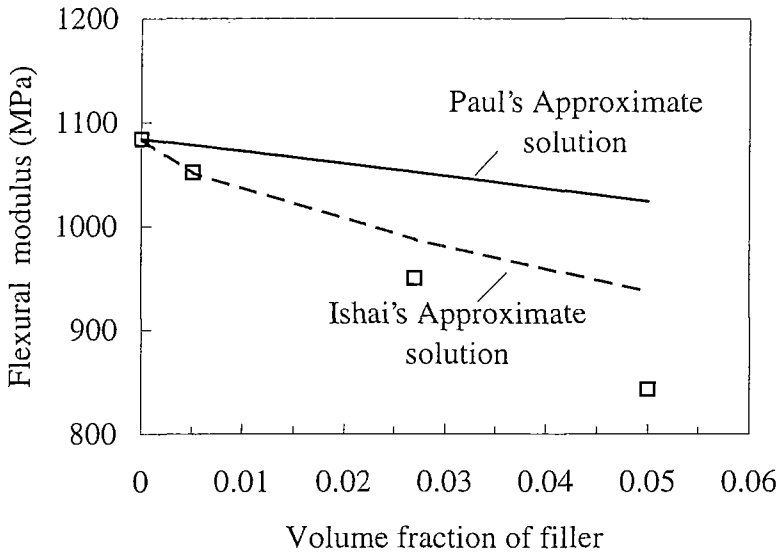

Figure 4.4.22.b : Flexural modulus versus filler volume fraction for paint particle (63 μm) dispersed PP/rubber/talc composites.

4.4.3 Impact strength

4.4.3.1 Base material and melt filtered material

The Izod impact strength was performed on notched specimens at room temperature and are tabulated in appendix E, table E.1. The impact strength of batch 1 and 2 decreased drastically (about 50%) compared to the base material without any paint. The paint particles acted as stress concentrators and crack initiators thus reducing the matrix strength. Though no significant variation was observed between the strength of unfiltered and melt filtered composites, there was a trend of decreasing values with filtration process. Only the unfiltered batch 2 material with 2.48% paint showed lower strength compared to its filtered batches. For batch 3 (recycled bumper material), the initial reduction for unfiltered sample was lower (upto 21%) and with filtration process the reduction in strength was upto 28%. From these results it can be concluded that even a small fraction of foreign matter which can be as low as 0.5% is enough to reduce the strength of composites

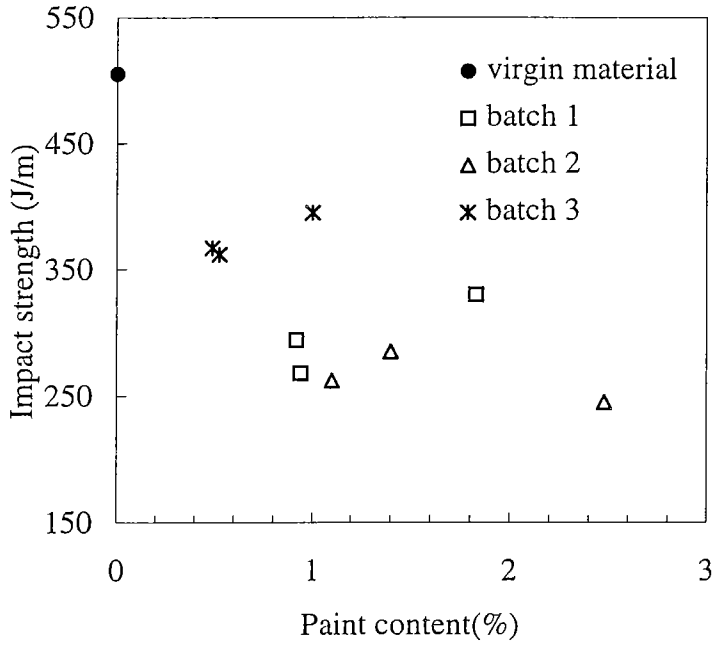

Figure 4.4.23 : Effect of paint content on impact strength before and after melt filtration for batch 1, 2 and 3 material.

when there is very poor adhesion between the matrix and the dispersed phase. It is difficult to conclude from these set of results whether particle size influence the strength or not as it was not a controlling factor. But conclusion can be drawn that concentration level of dispersed phase did not have significant effect on the impact strength. Figure 4.4.23 shows the effect of paint content on impact strength before and after melt filtration of batch 1, 2 and 3 respectively.

Analogous observation was reported by Tao *et al.* (1993), Asakawa (1992) and Miranda *et al.* (1994) for paint coated bumper material. Borkar and Lai (1993) studied the melt filtration of painted/plated recycled computer casing material and reported 80% reduction of impact strength for melt filtered material compared to the virgin sample.

4.4.3.2 PP/rubber based composites

The impact strength of the PP/rubber composite (506 J/m) was much higher than the neat PP itself (46 J/m) as it is well known that inclusion of rubber phase toughens the PP matrix. With the addition of dispersed paint particles and glass beads to this binary PP/rubber system the impact strength of the base matrix decreased drastically (Appendix E, Table E.3). In the region between matrix and filler for filled composites, a third phase is developed consisting of areas of imperfect adhesion, where stress concentrators, impurities and other defects develop. These micro defects lead to localised stress concentrations, which are in excess of the average stress in the bulk of the material. If the localised stresses are sufficiently high, they may lead to a growth of the defect and subsequent failure of the material. The same happened in case of these composites where poor adhesion was observed from the examination of fractured surfaces under the scanning electron microscope (section 4.2, figure 4.2.1 and 4.2.2).

Figure 4.4.24 shows the plot of impact strength of PP/rubber based composites versus volume fraction of the two different dispersed phases. For paint dispersed composites, the effect of particle size on impact energy was not significant though larger sized particles showed slightly higher strength. This is in contradiction with Nakamura *et al.*'s (1993) observation where they found that smaller sized particle filled composites absorbed more energy compared to bigger particles. Their work was performed on silica filled epoxy resin with particle size ranging from 2 ~ 47 μm. They did not observe significant difference between the values for particle content of 55 and 64%. The later observation was similar to the present studies though the content amount was much low.

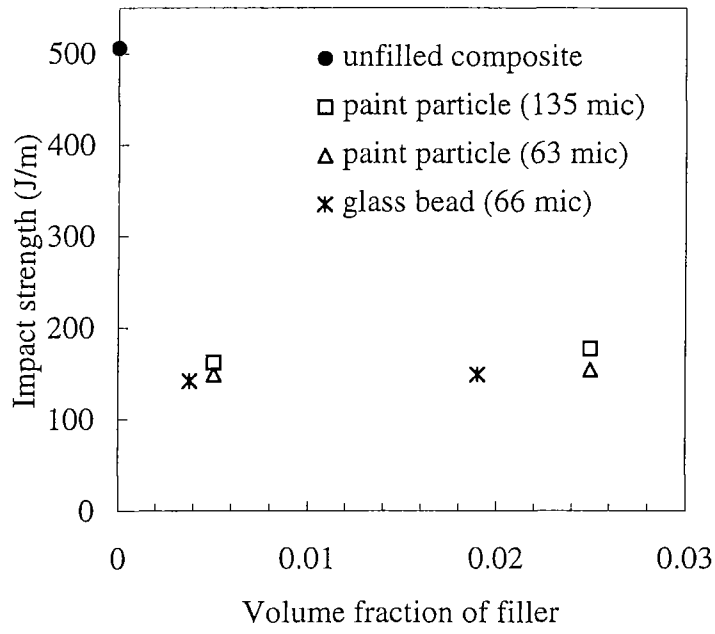

Figure 4.4.24 : Impact strength versus volume fraction of dispersed phase for PP/rubber composites.

Also observed from the graph that similar sized paint particle (63 μm) and glass bead (66 μm) dispersed composites showed insignificant difference in strength values. So it can be concluded that for low concentration level of filler, the shape and size of filler do not effect the material strength when the adhesion between the matrix and the dispersed phase is poor.

4.4.3.3 PP/rubber/talc based composites

The base matrix of PP/rubber/talc showed about 60% reduction in strength value (190 J/m) compared to the base PP/rubber matrix (506 J/m). Firstly, the effect of talc on impact strength was observed by increasing the talc fraction in PP/rubber matrix as shown in figure 4.4.25. A decrease in strength with increase in talc content was observed which may be attributed to the immobilisation of the matrix by the filler so that the filler fails to deform before failure. Lack of stress transfer between filler/matrix interphase also aided the fracture. Similar behaviour was observed by Maiti and Sharma (1992) for talc filled PP composites but was contrary to the observation of Maiti and Mahapatro (1991) where an initial increase of strength was reported for PP/$CaCO_3$ system.

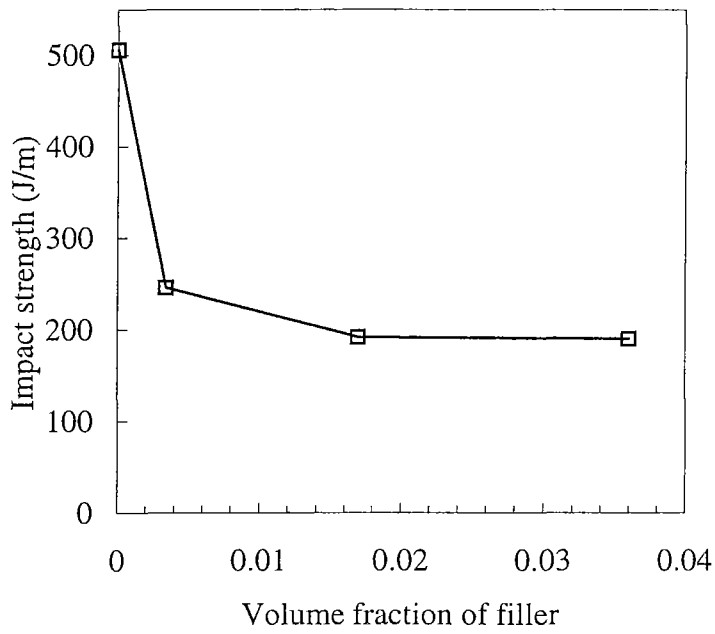

Figure 4.4.25 : Variation of impact strength of PP/rubber composite with volume fraction of dispersed talc particles.

The structure and properties of three component composites depend on composite properties, the characteristics of each component, miscibility and processing conditions. For PP-elastomer-filler systems, mutual miscibility and adhesion of the components are the crucial

factors influencing structure and properties. A desired microstructure can be obtained by controlling processing conditions and interfaces between various components. Matnois and Small (1969) and Matnois (1969) suggested that encapsulated structure would improve both stiffness and toughness where the elastomer particles have a filler core in them. Shanks and Long (1996) studied the PP-elastomer-filler (talc and $CaCO_3$) hybrids and showed that impact strength increased for encapsulated structure where elastomer particles had a filler core, compared to a separated microstructure. On the basis of the result they proposed a model to stimulate the deformation behaviour in these hybrids as illustrated in figure 4.4.26.

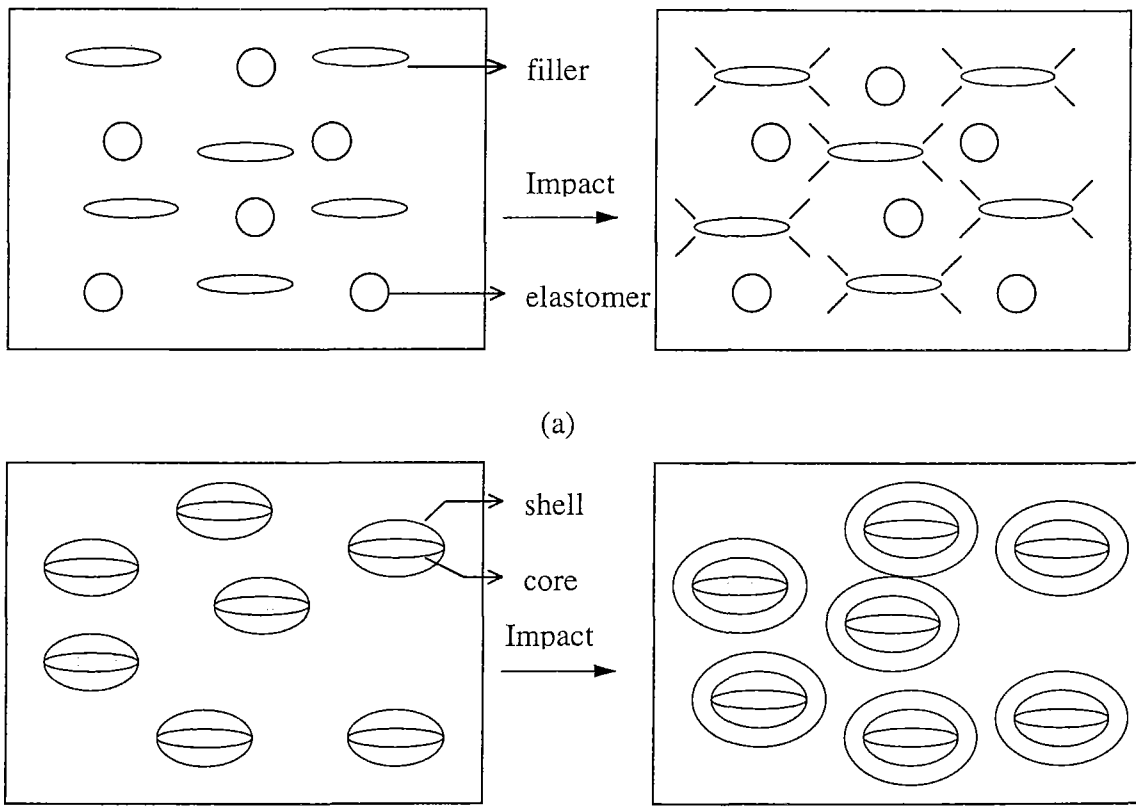

Figure 4.4.26 : Morphological model of microstructures and fracture of PP-elastomer-filler composites (a) separated and (b) core-shell microstructure (Shanks and Long, 1996).

They explained that with the application of an impact, filler particles tend to produce a range of microcracks for separated microstructure. The elastomer present are not able to stop the

crack propagation to full extent. On the other hand, for the core shell microstructure a yielded zone around the elastomer particle, with filler core, is established and original microcracks initiated at the fillers are prevented. Furthermore, the effect of elastomer on the toughness of PP depends on the distance between particles as well. The presence of filler as a core decrease the distance between elastomer particles thus making them more efficient.

In the present investigation, the hybrid had a separated microstructure and thus lower value for impact strength of the PP/rubber/talc system is expected according to the postulated model described above. The addition of talc increased the distance between PP and elastomer at some points thus making uneven absorption of impact energy throughout the fractured surface.

When paint particles were added to this separated microstructure hybrid, further reduction in impact strength was observed (Appendix E, Table E.4). This can be explained as for the case of addition of talc though here it was considered that PP-elastomer-talc now acts as the matrix for these components. The poorly adhered large sized particles again reduced the elastomer ability to absorb the applied strength by reducing the distance between particles. The reduction in strength was quite significant at lower level of particulate addition and became less adverse with increased volume fraction of particles as shown in figure 4.4.27. Similar effect was observed by Ghosh and Maiti (1996) for silver/PP composites. They explained that the fillers remained in agglomerated form producing stress concentration points. For interacting type of silver particles in PP matrix, the impact induced crack can readily propagate along the particle polymer interface.

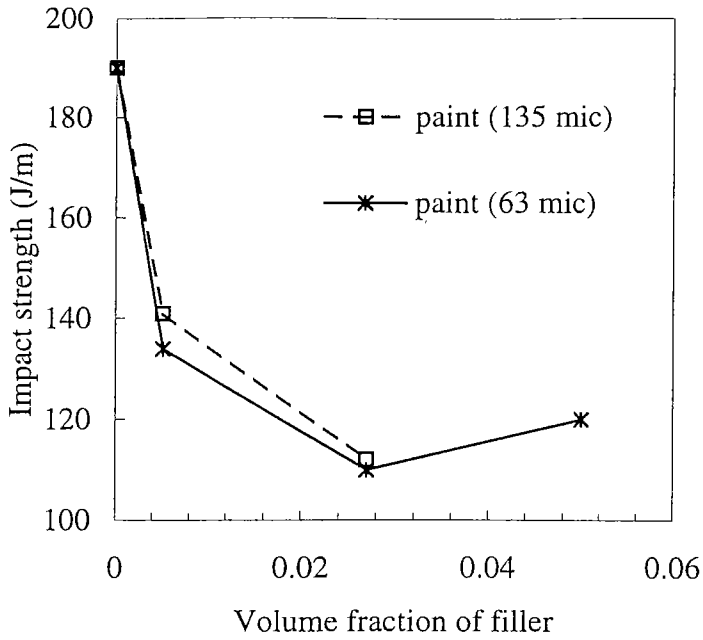

Figure 4.4.27 : Variation of impact strength of PP/rubber/talc composite with volume fraction of dispersed paint particles.

The result of impact test for glass filled composites was somewhat different compared to the paint dispersed systems as shown in figure 4.4.28. The initial addition of filler showed a drop in strength but further addition of dispersed phase ($\varphi > 0.019$) showed a gradual increase in strength upto the maximum filler level examined (10 vol%).

The observation was similar to Vollenberg and Heikens (1990) where they worked with chalk filled PP and observed that in case of excellently adhering chalk particles an increase in filler content decreased the impact strength, whereas in case of poor adhesion a maximum in impact strength was observed at a certain volume fraction of filler. The location of this maximum depended on the particle size of the filler where smaller particles showed the maximum at lower concentration compared to larger particles. They tried to explain the occurrence of maximum value due to a combination of two shearing processes : diffuse shearing and the formation of shear bands, which they observed by a slow tensile test.

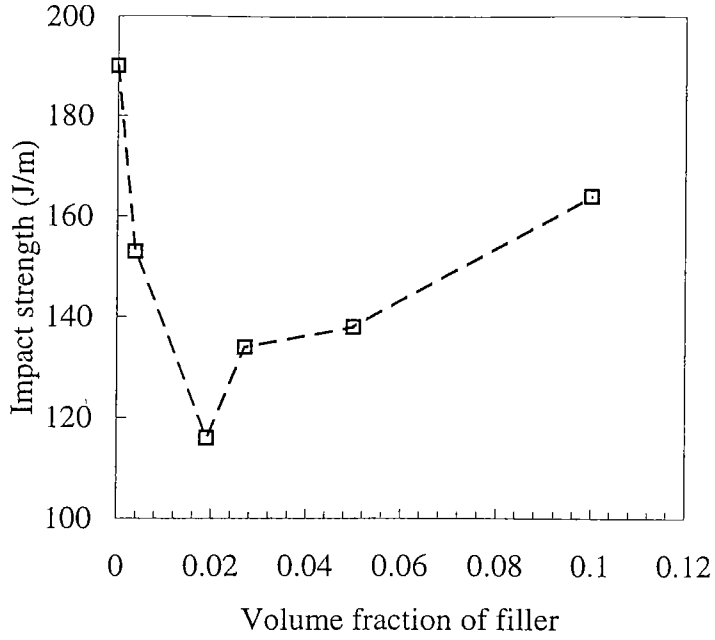

Figure 4.4.28 : Variation of impact strength of PP/rubber/talc composite with volume fraction of dispersed glass beads.

But it was pointed out that deformation behaviour may depend on speed on testing, so further study of the deformation mechanism at high speed test should lead to final conclusions. For filler concentration greater than maximum, the network continuity is upset leading to property deterioration. In this study though 10% glass bead (vol%) showed the highest value in strength, it is not possible to conclude whether this is the maximum or not as dispersed phase was not increased beyond this. Also no shear band formation was observed at this speed of test. To explain this phenomenon it was noticed that firstly, for the same volume fraction of dispersed phase, spherical glass beads had less detrimental effect on reducing strength compared to irregular paint particles. Also with increased volume fraction of glass beads the crack propagation path becomes longer and the distance between the elastomer and PP starts to decrease again thus providing better strength to the composite.

4.4.4 Fracture mechanism of composite materials

The fracture test of the blend composites were carried on an instrumented impact tester (IIT) as described in chapter three section 3.2.8.3 and a typical load displacement curve generated from the test is shown in figure 4.4.29. The area under the load displacement curve represents the energy absorbed during the fracture event, and these energy data can be plotted against $BD\phi$ where B and D are the specimen dimensions and ϕ is a compliance calibration function, to find the fracture energy or strain energy release rate, G_c. Investigating the curve obtained, it is reasonable to assume that crack initiation occurs at the maximum force (P_c) and the lower peaks, if any, result from specimen vibration and loss of contact with the striker. Then an initiation energy can be determined from the area upto the point P_c, but a gross energy, including the initiation, propagation and any ductility effects, would be represented by the total energy under the curve which should be similar to energy loss recorded in simple pendulum tests, as in those cases it is not possible to distinguish between crack initiation and propagation.

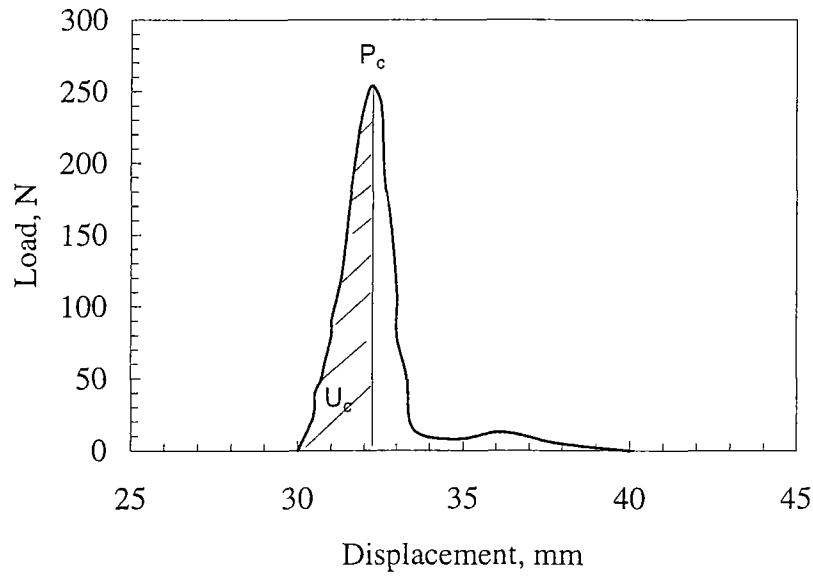

Figure 4.4.29 : Typical load displacement curve from IIT for a paint dispersed PP/rubber/talc sample.

In this work it was the initiation energy that was studied and so the energy upto the maximum load (U_c) was calculated by IIT software using mid-point trapezoid rule and plotted against $BD\phi$. It was explained in chapter two, section 2.6.3.3, that the impact fracture energy G_c, can be calculated from the slope of the plot :

$$U_c = G_c BD\phi + U_T \qquad ...(2.6.38)$$

where U_T is the intercept of the graph representing kinetic energy loss and can be calculated using the equation:

$$U_T = \frac{\pi}{2} m_s V^2 \qquad ...(2.6.47)$$

where m_s and V are the specimen mass and striker velocity respectively. Excepting for neat PP, plots of U_c vs. $BD\phi$ for all other composites were non linear explaining that brittle failure was observed for neat PP only and some degree of plasticity occurred for the others The fractured surfaces showed a small whitened plastic zone ahead of the crack tip and the failure was classified as semi brittle in nature. This type of failure was explained by Irwin and is described in section 2.6.3.1. As mentioned, equation (2.6.38) is still valid when $r_p < a$, where r_p is the radius of the circular plastic zone and a is the original crack length and (r_p/D) is not too large (< 0.2). Least square fitting technique was used in these situations, where small increment of r_p value was added to a until the data for the plot of U_c vs. $BD\phi$ gave minimum deviation from straight line. Figure 4.4.30 shows a typical plot of U_c vs. $BD\phi$ where plasticity effect causes non-linearity in the plot and also the corrected data for the same where the plastic zone correction factor has been used. Similar plots were obtained for all the composites to find the initiation fracture energy from the slope of the corrected line. At least six to eight measurements were taken for each notch depth as shown in figure 4.4.30. The G_c value was calculated from the slope of the corrected data. Then to simplify the process an average of energy was calculated from the measurements for each notch depth and the values were

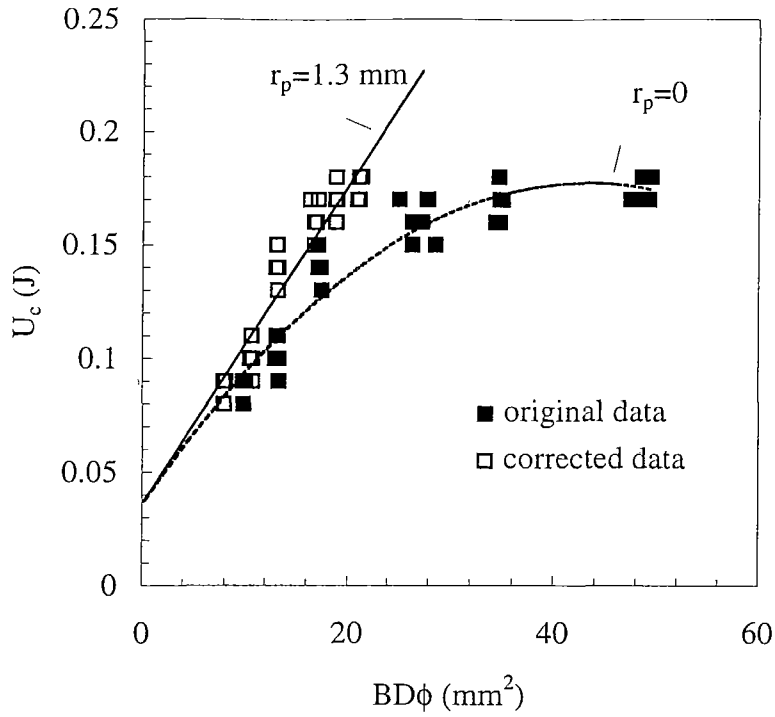

Figure 4.4.30 : Plot of original and corrected data of U_c versus $BD\phi$ for PP/rubber/talc composite (all data points).

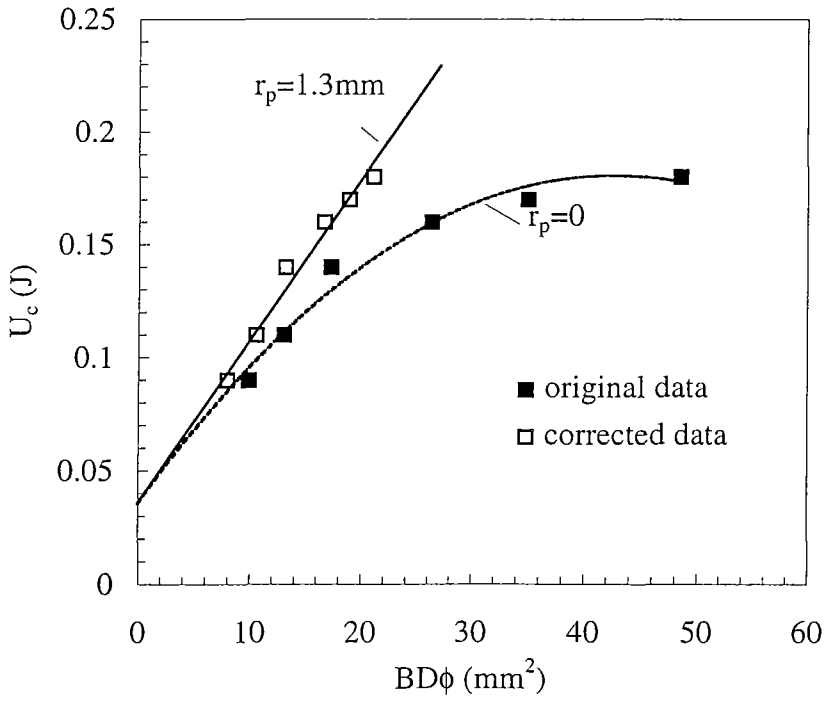

Figure 4.4.31 : Plot of original and corrected data of U_c versus $BD\phi$ for PP/rubber/talc composite (average data points).

replotted to calculate G_c (figure 4.4.31). The resultant values of G_c from both the methods were then found to be 7.0 kJ/m^2 (R^2 = 0.8971) and 7.2 kJ/m^2 (R^2 = 0.9722) respectively. As the agreement was reasonable so only the average energy values were used for calculating G_c for the rest of the composites.

To obtain the fracture toughness, K_c, the peak force (P_c) which is associated with crack initiation, was used to calculate the gross stress at fracture, σ_c , according to the equation:

$$\sigma_c = \frac{3}{2}\frac{P_c L}{BD^2} \qquad ...(4.4.1)$$

where L is the span of the specimen. These stresses were then used, together with appropriate crack length and finite width correction factor, Y, to determine the fracture toughness or critical stress intensity factor, K_c , as :

$$K_c = \sigma_c Y a^{1/2} \qquad ...(4.4.2)$$

where $$Y = 1.93 - 3.07\left(\frac{a}{D}\right) + 14.53\left(\frac{a}{D}\right)^2 - 25.11\left(\frac{a}{D}\right)^3 + 25.84\left(\frac{a}{D}\right)^4$$

A plot of $\sigma_c Y$ versus $a^{-1/2}$ was constructed where the resulting slope gave the fracture toughness K_c . Use of average reading for the stress values at a particular notch depth was applied similar to G_c value calculation. Figure 4.4.32 shows a typical plot of such a curve for paint dispersed PP/rubber/talc composite. The calculated values of G_c and K_c for PP/rubber and PP/rubber /talc composites are tabulated in tables 4.4.5 and 4.4.6 respectively.

In the following sections fracture mechanism of PP/rubber and PP/rubber/talc based composites are discussed in terms of the effect of filler concentration, filler size and filler nature .

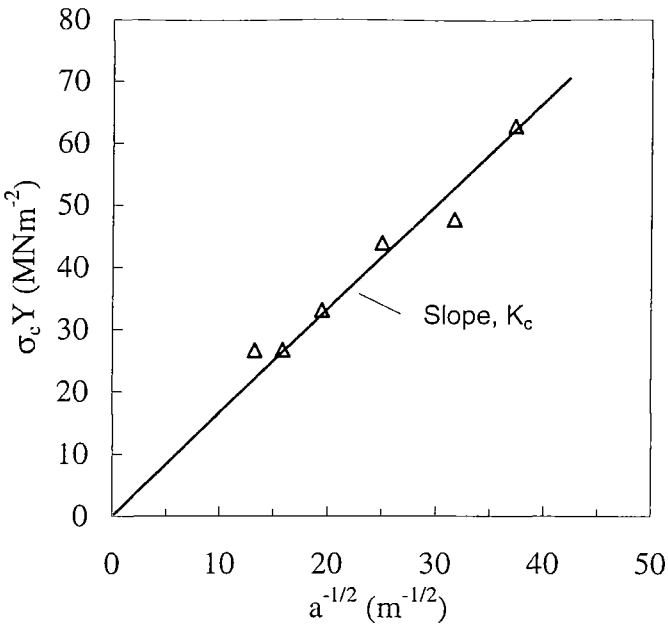

Figure 4.4.32 : $\sigma_c Y$ versus $a^{-1/2}$ for 2.7% paint (63 μm) filled PP/rubber/talc composite.

Table 4.4.5 : Fracture energy (G_c) and fracture toughness (K_c) for PP/rubber composites.

Filler	Volume fraction	G_c (kJ/m^2)	K_c (MNm$^{3/2}$)
Unfilled PP/rubber composite	-	3.6	1.52
Glass beads	0.0038	4.0	1.54
	0.019	4.3	1.48
Paint particles (63 μm)	0.0051	3.5	1.44
	0.025	3.9	1.40
Paint particles (135 μm)	0.0051	3.5	1.58
	0.025	3.9	1.70
talc	0.0034	3.6	1.52
	0.017	4.0	1.7
	0.036	7.2	1.92

Table 4.4.6 : Fracture energy (G_c) and fracture toughness (K_c) for PP/rubber/talc composites.

Filler	Volume fraction	G_c (kJ/m^2)	K_c ($MNm^{3/2}$)
Unfilled PP/rubber/talc composite	-	7.2	1.92
Glass beads	0.0038	4.6	1.70
	0.019	4.3	1.69
	0.027	3.9	1.67
	0.05	3.5	1.65
	0.10	3.8	1.70
Paint particles (63 μm)	0.0054	4.3	1.63
	0.027	3.9	1.61
	0.05	3.5	1.48
Paint particles (135 μm)	0.0054	4.5	1.75
	0.027	4.0	1.73

4.4.4.1 PP/rubber composites

As stated, the fracture of PP/rubber based composites (filled and unfilled) was classified as semi brittle failure. The fracture energy, G_c, of the binary base matrix (3.6 kJ/m^2) was higher than neat PP (1.7 kJ/m^2) and the increase in toughness can be explained by matrix shear yielding and rubber particle cavitation.

In rubber toughened polymer blends, the rubber gives rise to volume increase if the strain rate is sufficiently high. This expansion is called cavitation of rubber particles. Rubber particles dissipate bulk strain energy by cavitation, which leads to a local reduction of yield stress of the blend. In the presence of a sharp crack, a triaxial stress exists ahead of the crack tip. This promotes gradual dilation of the matrix and gives rise to rapid cavitation and growth of resulting voids. In addition, as the crack opens up, the increasing presence of stress concentration around the rubber particles promote both crack initiation and growth of shear yielding. The degree of shear yielding generated would be much greater because of large number of particles present. However, since the particles also act as sites for crack termination, the yielding would remain localised in the vicinity of the crack tip. So both the cavitation and the shear yielding process occur at the early stage of load application. Once initiated, the rubber particles toughen the matrix by acting as stress concentrators, enhancing shear yielding and then cavitate, dissipate energy and give rise to more shear yielding. In addition, void formation would considerably reduce the level of constraint on the matrix adjacent to voided particles. This ultimately relieves the degree of triaxiality experienced by the matrix in the interparticle regions and in turn lower yield stress thus promoting further shear yielding. As a result of voiding crack tip blunting occurs which in reality causes an even larger plastic zone formation. Thus increasing size of the plastic zone acts as the principal toughening mechanism.

The mechanism was proposed independently by Kinloch *et al.* (1983) and Pearson and Yee (1983) explaining the improved toughness for rubber modified epoxy compounds. For the blends under the present study, crazing was not observed and so the above mechanism seems to explain the increased toughness for the PP/rubber blend over the neat PP. To obtain an insight into the toughening mechanism the fractured surfaces were examined under scanning electro microscope (SEM). Figure 4.4.33 shows an example of a micrograph of a fractured PP/rubber composite.

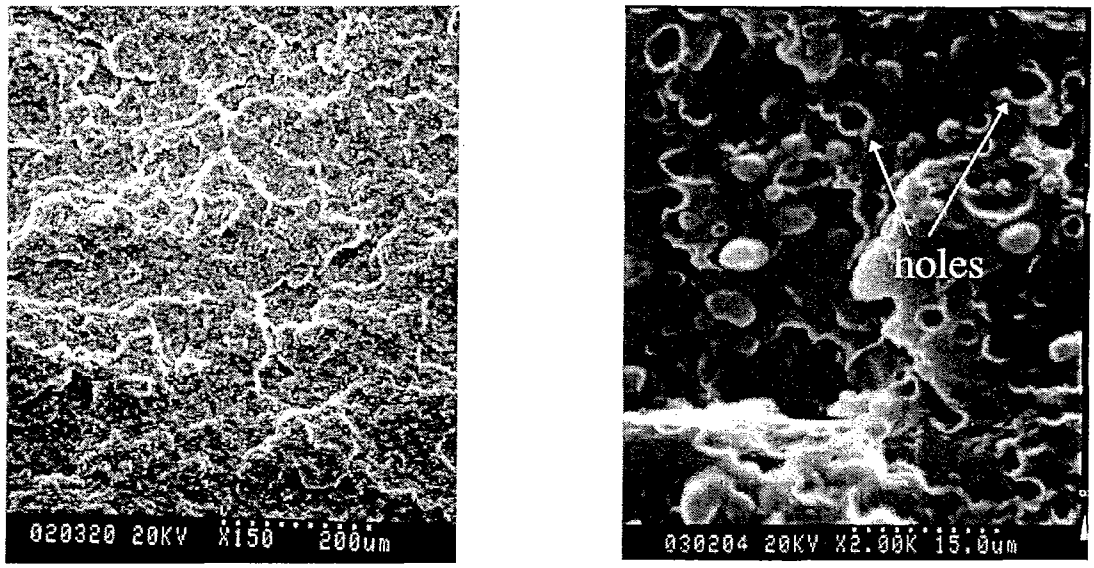

(a) (b)

Figure 4.4.33 : (a) SEM micrograph of fractured surface of PP/rubber composite.

(b) Enlarged SEM micrograph of the centre of (a).

As observed in the figure the dilation of the matrix and cavitation of rubbery particles causes the rubber phase to appear as holes. The rubber collapse back into the holes to give a cavity lined with rubber. Also, the enhanced shear deformation that occur in the matrix lead to a very rough, torn like surfaces containing river marks and furrows. Similar feature were also observed by Hodgkinson *et al.* (1983) and by Shanks and Long (1996) for PP/rubber blends.

For blends of PP/rubber dispersed with paint or glass particles a small extent of increased toughness was observed over the toughness of PP/rubber blend (table 4.4.5). Similar observation was made by Kinloch *et al.* (1985) for glass filled toughened epoxy material. The localised plastic deformation for the rubbery phase would still be dominant for higher G_c but crack pinning mechanism seems to work as well for the presence of dispersed glass and paint phase. This mechanism was described in chapter two, section 2.6.4.3 and it basically assumed that cracks can be impeded by rigid, impenetrable, well bonded particles. As crack meets an array of particles, it becomes pinned and tend to bow out between particles, forming secondary cracks. This leads to an increase in the length of crack front and some energy is supplied to this newly formed non-linear crack front as well. This in turn lead to enhanced crack resistance. For poorly bonded particles this mechanism has less effect on increased toughness. In the present study, no particular attention was focused on improving adhesion between the matrix and the dispersed phase. Also the micrographs of fractured surfaces of glass bead and paint particle dispersed composites presented in section 4.2 (figure 4.2.1 and 4.2.2) suggested that the fillers were debonding from the matrix at the interface and also did not show any characteristic tail which is consistent with the conclusion that less crack pinning occurred and lower increase in G_c resulted with inclusion of dispersed phase.

With the addition of talc to the PP/rubber system again a gradual increase in fracture energy was observed as shown in figure 4.4.34 upto the level of 3.6% which was later used as the base matrix composition for further studies. Here debonding at the interface was not so obvious from the micrograph (figure 4.2.3) and it can be assumed that bonding between talc and PP/rubber was somewhat better thus leading to higher G_c values.

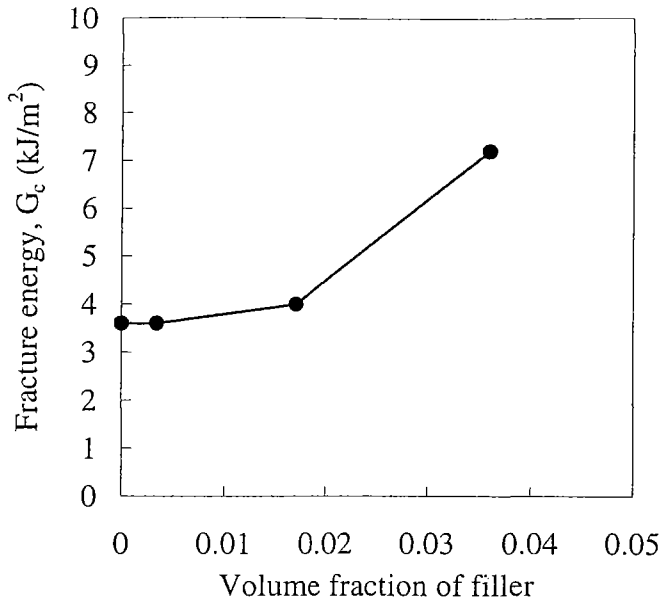

Figure 4.4.34 : Fracture energy versus volume fraction of talc for PP/rubber/talc systems.

4.4.4.2 PP/rubber/talc composites

As described in the previous section, the fracture energy of PP/rubber/talc composite was higher than PP/rubber one (figure 4.4.34) and the increased toughness was explained by crack pinning mechanism and localised plastic shear yielding. The composite with 3.6% talc (vol%) was used as the second base matrix and glass beads or paint particles were used as the dispersed phase into them as before. Generally a decrease in fracture energy was observed with increased filler phase (table 4.4.6). The result follows the poor interfacial bonding between the matrix and filler, where particles detach from matrix under impact. The fracture energy of these composites were similar to those without talc particles. Fillers such as talc, $CaCO_3$ silica and various other minerals added to PP generally increase the modulus but reduce the toughness of composites (Wong and Truss, 1994). But a range of behaviour has been found for these composites depending on the nature of filler, polymer matrix used and the strength of the interphase between polymer and filler. In general the presence of filler could either have a toughening or a weakening effect. On one hand, fillers tend to increase

surface roughness thus increasing fracture toughness for brittle matrix when filler-matrix adhesion is poor. On the other hand, they tend to inhibit plastic deformation by constraints or simply by volume replacement thus reducing the toughness. Thus, a competition exists between these two, and the toughening of the composite depends on which of the two mechanisms predominates. From the present result, it was observed that though PP/rubber/talc matrix had increased fracture energy over neat PP or PP/rubber matrix, the addition of paint particles or glass beads resulted in lowering the G_c value where the later mechanism predominated. So it becomes obvious that it is the second dispersed phase of paint particles or glass beads that reduces the matrix strength. The reinforcing talc filler does not overshadow its effect on deteriorating the matrix property.

One thing was noticed that at high volume fraction of glass beads there is a tendency in increasing G_c values which might be for localised crack tip blunting. But further investigation is required to establish this statement which was not performed in this present study.

4.4.4.2.1 Effect of filler nature on G_c

The fracture energy and fracture toughness of composites depend on factors like temperature; filler type, geometry, size and content; and interfacial bonding. In some special cases the fracture energy increases when small amount of filler is added which is explained by crack pinning mechanism, although it falls away again at higher volume loading. More generally the addition of filler causes a continuous and drastic reduction in fracture energy, resulting in a brittle, weak product. Similar detrimental effect was observed for both glass and paint particle filled matrices as shown in figure 4.4.35 which can be explained by debonding occurring at the interface. But the variation of fracture energy was insignificant at a constant concentration level for the different fillers dispersed in the matrix. The observation was similar to Jancar and Dibendetto (1995) who looked into the fracture mechanisms of ternary composites of PP with

inorganic fillers ($CaCO_3$, $Mg(OH)_2$) and elastomer inclusions. Here the $Mg(OH)_2$ used was platelet shaped and $CaCO_3$ was irregularly shaped. They found that for constant filler and elastomer concentration level in matrix, variation of G_c was insignificant for the different fillers. Kendall (1978) worked on carbon black (20 nm dia.) and silica (7-40 nm dia.) filled LDPE and found similar reduction in fracture energy. He proposed a theory based on it where the idea was, when the adhesion between particles and polymer is poor, the filler becomes detached from the polymer and composite fractures as a weak foam. Moloney *et al.* (1983) looked at fracture properties of commercial epoxide resin filled with irregular sharp edged silica and irregular rounded edged alumina with mean particle size of 1~300 and 0~6 μm respectively. The silica particles were well-bonded to and alumina particles were de-bonded from the resin. From their observation it was concluded that for these irregularly shaped relatively rigid particles neither the particle size at a constant volume fraction of filler nor the particle filler adhesion greatly influence the toughness.

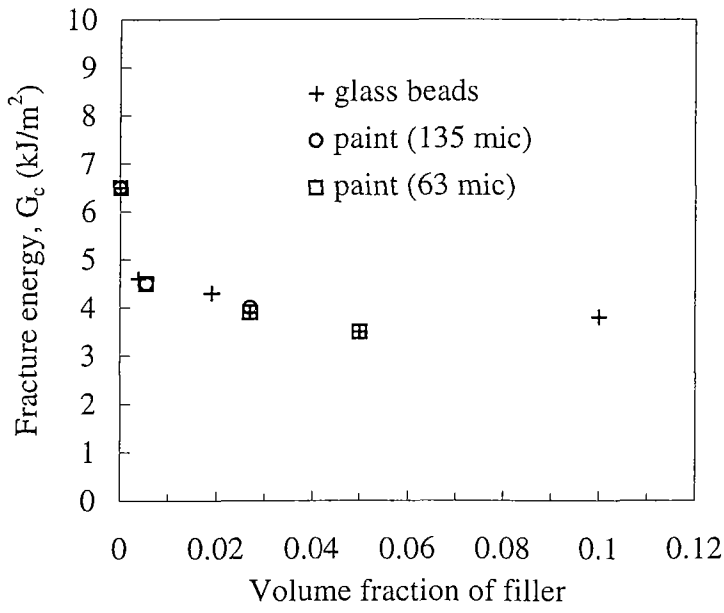

Figure 4.4.35 : Effect of filler nature on fracture energy for PP/rubber/talc composites.

4.4.4.2.2 Effect of filler concentration on G_c

For the PP/rubber composites the addition of filler showed a tendency of slightly increasing fracture energy with increased filler concentration (table 4.4.5). Kinloch *et al.* (1985) observed similar effect for hybrid particulate composites where epoxy material was used as the base matrix. For epoxy-glass and epoxy-rubber-glass composites the G_c value passed through a maximum at a certain volume fraction of glass beads and then decreased. Mallick and Broutman (1975) noticed similar behaviour for glass bead filled epoxy composites and explained that enhancement of fracture energy was due to the interaction of crack front with the dispersed particles. A drop in fracture energy was observed after a critical volume fraction when the effectiveness of the dispersed particles to pin down the crack front was reduced.

But for the PP/rubber/talc based composites, a sharp drop in fracture energy was observed with the addition of the second dispersed phase (glass beads or paint particles), after which the decrease in G_c was quite small with increasing filler fraction as shown in figure 4.4.35. The initial sharp drop in G_c indicates that the failure mechanism of the matrix was disturbed by the addition of the particles which had poor interaction with the polymer. As seen from the micrographs, debonding of particles occurred at the interface for these filled systems (figure 4.4.36 and 4.4.37) and thus the crack propagation was hindered reducing the fracture energy. With increased concentration of particles, the detrimental effect slowed down as it was only the initial disturbance that was increasing with more polymer being replaced by particulate phase. Kendall (1978) proposed that fracture energy of filled polymers decreases as the polymer detaches easily from the particles and creates a series of holes like a foamed material, through which crack propagate easily to give a linear fall in toughness with filler volume fraction. Friedrich and Karsch (1981) examined the decrease in G_c for silica filled PP and

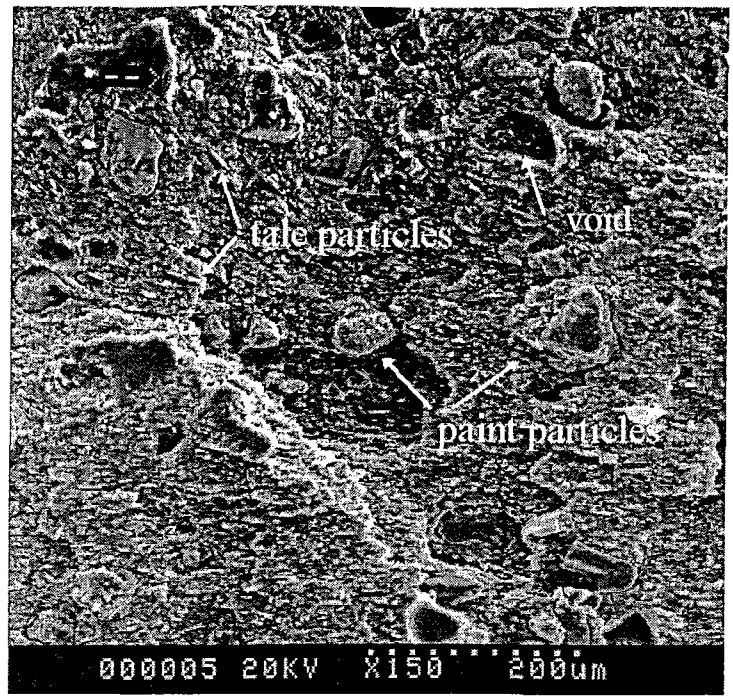

Figure 4.4.36 : SEM of an impact fractured surface of 2.7% paint particle (63 μm) filled PP/rubber/talc composite.

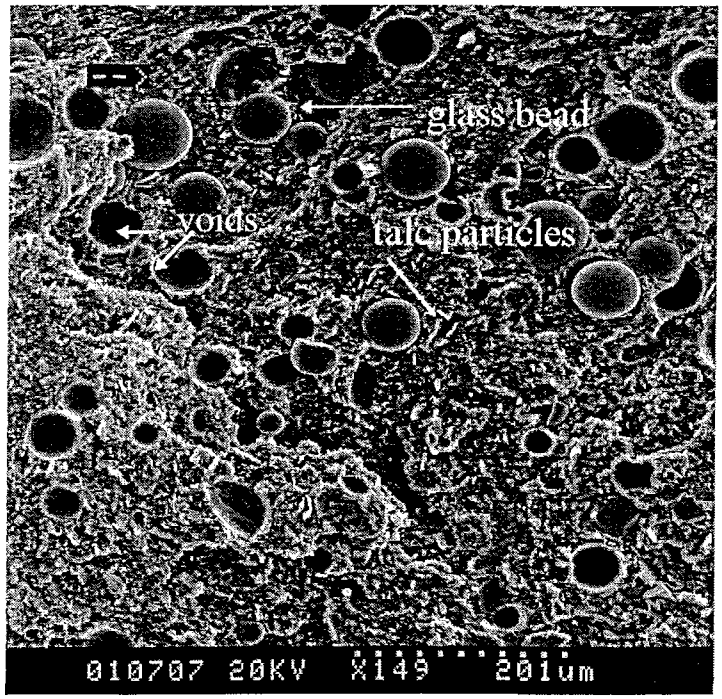

Figure 4.4.37 : SEM of an impact fractured surface of glass bead filled PP/rubber/talc composite.

suggested that as the interfacial energy is usually much smaller than the polymer fracture energy, the composite toughness drops when filler is added. Burford and Pittolo (1986)

studied the rubber crumb modified PS and found that for the addition of about 5% unmodified crumb to PS matrix, G_c value increased by about 100%. Further addition of crumb lead to reduction in G_c as crumb-PS adhesion is low and interfacial failure results. Srivastava and Shembekar (1990) studied the flyash filled epoxy resin and found that fracture energy reached a maximum at 6.5% flyash by volume and then decreased. The increase in energy was explained by increased surface area of fracture due to increase in surface roughness and interaction between crack front and dispersed phase. The decrease in energy for higher loading came from loss of tough matrix which was greater than the contribution from pinning process. On the other hand a continuos decrease in G_c was observed for flyash filled PP by Wong and Truss (1994). Nabi and Hashemi (1996) also noticed similar behaviour for glass bead filled acrylonitrile/styrene/acrylate (ASA) copolymers. For ternary composites of PP/rubber/filler ($CaCO_3$, $Mg(OH)_2$) similar reduction in energy was observed for constant PP/rubber fraction by Jancar and Dibenedetto (1995). They found that for volume fraction less than 0.055, the material fail by ductile tearing initiated around elastomer particles whereas with higher filler loading the failure mechanism changed to a quasi-brittle one. In all the cases it was noticed that the fracture energy was dependent on the particle volume fraction as well as degree of adhesion.

4.4.4.2.3 Effect of filler particle size on G_c

The fracture energy for the PP/rubber and PP/rubber/talc based composites was similar for the two sized paint particles used as seen in table 4.4.5-6 and as shown in figure 4.4.38.

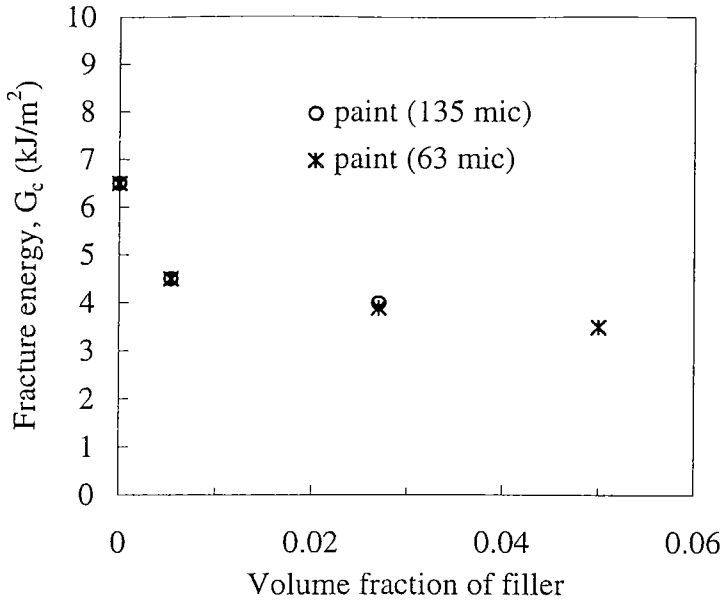

Figure 4.4.38 : Fracture energy versus volume fraction of paint particles for PP/rubber/talc composites.

The observation was different from similar studies where usually variation of fracture energy was noticed with change in filler size. Chen *et al.* (1989) worked on PP filled with 10 wt% $CaCO_3$ (~ 2.7 μm and ~ 75 nm) and found that fillers did not have any appreciable effect on G_c of copolymers based composites but improved G_c of homopolymer at low temperature (≤ 20°C) due to enhanced microplastic flow was observed on the fracture surface. Spanoudakis and Young (1984) studied the crack propagation in a glass particle filled epoxy resin where the filler particle size was varied from 4.5 to 62 μm and the filler fraction varied from 0.1 to 0.46. They observed that for a given value of volume fraction the particle size has a significant effect on fracture energy and the nature of crack propagation. For low volume fraction (φ=0.1), G_c dropped with increasing particle size to a minimum of particle size of 47 μm. For intermediate volume fraction (φ = 0.3), the initiation G_c peaks at diameter 32 μm. In composites containing a high volume fraction of particles (φ = 0.46), crack propagation was

continuous upto a certain diameter 32 μm above which it became stick/slip. So G_c increased at first, then reached a plateau level.

A different trend in fracture energy was again noticed by Nakamura *et al.* (1991, 1993) who worked on epoxy resin filled with angular shaped silica particles where the particle size varied between 2 to 47 μm. They found that impact absorbed energy increased with decreasing particle size but the fracture energy increased with increasing particle size. The explanation was that the starter crack for the small particle filled resin was sharp which was not the case for larger particle filled resin. In the later case many divergent cracks were present which redistributes the stress concentrated at the crack tip requiring greater energy for crack initiation. They concluded that increase in G_c with increasing particle size was due mainly to the differences in the starter crack.

The insignificant difference in fracture energy for the composites with two different sized paint particles used in the present study can be explained by the actual size of the particles. It was noted whenever a difference in fracture energy was observed the particle sizes under consideration was much smaller (all within about 60 μm). But in the present case the sizes used were 63 and 135 μm mean diameter, which was obviously much larger. It seems for larger particles the impedance of crack propagation is not affected by the size to that extent thus similar detrimental effect was observed for both of them.

4.4.4.2.4 Effect of filler nature on K_c

The effect of filler nature on fracture toughness for PP/rubber/talc composites for different volume fractions is shown in figure 4.4.39. As observed the data was very similar for both the dispersed phases. Moloney *et al.* (1983) found that for irregular sharp edged silica and round

edged alumina filled epoxy materials the data of K_c versus volume fraction was so similar that can be superimposed and K_c increased with filler fraction. But in the same matrix when irregular sharp edged dolomite was used it was observed that beyond 20% volume of filler a

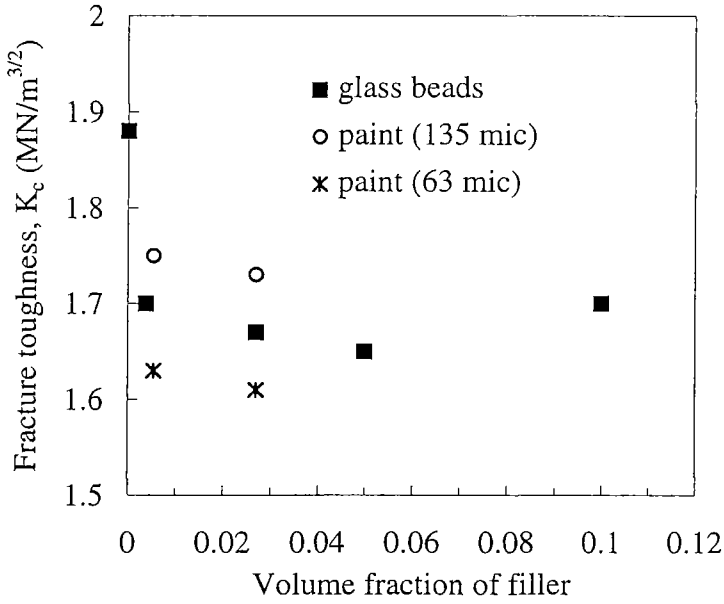

Figure 4.4.39 : Fracture toughness versus filler volume fraction for PP/rubber/talc composites.

plateau is reached for K_c. They explained that dolomite particles were rather weak and this plateau was caused by trans particle fracture which is not seen in case of strong particles like silica and alumina. Their observation was similar to Lange and Radford (1971) where they studied the toughness of relatively weak aluminium hydroxide filled epoxide resin.

Hashemi *et al.* (1996) Observed that addition of glass fibres enhanced but glass beads reduced the fracture toughness of plyoxymethylene (POM) matrix as the volume fraction of the filler was increased from 0 to 0.19. They explained that since the localised stress is highest at the notch tip, particle debonding occurs and a notch tip damage zone is formed which consists of

porous matrix. This damage zone is weaker than the surrounding undamaged composite and so a reduction in toughness is observed.

4.4.4.2.5 Effect of filler concentration on K_c

The addition of dispersed phase decreased the fracture toughness of the base composites for both PP/rubber and PP/rubber/talc systems as seen from figure 4.4.39, though the reduction was not as obvious as for the fracture energy case. With poor adhesion between the matrix and dispersed phase, the filler particles become easily debonded when struck with an impact and fractures more easily. Same behaviour was observed by Hashemi *et al.* (1996) for glass bead/POM system as discussed in the previous section. For flyash fillers epoxy (Srivastava and Shembekar, 1990) the K_c increased up to 6.5% filler volume but then decreased. This was because contribution from pinning process becomes less than reduction due to the loss of tough material. Friedrich and Karsch (1981) looked into the degradation effect of silicon oxide on fracture toughness of isotactic PP. They observed that for lower filler fraction (below 10%), K_c was only slightly affected by the amount of filler in the composite. They suggested that in this area K_c values do not represent real value as no crack instability occurred. Rather, crack propagated in stable manner under further increase of plastic zone ahead of crack tip. So these K_c data were only for crack propagation.

4.4.4.2.6 Effect of filler particle size on K_c

Figure 4.4.40 shows a slight increase in fracture toughness for paint dispersed composites with increasing particle size. The observation was similar to Nakamura and Yamaguchi (1993) where they noted an increase in fracture toughness with increasing weight fraction and particle size and explained the situation by showing the differences in starter crack for different sizes. Spanoudakis and Young (1984) observed that particle size had a secondary

effect upon K_c for a particular volume fraction of filler. For low filler fraction (φ=0.1), K_c decreased with increasing filler size. For volume fraction of 0.3, K_c had the highest value at 32 μm diameter and then dropped. For higher fraction K_c increased with increasing particle size. So it can be said that highest values of K_c are found for composites containing highest volume fraction of largest particles.

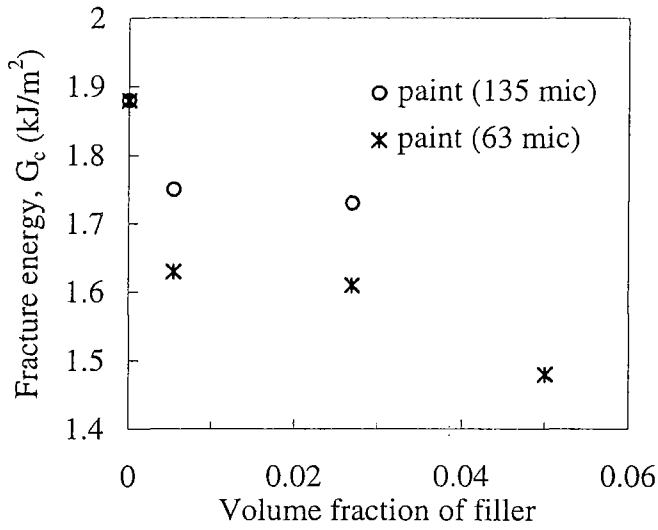

Figure 4.4.40 : Fracture toughness versus volume fraction of paint particles for PP/rubber/talc composites.

For the present study, though a slight variation was observed between two different particle sizes, it is not worthwhile to draw any conclusion based on that as the filler fraction was only up to 0.027 which might not be sufficient to show the full picture of the size variation effect.

4.4.4.3 Models of crack propagation in composite materials

Models for crack propagating through rigid particle filled matrix was first proposed by Goodier (1933). In later years similar approached was followed by many others. Mallick and Broutman (1975) worked on glass filled epoxy composites and illustrated the nature of stress

distribution around the particles for perfect adhesion and weak or no adhesion cases. If the interfacial adhesion is very strong, the stress is maximum at 90° and the matrix cracks at the same angle under an applied stress. In case of weak adhesion, the stress is maximum at 0° or 180° and the matrix breaks at the same angle between two particles. As soon as the crack reaches the interface, the weak interface may be debonded so that the crack will grow around the sphere along the particle matrix interface. The crack length is increased by a length πd without any appreciable increase in load. Figure 4.4.41 illustrates the possible location of crack for these two extreme cases. Kinloch *et al.* (1985) also worked on particulate systems and proposed that crack propagating through composites appear to be attracted to the equator of particles for glass-epoxy-rubber and glass-epoxy systems, but more towards poles of particles in hybrid composites containing silane coated glasses.

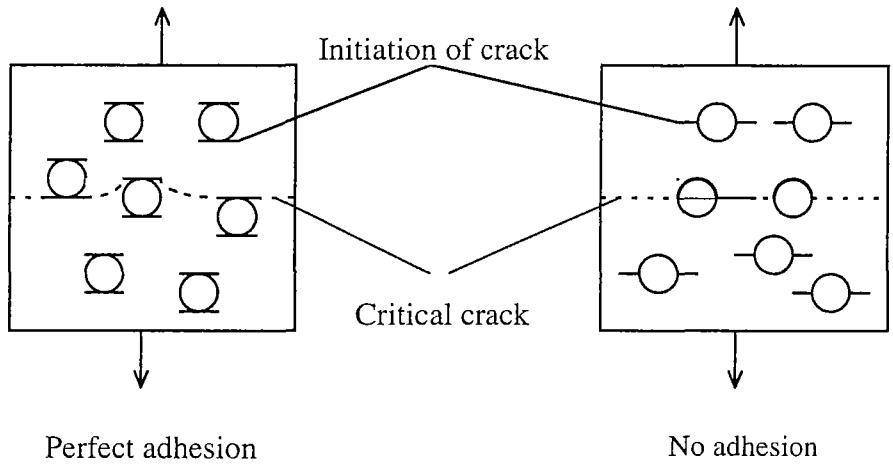

Figure 4.4.41 : Possible location of cracks in glass bead-resin matrix composites (Mallick and Broutman, 1975).

For poorly bonded or debonded particles the maximum tensile stress is at the equators of the particles and holes. Here the cracks propagating through the composite are attracted to the equator of particles and fractured surface consists of hemispherical holes and top surface of debonded particles. For well bonded rigid particles the maximum stresses are above and

below the poles of the particles. Since maximum stress is in the matrix, the cracks will propagate through the matrix above or below the particles leaving a layer of matrix covering the particles.

The same models can be used to explain the crack propagation in composites used in this study. Poor interfacial adhesion was observed from the micrographs for the glass filled PP/rubber/talc composites (figure 4.4.37), and according to the model described by Kinloch the maximum stress was observed at the equator of particles and holes. So, hemispherical holes and clean top surface of debonded glass particles were observed in the SEMs. The white flakey talc particles had much better interaction with the PP/rubber system and debonding was not so obvious for them. For this reason it was justified to consider the PP/rubber/talc composite to be a continuum phase.

For irregular shaped particles a different model was suggested by Xavier *et al.* (1990) as shown in figure 4.4.42 to describe the crack propagation characteristics where they examined PP-mica composites. Interfacial adhesion was again the crucial factor for different cases. For poor interfacial adhesion between PP and mica, the crack always followed the interphase no matter whether the flake was oriented parallel, perpendicular or inclined to the crack propagation direction. For strong interfacial adhesion, the crack propagated through the cleavage surfaces of the mica flake and thus caused fracture of the flake itself.

So it is seen that the poor bonding lets the flake debond from the matrix, providing sites of flake pull out along the propagation crack. On the other hand, if the adhesion between mica and matrix is good, high shear stresses are necessary to induce microvoiding across interphase, which weakens the composite and gives rise to microcracks. These microcracks initiate crazing and yielding of the matrix.

In the present case, poor bonding between irregular paint particles and the matrix was observed from the micrograph (figure 4.4.36) and clear sites of paint pull out was seen. Thus according to the model described crack always propagated following the interphase, debonding the paint particles. The talc particles were again seem to have higher interaction with the matrix and thus was considered as a part of the matrix.

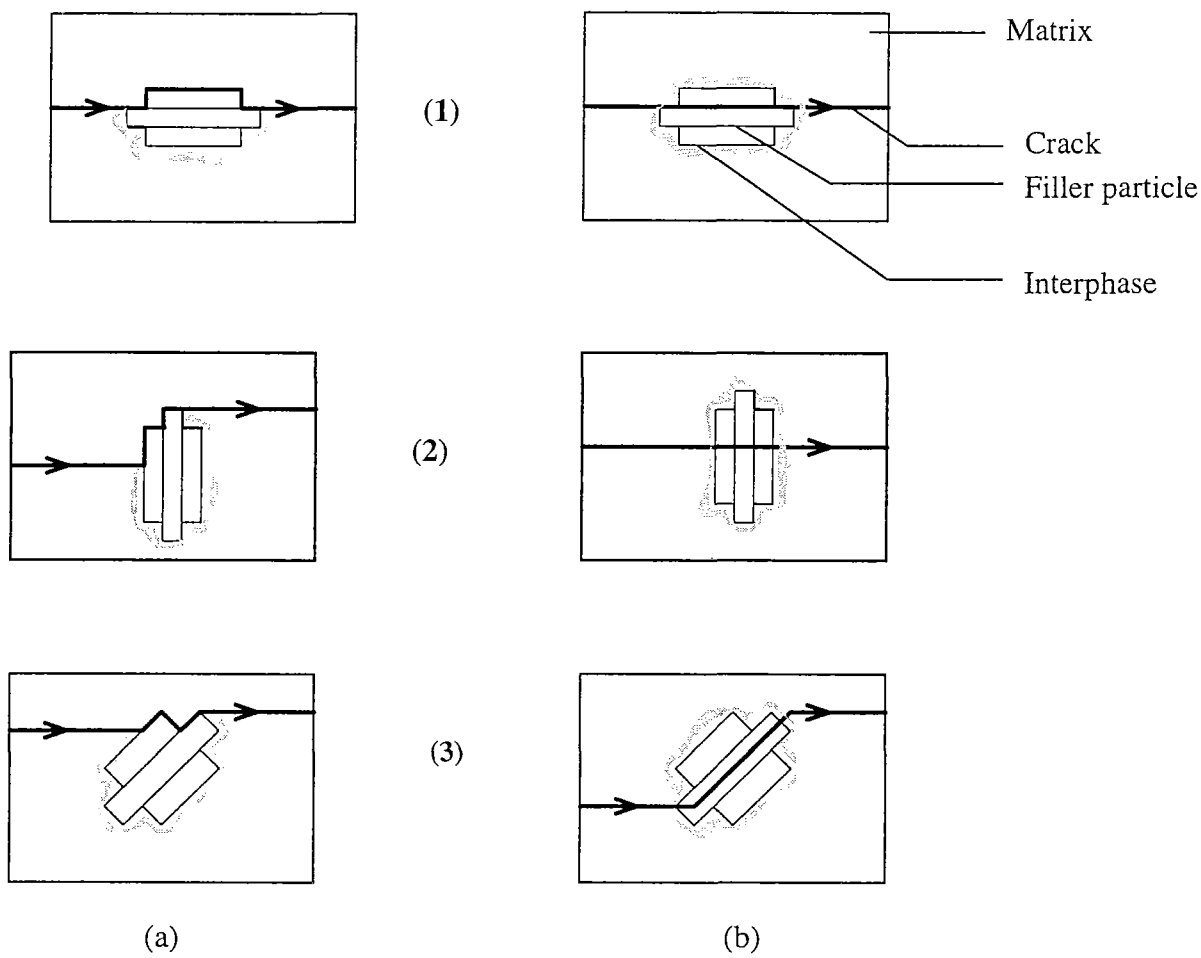

Figure 4.4.42: Models for fracture propagation through mica reinforced thermoplastic composites: orientation of flake (1) parallel (2) perpendicular and (3) inclined to the crack direction for (a) weak and (b) strong interfacial adhesion between mica and matrix (Xavier *et al.*, 1990).

4.5 Structure Property Relationship of PP/rubber/filler Composites

As discussed in chapter two, section 2.7, blends prepared under similar conditions can be compared and related in terms of their rheology, morphology, thermal and mechanical properties. Mechanical properties depend not only on the composition but also on the phase morphology. Morphology of ternary blends depends strongly on mixing conditions, the rheology and surface energies of the constituents and the geometry of the rigid fillers. In previous works (Jancar and Dibenedetto, 1995; Shanks and Long, 1995) three microstructures for three component thermoplastic/elastomer/filler systems were presented : (a) a separated microstructure where elastomer particles and filler are independently dispersed in polymer matrix (b) a core-shell microstructure where rubber particles with filler core are distributed in matrix and (c) a microstructure of mixed (a) and (b). The mixed microstructure having a random distribution of core-shell and separated filler elastomer inclusion arises from an uncontrolled mixing process. The controlled structure, on the other hand, can be produced using a polar functional group grafted onto the polymer matrix or the elastomer to improve the miscibility and adhesion between polymer and filler, or between polymer and elastomer.

During blend preparation in the present investigation, no such polar functional groups were used to obtain a specific controlled structure as this was not revealed in the commercial grades of the same kind available. Therefore, from the proposed models, a mixed microstructure would have been attained, as in PP/rubber/talc system, the adsorption of PP and elastomer onto talc has no particular preference, both of them being non-polar materials. But from the SEM micrograph of PP/rubber/talc composite (figure 4.2.3), a separated structure was revealed where talc (white flakes) and elastomer (dark holes) particles were separated in PP matrix showing poor interfacial adhesion. This corresponds more to type (a) rather than to type (c) structure. Similar observation was cited by Shanks and Long (1996) for PP/elastomer/talc hybrids. Also, the addition of the second dispersed phase of glass beads or

paint particles into the PP/rubber/talc system was found to have no affinity to either phase in the composite. Considering all these, the composites under investigation were categorised as to be of separated microstructure.

The rheological properties of the composites can be explained in terms of composite morphology. Firstly, the two base matrices PP/rubber and PP/rubber/talc were compared on the basis of effect of morphology on viscosity. PP/rubber/talc system showed higher viscosity compared to the PP/rubber system for the entire temperature range under investigation. As talc remained as a separate phase rather than being encapsulated by the elastomer in the polymer matrix, the composites showed characteristics as of particle filled compounds with increased viscosity over the binary composite. In these cases, as the filler fraction increased as a separate phase in the polymer matrix, it offered more constraint in polymer flow. Analogous behaviour was cited by Park and Kyn (1989) for PPTA/nylon 6 or 66 composites. A higher PPTA content, PPTA and nylon 6 or 66 phases separated during melt extrusion and increased viscosity was attained as for particulate systems. With the addition of the second dispersed phase of glass beads or paint particles, increased viscosity was noticed as the filler content increased. But at low concentration of the second filler ($\varphi < 1\%$), the presence of talc dominated the flow behaviour. Thus the filled composites showed similar or slightly reduced viscosity compared to the talc filled elastomer dispersed PP.

To relate the mechanical properties with the morphology of the composites, talc dispersed systems were first compared with the PP/rubber systems. The experimental results showed that the PP/rubber system had reduced modulus value compared to PP but the PP/rubber/talc matrix had a higher modulus than the neat PP or PP/rubber matrix. This was expected as it is well known that modulus is increased by rigid reinforcing particles and decreased by elastomer. As separate phases were present, the rigidity of the talc itself increased the modulus

of the composite. Shanks and Long (1996) observed similar behaviour for completely separated microstructure of PP/rubber/talc or $CaCO_3$ system. Jancar and Di Benedetto (1993) also reported an increased modulus for separated structure compared to an encapsulated one for PP/elastomer/$Mg(OH)_2$ or $CaCO_3$ system. But a decrease in modulus occurred with inclusion of glass beads and paint particles into the system. This was attributed because of poor bonding between the matrix and the second dispersed phase as revealed from the micrographs of the tensile test samples (figures 4.2.4 and 4.2.5). A decrease in tensile strength and elongation was also observed for the same composites. Usually, elongation is increased by elastomer and decreased by fillers. The PP/rubber system thus showed an increase in percentage strain at break (73.6%) over PP (31.63%). But the addition of talc and paint or glass beads restricted the polymer to provide strength between packed particles. Also the particles that do not bond well to the polymer caused cavitation thus reducing the percentage strain at break. Park and Kyn (1989) noticed similar reduction in tensile strength and elongation of composites for PPTA/nylon (6 or 66 and 11 or 12) systems. Shanks and Long (1996) also reported a decreased extent of elongation for the separated structure compared to core-shell microstructure. They explained that in the later case, as the filler was covered by the elastomer, the core particles behave partly like rubber particles thus showing higher elongation.

The impact strength of the PP/rubber/talc matrix and its composites were also lower compared to PP/rubber binary blends. Here the fillers impeded the crack growth thus reducing matrix strength. Shanks and Long (1996) observed similar behaviour for blends of PP/elastomer and PP/elastomer/talc or $CaCO_3$. They compared all three types of microstructure and found that the core-shell structure showed the highest strength.

The toughening mechanism activated by rubbery particles and rigid particles are also different. The elastomer particles enhance the extent of shear yielding deformations in polymer matrix at the crack front due to interaction between stress field ahead of the crack and the rubbery particles, thus increasing the fracture energy (Sultan and McGarry, 1973; Kinloch *et al.* 1983). In case of rigid particles, the toughening mechanism has been mainly ascribed to a crack pinning mechanism where the particles act as obstacles that pin the crack and cause the crack front to divert between particles. Furthermore, increased toughness by rigid inclusions has to meet the conditions of small particle size and the number (diameter of particle) is less than the number of particles that can be fully packed into the matrix.

In this study, the PP/rubber/talc matrix had higher fracture energy than the neat PP and the binary PP/rubber system as both the toughening mechanisms stated above acted simultaneously. Martinatti and Ricco (1994) investigated the separated PP/rubber/filler ($CaCO_3$ and talc) system and observed that in certain ranges of compositions, the inclusions of the secondary phase produces optimisation of the impact fracture properties compared to the corresponding binary system. Their results for the ternary system with rubber content of 5% and 16 vol% and about 4 vol% of talc inclusions, showed a broad maximum for the total energy required to fracture a specimen and the maximum energy on the load time curve. Hence, the fracture energy of the ternary blend PP/rubber(16 vol %) /talc (4 vol%) was greater than the corresponding binary systems. Kinloch *et al.* (1985) also observed increased fracture energy for separated epoxy-rubber-glass system. In the present work, the addition of talc was only upto 3.6 vol%, so no such comment can be made as to whether this is the optimum level of talc beyond which a reduction in impact properties would be observed or not. But the ternary blend of PP/rubber (20%)/talc (3.6%) indeed had a higher fracture energy (7.2 kJ/m^2) than the corresponding PP/rubber (20%) system (3.6 kJ/m^2).

For the composites with inclusions of glass beads or paint particles, a reduction in fracture energy was observed compared to the base PP/rubber/talc matrix implying that toughening mechanism was impaired by the presence of this secondary phase. The inclusions inhibit plastic deformation of the matrix and because of poor bonding between filler and polymer there is little possibility of stress transfer from polymer to filler thus giving a weaker structure. The micrographs (figure 4.4.36 and 4.4.37) suggest that the paint particles and glass beads debond at the matrix inclusion interface which was not evident for talc particles. Low adhesion of the second dispersed phase was considered to impair the efficiency of the crack pinning mechanism thus reducing the fracture energy values.

CHAPTER FIVE

CONCLUSIONS AND RECOMMENDATIONS

The following conclusions can be drawn from the results and discussions:

1. Image analysis technique was found to be a suitable method for the determination of dispersed paint fraction in polymer phase. The results from image analysis on melt filtered and unfiltered samples showed that only about 50% paint was removed following the filtration. The filtration here was done on a batch process where meshes were changed only between different samples. As no continuous rotary disk filter was used, the meshes allowed more paint to pass through after only partial removal of it.

2. The steady shear measurements for the commercial grade virgin and painted PP based bumper material showed that small increase in viscosity was obtained for unfiltered batches as paint acted as the particulate phase of the filled composite. On the other hand, lower viscosity of filtered samples at high temperature was attributed to the second heat history stage where material deteriorated with chain scission of PP.

3. For the PP/rubber blend systems the effect of filler concentration, filler size and filler geometry was insignificant upto the filler level examined (1.9 vol% for spherical glass beads and 2.7 vol% for irregular paint particles). With increased temperature the filled systems retained their trend and the flow curves were only shifted downwards.

4. The PP/rubber/talc base matrix showed increased viscosity over PP/rubber matrix specially at lower shear rate range as talc particles put restrain on material flow. But the addition of the second dispersed phase of glass beads or paint particles at low concentration level showed insignificant effect on viscosity values of the PP/rubber/talc matrix as higher proportion of talc dominated the flow behaviour. With increased filler fraction (5 vol%), a trend of increase in viscosity over the base matrix was revealed. But the overall variation was within 25%.

5. For PP/rubber/talc composites the larger sized paint particles (135 μm) showed slightly higher viscosity values over the smaller size (63 μm) which was explained by the behaviour of the polydisperse systems.

   The effect of particle geometry on viscosity was only significant at high concentration level of filler (5 vol%) where irregular paint particles showed slightly increased viscosity values over glass beads.

6. The filler volume fraction, filler size and geometry showed insignificant effect on the storage and loss moduli for all the composites studied. Only at higher filler level (5 vol%), an increase in moduli value was observed for the PP/rubber/talc composites.

7. A general conclusion can be drawn from the rheological studies that the small fraction of dispersed phase do not effect the flow behaviour and at this level, effect of particle size and geometry can be neglected. So processing of recycled material would not pose any difficulty as the dispersed phase is usually only around 1 vol%.
8. The retention of tensile yield strength was nearly 100% for both the unfiltered and melt filtered paint dispersed batches but the percentage strain at break for paint dispersed

composites dropped by about 90% compared to the virgin material. This suggested that though the small amount of particulate phase was not able to control the strength measured at high deformations, it could pose restraint to matrix deformability. The rigidity of the samples attained from the modulus values showed that filtered batches were weaker compared to the unfiltered batches.

9. For the blends prepared with PP/rubber as the base matrix, low fraction of the dispersed glass beads or paint particles again showed good retention of yield strength. Whereas, the percentage strain at break decreased with increasing filler fraction for poor adhesion between filler and the matrix. Young's modulus of the glass microsphere filler composites showed an increasing tendency because of its high rigidity over matrix. On the other hand, for paint dispersed systems, modulus values decreased below the matrix for imperfect adhesion between them.

10. The tensile yield strength of PP/rubber/talc based composites showed a gradual decrease with increasing filler fraction. The experimental data were fitted to the available theoretical models showing good prediction of the experimental results. The reduction of relative strain for the filled composites was caused by poor wetting of the fillers by the matrix which was also observed from the photomicrographs. The Young's modulus also decreased for all the filled systems implying that the presence of inclusions into the matrix formed a weak structure. Though addition of high modulus talc particles showed improved rigidity over PP/rubber system, the dispersion of paint particles or glass beads into the PP/rubber/talc system decreased the rigidity instead. Lower modulus of these fillers compared to talc was responsible for such behaviour.

11. The impact strength of the painted samples decreased drastically compared to the base virgin material though no significant variation was observed between the impact strength of unfiltered and melt filtered composites. The paint particles acted as stress concentration and crack initiators thus reducing the matrix strength.

12. Similar detrimental effect on impact strength was observed for the PP/rubber and PP/rubber/talc composites with addition of glass beads or paint particles. The composites had separated microstructure and so the poorly adhered inclusions reduced the ability of the elastomer phase to absorb applied strength by reducing the distance between particles.

13. The PP/rubber system showed increased fracture energy and toughness over neat PP as localised plastic deformation of the rubbery phase occurred. Inclusion of glass beads or paint particles to the matrix showed an increasing tendency over this value as crack pinning mechanism also occurred. But with high fraction of rubber particles present, the shear yielding mechanism dominated to control the fracture energy value.

14. For PP/rubber/talc composites the dispersed phase decreased the matrix fracture energy and toughness as the particles were easily detached from the polymer. Though the much smaller talc particles (~ 8 μm) adhered comparatively well to the polymer, the larger sized second phase of glass beads and paint particles were loosely bonded as seen from the micrographs of the fractured surfaces. The effect of filler geometry and filler size on fracture energy and toughness was insignificant upto the volume fraction examined.

15. Models were proposed to predict the crack propagation through glass and paint dispersed PP/rubber/talc matrix. For glass beads, crack propagation through the composite was attracted to the equator of particles, so fractured surfaces showed clear hemispherical

holes and top surfaces of debonded particles. For irregular paint dispersed composites, crack propagated through the interphase of filler and matrix thus debonding the whole paint particle.

16. The composites under study were related in terms of their rheology, morphology and mechanical properties. A separated microstructure of the composites as observed from the micrographs leads to the explanation of increased viscosity of filled composites over unfilled ones. Also poor interphase between filler and matrix leads to decreased property values in mechanical tests compared to base matrices.

The recommendations for further study in this area are as follows:

1. As lack of adhesion between filler and matrix was found to be one of the factors for detrimental mechanical property values, further study can be done to improve filler matrix interphase and observe the effect of this modification on the composites.

2. It was evident from published literature that encapsulated microstructure gave better mechanical properties compared to the separated one. So, further work can be performed to see whether encapsulation of paint particles is possible while dispersing it into polymer matrix which might lead to improved material properties.

REFERENCES

- Abbott, K. E. (1989), *SAE Publication* 890917.
- Ahmed, S. and Jones, F. R. (1990), *J. Mater. Sci.*, **25**, 4933.
- Alkire, T. (1993), *Products Finishing*, June, 119.
- Asakawa, K. (1992), in ACS Symposium Series, Emerging Technologies in Plastics Recycling, chapter 5 (eds., Andrews, G. D. and Subramanian, P. M).
- Baloch, M. K. (1989), *Rheol. Acta*, **28**, 316.
- Barnes, H. A. (1989), *J Rheol.*, **33 (2),** 329.
- Barro, L. and Bhattacharya, S. N. (1980), VIII Int. Cong. on Rheology, Naples, Italy, **2**, 165.
- Batchelor, G. H. (1977), *J. Fluid Mech.*, **83**, 97.
- Batchelor, G. K. (1970), *J. Fluid Mech.*, **41**, 545.
- Beaumont, P. W. R., Ashby, M. F. and Douglas, S. K. (1980), *J. Mater. Sci.*, **15**, 1109.
- Bhattacharya, S. N., Chin, C., Pullum, L. and O'Donnell, J. (1994), *Int. J. Soc. of Mater. Eng. for Resources*, **2 (1)**, 47.
- Bigg, D. M. (1982), *Polym. Eng. Sci.*, **22(8),** 512.
- Birch , M. W. and Williams, J. G. (1978), *Int., J. Frac.*, **14(1)** , 69.
- Birch, M. W. and Willams, J. G. (1977), Proceedings of 4th International Conference on Fracture (ICF4), University of Waterloo, Canada, June ,**1** , 501.
- Borggreve, R. J. M. and Gaymans, R. J. (1989), *Polymer*, **30**, 63.
- Borkar, P. and Lai, F. (1993), *Antec*, 877.
- Bretas, R. E. S. and Powell, R. L. (1985), *Rheol. Acta*, **24**, 69.
- Brown, H. R. (1973), *J. Mater. Sci.*, **8**, 941.

- Brown, W. F. and Srawley, J. E. (1966), ASTM STP 410.
- Brunger, D. (1993), *Modern Plastics*, **70(9)** , 96.
- Burford, R. P. and Pittolo, M.(1986), *J Mater. Sci,*. **21**, 2308.
- Chan, S. L. (1989), Fractography and failure mechanism of polymers and composites, chapter 4, (ed. Anne C. Roulin-Moloney), Elsevier Applied Science, New York.
- Chen, Le Shang, Mai, Y. W. and Cotterell, B. (1989), *Polym. Eng. Sci.*, **29 (8)**, 505.
- Chong, J. S., Christiansen, E. B. and Baer, A. D. (1971), *J. App. Polym. Sci.*, **15**, 2007.
- Clarke, B. (1967), *Trans. Inst. Chem. Engs.* **45**, 251.
- Cohen, A. and Richon, D. (1986), *Fuel*, **65**, 117.
- Crawford, R. J. (1987), Plastics Engineering, Perganon Press, London.
- Daniels, C. (1991), *Products Finishing*, August, 65.
- Davis, K. K. and Clark, P. D. (1991), *SAE publication* 910092.
- Donald, A. M. and Kramer, E. J. (1982), *J. Mater. Sci.*, **17**, 1765.
- Einstein, A. (1911), *Ann. Physik*, **34**, 591.
- Evans, A. L. (1972), *Phil. Mag.*, **26**, 1327.
- Eveson, G. F. (1959), Rheology of dispersed systems, (ed. C. C. Mill), Pergamon, London, 61.
- Faulkner, D. L. and Schmidt, L. R. (1977), *Polym. Eng. Sci.*, **17 (9)**, 657.
- Ferrini, F., Ercolani, D., Cindio, B., Di Nicodemo, L., Nicolois, L. and Ranaudo, S. (1979), *Rheol. Acta*, **18**, 289.
- Ferry, J. D. (1980), Viscoelastic Properties of Polymers, John Wiley and Sons, New York.
- Fisa, B. and Utracki , L. A. (1984), *Polym. Comp.*, **5 (1)**, 36.
- Flaris, V. (1992), PhD thesis, " Improving the impact properties of polypropylene at low temperatures", University of Melbourne, Australia.

- Folkes, M. J. and Hope, P. S. (1993), Polymer Blends and Alloys, Blackie Academic and Professionals, London.
- Friedrich, K. and Karsch, U. A. (1981), *J. Mater. Sci.*, **16**, 2167.
- Gandhi, K. and Solovey, R. (1988), *Polym. Eng. Sci.*, **28 (24)**, 1626.
- Gardner, J. (1985), *SAE Publication* 850713.
- Garg, A. C. and Mai, Y. W. (1988), *Comp. Sci. Technol.*, **31**, 179.
- Ghosh, K. And Maiti, S. N. (1996), *J. App. Polym. Sci.*, **60**, 323.
- Goodier, J. N. (1933), *Trans. Amer. Soc. Mech. Eng.*, **55**, 39.
- Graves, B.A. (1991), *Products Finishing*, April, 42.
- Green, D. J., Nicholson, P. S. and Embury, J. D. (1979:a), *J. Mater. Sci.*, **14**, 1413.
- Green, D. J., Nicholson, P. S. and Embury, J. D. (1979:b), *J. Mater. Sci.*, **14**, 1421.
- Griffth, A. A. (1920), *Phil. Trans. R. Soc.*, **A221**, 163.
- Guild, F. J. and Summerscales, J. (1993), *Composites*, **24(5)**, 383.
- Gupta, A. K. and Purwar, S. N. (1984), *J. App. Polym. Sci.*, **29**, 3513.
- Guth, E. and Simha, R. (1936), Kolloidzeitschrift, 74, 195 in Sherman, P. (1970) Industrial Rheology, Acedemic Press Inc., (London), Ltd.
- Haaf, F., Breuer, H. and Stabenow, J. (1977), *J. macromol. Sci. Phys.*, **B14**, 387.
- Halpin, J. C. and Kardos, J. L. (1976), *Polym. Eng. Sci.*, **16**, 344.
- Han, C. D. (1976), Rheology in polymer processing, Academic Press, New York, 182-189.
- Hashemi, S., Gilbride, M. T. and Hodgkinson, J. (1996), *J. Mater. Sci.*, **31**, 5016.
- Hassell, A. (1991), *Plastics World*, October, 20.
- Herchun, Y. and Colton, J. S. (1994), *Polym. Compos.*, **15 (1),** 46.
- Hobbs, S. Y., Dekkers, M. E. J. and Watkins, V. H. (1989), *J Mater. Sci.*, **24**, 2025.
- Hodgkinson, J. M., Savadori, A. and Williams, J. G. (1983), *J. Mater. Sci.*, **18**, 2319.

- Hodkinson, J. M., Savadori, A. and Williams, J. G. (1983), *J. Mater. Sci.*, **18**, 2319.
- Hoffman, R. H. (1992), *J. Rheol.*, **36(5)**, 947.
- Husband, D. M. and Galada-Maria, F. (1987), *J. Rheol.*, **31(1)**, 95.
- Irwin, G. R. (1964), *Appl. Mats. Res.*, **3**, 65.
- Irwin, G. R. and Paris, P. C. (1971), Fracture, an advanced treatise- Vol.3, (ed. H. Liebowitz), Acedemic Press, New York.
- Ishai, O. and Cohen, L. J. (1967), *Int. J. Mech. Sci.*, **9**, 539.
- Jancar, J. and Dibenedetto, A. T. (1993), *Antec,* 1698.
- Jancar, J. and Dibenedetto, A. T. (1995:a), *J. Mater. Sci.*, **30**, 1601.
- Jancar, J. and Diebndetto, A. T. (1995:b), *J. Mater. Sci.*, **30**, 2438.
- Johnson A. E., Moore, O. R., Prediger, R. S., Reed, P. E. and Turner, S. (1986), *J. Mater. Sci.*, **21**, 3153.
- K'92 preview (1992),*European Platics News*, October, 85.
- Kamal, M. R. and Mutel, A. (1985), *J. Polym. Eng.*, **5(4)**, 294.
- Kambe, H. and Tanako, M. (1963), *Fourth Int. Congress on Rheol.*, 557.
- Kao, S. V., Nielsen, L. E. and Hill, C. T. (1975*), J. Colloid and Interface Sci.*, **53(3)**, 358.
- Kataoka, T.,Kitano, T., Sashara, M. and Nishijimo, K. (1978), *Rheol. Acta*, **17**, 149.
- Kendall, K. (1978), *Brit. Polym. J.*, **10**, 35.
- Kerner, E. H. (1956), *Proc. Phys. Soc.*, **69B**, 808.
- Kim, S. K., Kim, M. S. and Kim, K. J. (1993), *J App. Polym. Sci.*, **48**, 1271.
- Kinloch , A. J., Shaw, S. J. and Hunston, D. L. (1983), *Polymer,* **24,** 1355.
- Kinloch, A. J. and Young, R. J. (1983), Fracture Behaviour of Polymers, Applied Science Publishers, London.
- Kinloch, A. J., Maxwell, D. and Young, R. J. (1984), *J. Mater. Sci. Letters*, **3**, 9.

- Kinloch, A. J., Maxwell, D. and Young, R. J. (1985), *J. Mater. Sci.*, **20**, 4169.
- Kinloch, A. J., Shaw, S. J., Tod, D. A. and Hunston, D. L. (1983), *Polymer,* **24,** 1341.
- Kitano, T., Kataoka, T. and Nagatsuka, Y. (1984), *Rheol. Acta*, **23**, 408.
- Kitano, T., Kataoka, T. and Nishimura T. (1980), *Rheol. Acta*, **19**, 764.
- Kitano, T., Kataoka, T. and Shirota, T. (1981), *Rheol. Acta*, **20**, 207.
- Kunori, T. and Geil, P. H. (1980) ,*J. Macromol. Sci. Phys.*, **B(18)**), 35.
- Kunz, S. and Beaumont, P. W. R. (1981), *J. Mater. Sci.*, **16**, 3141.
- Kunz-Douglass, S., Beaumont, P. W. R. and Ashby, M. F. (1980), *J. Mater. Sci.*, **15**, 1109.
- Lange, F. F. (1971), *J. Amer. Ceram. Soc.*, **54 (12)**, 614.
- Lange, F. F. and Ladford, K. C. (1971), *J. Mater. Sci.*, **6**, 1197.
- Lau, E. and Edge, D. (1993), *Antec*, 2487.
- Le, Do T. C. (1991), Masters Thesis, Rheology of concentrated coal-oil suspensions at elevated temperatures, RMIT, Melbourne, Australia.
- Lee, D. D, Mrochek, J. E., YoungBlood, E. L., oswald, G. E., Hightower, J. R. (1981), *16th Int. Energy Conv. Ens. Conf.*, 819484.
- Leinder, J. and Woodhams, R. T. (1974:a), *J. App. Polym. Sci.*, **18**, 2637.
- Leinder, J. and Woodhams, R. T. (1974:b), *J. App. Polym. Sci.,* **18**, 1639.
- Lepez, O., Choplin, L. and Tanguy, P. A. (1990), *Polym. Eng. Sci.*, **30 (14)**, 821.
- Lewis, T. B. and Nielsen, L. E. (1970), *J. App. Polym. Sci.* **14**, 1449.
- Li, L. and Masuda, T. (1990), *Polym. Eng. Sci.*, **30 (14),** 841.
- Lobe, V. W. and White, J. L. (1979), *Polym. Eng. Sci.*, **19 (9),** 617.
- Long Yu and Shanks R. A. (1996), *J. App. Polym. Sci.*, **61**, 1887.
- Long Yu, Tiganis, B. E. and Shanks R. A. (1995), *J. App. Polym. Sci.*, **58**, 527.
- Long Yu, Stachurski, Z. H. and Shanks, R. A. (1991), *Polym. Int.,* **26**, 143.

- Long Yu, Stachurski, Z. H. and Shanks, R. A. (1991), *Scanning*, **13**, 107.
- Long Yu, Stachurski, Z. H. and Shanks, R. A. (1992), *Chemistry in Australia* , **59**, 62.
- Long Yu, Stachurski, Z. H. and Shanks, R. A. (1992), *Materials Forum*, **16**, 173.
- Maiti S. N. and Mahapatro P. K. (1991), *J App. Polym. Sci.*, **42**, 3101.
- Maiti S. N. and Sharma K. K. (1992), *J Mater. Sci.* **27**, 4605.
- Mallick, P. K. and Broutman, L. J. (1975), *Mater. Sci. Eng.*, **18**, 63.
- Manson J. A. and Sperling, L. H. (1971), Polymer blends and composites, chapter 12, Plenum press, New York.
- Maron, S. H. and Pierce, P. E. (1956), *J Colloid Sci.*, **11**, 80.
- Marshall, G. P., Williams, J. G. and Turner., C. E. (1973), *J. Mater. Sci.*, **8**, 949.
- Martinatti, F. and Ricco, T. (1994), *J. Mater. Sci.*, **29**, 442.
- Matnois V. A. (1969), *Polym. Eng. Sci.* **9**, 100.
- Matnois V. A. and Small N. C. (1969), *Polym. Eng. Sci.* **9**, 90.
- Mayadunne, A., Boontanjai, C., Bhattacharya, S. N. and Kosior, E. (1993), 3rd Pacific Polymer Conference, gold Coast, Australia.
- Mayadunne, A., Bhattacharya, S. N. and Kosior, E. (1996), *Plastics, Rubber and Comp. Processing App.*, **25(3)**, 126.
- McCartney, P. and Associates (1993), Mechanical Engineering Consultants, internal report.
- McElhaney, R. D. and Plaver, F. M. (1991), SAE Technical Paper Series, 93.
- Merz, E. H., Claver, G. C. and Baer, M. (1956), *J. Polym. Sci.*, **22**, 325.
- Metzner. A. B. (1985), *J. Rheol.*, **29 (6),** 739.
- Mills, N. J. (1971), *J. App. Polym. Sci.*, **15**, 2791.
- Miranda, V., Lai, F. S. and Ferdinand, R. L. (1994), *Antec*, 2888.

- Mitsuishi, K., Kodama, S. and Kawasaki, H. (1985), *Polym. Eng. Sci.*, **25**, 1069.
- Moloney, A. C., Kausch, H. H. and Stieger, H. R. (1983), *J. Mater. Sci.*, **18**, 208.
- Mooney, M. J. (1951), *J. Colloid Sci.*, **6**, 162.
- Moore, S. (1993), *Modern Plastics Int.*, February, 13.
- Munstedt, H. (1976), Proceedings VII th International Congress on Rheology, 494 .
- Nabi, Z. U. and Hashemi, S. (1996), *J. Mater. Sci.*, **31**, 5593.
- Nakamura, Y., Yamaguchi, M., Okubo, M. and Matsumoto, T. (1991), *Polymer*, **32 (16)**, 2976.
- Nakamura, Y., Yamaguchi, M. and Okubo, M. (1993), *Polym. Eng. Sci.*, **33 (5)**, 279.
- Nicolais, L. (1975), *Polym. Eng. Sci.*, **15**, 137.
- Nicolais, L. and Narkis, M. (1971), *Polym. Eng. Sci.*, **11**, 194.
- Nicolais, L. and Nicodemo (1975), *Polym. Eng. Sci.*, 469.
- Nicolais, L., Drioli, E (1973), *Polymer*, **14**, 21.
- Nielsen, L. E. (1966), *J. App. Polym. Sci.*, **18**, 97.
- Nielsen, L. E. (1967), *J. Comp. Mater.*, **1**, 100.
- Nielsen, L. E. (1974), Mechanical properties of polymers and composites, vol. 2, Dekker, New York, chapter 7.
- Nielsen, L. E. (1975), *J .App. Polym. Sci.*, **15**, 137.
- Nikpur, K. and Williams, J. G. (1978), *Plast. Rubber: Mater. Appl.*, **3** , 163.
- Orowan, E. (1948), *Rept. Prog. Phys.*, **12**, 185.
- Ottani, S. and Valenza, A. F. R. La Mantia (1988), *Rheol. Acta*, **27**, 172.
- Owen, A. B. (1979), *J. Mater. Sci.*, **14**, 2521.
- Park. H. S. and Kyn, T. (1989), *Polym. Compos.*, **10 (6),** 429.
- Papadopoulos, C. (1995), Master thesis, " The oscillatory shear properties of glass and rubber filled low density polyethylene composites", RMIT, Australia.

- Passmore, E. M., Spriggs, R. M. and Vasilos, T. (1965), *J. Amer. Ceram. Soc.*, **48**, 48.
- Paul, B. (1960), *Trans. Metallurg. Soc. AIME*, **218**, 36.
- Peraro, J. S. (1985), Instrumented Impact Testing of Plastics and Composite Materials, (eds, Kessler, S. L., Adams, G. C., Driscoll, S. B. and Ireland, D. R.) ASTM STP 936, Philadelphia, Houston , 188.
- Peron, P. and Denison, B. (1992), *SAE publication* SP-902.
- Person, R. A. and Yee, A. F. (1983), NASA Contractor Report 3718 (NASA, Langley, Virginia, USA).
- Piggott, M. R. and Leidner, J. (1974), *J. App. Polym. Sci.*, **18**, 1619.
- Plati, E. and Williams, J. G. (1975), *Polym. Eng. Sci.*, **15**(6), 471.
- Poslinski, A. J., Ryan, M. E., Gupta, R. K., Seshadri, S. G. and Frechete, F. J.(1988), *J. Rheol.*, **32 (8),** 751.
- Pukanszky, B., Maurer, F. H. J. and Boode, J. W. (1995), *Polym. Eng. Sci.*, **35 (24)**, 1962.
- Pukanszky, B., Kolarik, J., Lednicky, F. and Tudos, F. (1990), *Polym. Compos.*, **11 (2),** 86.
- Pukanszky, B., Tudos, F. and Kelen, T. (1985), Polym. Comp. Proc. 28th Microsymposium on macromolecules Prague, Czechoslovakia, July (8-11), (ed. Sedlacek, B), Walter de Gruyte and Co. Berlin.
- Quemada, D. (1977), *Rheol. Acta*, **16**, 82.
- Reed, P. E. and Turner, S. (1987), *Plast. & Rubb. Proc. Appl.*, **8 (3)**, 173.
- Rice, J. R., Paris, P. C. and Merkle, J. M. (1973), ASTM STP 536, 231.
- Roberts, R.A. (1985), *SAE Publication* 850712.
- Rutgers, R. (1962), *Rheol. Acta*, **2**, 305.
- Sahu, S. and Broutman, L. J. (1972), *Polym. Eng. Sci.*, **12** , 91.
- Savadori, A., Bramuzzo, M. and Marega, C. (1984), *Polymer Testing*, **4** , 73.

- Sheldon, R. P. (1982), Composite Polymeric Materials, Applied Science Publishers Ltd, England.
- Shouche, S. V., Chokapp, D. K., Naik, V. M. and Khakhar, D. V. (1994), *J. Rheol.*, **38 (16),** 1871.
- Spanoudakis, J. and Young, R. J. (1984), *J. Mater. Sci.*, **19**, 473.
- Srivastava, V. K. and Shembekar, P. S. (1990), *J. Mater, Sci.*, **25**, 3513.
- Stott, T., Sexton, J. and Wilson, F. G. (1986), *Filteration and Separation*, March / April, 107.
- Studt, T. (1993), *R & D Magazine*, March, 32.
- Sultan , J. N. and McGarry , F. J. (1973), *Polym. Eng. Sci.*, **13,** 29.
- Takabori, Y., Ohba, S. and Tanaka, T. (1985), *SAE publication* 852225.
- Tsai, S. C., Botts, D. and Plouff, J. (1992), *J Rheol.*, **36 (1)**, 1291.
- Utracki, L. A. (1988), Rheological measurements, (ed. A. A. Collyer and D. W. Clegg), London, Elesvier, 490.
- Utracki, L. A. and Fisa, B. (1982), *Polym. Compo.*, **3 (4),** 193.
- Van der Werff, J. C. and Kruif C. G. D. (1989), *J. Rheol.*, **33(3)**, 421.
- Vincent, P. I. (1971), Impact Tests and Service Performance of Thermoplastics, PRI, London.
- Vollenberg, R. N. Th. and Heikens, D. (1990), *J. Mater. Sci.*, **25**, 3089.
- Walker, I. and Collyer, A. A. (1994), Rubber Toughened Engineering Plastics, chapter2, (ed. Collyer, A. A.), Chapman and Hall, London.
- Warman, K. (1991), presented at the "Elements of Color and Appearance for the Thermoplastics Processor" RETEC, New Orleans, October 15-17.
- Weber, A. (1991), *Mater. and Design*, **12 (4)**, 199.

- Weibel, E. R. (1979), Stereological Methods, Volumes 1 and 2, Academic press, New York.
- Williams, J. G. (1988), *Polymer Preprints*, **29(2)**, 149.
- Wong, K. W. Y. and Truss, R. W. (1994), *Compo. Sci. and Tech.*, **52**, 361.
- Xavier, S. F., Schultz, J. M. and Friedrich, K. (1990), *J. Mater. Sci.* ,**25**, 2411.
- Young, R. J., Maxwell, D. L. and Kinloch, A. J. (1986), *J. Mater. Sci.* ,**21**, 380.

APPENDICES

APPENDIX A : SPECIFICATION SHEETS FOR THE RAW MATERIALS

Table A.1 : Physical and mechanical properties of reinforced and modified polypropylene compound (Epalex 7095).

Supplier : Polypacific Pty.Ltd. Australia.

Property	ASTM method	Unit	Epalex 7095
Specific gravity	D792	-	1.01
Melt flow index	D1238	g/10 min	9
	2.16kg @ 230°C		
Tensile strength	D638	MPa	15
Elongation at break	D638	%	80
Flexural modulus	D790	MPa	1200
Notched Izod impact strength	D256	J/m	
@ 23°C			560
@ 0°C			420
@ -10°C			150
Heat deflection temperature	D648	°C	108
@450kPa			
Co-efficient of linear thermal	D696	10^{-5}/°C	8
expansion			

Table A.2 : Physical and mechanical properties of polypropylene (LYM 120).

Supplier : ICI Plastics Australia.

Property	Test method	Unit	LYM 120
Melt flow index	ASTM D1238 2.16kg @ 230°C	g/10 min	14
Density	AS1193 @ 23°C	kg/m^3	905
Tensile yield stress	ASTM D638 @ 23°C	MPa	26
Flexural modulus	ASTM D790	GPa	1.1
Notched izod impact strength @ 23°C	ASTM D256	J/m notch	75
Heat deflection temperature @ 455 kPa	ASTM D648	°C	95

TABLE A.3 : Typical properties of elastomer concentrate VM 42E.

Supplier : Kemcor Pty. Ltd., Australia.

Property		
Melt flow index	ASTM D1238 5.0kg @ 230°C	2 gm/10 min
Density	ASTM D 792	0.89 gm/cc
Volatiles (1h/105°C)	Exxon Chemical	< 0.1 %
Colour	Hunterlab pellets	< 5 b value
Product form	Free flowing pellets	
Additives	Processing heat stabiliser Anti agglomeration coating (0.4 % PE powder)	

Table A.4 : Typical chemical analysis of talc TX.

Supplier : Commercial Minerals Limited, Australia.

Typical chemical analysis		
Loss of ignition		6.0%
Silica	SiO_2	57.0%
Alumina	Al_2O_3	3.5%
Ferric Oxide	Fe_2O_3	1.0%
Lime	CaO	0.3%
Magnesia	MgO	31.9%

Table A.5 : Physical properties of talc TX.

Physical properties	
pH	9.5
Refrective index	1.59
Specific gravity	2.65
Hardness (Mohs)	1.0
Specific surface	9000 cm^2/g
Oil absorption (rub out)	44 ml/100 g
Bulk density (compacted)	1.0 g/cc
Reflectance (457 mu)	82

Table A.6 : Physical properties of Ballotini glass beads.

Supplier : Potters Industries Pty. Ltd., Australia.

Physical properties	
Shape	Spherical
Colour	Clear
Hardness	515 kg/mm
Comprehensive strength	36.00 psi (avg.)
Density	2.5 gm/cc
Specific gravity	2.45 - 2.50
Free silica content	0%

APPENDIX B : PARTICLE SIZE DISTRIBUTION AND PHOTOMICROGRAPHS OF DIFFERENT FILLERS

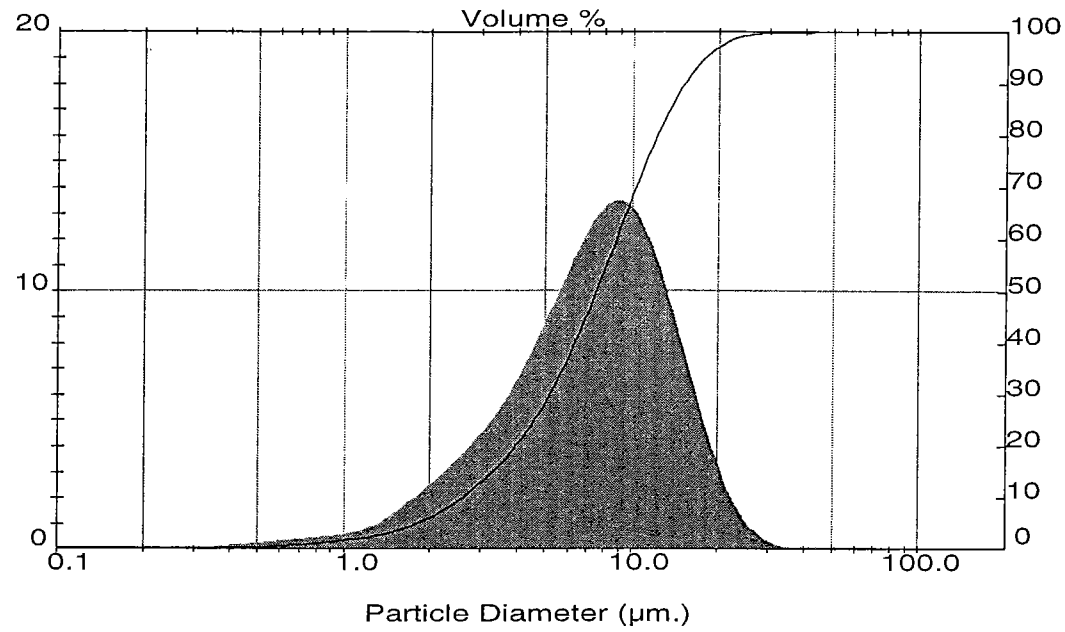

Figure B.1 : Particle size distribution of talc particles.

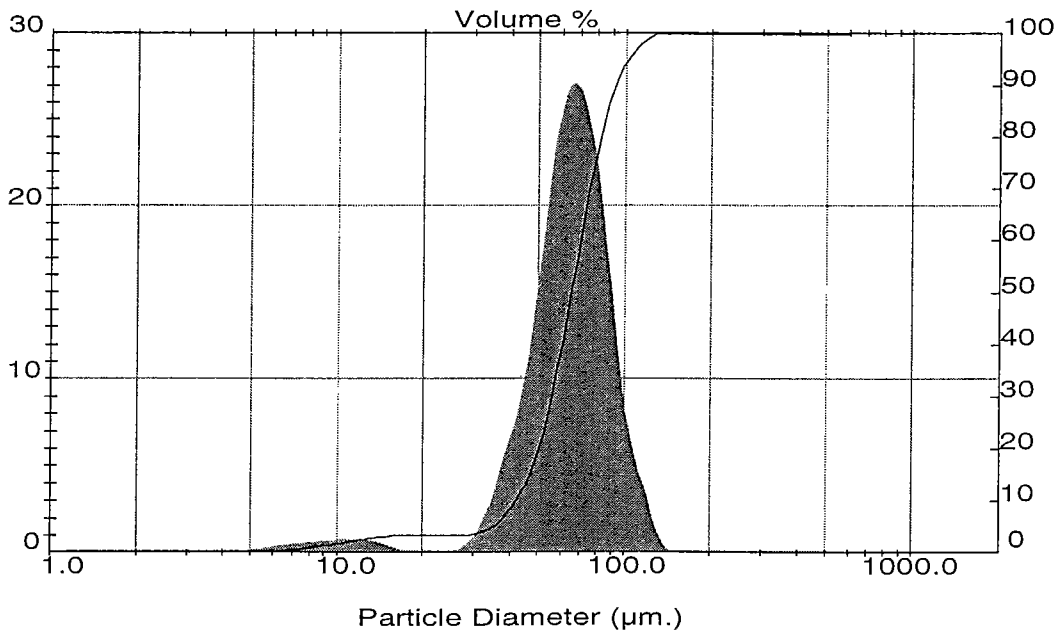

Figure B.2 : Particle size distribution of 106-53 µm glass beads.

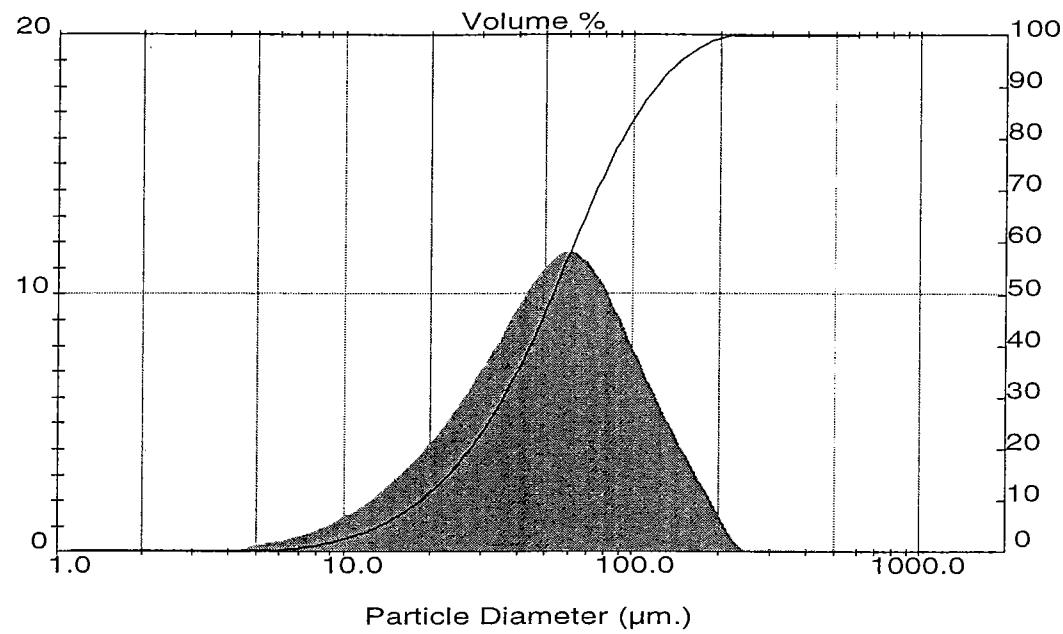

Figure B.3 : Particle size distribution of 75-53 µm paint particles.

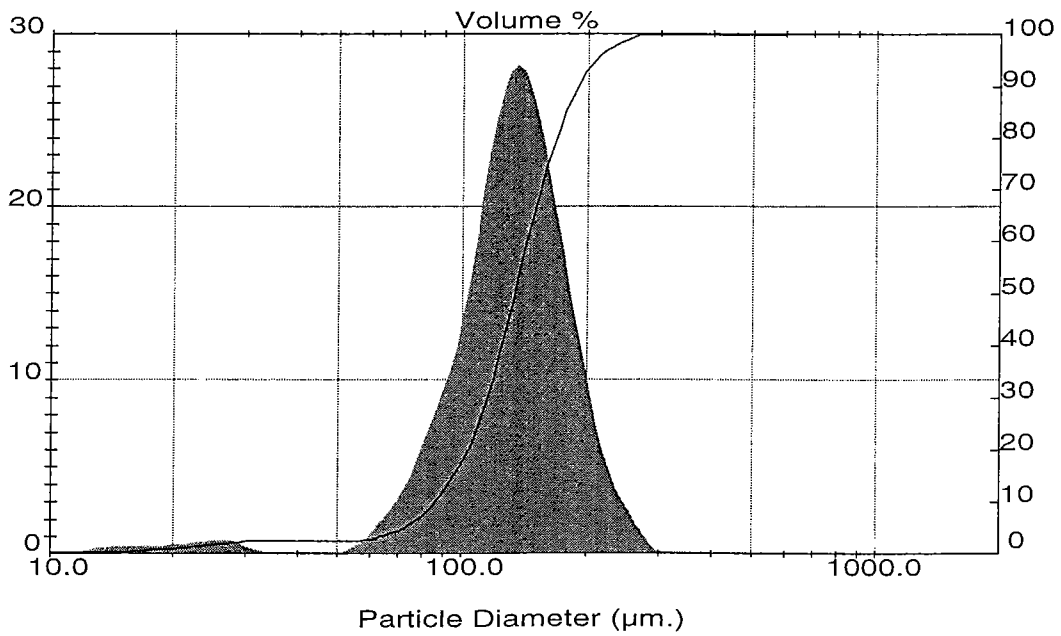

Figure B.4: Particle size distribution of 150-106 µm paint particles.

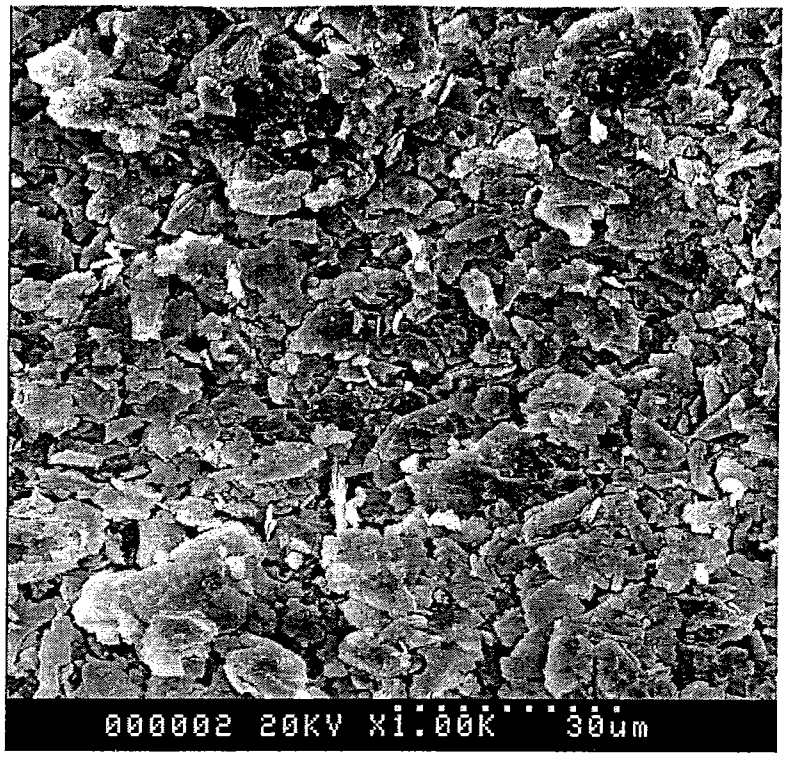

Figure B. 5 : Photomicrograph of talc particles (d = 8 μm).

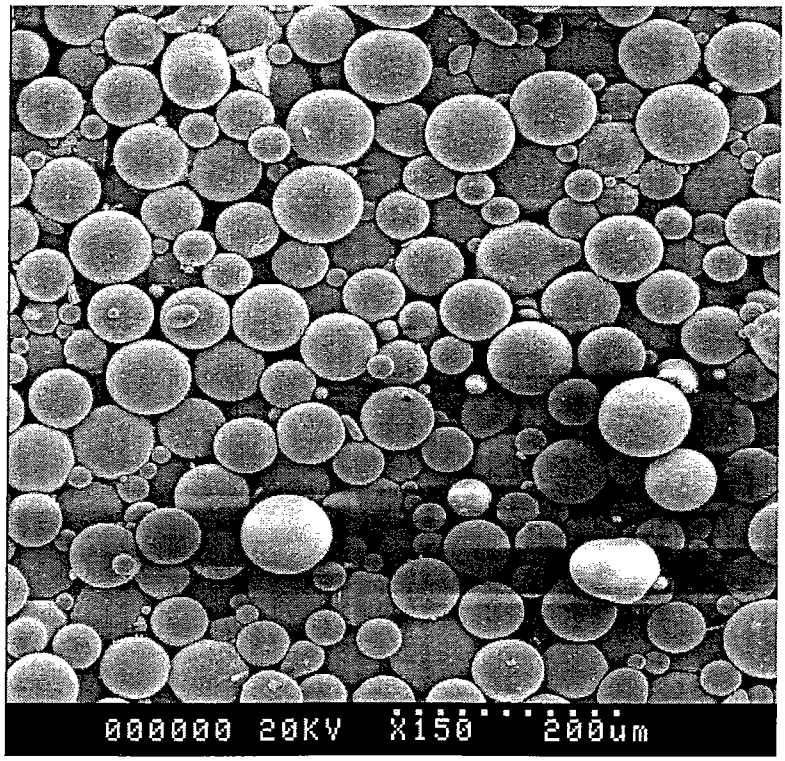

Figure B. 6 : Photomicrograph of glass beads (d = 66 μm).

Figure B. 7 : Photomicrograph of paint particles (d = 63 μm).

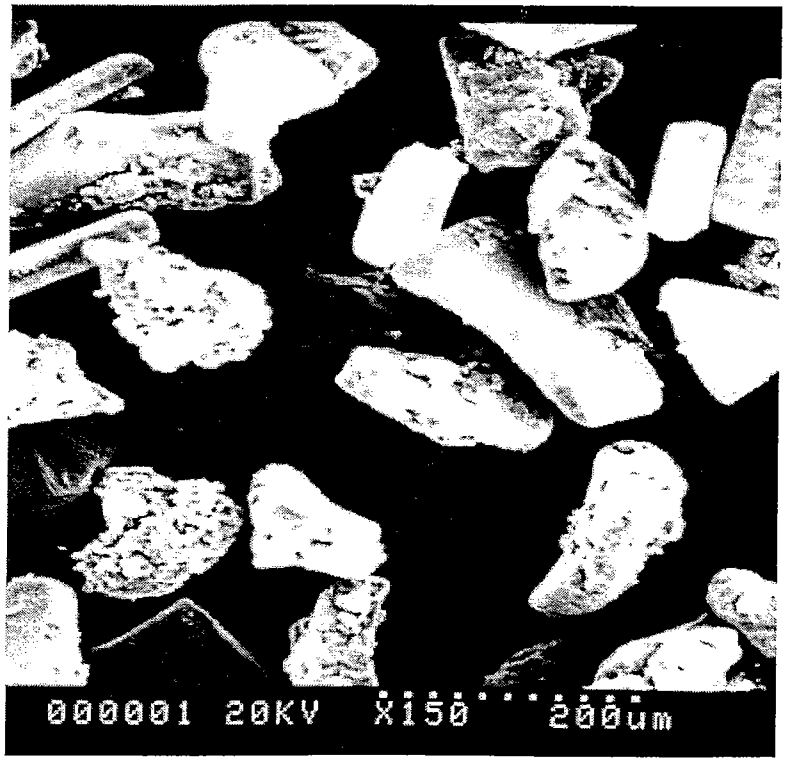

Figure B. 8 : Photomicrograph of paint particles (d = 135 μm).

APPENDIX C : INJECTION MOULDING DATA SHEET

Table C.1 : Conditions for injection moulding for PP/rubber and PP/rubber/talc blends.

Parameters	
Rear barrel heater	220°C
Middle barrel heater	210°C
Front barrel heater	210°C
Nozzle barrel heater	210°C
Mould temperature	40°C
Clamp force	425~450 kN
Mould protection force	7 kN
Injection high pressure	56 ~ 70 MPa
Injection low pressure	40 MPa
Screw back pressure	5 MPa
Multi ejection	8 sec
Air ejection delay	10 sec
Clamp open dwell	2 sec
Clamp dwell	30 sec
Injection dwell	8 sec
Injection full pressure	1.2 sec
Screw speed	300 rpm
Injection speed	Medium
Screw speed	Medium

APPENDIX D : RHEOLOGICAL RESULTS

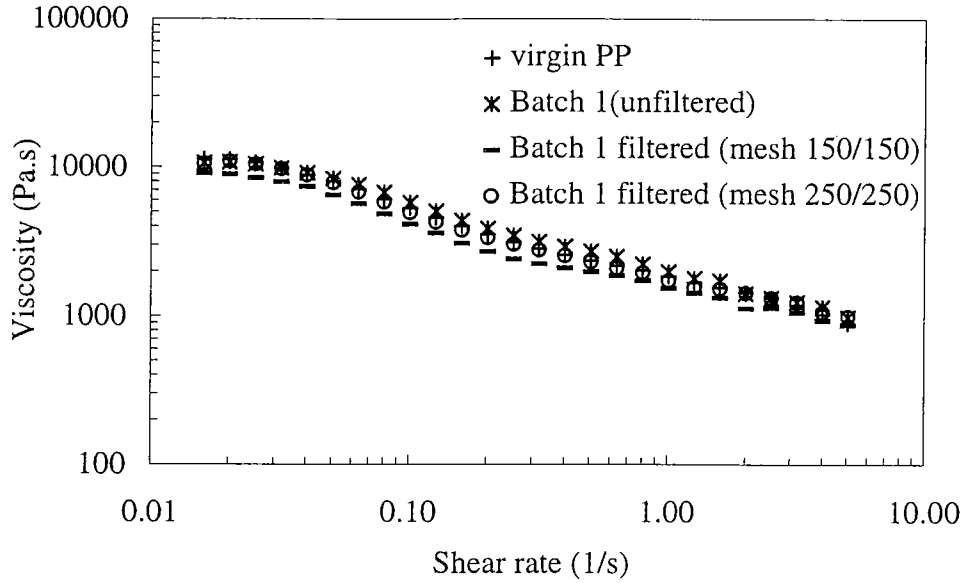

Figure D.1 : Flow curves for virgin material and batch 1 samples containing 1.83% paint (unfiltered and melt filtered) at 220°C.

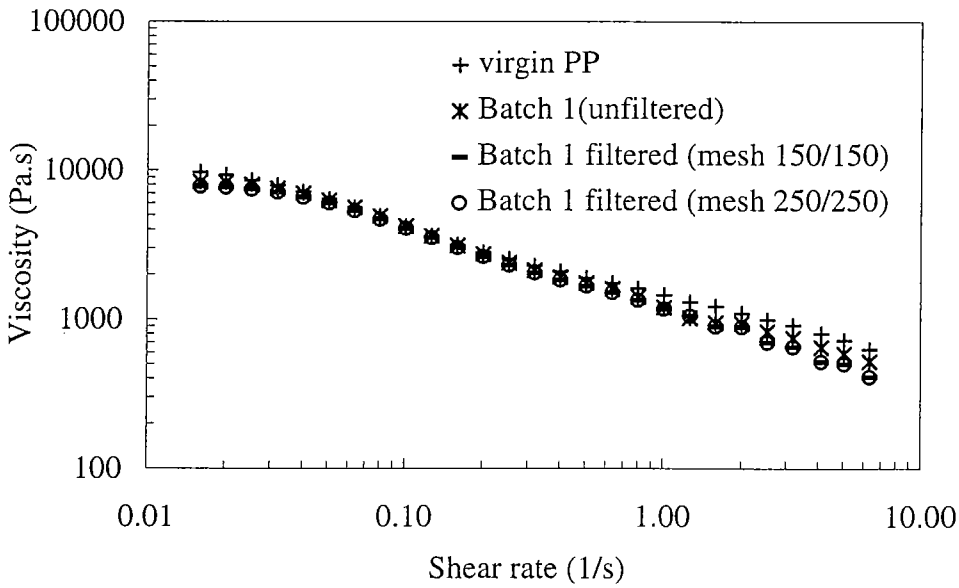

Figure D.2 : Flow curves for virgin material and batch 1 samples containing 1.83% paint (unfiltered and melt filtered) at 240°C.

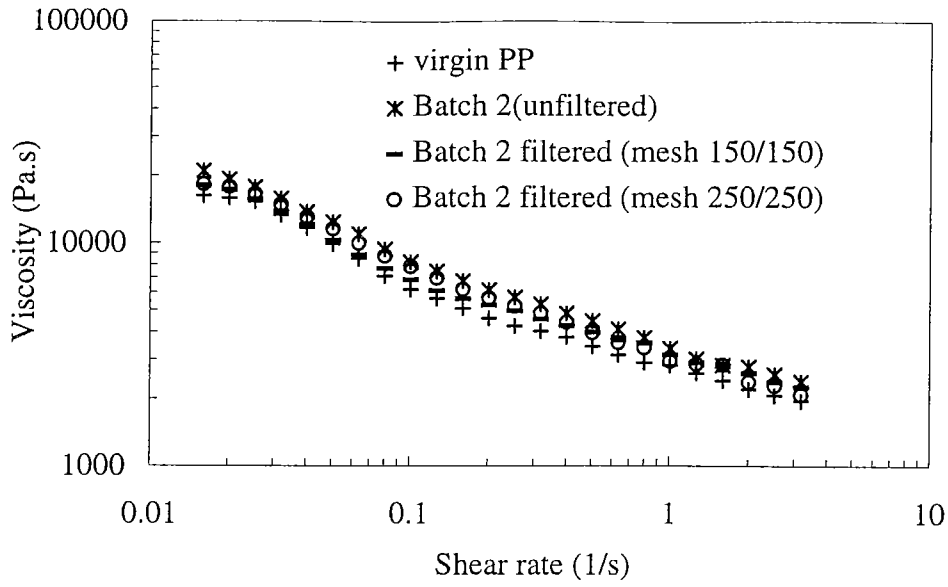

Figure D.3 : Flow curves for virgin material and batch 1 samples containing 2.48% paint (unfiltered and melt filtered) at 190°C.

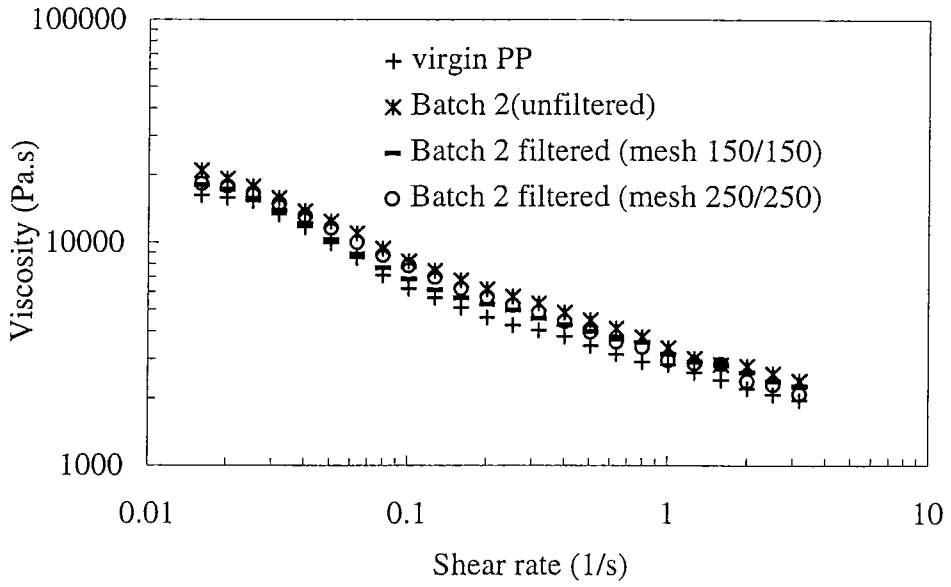

Figure D.4 : Flow curves for virgin material and batch 1 samples containing 2.48% paint (unfiltered and melt filtered) at 220°C.

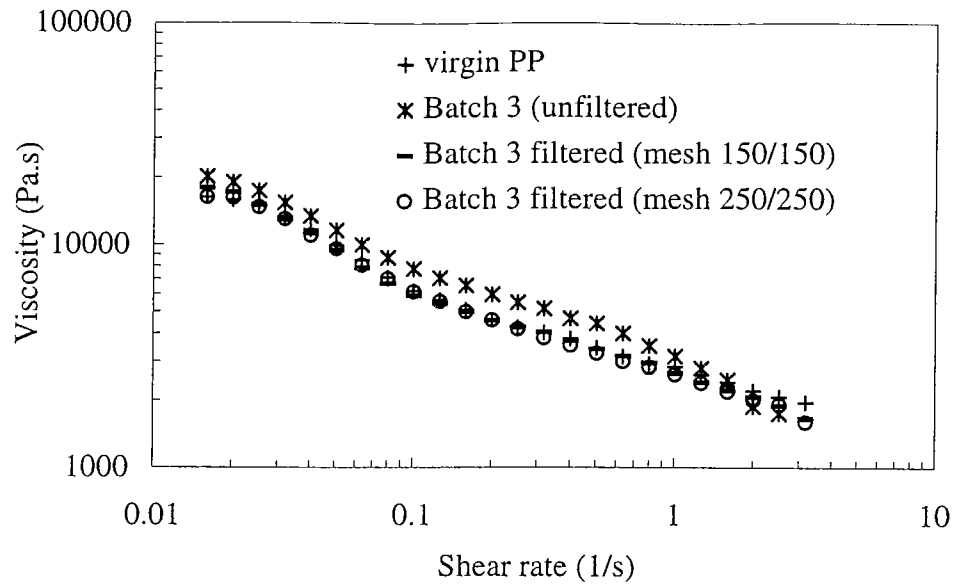

Figure D.5 : Flow curves for virgin material and batch 3 samples containing 1.00% paint (unfiltered and melt filtered) at 190°C.

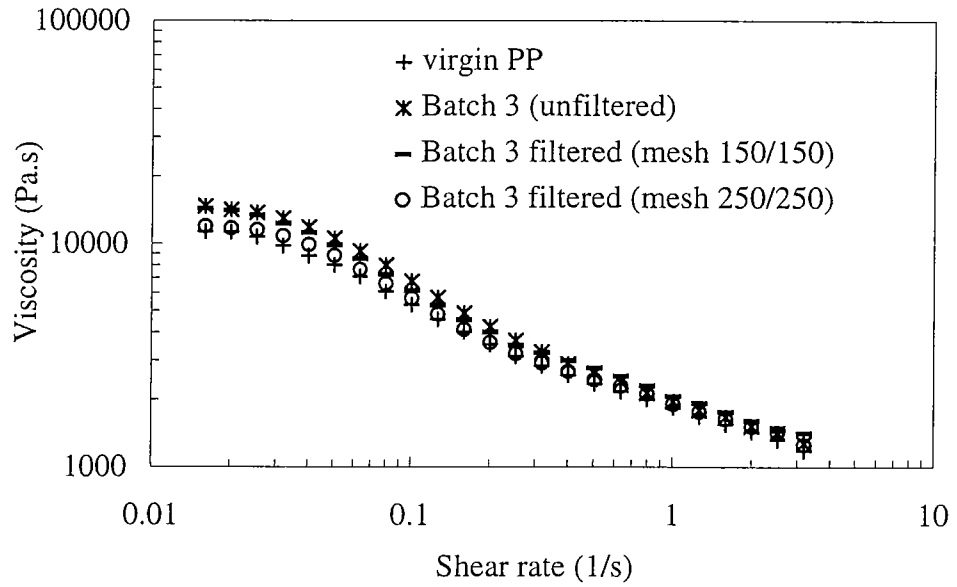

Figure D.6 : Flow curves for virgin material and batch 3 samples containing 1.00% paint (unfiltered and melt filtered) at 220°C.

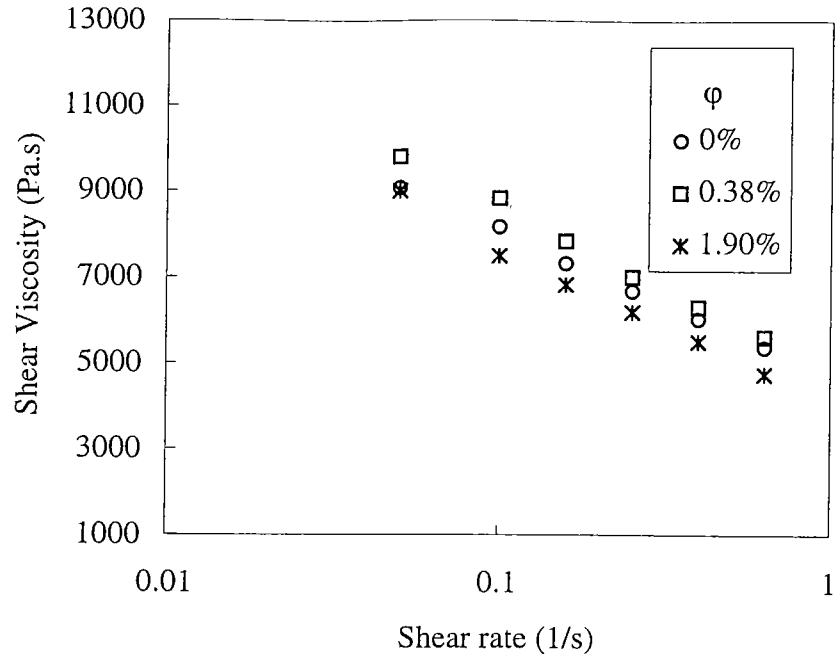

Figure D.7 : Steady shear viscosity versus shear rate for glass bead filled PP/rubber composites at 190°C.

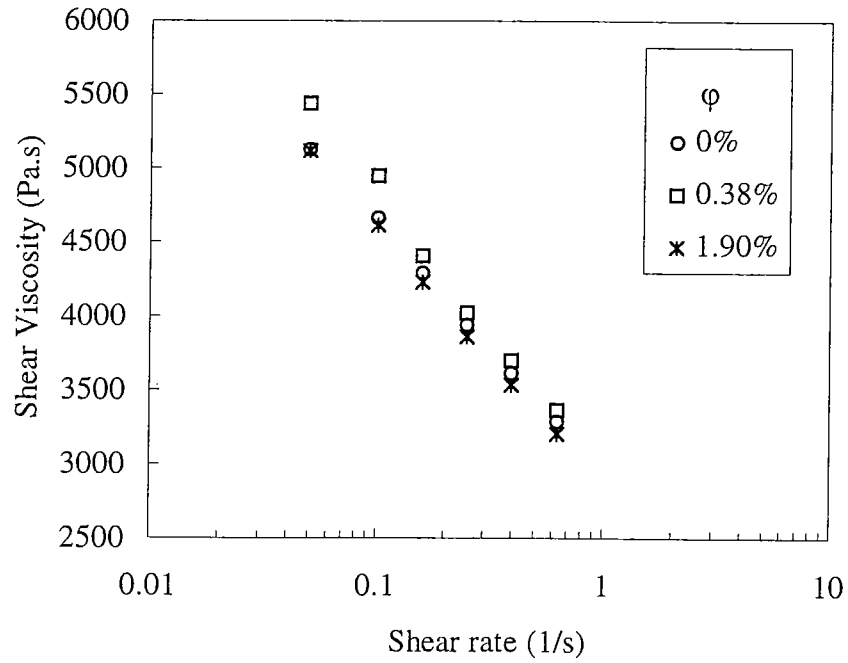

Figure D.8 : Steady shear viscosity versus shear rate for glass bead filled PP/rubber composites at 240°C.

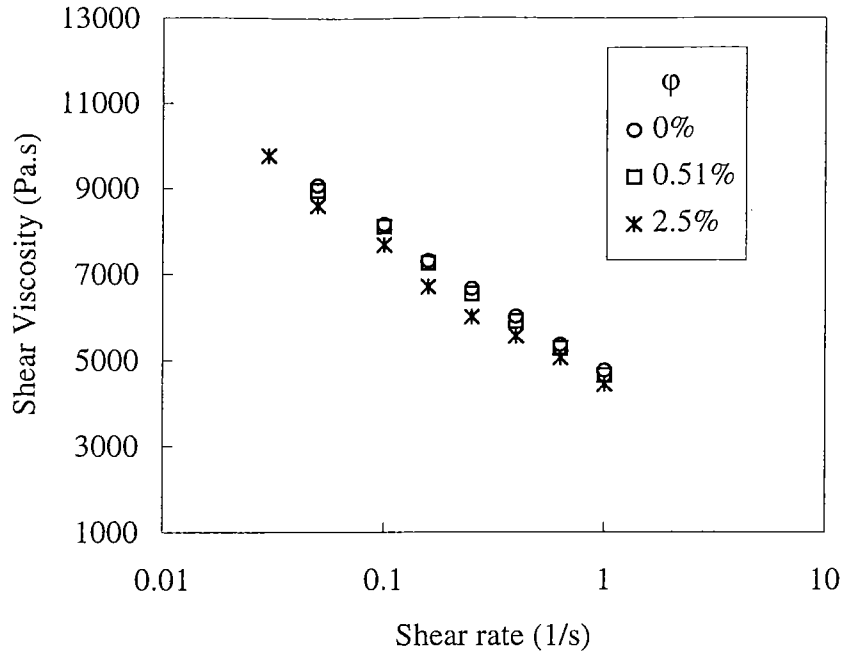

Figure D.9 : Steady shear viscosity versus shear rate for paint particle (63 μm) filled PP/rubber composites at 190°C.

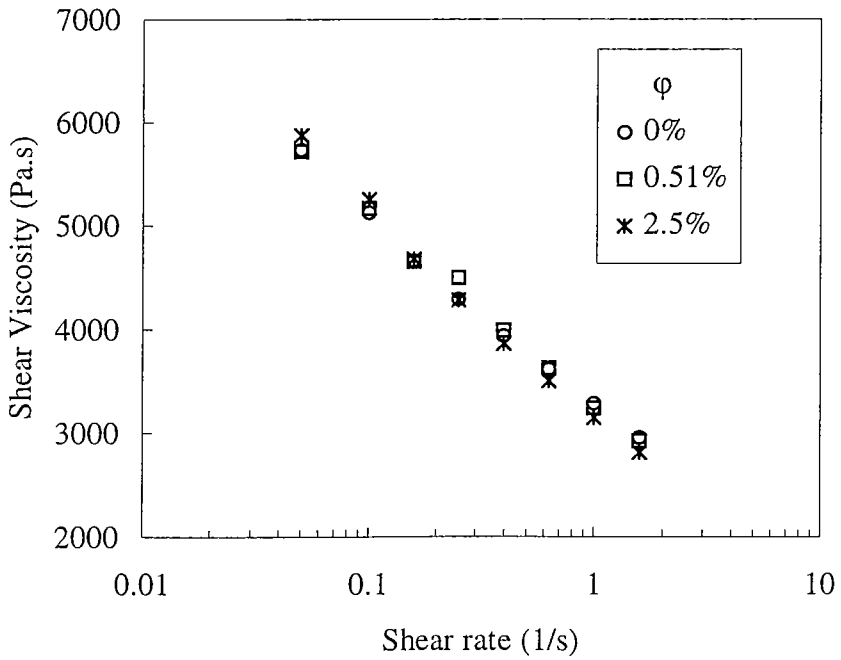

Figure D.10 : Steady shear viscosity versus shear rate for paint particle (63 μm) filled PP/rubber composites at 220°C.

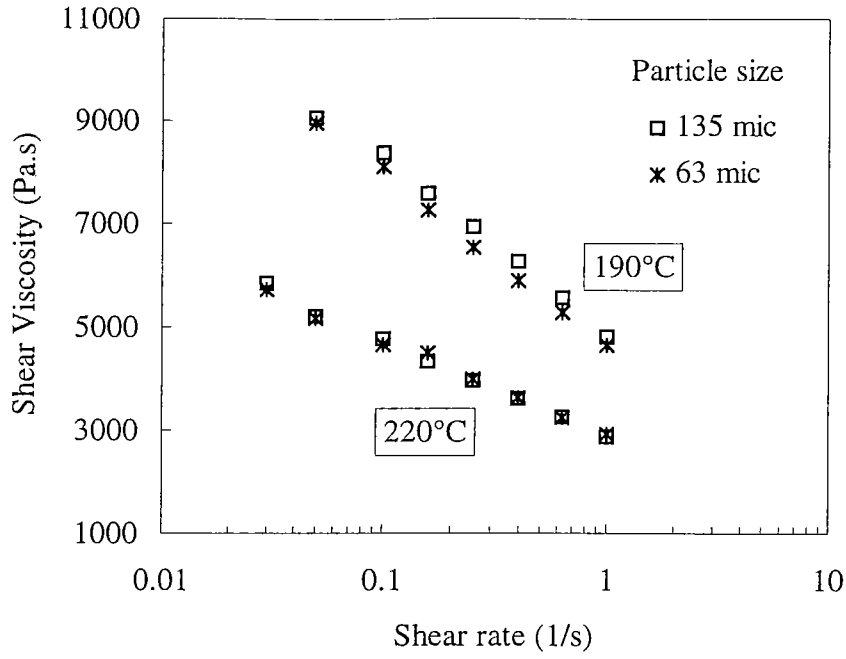

Figure D.11 : Steady shear viscosity versus shear rate for 2.5 vol% paint particle filled PP/rubber composites at 190° and 220°C.

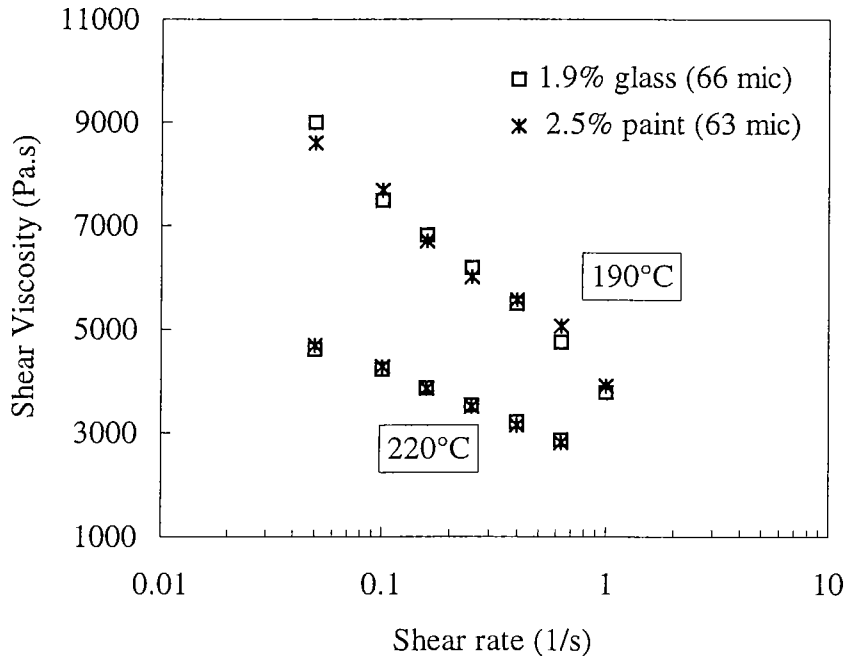

Figure D.12 : Steady shear viscosity versus shear rate for glass bead and paint particle filled PP/rubber composites at 190° and 220°C.

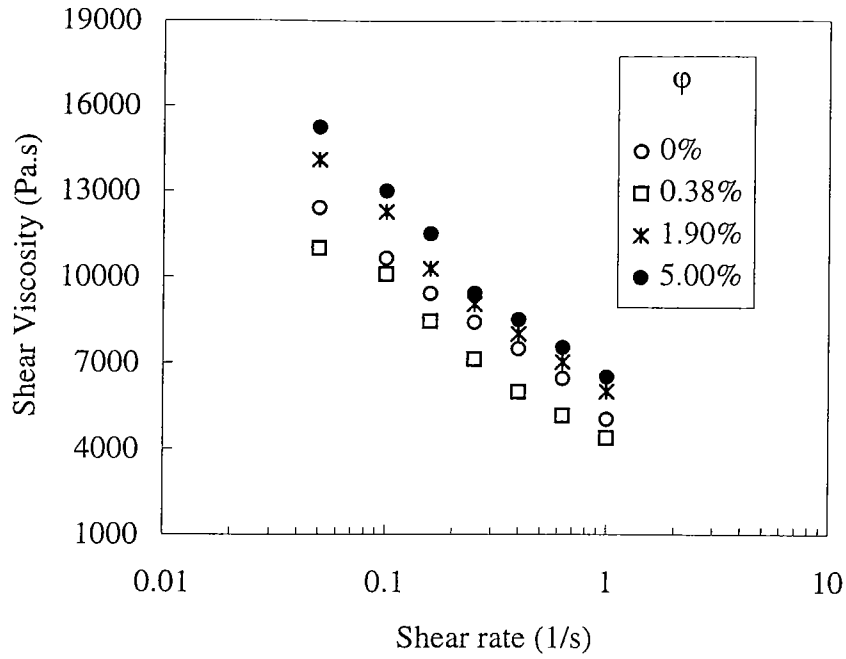

Figure D.13 : Steady shear viscosity versus shear rate for glass bead filled PP/rubber/talc composites at 190°C.

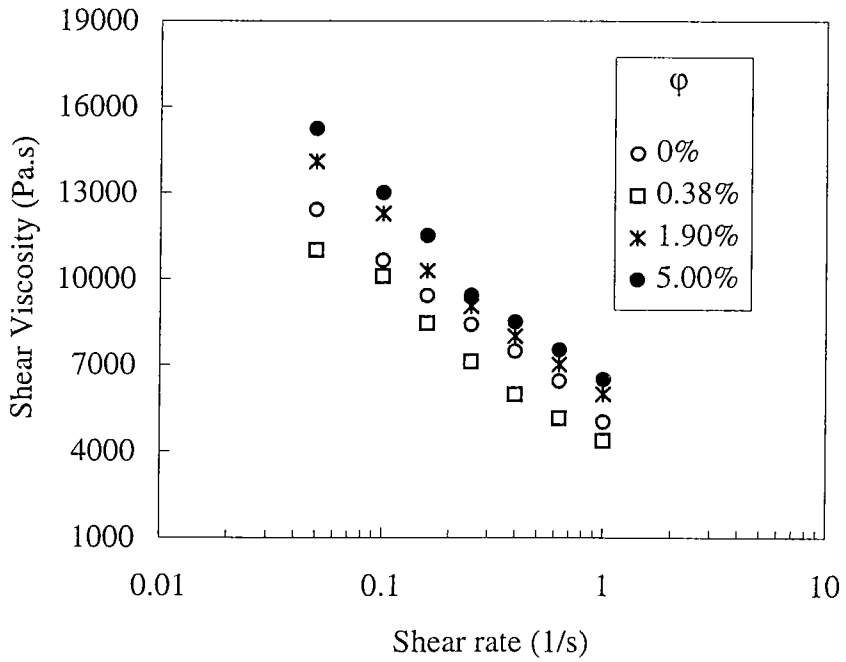

Figure D.14 : Steady shear viscosity versus shear rate for glass bead filled PP/rubber/talc composites at 220°C.

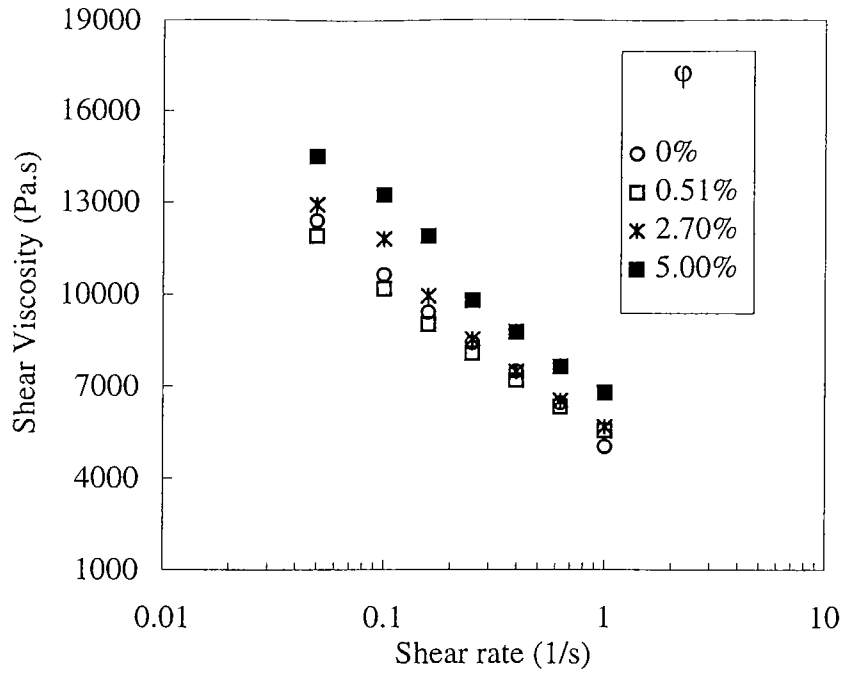

Figure D.15 : Steady shear viscosity versus shear rate for paint particle (63 μm) filled PP/rubber/talc composites at 190°C.

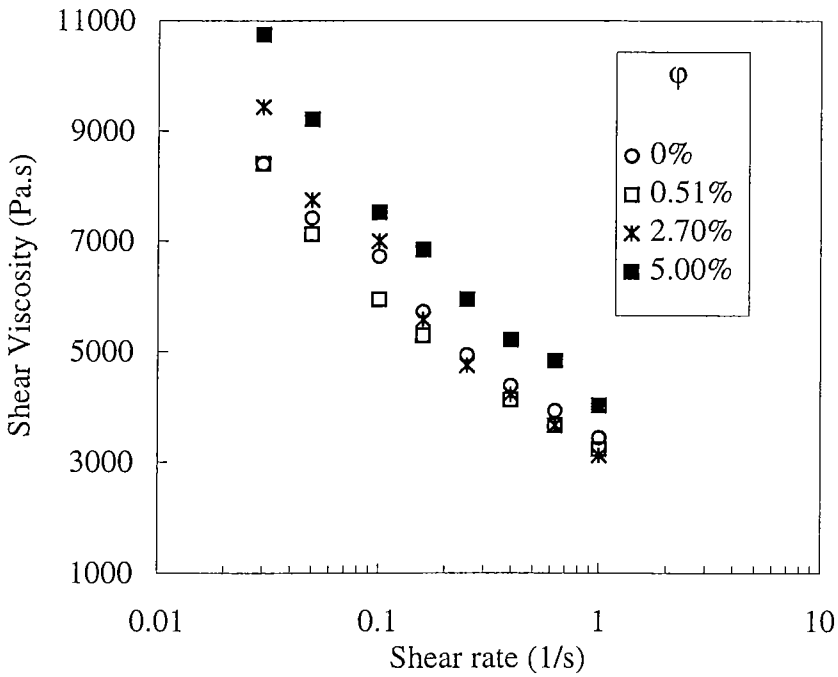

Figure D.16 : Steady shear viscosity versus shear rate for paint particle (63 μm) filled PP/rubber/talc composites at 220°C.

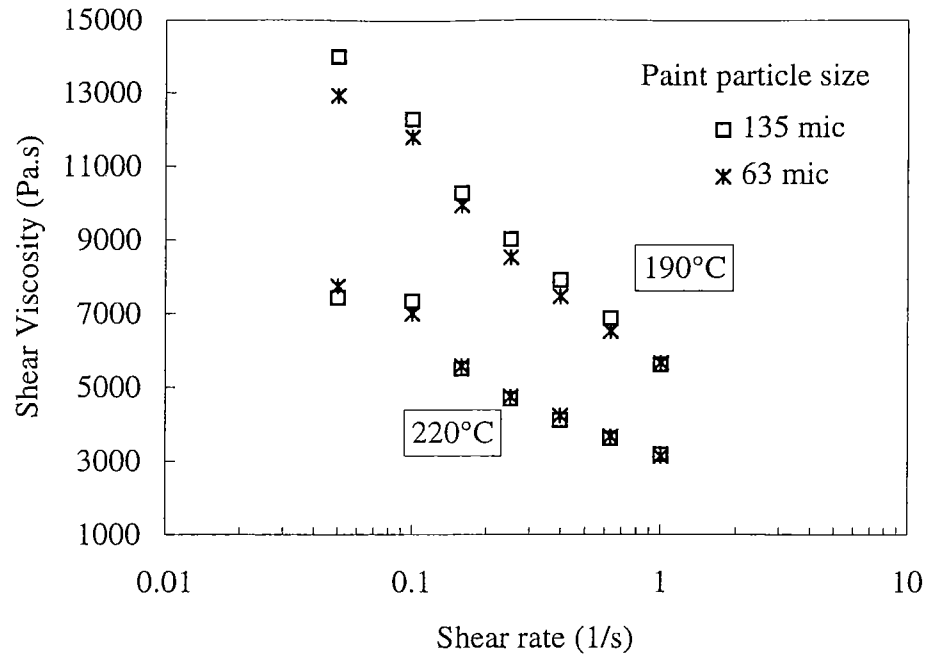

Figure D.17 : Steady shear viscosity versus shear rate for different sized paint particle filled PP/rubber/talc composites at 190° and 220°C.

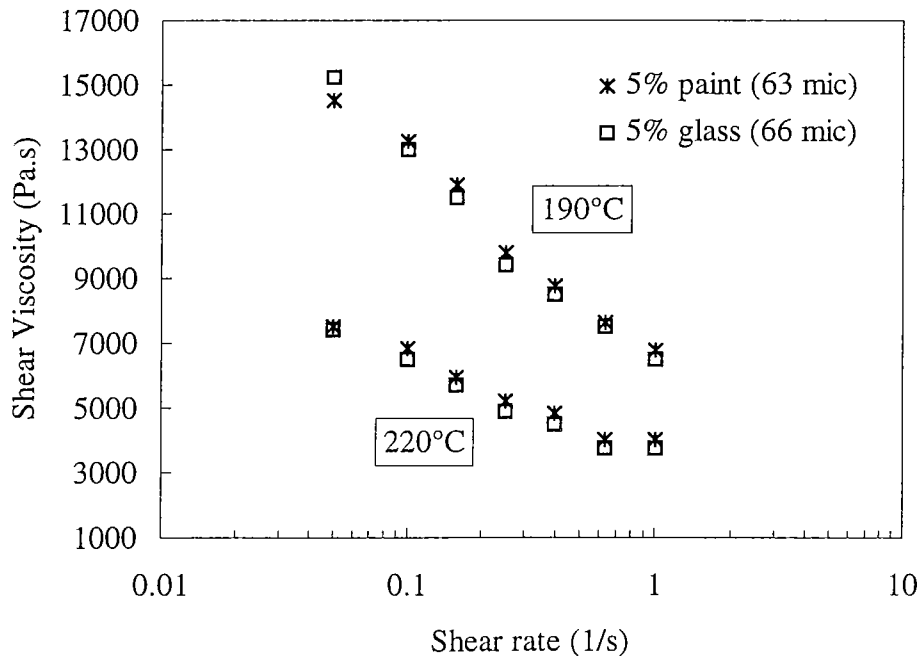

Figure D.18 : Steady shear viscosity versus shear rate for glass bead and paint particle filled PP/rubber/talc composites at 190° and 220°C.

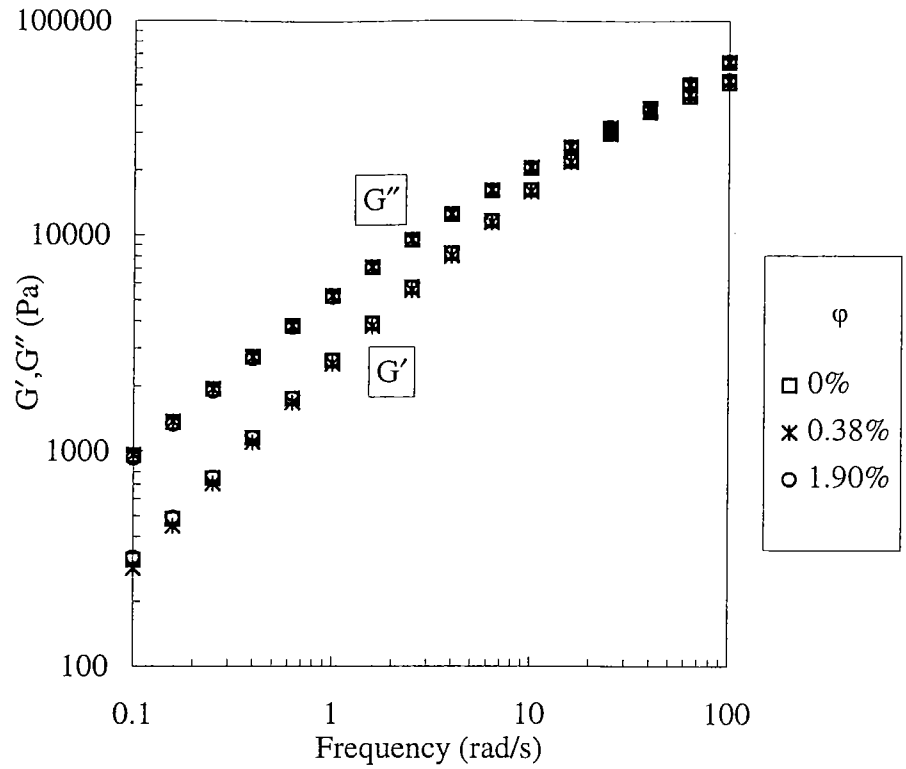

Figure D.19 : Storage and loss modulus of glass bead filled PP/rubber composites at 180°C and 5% strain.

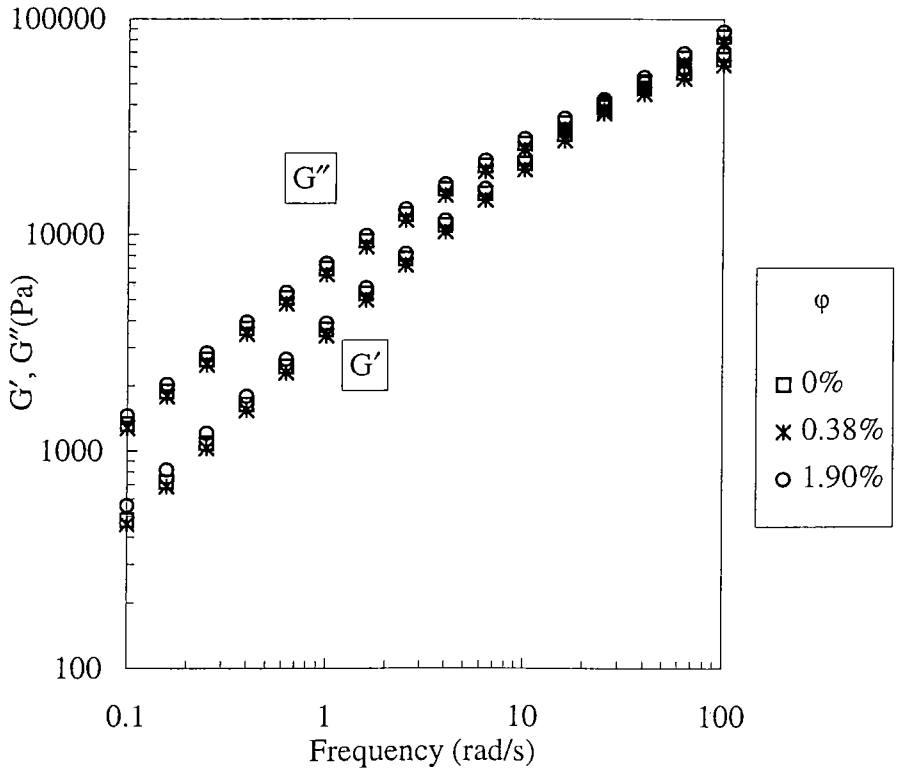

Figure D.20 : Storage and loss modulus of glass bead filled PP/rubber/talc composites at 180°C and 5% strain.

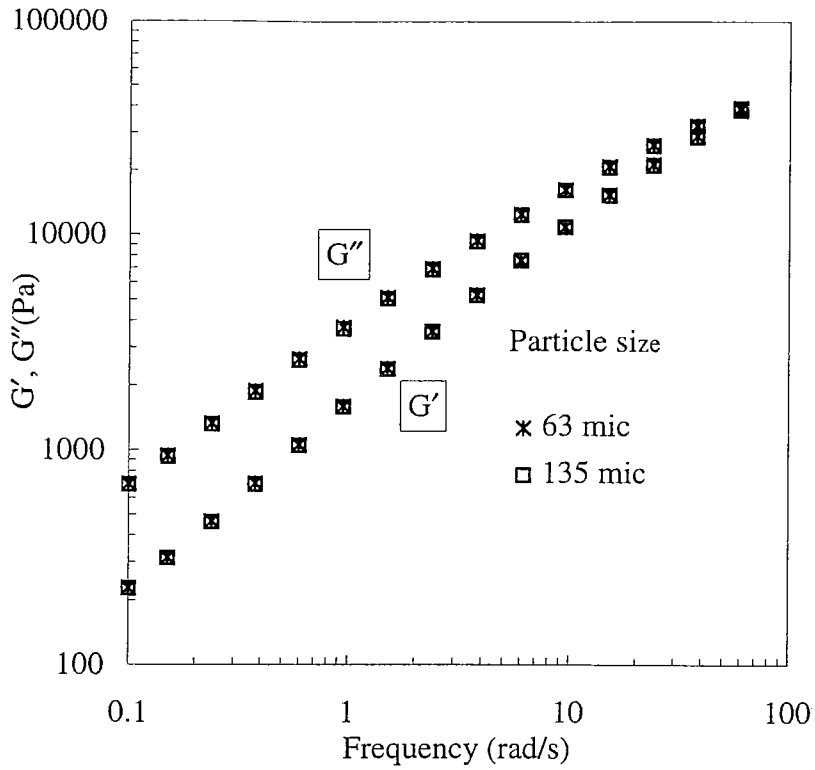

Figure D.21 : Storage and loss modulus of paint particle filled PP/rubber/talc composites at 220°C and 5% strain.

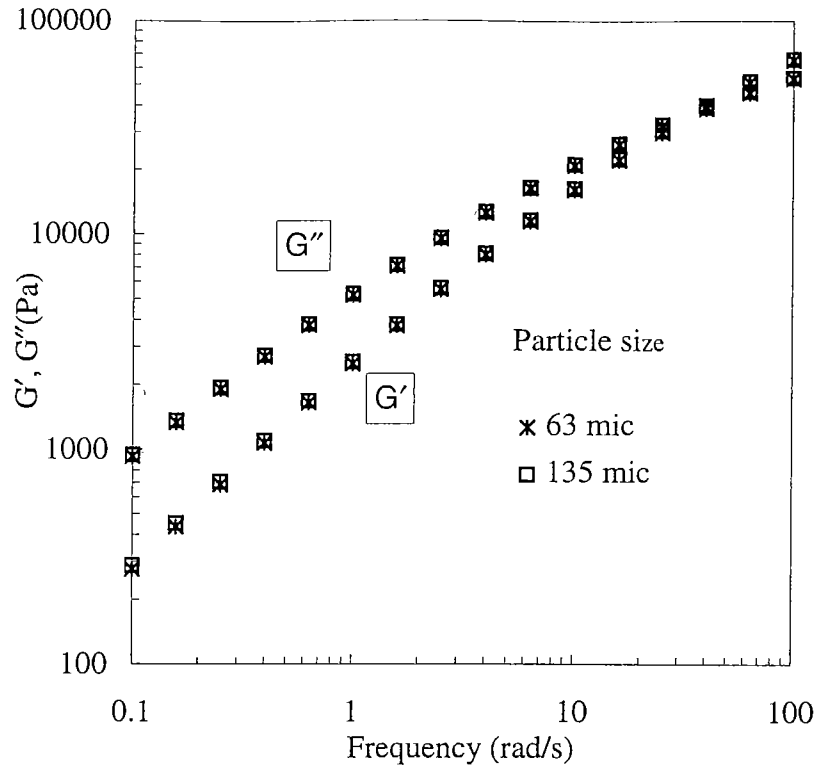

Figure D.22 : Storage and loss modulus of paint particle filled PP/rubber composites at 180°C and 5% strain.

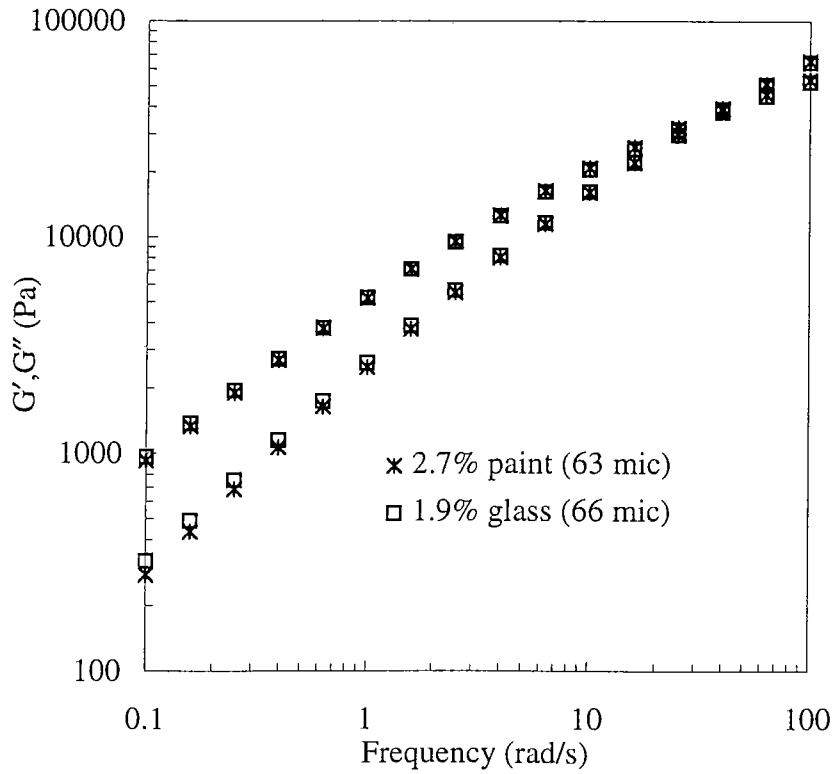

Figure D.23 : Storage and loss moduli of glass bead and paint particle filled PP/rubber composites at 180°C and 5% strain.

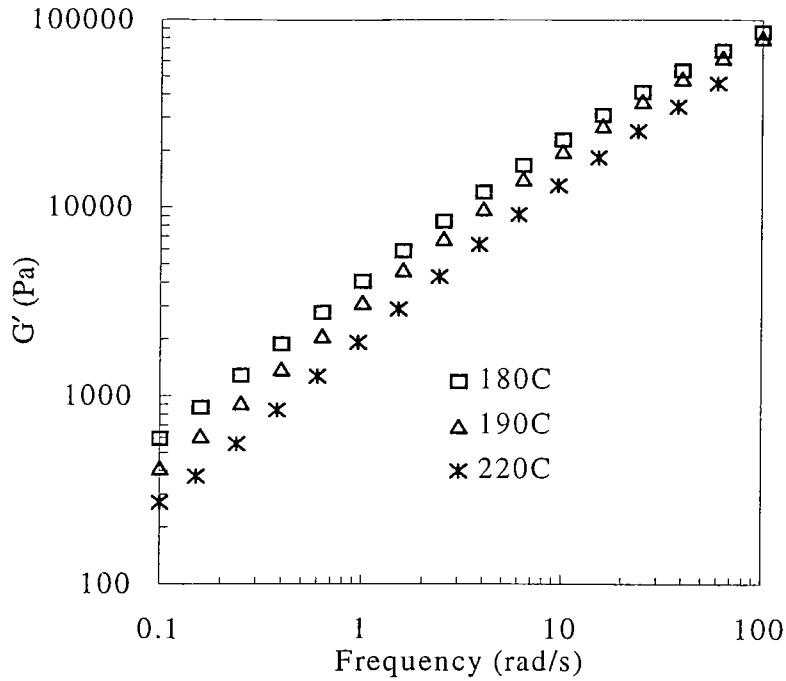

Figure D.24.a : Storage modulus of 2.7% paint particle (135 μm) filled PP/rubber/talc composite at different temperatures.

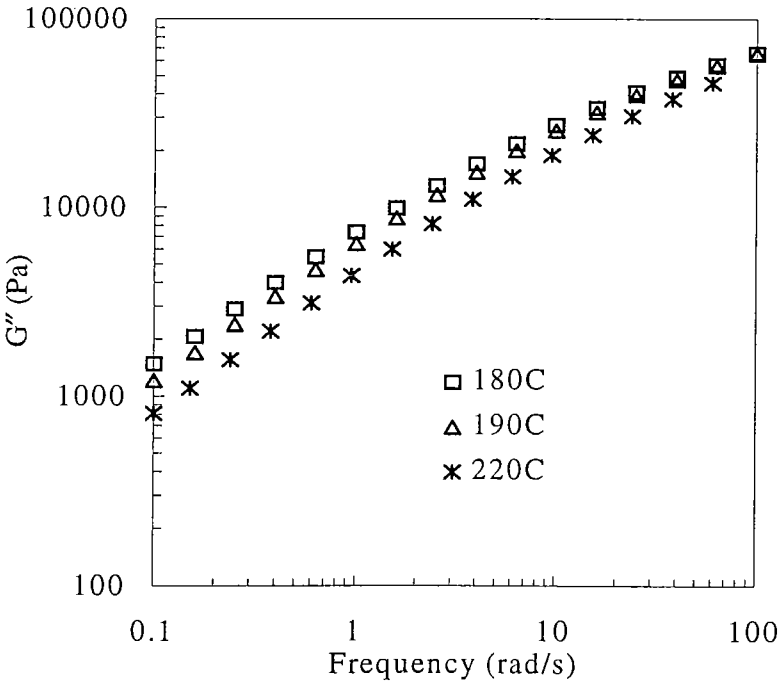

Figure D.24.b : Loss modulus of 2.7% paint particle (135 μm) filled PP/rubber/talc composites at different temperatures.

Table E.1: Mechanical test results of virgin PP and unfiltered and melt filtered PP/paint mixtures @ 10 mm/min and 23°C.

*(Standard deviation in the parenthesis)

		Tensile test (test speed 10 mm/min)				Imapct test
Samples	Paint content	Strength at yield (MPa)	% strain at break (%)	Elongation at break (mm)	Young's modulus (MPa)	Impact strength (J/m^2)
Virgin material		14.5 (0.2)*	79.5 (5)	60.8 (3.8)	576 (37)	505 (22)
Batch 1						
a. unfiltered	1.83	15.9 (0.1)	11.9 (0.5)	9.1 (1.9)	535 (44)	330 (15)
b. filtered (mesh 150/150)	0.92	14.9 (0.3)	9.6 (0.6)	7.3 (0.5)	554 (39)	294 (18)
c. filtered (mesh 250/250)	0.94	15.1 (0.3)	10.1 (0.7)	7.7 (0.5)	540 (18)	268 (14)
Batch 2						
a. unfiltered	2.48	15.3(0.1)	10.4 (1.1)	7.9 (1.0)	570 (52)	245 (9)
b. filtered (mesh 150/150)	1.40	15.3 (0.2)	10.5 (0.8)	8.0 (0.6)	469 (26)	285 (13)
c. filtered (mesh 250/250)	1.07	15.3 (0.2)	10.9 (0.9)	8.3 (0.7)	517 (65)	262 (13)
Batch 3						
a. unfiltered	1.00	14.5 (0.2)	10.3 (2.1)	7.9 (1.6)	527 (42)	395 (19)
b. filtered(mesh 150/150)	0.49	14.4 (0.1)	13.2 (2.1)	10.1 (1.8)	531 (22)	367 (12)
c. filtered(mesh 250/250)	0.52	14.2 (0.1)	11.9 (2.5)	9.1 (1.9)	562 (29)	362 (16)

Table E.2: Mechanical test results of virgin PP and unfiltered and melt filtered PP/paint mixtures @ 50 mm/min and 23°C.

*(Standard deviation in the parenthesis)

		Tensile test (test speed 50 mm/min)				Imapct test
Samples	Paint content	Strength at yield (MPa)	% strain at break (%)	Elongation at break (mm)	Young's modulus (MPa)	Impact strength (J/m^2)
Virgin material	-	17.5 (0.2)*	48.9 (4.0)	37.4 (3.2)	1497 (30)	505 (22)
Batch 1						
a. unfiltered	1.83	17.0 (0.1)	9.0 (1.0)	6.7 (1.5)	1460 (20)	330 (15)
b. filtered (mesh 150/150)	0.92	16.9 (0.1)	7.1 (1.2)	5.4 (1.0)	1443 (32)	294 (18)
c. filtered (mesh 250/250)	0.94	16.9 (0.4)	6.4 (2.0)	4.9 (1.7)	1417 (30)	268 (14)
Batch 2						
a. unfiltered	2.48	17.6(0.4)	8.9 (1.1)	6.8 (1.0)	1436 (25)	245 (9)
b. filtered (mesh 150/150)	1.40	17.3 (0.3)	9.0 (1.2)	6.9 (1.2)	1428 (40)	285 (13)
c. filtered (mesh 250/250)	1.07	17.3 (0.1)	8.5 (2.0)	6.5 (1.5)	1386 (50)	262 (13)
Batch 3						
a. unfiltered	1.00	17.9 (0.1)	10.0 (2.1)	7.6 (1.9)	1570 (20)	395 (19)
b. filtered(mesh 150/150)	0.49	17.6 (0.5)	9.0 (3.0)	6.9 (2.3)	1550 (10)	367 (12)
c. filtered(mesh 250/250)	0.52	17.6 (0.1)	10.0 (2.0)	7.6 (1.8)	1452 (34)	362 (16)

Table E.3 : Mechanical test results of PP/rubber composites at 23°C.

		Tensile test (test speed 50 mm/min)				Flexure test (test speed 10 mm/min)		Impact test
Filler	Volume fraction	Strength at yield (MPa)	%strain at break (%)	Elongation at break (mm)	Young's modulus (MPa)	Strength at yield (MPa)	Flexural modulus (MPa)	Impact strength (J/m)
PP/rubber (base matrix)	-	21.9 (0.1)	73.6 (2.9)	56.6 (2.2)	910 (40)	28.9 (0.3)	924 (13)	506 (18)
Glass beads (66 µm)	0.0038	21.9 (0.1)	59.6 (2.2)	45.8 (1.7)	920 (37)	29.1 (0.2)	938 (6)	142 (17)
	0.0190	21.1 (0.4)	58.6 (3.6)	45.0 (2.8)	940 (36)	28.7 (0.1)	940 (5)	149 (22)
Paint particles (63 µm)	0.0051	21.5 (0.1)	60.0 (5.2)	49.2 (4.0)	881 (15)	29.7 (0.1)	823 (6)	149 (9)
	0.0250	19.0 (0.9)	55.3 (1.9)	42.5 (1.5)	847(17)	28.7 (0.1)	813 (4)	154 (18)
Paint particles (135 µm)	0.0051	21.4 (0.2)	55.0 (3.0)	42.2 (3.4)	890 (64)	29.8 (0.5)	900 (10)	162 (18)
	0.0250	21.1 (0.1)	50.0 (2.0)	38.4 (2.0)	840 (43)	28.7 (0.1)	813 (6)	177 (14)
Talc particles (8 µm)	0.0034	22.0 (0.5)	69.2 (2.3)	53.2 (1.8)	970 (46)	29.0 (0.5)	930 (22)	246 (20)
	0.0170	21.9 (0.2)	68.7 (4.8)	52.8 (3.7)	1122 (57)	31.3 (0.4)	1004 (20)	192 (9)
	0.0360	21.2 (0.5)	53.9 (4.8)	41.5 (3.7)	1431 (51)	32.2 (0.1)	1084 (26)	190 (18)

Table E.4 : Mechanical test results of PP/rubber/talc composites at 23°C.

		Tensile test (test speed 50 mm/min)				Flexure test (test speed 10 mm/min)		Impact test
Filler	Volume fraction	Strength at yield (MPa)	%strain at break (%)	Elongation at break (mm)	Young's modulus (MPa)	Strength at yield (MPa)	Flexural modulus (MPa)	Impact strength (J/m)
PP/rubber/talc (3.6%)	-	21.2 (0.5)	53.9 (4.8)	41.5 (3.7)	1431 (51)	32.2 (0.1)	1084 (26)	190 (18)
Glass beads (66 µm)	0.0038	21.0 (0.1)	52.1 (1.0)	39.9 (0.8)	1370 (60)	31.3 (0.1)	1032 (3)	153 (6)
	0.0190	20.0 (0.2)	45.0 (0.1)	34.6 (0.1)	1320 (6)	29.9 (0.1)	1017 (20)	116 (7)
	0.027	18.0 (0.2)	44.0 (4.0)	33.8 (3.1)	1310 (17)	28.0 (0.4)	977 (25)	134 (6)
	0.0500	16.7 (0.2)	42.0 (2.0)	32.2 (7.0)	1210 (24)	25.5 (0.3)	951 (20)	138 (9)
	0.1000	14.3 (0.2)	36.0 (3.7)	27.8 (3.0)	1090 (48)	22.4 (0.4)	900 (10)	164 (10)
Paint particles (63 µm)	0.0054	20.8 (0.1)	48.9 (3.6)	37.6 (2.7)	1386 (46)	32.0 (0.2)	1052 (23)	134 (14)
	0.0270	18.6 (0.6)	29.5 (4.4)	22.7 (1.8)	1210 (33)	29.0 (0.3)	950 (20)	110 (5)
	0.050	17.4 (0.1)	22.1 (4.1)	16.9 (3.1)	1097 (23)	25.8 (0.2)	843 (30)	120 (3)
Paint particles (135 µm)	0.0054	20.7 (0.1)	44.2 (3.6)	33.9 (3.0)	1393 (50)	61.3 (0.2)	1040 (15)	141 (8)
	0.0270	19.0 (0.1)	26.7 (1.8)	20.6 (1.4)	1260 (60)	29.7 (0.1)	993 (28)	112 (11)

APPENDIX F

PUBLICATIONS ARISING FROM THIS WORK

Referred Journal :

- Quazi, R. T., Bhattacharya, S. N., Kosior, E. and Shanks, R. A. (1996), Digital image analysis applied to painted automotive bumper materials, *Surface Coating International*, **79(2)**, 63.

- Quazi, R. T., Bhattacharya, S. N. and Kosior, E., The effect of dispersed paint particles on the mechanical properties of rubber toughened polypropylene composites, *Journal of Materials Science*, (submitted).

Conference Proceedings :

- Quazi, R. T., Bhattacharya, S. N., Kosior, E. and Shanks, R., A. (1994), Rheological and mechanical properties of reprocessed automotive bumper materials, Proc. *7th Nat. Conf. Rheol.*, Brisbane, July 6-8, p. 183.

- Quazi, R. T., Bhattacharya, S. N. and Kosior, E. (1997), Rheological and mechanical properties of PP/rubber matrix filled with talc and paint particles, Proc. *2nd Pacific Rim Conf. Rheol.*, Melbourne, July 27-31, p. 235.